DISSERTATION

submitted to the

Combined Faculties for the Natural Sciences and for Mathematics

of the Ruperto-Carola University of Heidelberg, Germany

for the degree of

Doctor of Natural Sciences

presented by

Diplom Biochemikerin Felicia Maria Truckenmüller

Born in: Mosbach

Oral examination: 20.01.2021

Dysregulated Micro-RNAs in Biliary Tract Cancer and Characterization of the target Tumor Suppressor FHL1

Referees: Prof. Dr. Ralf Bartenschlager

PD Dr. Stephanie Rössler

For my mom,

who did not lose a battle, but ended a fight.

Thank you for every minute I had you by my side.

SYNOPSIS

Gallbladder cancer (GBC) and cholangiocarcinoma (CCA) comprise the group of biliary tract cancers (BTC). They are a rather rarely occurring group of gastrointestinal tumors, however, with bad prognosis. Due to the lack of specific symptoms and late diagnosis, the only potentially curative treatment is surgical resection, but only few patients are eligible, while the only treatment option for unresectable patients lies in general chemotherapy with a platinum-derived agent and gemcitabine. However, this is usually not extending the life expectancy substantially. BTCs are understudied cancers, of which the pathological mechanisms behind tumor formation are mostly unknown, but it is thought that chronic inflammatory processes can contribute to carcinogenesis. In preceding studies to the here presented doctoral thesis, miRNA profiling of a large German cohort of 40 GBC and 8 healthy gallbladder samples was performed. This led to the identification of 24 human miRNAs, which are differentially expressed between healthy gallbladder epithelium and gallbladder cancer. These miRNAs could further be classified into pro-survival and anti-survival-associated miRNAs, with miR-145-5p being the most downregulated miRNA and miR-4502 representing a potentially oncogenic miRNA. Furthermore, it was shown that CCA cells overexpressing miR-145-5p, significantly upregulated the STAT1 signaling pathway. This led to a tumor suppressive phenotype, as assessed by decreased colony formation and cell viability in CCA cells.

Within the scope of this study, two projects were pursued: firstly, confirming the upregulation of STAT1 signaling by miR-145-5p and sustained tumor suppressive STAT1 signaling by concomitant downregulation of the phosphatase PTPRF and secondly: proteomic profiling of FFPE (formalin fixed paraffin embedded) GBC and healthy gallbladder samples of the same cohort as mentioned above, were analyzed by in-depth quantitative proteomics. This resulted in the identification of differentially expressed proteins, leading to the identification of the tumor suppressor FHL1, which is also a target of the oncogenic miRNA miR-4502.

Regarding the first part, STAT1 gene and protein expression, as well as STAT1-induced target genes were investigated in CCA, GBC and hepatocellular carcinoma (HCC) cells under the ectopic overexpression of miR-145-5p. This showed that miR-145-5p induced STAT1 upregulation is functional and predominantly occurs in CCA. This emphasizes the molecular distinction between these cancer entities. Additionally, it was shown that along the axis of miR-145-5p and STAT1 activation, the phosphatase PTPRF is downregulated. PTPRF has been predicted to be a miR-145-5p target, however, proving the direct binding and subsequent downregulation was not successful so far. Nevertheless, as STAT1 and PTPRF co-precipitate, it is likely for PTPRF to be able to dephosphorylate STAT1, thereby negatively regulating STAT1 signaling. This led to the conclusion that the tumor suppressive miR-145-5p can lead to the induction of STAT1 expression, along with sustained phosphorylation by concomitant downregulation of PTPRF. Thereby, STAT1 signaling was further enhanced, since the attenuation of tumor suppressive signaling by PTPRF was decreased. These findings suggest the use of the miR-145-5p/STAT1/PTPRF axis to develop a targeted therapy for CCA.

For the second part of the studies, a new proteomic approach from FFPE-tissues of GBC and healthy gallbladder was established. Up to date, only few studies using this technology exist as it still challenging. However, the successful performance of quantitative proteomic profiling with a deep resolution of differentially expressed proteins of the GBC cohort is described here. This created the possibility to integrate the miRNA array data with the protein expression data. It was found that FHL1 is one of the topmost downregulated proteins in GBC. Furthermore, miR-4502 is an upregulated miRNA in the short-survival group and it was predicted by miRNA-binding algorithms to target FHL1. These predictions were confirmed by a luciferase assay, proving direct binding of miR-4502 to the 3'-untranslated region (3'UTR) of FHL1. In addition, miR-4502 is downregulating FHL1 in GBC cells after overexpression of mimic-4502 and miR-4502-inhibitor is upregulating FHL1 levels. FHL1 exhibited tumor suppressive properties by reducing colony formation, cell proliferation and cell viability in GBC cells. FHL1 contains protein-protein interaction domains and it has previously been shown to associate with transcription factors, such as the cofactor RBPJ, without being capable of binding DNA itself. In this study, the binding of FHL1 to RBPJ was confirmed and thus FHL1 is likely to replace the intracellular domain of NOTCH1 (N1ICD) in the N1ICD-RBPJ-complex, as N1ICD-mediated transcriptional activity is reduced after overexpression of FHL1. Concomitantly, NOTCH1 target genes are also reduced. As NOTCH1 signaling is frequently overactive in BTCs while FHL1 expression is decreased, this suggests an imbalance between FHL1 binding to RBPJ and N1ICD binding to RBPJ, thereby resulting in expression of oncogenic target genes. Reconstitution of FHL1 leads to tumor suppression, which could partially be attributed to attenuated NOTCH1 signaling. After co-immunoprecipitation of FHL1 and subsequent mass-spectrometric analysis of the associated proteins, additional transcription factors have been found, such as GTF2I. Thus, this study shows that FHL1 is a tumor suppressor in GBC and indicates that the miR-4502/FHL1 axis with subsequently affected genes, can be an important new pathway in order to develop a targeted therapy for GBC. This may in the long term improve the outcome of GBC patients.

ZUSAMMENFASSUNG

Gallenblasenkrebs (GBK) und Gallengangskrebs (GGK) gehören zur Gruppe der Gallenwegs-Krebserkrankungen. Dies sind selten auftretende, gastrointestinale Tumoren, die häufig mit einer schlechten Prognose einhergehen. Aufgrund des Fehlens von spezifischen Symptomen und der häufig erst späten Diagnosestellung ist die einzig heilende Behandlung nur durch die vollständige Resektion der Gallenblase erreichbar, dies ist allerdings nur für einen kleinen Teil der Patienten möglich. Für die inoperablen Patienten bleibt bisher nur die Chemotherapie aus einem Platin-basierten Zytostatikum in Kombination mit Gemcitabin. Diese Therapie verlängert das Leben jedoch meist nicht wesentlich. Gallenwegs-Krebserkrankungen sind schlecht erforschte Krebserkrankungen, deren zugrundeliegenden pathologischen Mechanismen größtenteils unbekannt sind, aber man geht davon aus, dass chronische Entzündung der entsprechenden Organe zum Prozess der Krebsgenese beitragen. Dieser Doktorarbeit vorangegangene Studien haben ein miRNA Profiling von einer großen deutschen Kohorte von 40 Gallenblasenkarzinomen und 8 gesunden Gallenblasenepithelien durchgeführt. Dadurch konnten 24 humane miRNAs identifiziert werden, die unterschiedlich stark zwischen Gallenblasenkrebsgeweben und gesunden Gallenblasengeweben exprimiert werden. Diese konnten weiter unterteilt werden in pro- und anti-Überlebens-assoziierte miRNAs, dabei ist miR-145-5p die miRNAs die am stärksten herunter regulierte miRNA und miR-4502 eine potentiell onkogene miRNA. Des Weiteren wurde in diesen Studien gezeigt, dass miR-145-5p überexprimierende GGK-Zellen den STAT1 Signalweg hochregulieren, was zu einem tumor suppressiven Phänotyp, gezeigt durch gehemmte Koloniebildung und Zellviabilität, führt.

Im Rahmen dieser Studie wurden zwei Projekte verfolgt: zum einen, die Bestätigung, dass die miR-145-5p den STAT1 Signalweg hochreguliert und die anhaltende Tumorsuppression durch STAT1 mit der einhergehenden Runterregulierung der Phosphatase PTPRF verstärkt wird und zum anderen, die Proteom-Analysen von Formalin-fixierten-Paraffin-eingebetteten (FFPE) GBK- und gesunden Gallenblasengeweben der oben erwähnten Kohorte. Letzteres führte zu einer hochaufgelösten Analyse von quantitativ unterschiedlich exprimierten Proteinen, die wiederum zur Identifikation des Tumor-Suppressors FHL1 führte, der ein Zielprotein der onkogenen miRNA miR-4502 ist.

Für den ersten Teil, wurde die STAT1-Gen- und Protein-Expression in GBK-, GGK- und Zellen des hepatozellulären Karzinoms nach der Überexpression der miR-145-5p untersucht. Dies hat gezeigt, dass die Hochregulierung von STAT1 funktional ist und hauptsächlich in GGK vorkommt. Damit wird verdeutlicht, dass die genannten Krebs-Entitäten sich in ihrem molekularen Hintergrund unterscheiden. Ferner, wurde auf der miR-145-5p/STAT1 Achse gezeigt, dass die Phosphatase PTPRF herunter reguliert wird. PTPRF ist als Zielprotein der miR-145-5p prognostiziert, aber die direkte Bindung und damit einhergehende Repression von miR-145-5p an PTPRF, konnte bisher nicht gezeigt werden. Es ist jedoch naheliegend, dass PTPRF STAT1 dephosphorylieren könnte, da PTPRF und STAT1 co-präzipitieren. Dies führte zur Schlussfolgerung, dass die tumor-supprimierende miR-145-5p zur Induktion der STAT1 Expression führt. Zusammen mit der

anhaltenden Phosphorylierung und der Herunterregulierung von PTPRF wird der STAT1 Signalweg verstärkt aufrechterhalten, da die negative Regulation durch PTPRF reduziert ist. Diese Ergebnisse können wegbereitend sein, um mit der miR-145-5p/STAT1/PTPRF-Achse gezielte Therapien für das Gallengangskarzinom zu entwickeln.

Im zweiten Teil der Studie wurde ein neuartiger Proteomics-Versuch etabliert, welcher FFPE-Gewebe von GBK und gesunden Gallenblasengeweben verwendet hat. Heutzutage existieren immer noch sehr wenige Studien mit dieser Technologie, da diese sehr schwierig ist. In dieser Studie wurde dies jedoch erfolgreich durchgeführt und eine quantitative Proteom-Analyse mit hoher Auflösung der unterschiedlich exprimierten Proteine der genannten Kohorte resultierte. Dadurch wurde die Möglichkeit geschaffen, die Daten des miRNA Microarrays mit den Proteom-Daten zu kombinieren. Dies führte zur Identifikation von FHL1, eines der am stärksten runterregulierten Proteine in GBK. Ferner wurde miR-4502 als onkogene miRNA identifiziert, die FHL1 als Zielprotein hat. Die von Algorithmen prognostizierte Bindung von miR-4502 an FHL1 konnte durch einen Luziferase-Assay bestätigt werden, welcher die direkte Bindung der miR-4502 an die 3‘-untranslatierte Region der FHL1 mRNA beweist. Ferner wurde gezeigt, dass das FHL1 Protein nach der Überexpression von miR-4502 herunterreguliert, sowie nach der Administration eines miR-4502 Inhibitors hochreguliert wird. FHL1 zeigte tumor-supprimierende Eigenschaften, durch die Reduktion von Kolonienbildung, Zellproliferation und der Zellviabilität in GBK Zellen. FHL1 besitzt einige Protein-Protein-Interaktionsdomänen und es wurde bereits gezeigt, dass FHL1 an Transkriptionsfaktoren bindet, ohne selbst eine DNA-Bindungsfähigkeit zu besitzen. In der vorliegenden Studie wurde die Bindung von FHL1 an RBPJ bestätigt und es ist wahrscheinlich, dass FHL1 die intrazelluläre Domäne von NOTCH1 (N1ICD) im Komplex N1ICD-RBPJ ersetzt, da die N1ICD-vermittelte Transkription nach der Überexpression von FHL1 reduziert wird. Damit einhergehend wurde die Hemmung von NOTCH1-Zielgenen beobachtet. Der NOTCH1 Signalweg ist häufig überaktiviert in Gallenwegs-Krebserkrankungen und gleichzeitig ist die Expression von FHL1 verringert. Dies lässt vermuten, dass damit ein Ungleichgewicht zwischen der Bindung von FHL1 an RBPJ und von N1ICD an RBPJ entsteht. Die Überexpression von FHL1 führt somit zur Tumor-Suppression, was zumindest teilweise dem verminderten NOTCH1 Signalweg zuzuschreiben ist. Nach der Co-Immunpräzipitation von FHL1 mit anschließender massenspektrometrischer Analyse der assoziierten Proteine, wurden zusätzliche Transkriptionsfaktoren identifiziert, darunter GTF2I. Die hier präsentierten Daten lassen sich als Anhaltspunkt nehmen, um die miR-4502/FHL1-Achse und die nachfolgend regulierten Gene, als wichtigen Signalweg in GBK genauer zu untersuchen. Dies dient dem langfristigen Ziel, potentielle zielgerichtete Therapien für das Gallenblasenkarzinom zu entwickeln, um das Überleben der GBK Patienten zu verbessern.

LIST OF ABBREVIATIONS

3'UTR	3' untranslated region
ADAM	A Disintegrin And Metalloproteinase
AGO2	Argonaute 2
AKT	Protein Kinase B
AMACR	Alpha-methylacyl-CoA racemase
AMPK	Adenosine-monophosphate (AMP) activated protein kinase
AP	Alkaline phosphatase
AP-1	Activator protein-1
APBJ	Anomalous pancreaticobiliary junction
APC	Adenomatous polyposis coli
APS	Ammonium persulfate
aqua dest.	Distilled water
ARID1A	AT-rich interactive domain-containing protein 1A
ASCO	American Sociation of Clinical Oncology
ATCC	American Type Culture Collection
attB1/B2	Attachment site B1/B2
BAP1	BRCA1 associated protein-1 (ubiquitin carboxy-terminal hydrolase)
BCLAF1	Bcl-2-associated transcription factor 1
BilIN	Biliary intraepithelial neoplasia
bp	Base pair
BRAF	B-Raf proto-oncogene
BrdU	Bromo-deoxyuridine
BSA	Bovine serum albumin
BTC	biliary tract cancer
c-MYC	MYC proto-oncogene, bHLH transcription factor
CBF1	see RBPJ
CCK8	Cell Counting Kit-8
CDH1	Cadherin-1
CDK	Cyclin-dependent kinase
CDKN2B	Cyclin-dependent kinase 4 inhibitor B
cDNA	Complementary DNA
CF	Colony formation
ChIP	Chromatin immunoprecipitation
ChIP-seq	Chromatin immunoprecipitation + sequencing
CISH	Cytokine-inducible SH2-containing protein
CK1∂	Casein kinase 1
cm, mm, µm	centimeter, millimeter, micrometer
Co-IP	Co-immunoprecipitation

CO_2	carbon dioxide
COX2	cyclooxygenase 2
CSF	see RBPJ
CTGF	Connective tissue growth factor
CV	cell viability
DAPI	4,6-Diamidino-2-phenylindole
DAPK	Death associated protein kinase
DGCR8	DiGeorge syndrome chromosomal [or critical] region 8
dH2O	Distilled DNAse, RNAse free water
DLL	Delta-like ligand
DLV2	Dishevelled 2
DMEM	Dulbecco's Modified Eagle Medium
DMSO	Dimethyl sulfoxide
DNA	Deoxyribonucleic acid
dNTP	Deoxyribonucleotide triphosphate
DOX	Doxycycline
dsRNA	Double-stranded ribonucleic acid
DTT	Dithiothreitol
e/iCCA	extrahepatic/ intrahepatic cholangiocarcinoma
EBNA2	Epstein–Barr virus nuclear antigen 2
ECM	Extracellular matrix
EDTA	Ethylenediaminetetraacetic acid
EGFR	Epidermal growth factor receptor
ELISA	Enzyme-linked immunosorbent assay
EMT	Epithelial-mesenchymal transition
ER	Estrogen receptor
ERBB2/3/4	Receptor tyrosine-protein kinase erbB-2/3/4
ERK	Extracellular signal-regulated kinases
EtOH	Ethanol
EZH2	Enhancer of zeste homolog 2
F-actin	Filamentous actin
FACS	Fluorescence-activated cell sorting
FBXW7	F-box/WD repeat-containing protein 7
FCS	Fetal calf serum
FDA	Food and Drug Administration
FFPE	Formalin fixed paraffin embedded
FGFR	Fibroblast growth factor receptors
FHL1	four and a half lim domain protein 1
FX1	Fragile mental X retardation
GAPDH	Glyceraldehyde 3-phosphate dehydrogenase
GAS	gamma activated sequence
GBC	gallbladder cancer

GEO	Gene Expression Omnibus
GO	Gene ontology
GP130	Glycoprotein 130
GSI	γ-secretase inhibitor
GTF2I	General transcription factor 2 I
GTP	Guanosine-5'-triphosphate
HCC	hepatocellular carcinoma
HDAC	histone deacetylase
HES1	Hairy and enhancer of split-1
HEY1	Hairy/enhancer-of-split related with YRPW motif protein 1
hMLH1	Human mutL homolog 1
HNSCC	Head and neck squamous cell carcinoma
HSPB6	Heat shock protein B6
IDH1/2	Isocitrate dehydrogenase 1/2
IF	Immunofluorescence
IFI16	Interferon-inducible myeloid differentiation transcriptional activator
IFI27/35	Interferon alpha-inducible protein 27/35
IFN	Interferon
IL-6	Interleukin 6
iNOS	Inducible nitric oxide synthase
IPNB	Intraductal papillary neoplasm
IRF9	Interferon regulatory factor 9
ISRE	Interferon-stimulated response element
JAG	Jagged
JAK	Janus kinase
KRAS	Kirsten Rat Sarcoma
KyoT	see FHL1
LRA	luciferase reporter assay
MAML	Mastermind-like protein
MEK	Mitogen-activated protein kinase kinase
MEM	Minimum Essential Medium
MET	Hepatocyte growth factor receptor
miRNA	micro RNA
mRNA	messenger RNA
MS	mass spectrometry
mTOR	Mammalian target of Rapamycin
MX1	Interferon-induced GTP-binding protein Mx1
N1ICD	NOTCH1 intracellular domain
NCT	National Center for Tumor Diseases
NF-κB	Nuclear factor 'kappa-light-chain-enhancer' of activated B-cells
NRP1	Neuropilin-1
NSCLC	Non-small cell lung cancer

P/S	Penicillin-streptomycin
p16/	Cyclin-dependent kinase inhibitor 2A
p73	Tumor protein p73
PARP9	Poly(ADP-Ribose) Polymerase Family Member 9
PBRM1	Polybromo1
PBS(T)	phosphate buffered saline (Tween20)
PCR	polymerase chain reaction
PD-L1	Programmed death-ligand 1
PECR	Peroxisomal trans-2-enoyl-CoA reductase
PEI	Polyethylenimine
PFA	Para-formaldehyde
PI3K	Phosphoinositide 3-kinase
PIAS	Protein inhibitors of activated STATs
PIK3CA	Phosphatidylinositol-4,5-bisphosphate 3-kinase, catalytic subunit alpha
PLA	Proximity Ligation Assay
PLL	Poly l-lysine
PMSF	Phenylmethylsulfonyl fluoride
PSM	Peptide-spectrum match
PTP	Protein tyrosine phosphatase
PTPRF	Protein tyrosine phosphatase receptor type F
qRT-PCR	Quantitative real-time polymerase chain reation
RAB14	Ras-related protein Rab-14
RAF	Rapidly accelerated fibrosarcoma
RB	Retinoblastoma
RBPJκ = RBPJ	Recombination signal-binding protein for Ig of κ region
Rho	RAS homologue
RISC	RNA-induced silencing complex
RNA	Ribonucleic acid
RPMI	Roswell Park Memorial Institute
Rs	Spearman's rank coefficient
RT	Room temperature
RT	Reverse transcriptase
SAV1	Salvador family WW domain containing protein 1
SCF	Skp, Cullin, F-box containing complex
SDS-PAGE	Sodium dodecyl sulfate polyacrylamide gel electrophoresis
SH2	Src homology 2
SIE	Sis inducible elements
siRNA	Small interfering RNA
SMAD2/3	Mothers against decapentaplegic homolog 2/3
SNA1	Snail Family Transcriptional Repressor 1
SNORD48	Small nucleolar RNA 48
SOC	Super optimal broth with catabolite repression

SOCS	Suppressor of cytokine signaling
SRSF4	Serine/arginine-rich splicing factor 4
STAT1/3/4/5	Signal transducer of activation 1/3/4/5
SUMO	Small Ubiquitin-Related Modifier
T-ALL	T-cell acute leukemia
TAE	Tris acetate EDTA
TBS	Tris buffered saline
TBST	Tris buffered saline + Tween
TCGA	The Cancer Genome Atlas
TE	Tris EDTA
TEMED	N, N, N' ,N'- Tetramethylethylenediamine
TFA	Trifluoroacetic acid
TGFbeta	Transforming growth factor beta
Tm	Melting temperature
TMA	Tissue microarray
TMB	Tetramethylbenzidine
TMT	Tandem mass tag
TNM	TNM Classification of Malignant Tumors (Tumor, Nodes, Metastasis)
TP53	Tumor suppressor protein 53
TRBP	TARBP2 Subunit Of RISC Loading Complex
TWIST1	Twist Family BHLH Transcription Factor 1
TYK2	Non-receptor tyrosine-protein kinase
UBE2L6	Ubiquitin/ISG15-conjugating enzyme E2 L6
UPLC	Ultra-performance liquid chromatography
VEGF	Vascular endothelial growth factor
VIM	Vimentin
WB	Western Blot
ZEB1	Zinc finger E-box-binding homeobox 1

TABLE OF CONTENTS

1. Introduction

1.1. The Gallbladder and Cancers of the Biliary Tract

1.1.1. The Gallbladder and Bile Ducts

The gallbladder (*Vesica fellea* or *Vesica biliaris*) is a small pear-shaped hollow organ commonly occurring in most vertebrates. It is located beneath, or in the liver and is largely covered by the peritoneum. The main task of the gallbladder is the storage of bile acids. The bile is produced by the liver and its main task is helping with the emulsion and digestion of fats from food intake. The gallbladder is connected to the *Ductus cysticus* and together with the *Ductus hepatis communis* from the liver, it is leading into the *Ductus choledocus*. This duct is entering the duodenum. The ampulla of Vater is located, where the *Ductus pancreaticus* and the *Ductus choledochus* unite. This marks the beginning of the second part of the duodenum [1]. In between food intake (interdigestive periods), the bile is being held back by the *Musculus sphincter ductus choledochi* which leads to a concentration of the bile liquids. The bile can then be released to the small intestine by relaxation of the sphincter and contraction of the extrahepatic bile ducts. The bile in the gallbladder contains more gall acids, lecithin, bile pigments and cholesterol than the bile produced by the liver due to the concentration during interdigestive periods [2]. Figure 1-1 shows the location of the gallbladder in humans, together with the main branches of the bile duct system.

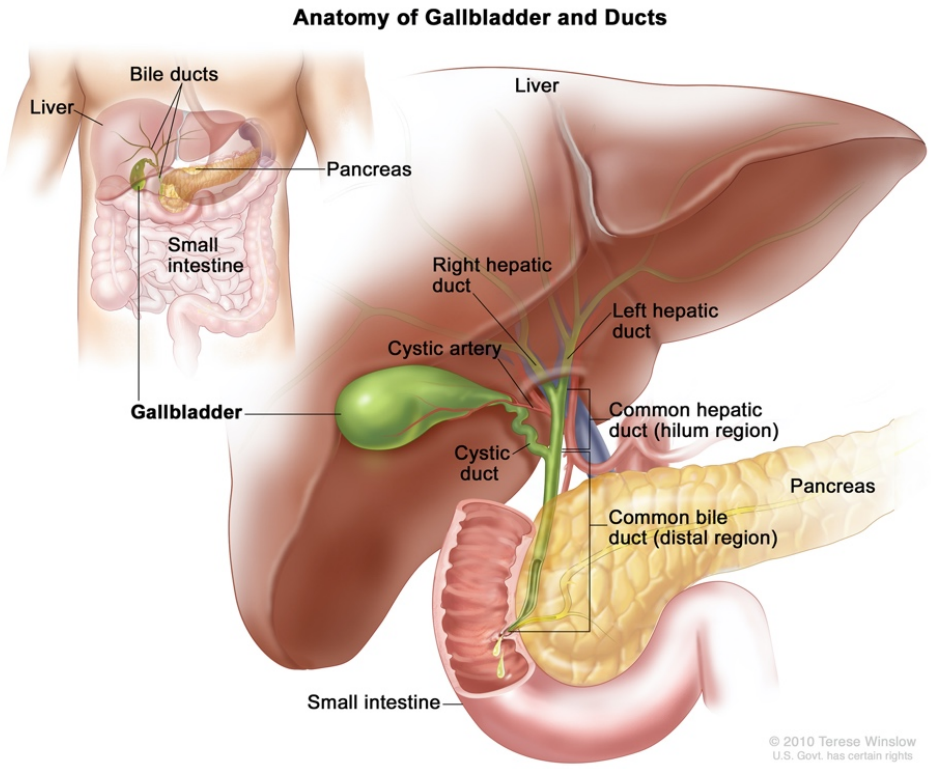

Figure 1-1: Anatomy of the gallbladder and bile ducts[1]. The gallbladder is a small hollow organ beneath the right liver lobe. The bile ducts start in the liver and are connected with the gallbladder. The gallbladder can retain bile produced by the liver and only releases bile when needed. The *Ductus cysticus* joins the *Ductus hepaticus* to form the *Ductus choledochus*, the main bile duct. This duct is joined to the duodenum, where it meets the *Ductus pancreaticus* to form the ampulla of Vater.

The bile ducts are usually referred to as intrahepatic (the left and right hepatic ducts in Figure 1-1), perihilar (the hilum region, where the cystic duct and the *Ductus hepaticus major* form the *Ductus choledochus*) or distal bile ducts (distal region of the extrahepatic common bile duct). This differentiation is also important for the classification of bile duct tumors.

The gallbladder wall is approximately 0.4 cm broad and consists of three layers. On the luminal side, the *Tunica mucosa* (with the epithelium and the *Lamina propria*) is followed by the *Tunica muscularis* and then the *Tunica serosa.* The mucous membrane is pleated and can be stretched, once the gallbladder is accumulating bile. The pleats in the tunica mucosa can form 'bridges', which is a characteristic feature of the gallbladder histology. The *Lamina propria* contains blood vessels. The epithelium is a cell monolayer of cells connected with each other through nexuses and desmosomes. Generally, the function of these cells is the withdrawal of water and concentration of the bile, but in carnivorous animals, often mucins are also secreted. Sometimes in chronic inflammation, the number of the mucin-secreting glands can be elevated [3]. If the gallbladder is diseased with chronic inflammation or tumors, it can be removed without having a strong impact on the intestinal functions, therefore, it is not essential for survival.

[1] https://www.roswellpark.org/sites/default/files/gallbladder_anatomy_with_cystic_artery.jpg

The liver stem cells that are giving rise to epithelial cells of the bile ducts in mice, are called oval cells. They have not yet been identified in humans yet. Oval cells contribute to liver regeneration and can differentiate into hepatocytes or cholangiocytes. The stemness properties of these cells could contribute to the formation of primary liver or bile duct cancers after, for instance, prolonged cell proliferation stimuli, which can lead to altered nuclear factor 'kappa-light-chain-enhancer' of activated B-cells (NF-κB) induced gene expression [4]. However, the stem cells giving rise to epithelial cells of the gallbladder, seem to be distinct from those preceding the intrahepatic biliary ducts, with their own unique expression of surface proteins [5]. It is likely that more than only one kind of stem cells for the gallbladder and bile ducts exist in humans.

1.1.2. CANCERS OF THE BILIARY TRACT

Cancers of the biliary tract (BTC) are rather rare but the incidence rates are rising and the general prognosis is often poor [6]. The BTC are generally malignancies of the epithelial cells and divided into gallbladder cancer (GBC), extrahepatic bile duct cancer (eCCA=extrahepatic cholangiocarcinoma including distal and perihilar cholangiocarcinoma) and intrahepatic bile duct cancers (iCCA=intrahepatic cholangiocarcinoma), see Figure 1-2. BTCs are accounting for approximately 3% of all gastrointestinal cancers and are the second most common hepatobiliary cancers after hepatocellular carcinoma. There is a very interesting distinct and differential distribution of BTCs around the globe. In 2016 in Western countries, CCA rates are modest with 0.35-2 per 100,000/year, however, in Asia this number is 6+ per 100,000/year [7], which is likely to be associated with a higher prevalence of endemic liver fluke infections. For gallbladder cancer, the incidence rates are highest in populations of the Andean region of Chile and Bolivia (up to 23 per 100,000 in women and up to 7.5 per 100,000 in men) and lowest in US Americans (1.5 per 100,000). Additionally, there are high rates in India and Pakistan, in Japan and North-American Indians [7]. Possible explanations for these observations could be the close association of GBC with cholelithiasis and cholecystitis, aflatoxin exposure or regional differences chronic *Salmonella* or *Helicobacter bilis* infections [8].

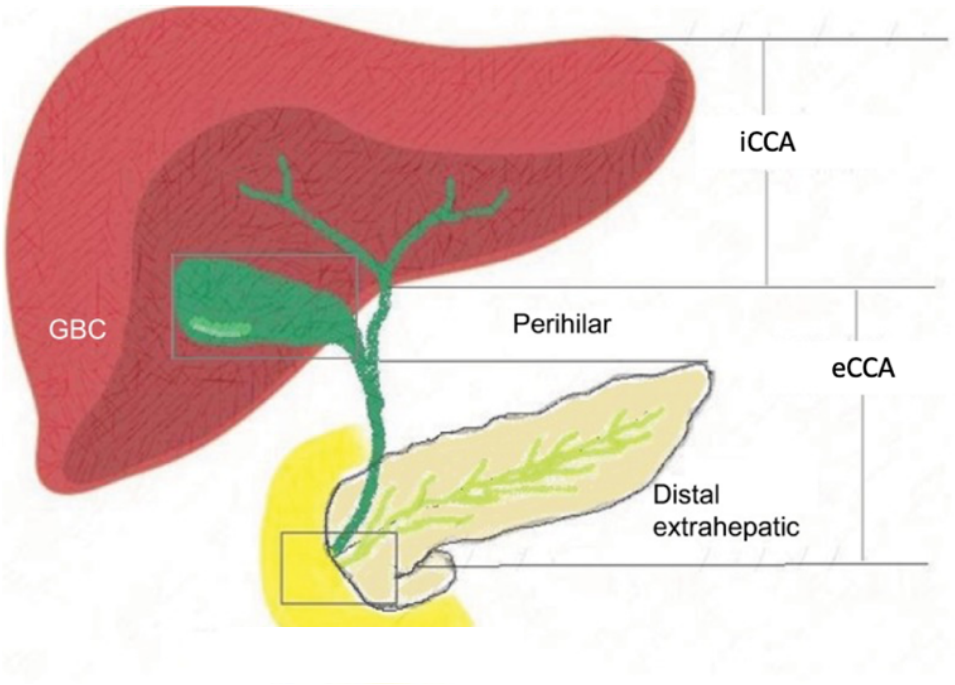

Figure 1-2: Anatomic sub-variants of biliary tract cancers. Intrahepatic cholangiocarcinoma (iCCA) affects that bile ducts in the liver. Gallbladder cancer (GBC) affects the gallbladder, which lies beneath the right liver lobe. Extrahepatic cholangiocarcinoma (eCCA) can be divided into perihilar and distal cholangiocarcinoma and they occur in bile ducts outside of the liver. Taken and modified from [1].

However, both CCA and GBC have a poor prognosis. For iCCA the 5-year survival rate is 2-24% and for eCCA 2-26%. The highest 5-year survival rates have patients with early diagnosis compared to patients with localized or distant spreading of the tumor [9]. In GBC, if the cancer is diagnosed without having spread outside the gallbladder, the 5-year survival rate is 62%. Still, this occurs infrequently due to the lack of specific symptoms. With the cancer having spread to regional lymph nodes, the 5-year survival rates decrease to 27% and if metastases occur in distant parts of the body, the survival rate is only 2%, according to the American Society of Clinical Oncology (ASCO) patient information on cancer in 2020 [10].

The treatment options for BTCs are still very limited. Complete surgical resection is the only potentially curative treatment, but due to the lack of early symptoms and not yet identified specific prognostic markers, the majority of the advanced-stage tumors are unresectable [11]. Since GBC and CCAs are occurring so rarely, they are usually treated in the same way, although evidence is growing that they are different tumor entities with different underlying genetically disturbed backgrounds [8]. However, the up to date most effective treatment options for unresectable BTC are combined chemotherapy with gemcitabine and a platinum-derived agent [12], but unfortunately the results and the benefit for survival are only marginal and curation is not possible any more. This orchestrates the requirement for new targeted therapies, based on the molecular disturbances of CCAs and GBCs.

The pathogenesis of GBC is still poorly understood. There are a number of general risk factors, above all the presence of gallstones, which can lead to chronic cholecystitis and later on to oncogenesis. More precisely: the sustained injuries of the epithelial cells as result of chronic inflammation can lead to aberrant

regeneration and proliferation of the cells. This leads to impaired growth control and the downregulation of apoptosis or cellular senescence, ultimately resulting in the formation of malignant tumors and metastases [6]. Further, GBC is strongly correlated with age over 65, female gender, genetic disposition and gallstones or past medical history of gallstones. Another risk factor is the presence of anomalous pancreaticobiliary junctions (APBJ). This seems to occur more frequently in younger patients and is less associated with cholelithiasis [13]. An overview of the two main routes to invasive gallbladder carcinoma together with the most commonly occurring genetic mutations [14] in GBC formation is displayed in Figure 1-3.

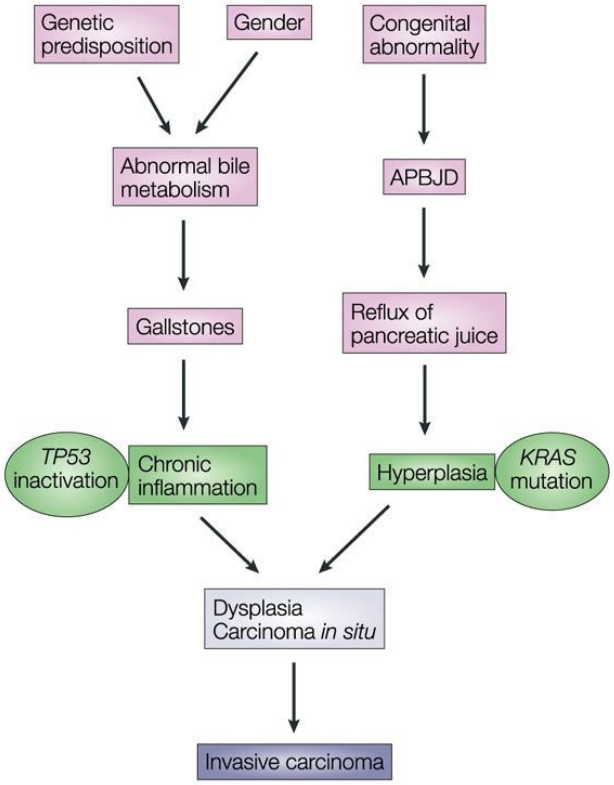

Figure 1-3: Overview of the two routes leading to gallbladder cancer. There are two main routes to the development of gallbladder cancer. The first arises from the presence of gallstones as a result of abnormal bile metabolism. Gallstones can lead to chronic inflammation and subsequently to dysplasia. The second way is a consequence of anomalous pancreaticobiliary junctions (APBJ), which leads to sustained reflux of pancreatic juice. After time and the acquisition of mutations, this can result in hyper- and dysplasia and subsequently lead to invasive carcinoma. Figure from [14].

The main genetic mechanisms leading to GBC are mutations in *TP53* and *KRAS*, accompanied by chronic inflammation. In addition, cyclooxygenase 2 (COX2) overexpression in GBC subsequently leads to the formation of prostaglandins and therefore sustained inflammation. Another by-product is the synthesis of reactive oxygen species, which can damage DNA and lead to mutations. Over the years all these events combined can lead to invasive carcinoma [14]. There are also epigenetic events that can occur, such as methylations of promotors from tumor suppressor genes. For instance, in the carcinogenesis of

cholangiocarcinoma, it is believed that EZH2 could induce hypermethylation of the *p16* promoter, a major cell regulator, thus leading to multi-step cholangiocarcinogenesis after intraepithelial neoplasms (BilIN) [15]. In gallbladder cancer, a study by House *et al.* investigated aberrant methylation of candidate tumor suppressor genes. They found increased methylation of *p16, p73, APC* and *hMLH1* promoters from normal gallbladder, to chronic cholecystitis, to gallbladder neoplasms. Thereby, they suggested that the acquisition of promoter hypermethylation may contribute to tumor formation and progression in the inflamed gallbladder [16].

The pathogenesis of CCA is also relatively unknown. Up to date, there is general consent that pro-inflammatory mediators play an important role. This leads to chronic inflammation of the bile duct epithelium resulting in cholestasis, which in turn leads to aberrant bile acid signaling. Together with subsequently activated growth factors, the cholangiocytes proliferate and are forming two key pre-malignant precursor lesions. BilIN, biliary intraepithelial neoplasia, and IPNB, intraductal papillary neoplasm of bile ducts, which can progress to invasive carcinomas [13] [17]. Thus, BTCs are most likely evolving in a stepwise process and inflammation is promoting the tumorigenic process.

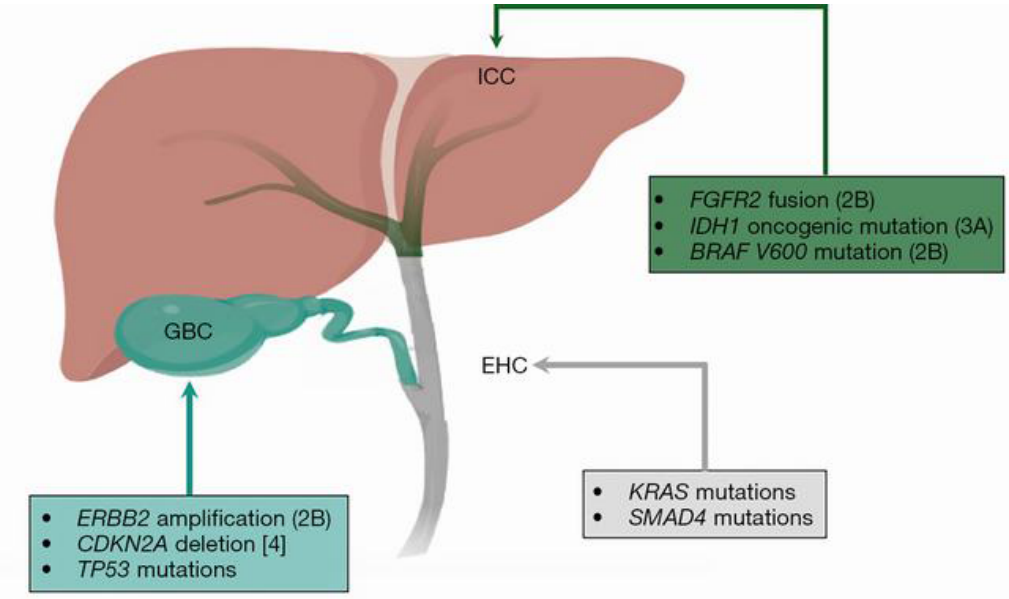

Figure 1-4: Overview of the most frequent genetic aberrations in biliary tract cancers and their actionability according to OncoKB [8] [18].

Several mutations that are associated with biliary tract cancers have been identified in BTC. These mutations occur at different frequencies in the anatomical subgroups [8]. There are also commonly occurring mutations, especially in the cell cycle regulation gene *CDKN2B* and chromatin remodeling gene *ARID1A* [19]. Intrahepatic cholangiocarcinoma frequently shows fusions of *FGFR*, *IDH1/2* mutations, *BRAF* substitutions and *MET* amplifications, together with a low mutational frequency of *KRAS* (Figure 1-4). Extrahepatic cholangiocarcinoma and gallbladder cancer often show ERBB2 amplifications and PIK3CA/mTOR pathway alterations. *KRAS* is frequently mutated in eCCA, but not in GBC [14] [19] [20] [21]. In GBC, the most frequently mutated pathway is the ErbB signaling pathway, including EGFR, ERBB2, ERBB3, ERBB4 and their

downstream targets. Patients with ErbB pathway mutations have a worse outcome, than those without mutations in the respective pathway [22]. The observed genetic alterations are differing between the subtypes of BTCs whereby iCCA, eCCA and GBC show specific aberrant genes. This is once more reflecting the fact that the different BTCs are more distinct from each other than initially assumed.

It is quite clear to see that the affected genes are also general tumor-relevant genes. In a comprehensive study for genomic profiling, it was found that only of a subset of iCCA, eCCA and GBC patients present clinically relevant mutations [19], which are more targetable than others (e.g. FGFR2 fusions or ERBB2), yet, most patients do not have targetable mutations. Thus, targeted therapies are currently being evaluated in clinical studies. Patients suffering from iCCA with IDH1/2 mutations, are responding well to a multi-tyrosine kinase inhibitor and there is clinical data showing that the use of FGFR inhibitors is promising, as the side effects are comparable to other anti-cancer therapies. However, inhibiting angiogenesis with already used agents like bevacizumab, or targeting EGFR by cetuximab shows no effect in treating BTC. Neither does the administration of KRAS or ERBB2 inhibitors. Other therapeutics disturbing the WNT/catenin, Hedgehog, KRAS-RAF-MEK-ERK or PI3K-AKT-mTOR pathways are still studied extensively. The most promising targets so far are IDH inhibitors and FGFR2 fusion-inhibitors, however, these are most relevant only for patients with iCCA. As many of the already tested molecular targets showed disappointing and conflicting results, there is a new window of opportunity open for drugs targeting the mutations of chromatin remodeling proteins (such as ARID1, BAP1 and PBRM1) [23] [24]. As mentioned before, the ErbB pathway is frequently mutated in GBC. It has been shown that ERBB2/ERBB3 mutants can upregulate PD-L1 expression, thereby contributing to the immune evasion of cancer cells from cytotoxic T-cells. By administrating ERBB2/ERBB3 inhibitors with a PD-L1 antibody, this immunosuppressive effect was reversed, thereby suggesting a therapeutic potential in the treatment regimen for GBC patients with ERBB2/ERBB3 mutations [25].

However, the assumption up to date is that the efficacy of targeted therapies will remain low, as the genetic aberrations are not occurring very frequently and many biliary tract tumors seem to rely on epigenetic regulation mechanisms [7]. Therefore, it is of great importance to investigate further mechanisms of dysregulation in tumors to generate a broader picture and to be able to identify novel potential targets, complementing the ‘traditional’ approach of targeting proteins by using small molecule inhibitors or monoclonal antibodies.

1.2. Gene Regulation by MicroRNAs

1.2.1. Synthesis of MicroRNAs and Canonical Mode of Action

MicroRNAs are short single-stranded RNA molecules of ~22-23 nucleotides in length and it is undoubtedly accepted nowadays that they play important roles in many biological processes, most important of all, the mediation of post-transcriptional regulation of gene expression [26]. Hence, they are implicated in

processes that can be relevant for cancer development, such as cell proliferation, differentiation and tumorigenesis.

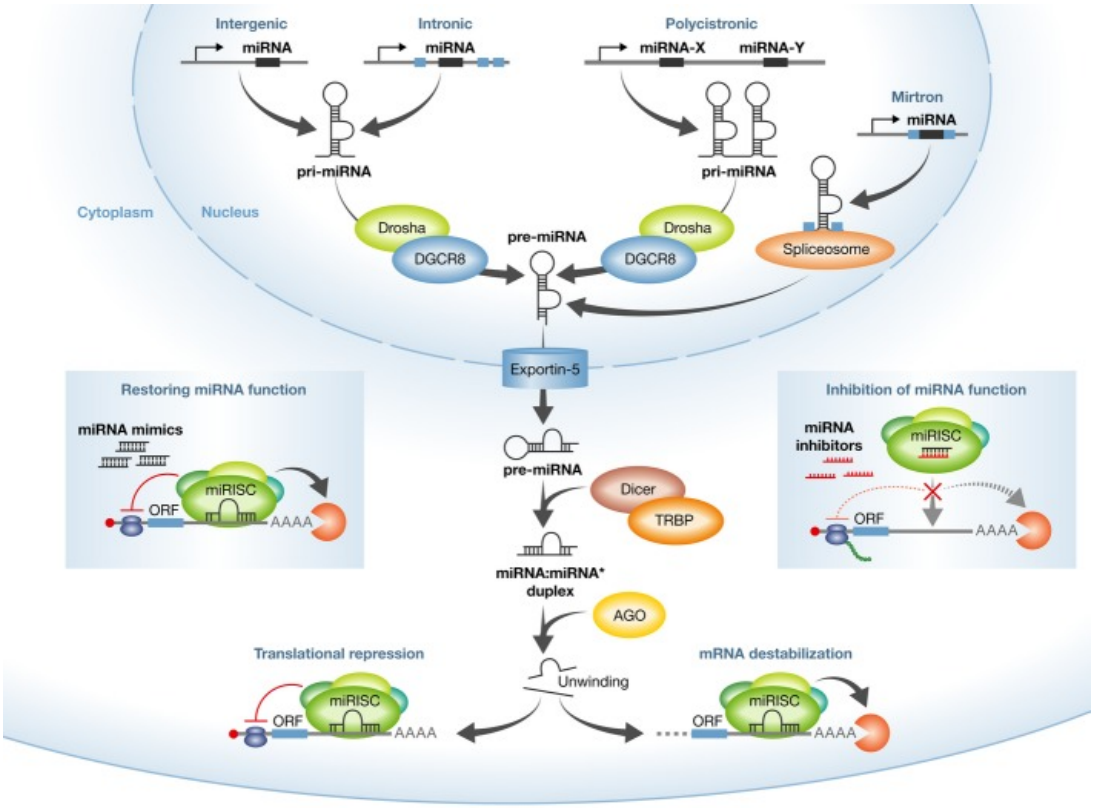

Figure 1-5: Synthesis of animal miRNAs and their main potential targetability. The microRNA transcripts are transcribed from DNA sections in intergenic, intronic or polycistronic regions into pri-miRNAs. They are capped and polyadenylated for stabilization and processes by DGCR8/Drosha to pre-miRNAs. Subsequently they are exported in a GTP-dependent manner into the cytoplasm and undergo further nucleolytic cleavage by Dicer/TRBP to yield the mature miRNA:miRNA* duplex. The mature miRNA is then incorporated into the RISC complex by the help of Ago proteins. Once incorporated into the RISC complex, the miRNA is leading to the downregulation of the target mRNA by translational repression and/or mRNA destabilization, followed by degradation. The targetability of miRNAs is either by restoring miRNA function through miRNA mimics (left) or by the prevention of miRNA-guided downregulation of target genes through the inhibition of the miRNAs themselves with miRNA inhibitors (right, often referred to as antago-miRs). Figure taken and modified from [27].

In animals, miRNAs are usually transcribed by RNA polymerase II (Figure 1-5). Their DNA sequences are located in intergenic, intronic or polycistronic regions. In the first step, the transcripts are several hundred nucleotide long pri-miRNAs with an 80-nucleotide stem loop. These pri-miRNAs can contain up to six miRNAs precursors. The processing starts at pri-miRNA level by capping of the 5'-end and the attachment of a poly-A tail [28]. Then, the pri-miRNAs associate with DCCR8 (Pasha in invertebrates) and Drosha, which catalyze the cleavage to yield the pre-miRNAs [29]. In the nucleus, about 16% of all miRNAs are edited and modified, for example transitions of adenosine to inosine take place [30]. The next step is the energy-

dependent nuclear export of the pre-miRNAs mediated through the shuttling protein Exportin-5, which recognizes a two-nucleotide overhang on the 3'-end left by Drosha. In the cytoplasm, the RNase Dicer cleaves the pre-miRNA hairpin, thereby creating an imperfect miRNA:miRNA* duplex. Technically, both strands of the miRNA duplex could act as functional miRNA, but usually only one strand is incorporated into the Agonaute-containing RISC (RNA-induced silencing complex), leading to the miRISC complex. The miRNA in the miRISC complex is directing the protein complex towards the complementary sites of the target mRNAs, which is leading to transcriptional repression or induction of target mRNA degradation [31]. The interaction between miRNAs and mRNAs is initiated by the complementary binding of the two different RNA species through the so-called seed sequence, which is a 2-7 nucleotide long sequence in the miRNA with a corresponding site in the 3'UTR of the target mRNA [32]. The here described mechanism is the canonical mode of action by miRNAs, resulting in the downregulation of target mRNAs and lastly also of proteins. There are also miRNAs exerting their functions in non-canonical ways. These are for example: miRNAs, which are recruiting transcription factors to their respective promoters or exerting their functions as negative transcription regulators. Furthermore, it has been studied that miRNAs can also upregulate transcription and there is increasing evidence that miRNAs could associate with other proteins in a RISC-independent manner (reviewed in [33]).

So far, miRNAs have been shown to be involved in many cellular and developmental processes [34] and potentially affect over 60% mammalian protein-coding genes, making them highly abundant and important regulators for gene expression [35]. Therefore, it is not surprising that dysregulated miRNA turnover can contribute to tumorigenesis and can potentially also be targeted by anti-cancer therapies [36].

1.2.2. MicroRNAs in Cancer

Since miRNAs are able to regulate the step between transcription of genes from DNA and the translation into functioning proteins, it seems very likely that aberrant miRNA function is having a huge impact on the cell metabolism. In this context, miRNAs are called oncogenic miRNAs, if they lead to the sustained expression of oncogenic proteins and the opposite being tumor suppressive miRNAs [37]. As a single miRNA can regulate hundreds of genes, miRNAs also became an interesting therapeutic target – and especially regarding BTCs, as they are not as frequently mutated as other cancer entities and where the commonly used small molecule inhibitors are not applicable. Furthermore, the dysregulation of miRNAs can be with the miRNAs themselves, through e.g. chromosomal abnormalities, transcriptional control changes, epigenetic changes or defects in the miRNA biosynthesis [38].

The first miRNA implication in cancer was found in chronic lymphocytic leukemia, where miR-15a and miR-16-1 were frequently deleted and hence their expression was reduced in the according cancer samples [39]. This also led to the idea of using miRNA signatures in healthy or cancerous tissues, in order to use their expression as prognostic markers. For example either high miR-185 or low miR-133b levels in colorectal

cancer might correlate with poor prognosis and metastasis levels [40]. This can go even further, as in one study the expression signature of 6 miRNAs is used to predict the survival of gastric cancer patients [41]. The use of miRNA signatures or expression levels as prognostic markers gave rise to the thought, whether they can also be used as diagnostic markers, which would be of great interest for rare tumors that lack initial symptoms. Here again, this would be beneficial for the diagnosis of BTC, but also for instance for the diagnosis of pancreatic cancer, where the problem of non-specific early symptoms is also common. However, a 'quick-and-easy' approach for diagnosis or prognosis like this is only then possible, if there are cell-free miRNAs, which circulate in the blood serum or other body fluids. Luckily, this is quite common, even though the cell-free miRNA signatures cannot be found in the same fashion, as inside the cells. A study found a specific signature of pancreatobiliary cancer biomarkers in patient sera, consisting of 8 miRNAs (miR-6075, miR-4294, miR-6880-5p, miR-6799-5p, miR-125a-3p, miR-4530, miR-6836-3p, and miR-4476) to predict pancreatobiliary cancers among healthy individuals and other cancer-diseased patients [42]. However, further studies using large cohorts are required to validate this miRNA signature independently and the functions of most of these miRNAs are largely unknown. Another interesting study shows, how tricky the work with miRNAs can be. For instance, miRNA-21 in serum has been shown to play roles in different cancers, such as esophageal and colorectal cancer. In BTC, miR-21 serum markers are helpful, if used together with other diagnostic modalities to detect early stage of disease and to discriminate malignant from benign disease [43]. This means, the serum levels of miR-21 can be very useful, if the previous knowledge of a biliary tract disease exists, but it could also hint towards different cancers or, in the worst case, disguise other cancers. In addition, the miRNA levels in bile might be more specific than the ones in blood serum for BTC, and miR-9 seems to be a potential novel biomarker for diagnosis and clinical management of BTC [44].

Above described are only a few examples as to how miRNAs can be used as predictive markers for survival, prognostics or diagnostics. There is a multitude of studies (reviewed in [38]), investigating either miRNA profiles of one or a few miRNAs and their relevance in different cancers. For research however, it would be important to deduce the actual mechanisms of action for interesting miRNAs in different cancer entities, to be able to exploit these properties and directly interact with the mechanism, as miRNAs have multiple levels of regulations. One example is miR-200, in the progression of formation of hepatocellular carcinoma (HCC) formation. In early stages when the cells become invasive and under epithelial-mesenchymal transition, miR-200 is downregulated. It becomes upregulated again, when metastases re-epithelialize [45]. Another example is miR-451, which is strongly downregulated in non-small cell lung cancer (NSCLC) and is directly targeting RAB14. RAB14 rescue however, can attenuate the tumor suppressive function of miR-451, thereby suggesting that miR-451 exerts its tumor suppressive at least partially via inhibiting RAB14 [46]. For the promotion of tumorigenesis, a study describes that miR-27a is upregulated in gastric carcinoma and can target prohibitin. Since prohibitin protein levels are upregulated after knockdown of the miRNA, concomittant with the attenuation of cancer cell growth, the authors conclude that miR-27a functions as an oncogene, at least to some extent by downregulating prohibitin [47]. Up to date, it has also been shown that promoters of miRNA genes can be hypermethylated leading to decreased miRNA expression, as with miR-9 in breast cancer for instance [48]. This can subsequently have an impact on the cell function. However generally, it should be mentioned again that miRNA dysregulation in cells is mostly leading to functional differences of target proteins. For a huge number of miRNAs, the target proteins are only predicted and not

confirmed. In addition, some of the miRNA targets are cell type specific and therefore, only play a role in certain tumor entities.

The therapeutic potential of interfering with miRNAs for therapies of all kinds, not only for cancer, lies in either the suppression of certain miRNAs by antago-miRs or in restoring the expression by use of miRNA mimics. This is schematically shown in Figure 1-5 in the right and left boxes within the diagram. The first pharmaceutical drug targeting miRNAs is Miravirsen (Santaris Pharma A/S), which is inhibiting liver-specific miR-122. This miRNA is necessary for the hepatitis C virus to replicate and in the clinical phase IIa of the study, 4 out of 9 patients did not show any detectable virus RNA anymore after 5 weekly doses [49]. Miravirsen is considered a flagship product of the miRNA therapeutic market, however, up to date, there are still ongoing clinical trials and it has not yet reached FDA approval. One of the first miRNA-based therapeutics for cancer treatment was MRX34 by Mirna Therapeutics Inc. It was intended to restore the tumor suppressive function of miR-34 in patients with inoperable liver tumors. However, the clinical trials had to be stopped due to high toxicity and adverse effects. On the other hand, the TargomiR/Mesomir phase I trial was aiming to deliver the tumor suppressive miR-16 mimics to the target tissues of patients with malignant pleural mesothelioma and NSCLC patients. The administration of the mimics was done by using a presumably safer bacterial-derived transfection system [50] and is now entering phase II clinical trials.

Thus, miRNA synthesis, degradation and mode of action are a very important research field, opening up the cellular functions to a multitude of additional regulations and modifications. Some are certainly very slight and only fine-tune the cell homeostasis, but some can have a huge impact and might be responsible for the malignant development of the cells. Taken together, there has been extensive research on miRNAs since the discovery that they are implicated in human disease in 2002. Many of the studies are showing promising results for future diagnostic and therapeutic use of these RNA molecules in order to bring them from bench to bedside.

1.3. STAT AND NOTCH SIGNALING

1.3.1. THE JAK-STAT PATHWAY AND ITS DYSREGULATION IN CANCER

One main mechanism for the cells to maintain homeostasis and exert their specific function, is the reaction towards extracellular stimuli, often leading to the activation or inactivation of genes. This is mostly achieved by receptor activated signaling cascades and results in transcription factor regulation. STAT signaling is a major pathway in inflammation, which it is induced by cytokines and interferons. As described above, chronic inflammation is a frequently occurring event in the formation of gallbladder carcinoma and cholangiocarcinoma, therefore, dysregulated STAT signaling might be implicated in the tumorigenesis of BTC. The main proteins involved in STAT signaling, apart from cyto- and chemokines are STAT (signal transducer and activators of transcription) proteins and Janus kinases (JAK). STAT proteins are a class of

transcription factors and they are involved in different cellular processes like immune response, cell division, cell death or tumor formation. When dysregulated, STATs can lead to diseases, such as cancer and immune system disorders. Another important mediator for STAT signaling are Janus kinases (JAKs) and special receptor proteins preceding the JAK enzymes [51].

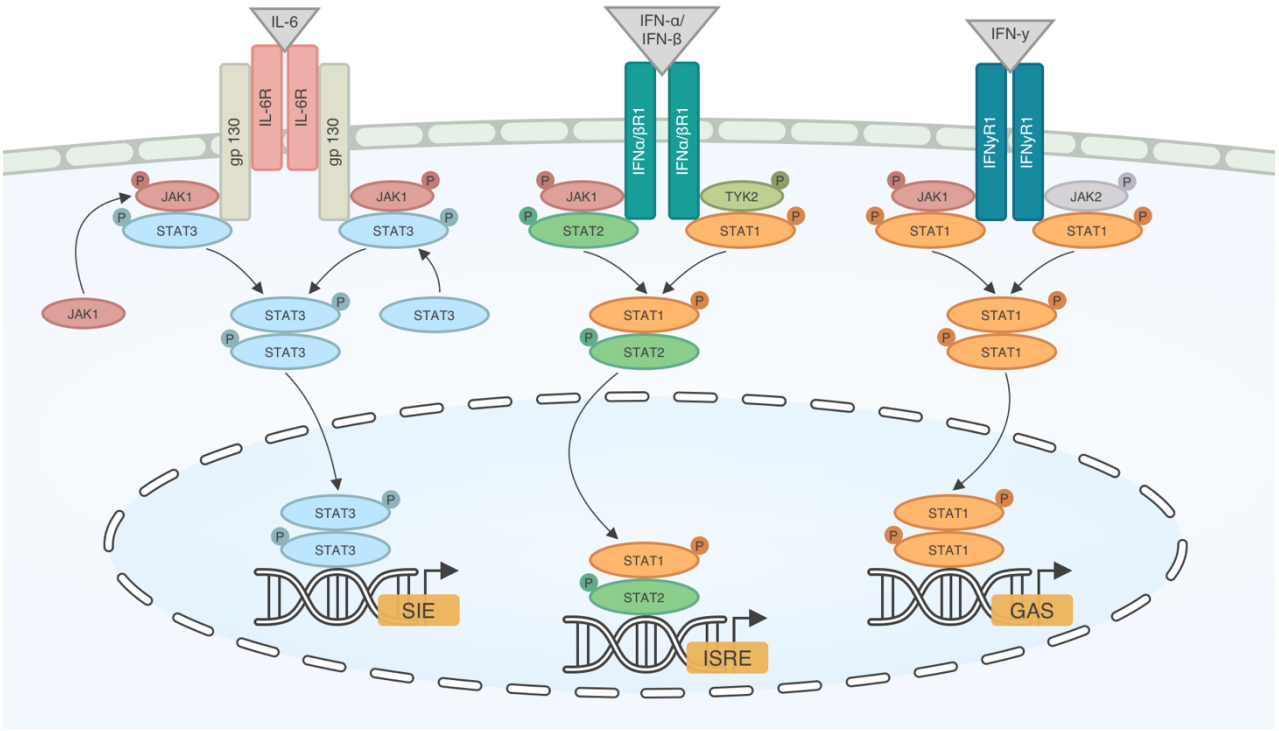

Figure 1-6: JAK-STAT signaling pathway of STATs1-3. STAT3 signaling is triggered by IL-6 binding to the IL-6-receptor/GP130 complex, this leads to the activation of JAK1. JAK1 is mainly responsible for the phosphorylation of STAT3. STAT3 dimerizes upon phosphorylation, translocates to the nucleus and binds to SIE (sis-inducible elements) sequences, leading to the activation of gene transcription. IFNα and IFNβ bind to the IFNαR/IFNβR receptors, leading to activation of JAK1 and TYK2. Subsequently, STAT1 and STAT2 are phosphorylated and form heterodimers. STAT1/STAT2 heterodimers bind to ISRE (interferon-stimulated response element) sequences on the DNA. IFNγ binds to the IFNγ-receptor, thereby activating JAK1 and JAK2. They phosphorylate STAT1, which then forms homodimers, translocates to the nucleus and activates genes after binding to the GAS (gamma-activated sequence).

JAK enzymes are tyrosine kinases, permanently associated with the intracellular domains of cytokine or growth factor receptors. After binding of a respective extracellular ligand to the receptor, the receptor dimerizes and is trans-phosphorylated by JAKs (see Figure 1-6). This creates phosphotyrosine residues that can be bound by the Src homology 2 (SH2) domains of the STAT proteins. Once present, JAKs are further phosphorylating the STAT proteins. Phosphorylated STATs can homo- or heterodimerize and in this phosphorylated and dimeric state, they enter the nucleus by the help of importins and bind to the DNA [52]. In mammals there are 4 different JAKs (JAK 1-3 and TYK2) and 7 STATs (1-4, 5A and 5B and 6), which are

expressed to different extents in different tissues. In mouse knock-out studies, some STATs were shown to be essential for life and when dysregulated lead to neoplastic diseases [53]. STAT1 is a main mediator of type I and II interferons. Type I interferons comprise IFN-α and -β and are able to activate STAT1 and STAT2, which are forming heterodimers and can bind to ISRE (interferon-stimulated response elements) on the DNA, subsequently leading to target gene transcription. IFNγ is the only type II interferon, which is leading to STAT1 homodimers and their binding to GAS (gamma-activated sequences) on the DNA [54].

The regulation of JAK-STAT signaling is occurring on many levels. As with every membrane-bound receptor, the endocytic membrane turnover is one early level of regulation. Further important mediators in the downregulation of JAK-STAT signaling are SOCS proteins (suppressor of cytokine signaling). SOCS proteins comprise SOCS1-7 and cytokine-inducible SH2-containing protein (CISH). They function through different mechanism to achieve negative regulation of STAT signaling, such as binding to the receptors themselves (SOCS2, SOCS3 and CISH) [55] or binding to JAKs (SOCS1 and SOCS3) [56]. However, it is not fully clear for all SOCS proteins, where exactly they are interfering with the signaling cascade. Furthermore, protein tyrosine phosphatases (PTPs) are a relevant group of regulatory enzymes, as they remove the phosphate groups from receptors, JAKs or STAT proteins, thereby interfering with the signaling cascade at different branch points, leading to an attenuation of signal propagation [57]. Among these phosphatases negatively affecting JAK-STAT signaling is PTPRT, which is a cell membrane spanning receptor-like protein phosphatase. There are a number of these receptor-like phosphatases, such as PTPRF, but even though the nomenclature suggests that they are related and could be relevant for the same molecules, this is not necessarily the case. PTPRF has been suggested to be involved in negatively affecting insulin signaling [58] and regulating cell adhesion by dephosphorylating ß-catenin [59]. Further, PTPRF is also implicated in other pathways. For instance, it can inhibit breast cancer progression by being activated through PPARγ [60]. Its growth-inhibitory role has also been shown in hepatocarcinogenesis, by negatively regulating ERK-dependent proliferation signaling [61]. In terms of cell adhesion, PTPRF can impact focal adhesions through regulating CDK1. When PTPRF is lost, CDK1 activity is reduced and leads to less focal adhesion complex formation, which may play a role in cancer progression [62]. Another level of JAK-STAT signaling regulation is carried out by PIAS (protein inhibitors of activated STATs) proteins. There are PIAS1, PIAS3, PIASx, and PIASy in mammals. These proteins function in three different ways. A) by adding a small protein called SUMO onto the STATs which blocks phosphorylation sites, B) by inhibiting the DNA binding capacities of STAT proteins and C) by recruiting histone deacetylases (HDACs), which remove acetyl residues from the DNA, thereby keeping the DNA inaccessible for the transcriptional machinery [63]. Thus, STAT signal transduction is tightly regulated by the interplay of kinases and phosphatases, which depends on the cellular context and type of cytokine.

There are numerous consequences for human diseases if JAK-STAT signaling is dysregulated, such as immune defects and tumor formation. Due to reasons of clarity and comprehensibility, this introduction will only focus on STAT proteins in the role of cancerogenesis. STAT3 and STAT5 are best studied for their roles in tumor promotion, whereas STAT1 is generally seen as a tumor suppressor [64]. STAT3 is constitutively active in different solid and hematological cancers, thereby sustaining pro-proliferative signaling [65]. The same has been observed for STAT5 [66]. The tumor suppressive functions of STAT1 are mediated by multiple mechanisms. Firstly, by being able to induce apoptosis ([67] [68]) and by negatively regulating the cell cycle. Further, the oncogenes *C-MYC* and *ERBB2* are suppressed by STAT1 [64]. STAT1 has

also been shown to inhibit angiogenesis [69] and there are hints towards the loss of immunosurveillance through defects in IFNγ/STAT1 signaling, which can contribute to tumor progression [70]. The full picture of STAT involvement is still not clear, bearing in mind its proinflammatory signaling, which might be oncogenic too. This could be especially important in BTC, as inflammation is commonly occurring and is likely to contribute to tumorigenesis. So far, the implications of STAT proteins in BTC are poorly studied. It has been shown that STAT3 expression in cholangiocarcinoma correlates with poorer histological differentiation and it has been suggested that pro-inflammatory signaling of STAT3 contributes to CCA carcinogenesis [71]. Our own study revealed that STAT1 can be induced by the tumor suppressive microRNA (miR-145-5p) in CCA cells. The activation of STAT1 signaling and might lead to tumor suppression via STAT1 targets [72]. Taken together, STAT signaling is involved in BTC, but only few players of this signaling cascade have been studied in detail and further studies are required to unravel potential therapeutic opportunities.

1.3.2. The NOTCH Pathway and its Dysregulation in Cancer

The NOTCH pathway was first described in 1914, by John S. Dexter, when he noticed the appearance of a notch in *D. melanogaster* wings [73]. Today, NOTCH signaling is understood as a highly conserved pathway in metazoans and it is a main pathways for embryonic development and tissue homeostasis [74]. NOTCH signaling is absolutely crucial as cell fate determinator, hence, dysregulation of the pathway can lead to hematological and solid tumors, [75] but also to a variety of other diseases [76]. In mammalians, there are four NOTCH receptors (NOTCH1-4) and diverse ligands, belonging either to the Delta-like (DLL1, DLL3 and DLL4) or the Jagged (JAG1 and JAG2) family. They are temporarily and spatially differentially expressed [77].

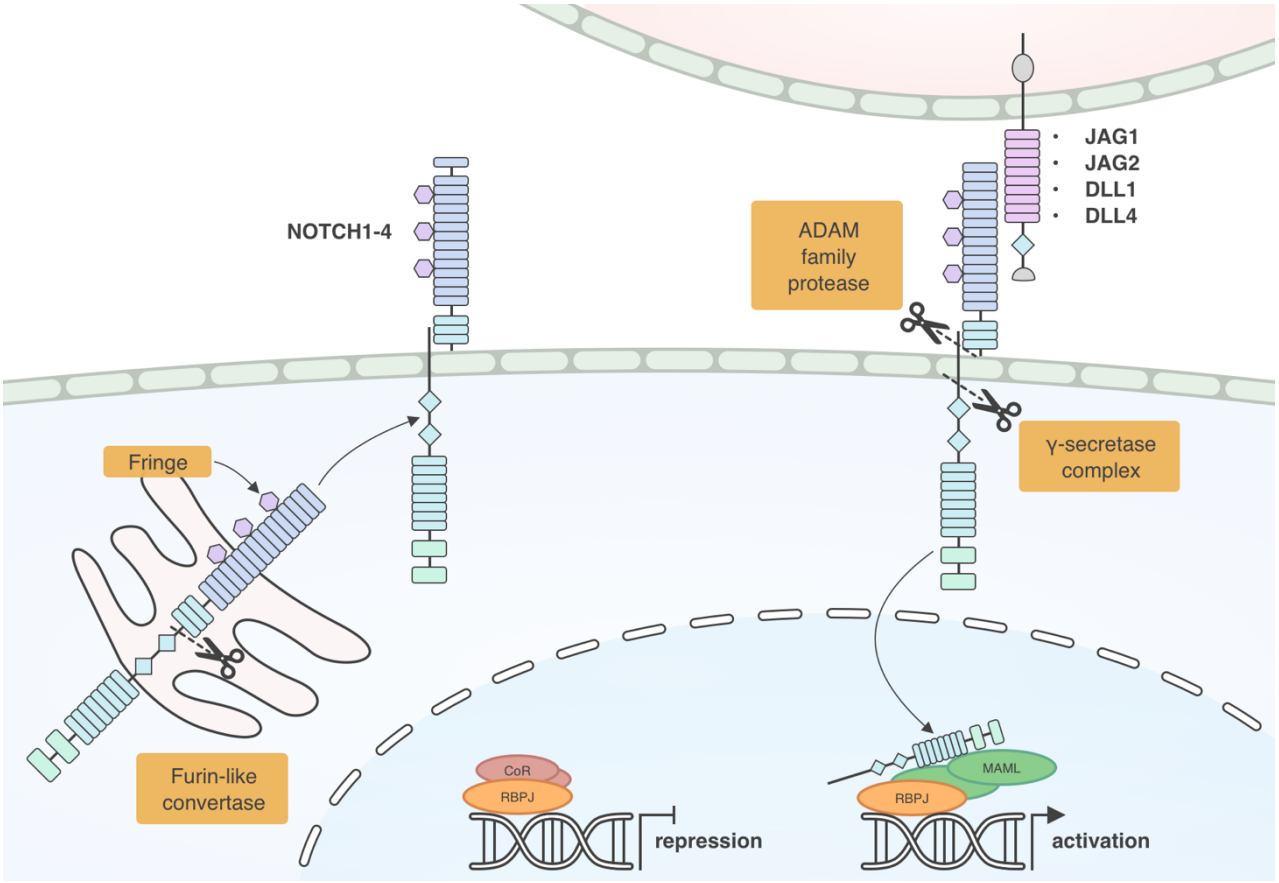

Figure 1-7: Schematic overview of the NOTCH signaling pathway. Final maturation of the NOTCH receptor is carried out through S1-cleavage by a Furin-like convertase, glycosylation by Fringe and transport to the cell membrane. At the cell-cell interface *trans*-binding of JAG1/2 or DLL1/4 ligands to one of the NOTCH receptors takes place. This leads to two subsequent proteolytic cleavages S2 (through ADAM family proteases) and S3 (through γ-secretase complex). The product of the final cleavage is the NOTCH intracellular domain (NICD), which then translocates to the nucleus. There, NICD binds to RBPJ and replaces a co-repressor complex to form a co-activator complex, together with MAML proteins, and to subsequently induce target gene expression. Figure based on [78].

Figure 1-7 shows the principal NOTCH pathway. The final maturation of the NOTCH receptor is taking place in the Golgi complex, where it gets cleaved by a Furin-like protease (S1-cleaveage) and glycosylated by Fringe, leading to a large bipartite protein. NOTCH has a large extracellular domain, spans the membrane and has a smaller intracellular part [79]. Paracrine contact between the extracellular domain of the receptor to one of the ligand proteins results in a conformational change that exposes a proteolytic cleavage site in the NOTCH protein and two subsequent proteolytic cleavages are taking place [77]. The first one is carried out by ADAM family proteases (S2) and the second one by the γ-secretase (S3) complex. This leads to the release of the intracellular domain (NICD – NOTCH intracellular domain) to the cytoplasm of the NOTCH-receptor bearing cell. The NICD translocates to the nucleus and binds to the transcription factor RBPJ (alias

CSF or CBF1). NOTCH and RBPJ, together with Mastermind-like proteins (MAML1-3), form a co-activator complex, which is then able to induce target gene expression [80].

In contrast to many other signaling pathways involving kinases and second messenger amplifications, the NOTCH signaling pathway is a straight-forward pathway, where signal transmission irreversibly takes place after receptor cleavage. However, given the importance and the plethora of possible developmental decisions carried out by NOTCH signaling, additional regulatory levels exist (reviewed in [81] and extensively in [82]). For instance, the described mechanism of *trans*-activation between two adjacent cells has its counterpart in *cis*-activation. Here, ligand and receptor of the same cell interact, which can lead to pathway inhibition, termed lateral inhibition. But, as this also can lead to lateral induction, the expression patterns of receptors/ligands set for a level of regulation of NOTCH signaling [83]. Further, NOTCH signaling is dependent on proper protease function. The S2 cleavage is the rate-limiting proteolytic cleavage step in the juxtamembrane extracellular region [84]. The hereby arisen NOTCH fragment is very short-lived and immediately cleaved by γ-secretase to release the transcriptionally active NICD. Furthermore, there is evidence for ligand-independent NOTCH cleavage mechanisms that could also play a role in pathophysiological signaling [85]. Additional levels of regulation of NOTCH signaling are carried out by post-translational modifications. Ubiquitination of NOTCH through the critical tumor suppressor FBXW7 (which recognizes substrates for the SCF E3 ubiquitin ligase) leads to downregulation of NOTCH signaling [86]. Different glycosylation patterns can sensitize NOTCH receptors to some ligands compared to others, or affect the general NOTCH receptor sensitivity [87],[88]. As already mentioned above for JAK-STAT signaling, membrane turnover and endocytosis of receptors is a potential regulatory mechanism. One last example for NOTCH signaling regulation is the crosstalk with other pathways. For NOTCH it has been shown that Dishevelled 2 (DLV2), a mediator of the Wnt signaling pathway, can directly inhibit RBPJ, which leads to downregulation of NOTCH target gene transcription [89].

Dysregulated NOTCH signaling is implicated in carcinogenesis of a variety of tissues. Initially, it has been investigated in the context of acute T-cell leukemia (T-ALL), where activating NOTCH1 mutations have been found in the majority of patients [90]. However, in squamous cell carcinomas of skin and lung, about 75% and 12.5 % inactivating NOTCH1/2 mutations have been observed [91]. Both tumor suppressive and oncogenic implications have been described [92], which is attributed to the complexity of readouts of NOTCH signaling, depending on the cell types and the genetic landscape. Oncogenic signaling through NOTCH overactivation is mainly achieved by inducing its target gene *MYC* and induction of pro-proliferative PI3K/AKT signaling [78]. NOTCH dysregulation has been also investigated in biliary tract cancers. NOTCH1-4, as well as DLL4, are aberrantly highly expressed in GBC and eCCA and might contribute to tumor progression, as the expression correlates with advanced TNM stages [93]. Another study proved that NOTCH1 and NOTCH3 signaling is activated in iCCA cell lines, with subsequent overexpression of cyclin E, thereby suggesting the mechanistic link of NOTCH1-mediated tumorigenesis [94]. Further, a link between upregulated NOTCH1 signaling by nitric oxide through iNOS has been investigated in primary sclerosing cholangitis and CCA, which substantiates the great impact of inflammatory environment in the formation of BTC [95]. These and further observations has led to the idea of medical interference with the NOTCH signaling pathway in targeted therapies of BTC, among them are γ-secretase inhibitors (GSIs) the most common ones. They are still lacking FDA approval, but are currently in phase I/II and III clinical trials.

However, up to date, there is not enough data to confirm the efficacy of NOTCH pathway inhibitors in BTC [96].

2. OBJECTIVES

Biliary tract cancers (BTCs), comprising gallbladder cancer and cholangiocarcinoma, are rare and understudied cancer entities. Frequently, BTCs are diagnosed at late stages, due to the lack of early symptoms, and often have dismal prognosis with very little prospect of long-term survival. Therefore, it is of ample importance to understand the molecular mechanism leading to BTC. Up to date, neither much is known about the development of BTC, nor about the proteomic, genetic, as well as epigenetic alterations. Therefore, in preceding works of AG Rössler, a miRNA expression profiling of a cohort in 40 German GBC patients and 8 healthy gallbladder samples of patients undergoing cholecystectomy, has been performed. Due to the rareness and the different geographic incidence rates, this cohort constitutes a unique and relatively large study group with the advantage of reflecting the situation in patients of a relatively homogenous cohort. The results of the miRNA expression profiling elucidated miRNAs that are associated with short and long patient survival and have therefore been grouped in potentially oncogenic and tumor suppressive miRNAs [72].

In order to complement the miRNA array data with proteomic profiling of the same samples, and to enhance insight into the molecular background of gallbladder cancer, the aim of this work was firstly, to tie in with the earlier results from the miRNA microarray, by characterization of the tumor suppressive miR-145-5p in role of STAT1 signaling and secondly, to perform shotgun mass-spectrometric analysis for the identification of dysregulated proteins in gallbladder cancer versus healthy gallbladder samples. The resulting multitude of up- and downregulated proteins should then be carefully evaluated for candidate proteins in an oncogenic and tumor suppressive context. Further, the candidate proteins should be evaluated *in silico* for the potential regulation by oncogenic or tumor suppressive miRNAs.

Interesting chosen proteins ought to be characterized in pathways, in which they could be implicated, as well as functionally analyzed by cell culture-based assays to test their tumorigenic or tumor suppressive potential. Furthermore, their direct interaction partners were analyzed by functional assays and by renewed proteomics research. The long-term purpose of these studies lies in the elucidation of specific molecular disorders in gallbladder cancer, to approach targeted therapies for this dismal disease and enhance the patient outcome .

3. Material and Methods

3.1. Materials

3.1.1. Chemicals and Consumables

3.1.1.1. Chemicals

The chemicals used in this study were purchased from the listed manufacturers if not stated otherwise:

- AppliChem (Darmstadt, Germany)
- Carl Roth (Karlsruhe, Germany)
- Merck Millipore (Darmstadt, Germany)
- SERVA (Heidelberg, Germany)
- Sigma-Aldrich (Taufkirchen, Germany)

Chemicals for bacteria cultivation (agar, tryptone and yeast extract) were purchased form BD Biosciences (Heidelberg, Germany).
Distilled DNA/RNAse free water (dH_2O) was obtained from Gibco/Life Technologies (Darmstadt, Germany).

3.1.1.2. Consumables

Table 3-1: Overview general consumables

Consumables	*Supplier*
Agarose	Carl Roth GmbH &Co. KG, Karlsruhe, Germany
Amersham ™Protran ™Nitrocellulose blotting membrane, 0.45 µm	GE Healthcare, Buckinghamshire, UK
Cell culture plates (96-well, 24-well, 12-well, 6-well, 6 cm, 10 cm, 15 cm)	NeoLab, Heidelberg, Germany Orange Scientific (Braine-l'Alleud, Belgium)
Cell scrapers	Corning, New York, USA
Cryovials	Greiner Bio-One, Frickenhausen, Germany
Falcon tubes (15 ml, 50 ml)	Greiner Bio-One, Frickenhausen, Germany
MicroAmp Fast Optical 96-well reaction plates	Thermo Fisher Scientific, Waltham, USA
Microcentrifuge tubes	Eppendorf, Hamburg,Germany

(0.2 ml; 0.5 ml, 1.5 ml; 2 ml, 5ml)	Sarstedt, Nümbrecht, Germany
Microscope cover glasses	Marienfeld, Lauda-Königshofen, Germany
Microscope slides "Menzel-Gläser"	Thermo Fisher Scientific, Waltham, USA
Millex-HA filter (0.22 µm or 0.45 µm)	Merck Chemicals GmbH, Darmstadt, Germany
Mini-PROTEAN® TGX™ precast gels	Bio-Rad, Munich, Germany
Parafilm	Pechiney, Düsseldorf, Germany
Pasteur pipettes	Wilhelm Ulbrich, Bamberg, Germany
Pipette tips	Greiner Bio-One, Frickenhausen, Germany Steinbrenner, Heidelberg, Germany
Scalpels	Feather, Osaka, Japan
Sterile stripettes®	Corning, New York, USA
Syringes	BD Biosciences, Heidelberg, Germany
Whatman™ 3MM Chr	GE Healthcare, Buckinghamshire, UK

3.1.2. Reagents

3.1.2.1. General Reagents

Table 3-2: General reagents

Reagent	*Order number*	*Supplier*
Albumin fraction V, biotin-free (BSA)	0163	Carl Roth, Karlsruhe, Germany
Ammonium persulfate (APS)	1610700	Bio-Rad, Munich, Germany
Anti-FLAG M2 magnetic beads	M8823	Sigma-Aldrich GmbH, Taufkirchen, Germany
Bradford reagent	B6916	Sigma-Aldrich, Taufkirchen, Germany
Cell lysis buffer 10x	9803	Cell Signaling Technology, Frankfurt am Main, Germany
Cristal violet	C-3886	Sigma-Aldrich, Taufkirchen, Germany
CytoPainter Phalloidin-iFluor 488 reagent	ab176753	Abcam, Cambridge, UK
DAPI Fluoromount-G	0100-20	Southern Biotech, Birmingham, USA
Fisher's EZ-Run™ pre-stained Rec protein ladder	BP36031	Thermo Fisher Scientific, Waltham, USA

Gel loading dye blue (6x)	B7021	New England Biolabs, Frankfurt, Germany
GelRed™ nucleid acid gel stain	41003	Biotium, Hayward, USA
LE agarose	840004	Biozym, Hessisch Oldendorf, Germany
Milk powder	T145	Carl Roth, Karlsruhe, Germany
PhosStop 10x (PS)	4906845001	Roche, Mannheim, Germany
Protease-inhibitor mix G 1000x (PI)	39101	SERVA, Heidelberg, Germany
TRIzol® Reagent for RNA extraction	15596026	Thermo Fisher Scientific, Waltham, USA

3.1.2.2. TRANSFECTION REAGENTS

Table 3-3: Transfection Reagents

Transfection reagents	*Order number*	*Supplier*
Lipofectamine™RNAiMAX	13778	Life Technologies, Darmstadt, Germany
Lipofectamine™2000	11668	Life Technologies, Darmstadt, Germany
Polyethylenimine (PEI)	23966	Polysciences, Warrington, PA, USA

3.1.2.3. PCR AND CLONING REAGENTS

Table 3-4: Reagents for polymerase chain reactions and cloning

Reagents	*Order number*	*Supplier*
miScript Primer Assay	218300	Qiagen, Hilden, Germany
dNTP Mix	R0192	Thermo Fisher Scientific, Waltham, MA, USA
Gateway LR clonase II enzyme mix	11791020	Thermo Fisher Scientific, Waltham, MA, USA
GelRed™ nucleid acid gel stain	41003	Biotium, Hayward, USA
Gel loading dye blue (6x)	B7021	New England Biolabs, Frankfurt, Germany

GeneRuler™1 Kb plus DNA ladder	10787018	Thermo Fisher Scientific, Waltham, MA, USA
FastDigest Bsp1407I	FD0934	Thermo Fisher Scientific, Waltham, MA, USA
PrimaQUANT qPCR-CYBR-Green-MasterMix-high-ROX	SL-9912	Steinbrenner, Heidelberg, Germany
RevertAid H Minus	K1631	Thermo Fisher Scientific, Waltham, MA, USA

3.1.3. KITS

Table 3-5: Commercially bought laboratory kits

Kit name	*Order number*	*Supplier*
Dual Luciferase Reporter Assay	E1910	Promega GmbH, Mannheim, Germany
Duolink® In Situ Detection Reagents Orange	DUO92007	Sigma-Aldrich GmbH, Taufkirchen, Germany
Duolink® In Situ Mounting Medium with DAPI	DUO82040	Sigma-Aldrich GmbH, Taufkirchen, Germany
Duolink® In Situ PLA Probemaker Anti-MINUS	DUO92010	Sigma-Aldrich GmbH, Taufkirchen, Germany
Duolink® In Situ PLA Probe Anti-rabbit PLUS	DUO92001	Sigma-Aldrich GmbH, Taufkirchen, Germany
Duolink® In Situ Wash Buffers, Fluorescence	DUO82049	Sigma-Aldrich GmbH, Taufkirchen, Germany
MycoAlert™Mycoplasma Detection Kit	LT07	Lonza, Verviers, Belgium
miScript II RT Kit	218160	Qiagen, Hilden, Germany
miScript SYBR® Green PCR kit	218073	Qiagen, Hilden, Germany
Cell Proliferation ELISA Biotrak™ System	RPN250	GE Healthcare, Buckinghamshire, UK
PureYield™ Plasmid Midiprep System	A2495	Promega, Madison, USA
RevertAid H Minus First Strand cDNA Synthesis Kit	K1632	Thermo Fisher Scientific, Waltham, USA

3.1.4. BUFFERS AND SOLUTIONS

Table 3-6: List of buffers **and** composition

Buffer/solution	*Composition*	*Application*
2x Sample buffer	125 mM Tris HCl pH 6.8, 4% SDS, 20% glycerol, 0.02% bromphenol blue	FLAG co-IP, SDS-PAGE
4x Loading buffer	250 mM Tris HCl pH 6.8, 8% SDS, 40% glycerol, 0.04% bromphenol blue, 100 mM DTT	SDS-PAGE, Co-IP
Blocking solution	TBST + 5% milk powder or BSA	WB
Crystal violet staining solution	1% Crystal violet, 25% methanol	Colony formation assay
FLAG Co-IP lysis buffer for Dynabeads® protein G magnetic beads	50 mM Tris HCl pH 7.4, 150 mM NaCl, 1 mM EDTA, 1% Triton X-100 add 1 mM PMSF and 1 mM DTT, PS and PI directly before use	FLAG Co-IP
FLAG FHL1 Co-IP lysis buffer for Anti-FLAG® M2 Magnetic Beads	50 mM Tris HCl pH 7.5, 150 mM NaCl, 1 mM MgCl, 1% NP-40, 1 mg/ml BSA add PS and PI directly before use	FHL1 FLAG Co-IP
LB agar	LB medium + 1.5% agar	Bacteria cultivation
LB medium	2% LB broth in H_2O	Bacteria cultivation
PBS	140 mM NaCl, 2.7 mM KCl, 10 mM Na_2HPO_4, 1.8 mM KH_2PO_4	Cell harvest, Co-IP
PBST	PBS + 0.01% Tween 20	IF, PLA, Co-IP
Running buffer (pH 8.5-8.7)	0.25 M Tris base, 2 M glycine, 1% SDS	SDS-PAGE
TAE buffer	40 mM Tris base, 10 mM EDTA pH 8.0, 6% acetic acid	Agarose gel electrophoresis
TAE gel	TAE buffer + 1-2% agarose	Agarose gel electrophoresis
TBS (pH 7.4)	50 mM Tris HCl, 150 mM NaCl	FLAG co-IP
TBST (pH 7.6)	25 mM Tris base, 140 mM NaCl, 0.02% Tween 20	WB
TE buffer	70 mM Tris base, 1 mM EDTA pH 8.0	Gateway cloning
Transfer buffer	25 mM Tris base, 200 mM glycine, 20% methanol	WB

3.1.5. Cell Culture

3.1.5.1. Cell Lines Overview

The cell lines used in the study were either purchased from the American Type Culture Collection (ATCC; LGC Standards, Wesel, Germany), the German Collection of Microorganisms and Cell Culture (DSMZ; Braunschweig, Germany), the Japanese Collection of Research Bioresources Cell Bank (JCRB, Tokyo, Japan), the Korean Cell Line Bank (KCLB, Seoul, Korea) or have been gifted.

To prove the genetic identity, cells were routinely confirmed by short tandem repeat profiling. Further the cell lines were regularly checked for mycoplasma contamination.

Table 3-7: Human cell lines

Cell line	*Origin*	*Cultivation medium*	*Order number*
EGI-1	eCCA	MEM + 2x MEM amino acids + 4 mM L-glutamine + 1 mM sodium pyruvate	ACC385 (DSMZ)
G-415	GBC	RPMI	RBRC-RCB2640 (Gift from Justo)
Gb-d1	GBC	RPMI	RRID:CVCL_H705
HEK293T	Human embryonic kidney cells (expressing SV40 large T antigen)	DMEM	ATCC CRL-3216
HUCC-T1	iCCA	RPMI	JCRB0425
HuH1	Hepatoma	DMEM	JCRB0199
HUH7	HCC	DMEM	JCRB0403
HEP3B	HCC	MEM	ATCC HB-8064
Mz-CHA-1	GBC	DMEM	RRID:CVCL_6932
NOZ	GBC	William's E Medium	JCRB1033
OZ	iCCA	William's E Medium	JCRB1032
SNU182	HCC	RPMI	ATCC CRL-2235
SNU1196	Hilar CCA	RPMI	KCLB (01196)
SNU308	GBC	RPMI	KCLB (00308)
TGBC1	GBC	DMEM	RRID:CVCL_1769
TFK-1	eCCA	RPMI	ACC344 (DSMZ)

3.1.5.2. Cultivation Media and Additives

Table 3-8: Cell culture media and additives

Medium/additive	*Order number*	*Supplier*
Dimethyl sulfoxide (DMSO)	D8418	Sigma-Aldrich GmbH, Taufkirchen, Germany
Doxycycline hyclate	D9891	Sigma-Aldrich, Taufkirchen, Germany
Dulbecco's Modified Eagle Medium (DMEM)	D5796	Sigma-Aldrich, Taufkirchen, Germany
Dulbecco's Phosphate Buffered Saline (DPBS)	D8537	Sigma-Aldrich, Taufkirchen, Germany
Fetal Bovine Serum (qualified, heat inactivated)	10500064	Thermo Fisher Scientific, Waltham, USA
Hexadimethrine bromide (Polybrene)	107689	Sigma-Aldrich, Taufkirchen, Germany
L-Glutamine	G7513	Sigma-Aldrich, Taufkirchen, Germany
Minimum Essential Medium (MEM)	M4655	Sigma-Aldrich GmbH, Taufkirchen, Germany
Mitomycin C	-	Pharmacy, University Hospital Heidelberg, Heidelberg, Germany
Opti-MEM® I Reduced Serum Medium	31985047	Thermo Fisher Scientific, Waltham, USA
Penicillin-Streptomycin Solution	15140130	Thermo Fisher Scientific, Waltham, USA
Poly-L-Lysin hydrobromid (PLL)	P6282	Sigma-Aldrich, Taufkirchen, Germany
Puromycin	P8833	Sigma-Aldrich, Taufkirchen, Germany
Resazurin	AR002	R&D Systems, Minneapolis, USA
Roswell Park Memorial Institute 1640 (RPMI 1640)	R8758	Sigma-Aldrich, Taufkirchen, Germany
Trypsin-EDTA solution	T3924	Sigma-Aldrich, Taufkirchen, Germany

3.1.6. Bacteria

For cloning the bacterial strain 'One Shot™ Mach1™ T1 Phage-Resistant Chemically Competent E. coli' (Thermo Fisher Scientific, Waltham, USA) and was and the following media and additives were used:

Table 3-9: Bacterial medium and additives

Medium/additive	*Order number*	*Supplier*
Ampicillin sodium salt	A9518	Sigma-Aldrich GmbH, Taufkirchen, Germany
Carbenicillin disodium salt	6344	Carl Roth, Karlsruhe, Germany
Kanamycin sulfate	T832	Carl Roth, Karlsruhe, Germany
LB broth (Lennox)	X964	Carl Roth, Karlsruhe, Germany
SOCS outgrowth medium	15544034	Thermo Fisher Scientific, Waltham, USA

3.1.7. PRIMERS

The plasmids were purchased as indicated. Further plasmids have been kindly provided by Dr. Stefan Pusch, DKFZ Heidelberg or belong to AG Roessler, Institute of Pathology.

Table 3-10: List of plasmids used in cell lines

Plasmid	*Application*	*Origin*
pCMV-XL-5-PTPRF	Transient expression of PTPRF and subcloning to pDEST26, contains point mutation I to T	Origene, Maryland, USA
pDONR201-FHL1	Gateway entry vector for human FHL1	Gift from Stefan Pusch, DKFZ, Heidelberg, Germany
pDONR201-N1ICD	Gateway entry vector for human N1ICD	Generated by Sarah Luiken
pDONR201-N3ICD	Gateway entry vector for human N3ICD	Generated by Sarah Luiken
pDONT223-RBPJ-WT	Gateway entry vector for human RBPJ	Addgene, Cambridge; MA, USA
pDEST26	Gateway destination plasmid	AG Roessler, Institute of Pathology, Heidelberg, Germany
pDEST26-ctrl (w/o ccdB site)	Transient transfection control	AG Roessler, Institute of Pathology, Heidelberg, Germany
pDEST26-FLAG-C	Gateway destination plasmid for C-terminally FLAG-tagged gene products (transient transfection)	AG Roessler, Institute of Pathology, Heidelberg, Germany
pDest26-HA-N-STAT1α	Transient expression of human STAT1 with N-terminal HA-tag	Generated by Carolin Ploeger
pDEST26-FHL1	Transient expression of human FHL1	Personally generated
pDEST26-FHL1-FLAG-C	Transient expression of human FHL1 with C-terminal FLAG-tag	Personally generated
pDEST26-N1ICD	Transient expression of human N1ICD	Personally generated

pDEST26-N1ICD-FLAG-C	Transient expression of human N1ICD with C-terminal FLAG-tag	Generated by Sarah Luiken
pDEST26-RBPJ	Transient expression of human RBPJ	Personally generated
pDEST26-RBBJ-FLAG-C	Transient expression of human RBPJ with C-terminal FLAG-tag	Personally generated
pDEST26-PTPRF	Transient expression of PTPRF, re-mutated T to I	Gift from Stefan Pusch, DKFZ, Heidelberg, Germany
psPAX2	Lentiviral packaging plasmid	AG Roessler, Institute of Pathology, Heidelberg, Germany
pMD2.G	Lentiviral envelope plasmid	AG Roessler, Institute of Pathology, Heidelberg, Germany
pTRIPZ-GW (Gateway cloning-adapted)	Gateway destination plasmid for stable inducible expression	Gift from Stefan Pusch, DKFZ, Heidelberg, Germany
pTRIPZ-FHL1	Stable inducible expression	Personally generated
pTRIPZ-NOTCH1ICD	Stable inducible expression	Personally generated
pTRIPZ-NOTCH3ICD	Stable inducible expression	Personally generated
pRL-TK	Renilla expression	AG Roessler, Institute of Pathology, Heidelberg, Germany
pGL2-4xCSL-luciferase	Luciferase expression	Addgene, Cambridge; MA, USA

3.1.8. OLIGONUCLEOTIDES

3.1.8.1. OLIGONUCLEOTIDES FOR MIRNA EXPERIMENTS

The miRNA-mimics and negative control "AllStars" have been purchased from Qiagen (Hilden). The miRNA-4502 inhibitor is from Ambion, Thermo Fisher Scientific (Waltham, USA).

Table 3-11: List of RNA species used for experiments

RNA species	*Sequence (5'-3')*	*Order Number*
mimic-145-5p	GUCCAGUUUUCCCAGGAAUCCCU	MSY0000437
Mimic-4502	GCUGAUGAUGAUGGUGCUGAAG	MSY0019038
AllStars neg. control	-	1027280
miR-4502 inhibitor	-	219300

For the investigation of mature miRNA levels, the primer assays for the MiScript SYBR® Green PCR Kit have been purchased from Qiagen (Hilden). The levels of small nucleolar RNA 48 (SNORD48) have been used as reference. The unique primer sequences are not provided by the manufacturer.

Table 3-12: Primer assays for qRT-PCR of mature miRNA levels

Primer Assay	*Order Number*
SNORD48	MS00007511
mir-145-5p	MS00008708
mir-4502	MS00040922

3.1.8.2. Oligonucleotides for DNA Experiments

DNA oligonucleotides were either in stock, or purchased from Thermo Fisher Scientific (Waltham, USA).

Table 3-13: Sequencing primer

Primer	*Sequence (5'-3')*	*Application*
pDONR-5	TAACGCTAGCATGGATCTC	pDONR forward primer
pDONR-3	GCAATGTAACATCAGAGAT	pDONR reverse primer
CMV fwd	CGCAAATGGGCGGTAGGCGTG	pDEST forward primer
T7	TAATACGACTCACTATAGG	pDEST reverse primer
pTRIPZ CMV fwd	CAGAGCTCGTTTAGTGAACCG	pTRIPZ forward primer
pTRIPZ UbqC rev	CCGCGGGAGGCGCCAAAACC	pTRIPZ reverse primer

Table 3-14: Primers for quantitative Real-Time PCR

Gene name	*Accession Number*	*Sequence (5'-3')*	*Amplicon length bp*
ABCA8	NM_001288985.2	Fw: GTGTCAACAAACTTGGGCCTT Rv: TATCTACCCGTCCCAGGTCC	182
ABCD3	NM_002858.4	Fw: GGCCTGCACGGTAAGAAAAG Rv: CGAGACACCAGCATAACAGC	188
AMACR	NM_014324.6	Fw: CAGAGATTCTGCAGCGGGAA Rv: GGGGCATACGGATTCTCACC	163
CDH1	NM_001317185.2	Fw: CTTTGACGCCGAGAGCTACA Rv: TCGACCGGTGCAATCTTCAA	97

c-MYC	NM_002467.6	Fw: TGGTGCTCCATGAGGAGACA Rv: GTGATCCAGACTCTGACCTT	132
ERBB2	NM_001005862.2	Fw: TGCTGGACATTGACGAGACAG Rv: GTTTGGCCCCAAAAGTCATCA	159
ERBB3	NM_001982.4	Fw: CATCGTGAGGGACCGAGATG Rv: GGAGCACAGATGGTCTTGGT	141
FHL1	NM_001159699.2	Fw: GCGTGGATTGCTACAAGAACTTT Rv: TTACCAAACCCAGTGATGGGG	73
HES1	NM_005524.4	Fw: AAGAAAGATAGCTCGCGGCA Rv: CGGAGGTGCTTCACTGTCAT	71
HEY1	NM_012258.4	Fw: CGGCTCTAGGTTCCATGTCC Rv: AAAAGCACTGGGTACCAGCC	140
HSPB6	NM_144617.3	Fw: AGCCCATTTTCTGCCGTGAA Rv: AGAGTTGGGGCAGTCGAAAA	73
GAPDH	NM_002046.7	Fw: CTGGTAAAGTGGATATTGTTGCCAT Rv: TGGAATCATATTGGAACATGTAAACC	81
MX1	NM_002462.5	Fw: TGGCATAACCAGAGTGGCTG Rv: CCACATTACTGGGGACCACC	125
NOTCH1	NM_017617.4	Fw: TGCAGAACAACAGGGAGGAG Rv: CAGGTTGTACTCGTCCAGCA	188
PXPM2	NM_018663.3	Fw: GGCCTCTGAGATATGCCGTT Rv: ACCTCAGGAGGGATCCAATGT	94
PARP9	NM_031458.3	Fw: GGCCACATTGAATGGCAGAC Rv: TACCAACTGGGACCGTTGAA	165
PECR	NM_018441.6	Fw: GGAGCTGGGGAGTAATGTGG Rv: ATGGGAATGACTCGTGCCTG	114
PLEKHG2	NM_022835.3	Fw: AATTTCTGCACCGCATCCTG Rv: TCTTGAAACGGGGATACGGG	166
PTPRF	NM_002840.5	Fw: CTGCGAACCTGTATGTGCGA Rv: CATCCACTTCACGTAGGGCA	140
SNAI1	NM_005985.4	Fw: CTTCTCTAGGCCCTGGCT Rv: GACAGGAGAAGGGCTTCTCG	68
STAT1	NM_007315.4	Fw: CCTAACGTGCTGTGCGTAG	128

		Rv: GGTGAACCTGCTCCAGGAAT	
TWIST	NM_000474.4	Fw: GACAAGCTGAGCAAGATTCAGACC Rv: CTGGAGGACCTGGTAGAGGAAG	72
VIM	NM_003380.5	Fw: GAAAGTGTGGCTGCCAAGAACC Rv: CAGCCTCAGAGAGGTCAGCAA	76
ZEB1	NM_001323642.2	Fw: GATCCAGCCAAATGGAAATCAG Rv: CTGAGCTAGTATCTTGTCTTTCATC	47

3.1.9. ANTIBODIES

Table 3-15: List of primary antibodies used in this study with their respective application

Epitope (clone)	*Host species*	*Supplier*	*Order number*	*Applicat-ion*	*Dilution*	*Concentration 2nd antibody*
β-Actin (C4)	Mouse	MP Biomedicals	SKU 08691001	WB	1:10 000	1:2000
FHL1	Mouse	LS-Bio	LS-C115289	WB IF	1:1000 1:100	1:2000 1:250
FHL1	Rabbit	Novus Biologicals	NBP1-88745	WB IF, IHC, PLA	1:1000 1:100	1:2000 1:250
E-Cadherin	Mouse	BD Biosciences	610182	WB	1:1000	1:2000
N-Cadherin	Rabbit	QED Bioscience	42031	WB	1:1000	1:2000
VE-Cadherin	rat	BD Biosciences	555289	WB	1:1000	1:2000
GAPDH	Chicken	Merck Millipore	AB2302	WB	1:10 000	1:2000
*GAPDH (**10C10**)*	Rabbit	Cell Signaling	2118	WB	1:10 000	1:2000
Ki67	Rabbit	Abcam	ab15580	IF	1:100	1:250

Monoclonal ANTI-FLAG	Mouse	Sigma-Aldrich	F1804	WB	1:1000	1:2000
Notch1iCD/N1iCD (5B5)	Rat	Cell Signaling	3447S	WB	1:1000	1:2000
RBPJ	Rabbit	Invitrogen	PA5-35187	WB IF, PLA	1:1000 1:50	1:2000 1:250
RBPJ	Rabbit	Cell Signaling	5313	WB	1:1000	1:2000
Smad2/3 (D7G7) XP®	Rabbit	Cell Signaling	12747T	WB	1:1000	1:2000
Phospho-Smad2 (Ser465/467) (138D4)	Rabbit	Cell Signaling	12747T	WB	1:1000	1:2000
Phospho-Smad3 (Ser423/425) (C25A9)	Rabbit	Cell Signaling	12747T	WB	1:1000	1:2000
SNAIL (C15D3)	Rabbit	Cell Signaling	3879S	WB	1:1000	1:2000
STAT1 (D1IK9Y)	Rabbit	Cell Signaling	14994	WB	1:1000	1:2000
P-STAT1 (Tyr701) (D4A7)	Rabbit	Cell Signaling	7649	WB	1:2000	1:2000
*P-STAT1 (S727) **(D3B7)***	Rabbit	Cell Signaling	8826	WB	1:1000	1:2000
TFII-I	Rabbit	Cell Signaling	4562	WB	1:1000	1:2000
Vimentin(D21H3)	Rabbit	Cell Signaling	5741S	WB	1:1000	1:2000

Table 3-16: List of secondary antibodies with their respective application

Secondary Antibody	*Host Species*	*Ordering Number/ Supplier*	*Application*
IRDye® 680LT anti-mouse IgG	Donkey	926-68022/ LI-COR Biosciences	WB
IRDye® 680LT anti-rabbit IgG	Donkey	926-68023/ LI-COR Biosciences	WB

IRDye® 800CW anti-mouse IgG	Donkey	926-32212LI-COR Biosciences	WB
IRDye® 800CW anti-Chicken	Donkey	926-32218/ LI-COR Biosciences	WB
IRDye® 800CW anti-rat IgG	Goat	926-32219/ LI-COR Biosciences	WB
IRDye® 800CW anti-rabbit IgG	Donkey	926-32213/ LI-COR Biosciences	WB
Cy3 AffiniPure anti-Rabbit IgG	Goat	111-165-045/ Jackson ImmunoResearch	IF

3.1.10. Equipment and Material for Mass-spectrometry

Table 3-17: Technical equipment for mass-spectrometric experiment

Equipment	*Application*	*Supplier*
Bioruptor® Plus	For tissue cell lysis	B01020001, Diagenode, Liège, Belgium
Agilent 1260 Infinity HPLC System	High pressure liquid chromatography	Agilent Technologies, Santa Clara, USA
XBridge C18 column 3.5 µm, 100 x 1.0 mm,	Column for HPLC	186003127, Waters, Milford, USA
Gemini C18, 4 x 2.0 mm SecurityGuard	Security Column for HPLC	AJ0-4286, Phenomenex, Torrence, USA
speed vacuum centrifuge	Concentration of HPLC liquied fractions	Concentrator Plus, Eppendorf, Hamburg
nanoAcquity UPLC system	Separation of peptide samples	Waters
nanoAcquity Symmetry C18, 5 µm, 180 µm x 20 mm	Trapping column for UPLC	186006527, Waters
nanoAcquity BEH C18, 2.5 µm, 75 µm x 250 mm	Analytical column for UPLS	186007484, Waters
Orbitrap™ Fusion™ Lumos™	Mass spectrometer	Thermo Fisher Scientific, Waltham, USA
Pico-Tip Emitter 360 µm OD x 20 µm ID; 10 µm tip	Release of peptides to mass spectrometer	FS360-20-10-D-20, New Objective, Woburn, USA

Table 3-18: Reagents and chemicals for mass-spectrometric experiment

Equipment	*Application*	*Supplier*
Cell lysis buffer	Protein extraction after deparaffinization	Selfmade: 1 M DTT, 1 M Tris-HCl pH 8.0, 20% SDS
ProteinWorks µElution SPE Clean-up Kit	Purification of peptide samples	186008304, Waters
Reconstitution buffer: 5% (v/v) acetonitrile, 0.1% (v/v) TFA in water	Reconstitution of dried peptides	00069141A8BS, Biosolve, Vaalkenswaard, Netherlands
Mobile phase A: Ammonium formate (20 mM formic acid 20 mM ammonia, pH 10).	HPLC	00069141A8BS, Biosolve 9857, Fluka Honeywell, Charlotte, USA
Mobile phase B: 100% Acetonitrile	HPLC	0001204102BS, Biosolve
Solvent A 0.1 % formic acid v/v in water	Orbitrap	4724.3, Roth, Karlsruhe, Germany
Solvent B 0.1 % formic acid v/v in acetonitrile	Orbitrap	4724.3, Roth 0001204102BS, Biosolve

Table 3-19: List of software used for mass-spectrometric data analyses

Software	*Application*	*Supplier*
Proteome Discoverer v2.0	TMT-10plex™ data processing	Thermo Fisher, Waltham, USA
Mascot v2.5.1	Peptide annotation	Matrix Science, USA
R v3.4.1	Data processing	-

3.1.11. General Laboratory Equipment

Table 3-20: List of general laboratory equipment used in this study

Equipment	*Supplier*
12-Tube magnet	Qiagen, Hilden, Germany
Agarose gel electrophoresis systems	von Keutz Labortechnik, Reiskirchen, Germany
AlphaImager™ gel documentation system	Biozym, Hessisch Oldendorf, Germany
Axiovert 25 microscope	Zeiss, Oberkochen, Germany
Bacteria incubator	Memmert, Schwabach, Germany
BIOWIZARD Silver Line safety microbiological safety cabinet	Ewald, Bad Nenndorf, Germany
CAT RM5 tube roller	Neolab, Heidelberg, Germany
CKX31 and CKX41 inverted microscope	Olympus, Hamburg, Germany
Cover glass staining dish	Glaswarenfabrik Hecht, Sondheim, Germany
Cover glass staining rack	Thomas Scientific, Swedesboro, USA
E861 and EV231 power supplies	Consort, Turnhout, Belgium
EG scale	Kern, Balingen-Frommern, Germany
Eppendorf 5424R centrifuge	Eppendorf, Hamburg, Germany
Eppendorf pipettes Research Plus	Eppendorf, Hamburg, Germany
FLUOstar Omega Microplate Reader	BMG LABTECH GmbH, Ortenberg, Germany
INCOmed CO_2 incubator	Memmert, Schwabach, Germany
Intelli-mixer overhead shaker	NeoLab, Heidelberg, Germany
IX81 inverted fluorescence microscope	Olympus, Hamburg, Germany
KS15 orbital shaker with TH15 incubation hood	Edmund Bühler, Hechingen, Germany
Megafuge 16R centrifuge	Thermo Fisher Scientific, Waltham, USA
Microwave R-208	SHARP, Hamburg, Germany
Micro 200R centrifuge	Hettich, Tuttlingen, Germany
MicroAmp, Fast Optical 96-well reaction plate	Thermo Fisher Scientific, Braunschweig, Germany
Mini PROTEAN® multi casting chamber	Bio-Rad, Munich, Germany
Mini PROTEAN® 3 Cell SDS-gel electrophoresis system	Bio-Rad, Munich, Germany
Mini Trans-Blot Cell	Bio-Rad, Munich, Germany
Mr. Frosty™ freezing container	Thermo Fisher Scientific, Waltham, USA

myFUGE Mini microcentrifuge	Biozym, Hessisch Oldendorf, Germany
NanoDrop ND-1000 spectrophotometer	Thermo Fisher Scientific, Waltham, USA
NanoZoomer slide scanner	Hamamatsu, Hersching, Germany
Neubauer counting chamber	Brand, Frankfurt, Germany
Nikon C2+ confocal microscope	Heidelberg University, Nikon Imaging Center
Nikon NiE widefield microscope	Heidelberg University, Nikon Imaging Center
Nikon DS-Ri2 color camera	Heidelberg University, Nikon Imaging Center
Odyssey Sa Infrared imaging system	LI-COR Biosciences, Bad Homburg, Germany
Orbital shaker DOS-10L	neoLab, Migge Laborbedarfsbetrieb, Heidelberg, Germany
pH210 Microprocessor pH meter	Hanna Instruments, Kehl am Rhein, Germany
PowerPac™ HC High-Current power supply	Bio-Rad, Munich, Germany
PTC-200 thermal cycler	Biozym, Hessisch Oldendorf, Germany
QuantStudio™ 5 Real-Time PCR System, 96-well	Applied Biosystems, Darmstadt, Germany
Secuflow fume hood	Waldner, Wangen, Germany
StepOnePlus™ Real-Time PCR system	Thermo Fisher Scientific, Waltham, USA
Thermomixer comfort	Eppendorf, Hamburg, Germany
Transsonic T460/H ultrasound water bath	Elma, Singen, Germany
Universal 32R centrifuge	Hettich, Tuttlingen, Germany
Ventana BenchMark ultra	Roche Diagnostics, Rotkreuz, Switzerland
Vortexer	neoLab, Heidelberg, Germany

3.1.12. SOFTWARE

Table 3-21: List of software and online tools used in this study

Software/Algorithms	*Provider*
Adobe Illustrator CS6	Adobe Systems, San José, USA
Adobe Photoshop CS5	Adobe Systems, San José, USA
Ape v2.0.47 a Plasmid Editor	www.biologylabs.utah.edu/jorgensen/wayned/ape

BioRender	https://biorender.com
c bioportal webpage	https://www.cbioportal.org/
CellSens Dimension	Olympus, Hamburg, Germany
Human Protein Atlas	https://www.proteinatlas.org
FIJI/Image J v1.46J	www.fiji.sc
GOrilla gene ontology enrichment analysis and visualization tool	http://cbl-gorilla.cs.technion.ac.il
GraphPad Prism 8	GraphPad Software, San Diego, USA
Image Studio v3.1.4	LI-COR Biosciences, Bad Homburg, Germany
miR Walk v3.0	http://mirwalk.umm.uni-heidelberg.de/search_mirnas/
NIS-Elements	Heidelberg University, Nikon Imaging Center
PROMO transcription Factor prediction	http://alggen.lsi.upc.es/cgi-bin/promo_v3/promo/promoinit.cgi?dirDB=TF_8.3
Omega v3.00 R2 and MARS	BMG Labtech, Ortenberg, Germany
QuantStudio™ Design & Analysis Software	Applied Biosystems, Darmstadt, Germany
QuPath	https://qupath.github.io/
REVIGO reduce and visualize gene ontology	http://revigo.irb.hr
R Studio v1.0.136	www.rstudio.com
Seqbuilder Pro 15	DNASTAR, Madison, USA
SnapGene Viewer	GSL Biotech, Chicago, USA
StepOne v2.3	Applied Biosystems, Darmstadt, Germany
Venny v2.1	https://bioinfogp.cnb.csic.es/tools/venny/

3.2. METHODS

3.2.1. HUMAN PATIENT MATERIAL

3.2.1.1. HUMAN CANCER AND HEALTHY TISSUES

In total, tissue of 40 gallbladder cancer samples, as well as 8 healthy gallbladder samples was available for analysis. The FFPE tissue blocks were provided by the Tissue Bank of the National Center for Tumor Diseases (NCT, Heidelberg, Germany). Samples were taken in accordance with the regulations of the NCT and the ethics committee of the University of Heidelberg. Informed consent was given by all study participants and analyses were carried out in accordance with guidelines and regulations by the Heidelberg University Hospital. All GBC patients underwent surgery in the Heidelberg University Hospital without any treatment before resection and the GBC cases were histologically confirmed by at least two experienced pathologists from the Institute of Pathology from the University Hospital. The control tissues of healthy normal gallbladder were obtained from patients who underwent a cholecystectomy because of gallstone disease, but were only included in the study if the tissue was not strongly inflamed.

3.2.1.2. MICRO-RNA MICROARRAY

Previously to the studies performed in the present dissertation, a micro-RNA microarray was performed from the tissue samples described in 3.2.1.1. Therefore, miRNA samples from micro-dissected FFPE material was extracted and the Agilent SurePrint Human miRNA Microarray with 2006 human miRNAs was used [72]. After processing and analysis using R and the limma package [97] the final miRNA expression data were obtained. All of this data have been deposited into the Gene Expression Omnibus repository (GEO, http://www.ncbi.nlm.nih.gov/geo/), with the serial accession number GSE104165.

3.2.1.3. TISSUE MICROARRAY

Tissue cores of 1 mm ∅ have been punched from the FFPE tissue blocks of healthy gallbladder and the 40 GBC samples and have been embedded into a new paraffin block by using a tissue microarrayer (TMA Grand Master fa. Sysmex, Germany). For invasive GBCs, duplicate tissue punches from different areas have been taken.

Immunohistochemistry staining was carried out with an automated immunostainer (Ventana BenchMark ultra, Roche Diagnostics, Rotkreuz, Switzerland). Firstly, the FFPE TMA blocks were cut into 3 µm thin sections, de-paraffinized and rehydrated. Heat-induced epitope retrieval was performed by using Ultra CC1 (Cell conditions solutions), followed by blocking of endogenous peroxidase. Finally the slides were incubated with rabbit anti-FHL1 antibody (Table 3-15) at a dilution of 1:100. Lastly, incubation with OptiView Universal

Linker and OptiView HRP Polymer was performed. The visualization was achieved by using DAB-Chromogen and before mounting, counterstaining with hematoxylin was carried out [72].

For evaluation of FHL1 expression in the tissue samples, a scoring system as following was used: 0=no expression, 1=weak expression, 2-3=intermediate to strong expression.

3.2.2. CELL CULTURE

3.2.2.1. CULTIVATION OF CELLS

The model cell lines of this study are adherent cell lines of human origin. Details, as well as the commercial source, can be found in Table 3-7. The cell lines originated from different tumor entities. The cell lines OZ and HuCCT-1 are intrahepatic cholangiocarcinoma (iCCA) cells, whereas TFK-1 and EGI-1 are extrahepatic cholangiocarcinoma (eCCA) cells. SNU1196 are a special form of extrahepatic CCA called hilar cholangiocarcinoma (Klatskin tumor). The cell lines SNU182, HuH7 and Hep3B are hepatocellular carcinomas and HuH1 is a hepatoma cell line. The remaining cell lines NOZ, SNU308, Mz-ChA1, TGBC-1, GB-d1 and G-415 are gallbladder cancer cell lines. Further, HEK293T cells as fast growing cell line for a subset of experiments were used. For authentication of the cells, short tandem repeat (STR) analyses were routinely performed.

NOZ and OZ were cultivated in William's E medium, supplemented with 10% fetal bovine serum (FCS) and 1% penicillin-streptomycin (100 IU/ml and 100 g/ml). SNU1196, SNU308, SNU183, TFK-1, G-415, GB-d1 and HuCCT-1, were grown in RPMI1640 + 10% FCS and 1% P/S. HuH7, HuH1, Hep3B, HEK294T, Mz-ChA1 and TGBC-1 were grown in DMEM + 10% FCS + 1% P/S. EGI-1 were cultivated in MEM + 10% FCS + 1% P/S and 2x MEM amino acids, 4mM L-glutamine and 1mM sodium pyruvate. Cultivation took place in a 37°C incubator in a 5% CO_2 atmosphere. Routine checks for mycoplasma contamination with the MycoAlert kit were performed and in case of contamination cells were discarded. Cell lines were passaged according to their respective density every 2-4 days. In order to achieve de-attachment, the cells were washed with ~5 ml PBS, 2 ml of trypsin-EDTA was added, followed by 2-15 min incubation at 37°C. A fraction of cells were afterwards transferred to new 10 cm ∅ petri dishes containing 10 ml of the corresponding growth medium. After approximately 50-60 passages, cells were discarded.

3.2.2.2. CRYO-CONSERVATION OF CELLS

To preserve cells and stable clones for long-time storage, the cells of a 10 cm ∅ petri dish were trypsinized at around 80% of confluence and pelleted at 100 g for 5 min. The pellet was resuspended in freezing medium, consisting of the respective cell culture medium, 40% FCS and 10% DMSO and transferred to cryogenic vials. The cells were slowly frozen at a cooling rate of 1°C/min with aid of a Mr. Frosty freezing

container at -80°C for the first 24h, and subsequently transferred to the vapor phase of a liquid nitrogen tank (-196°C). Cells were thawed quickly at 37°C, resuspended in 10 ml of warm growth medium and pelleted at 100 g for 5 min, thus getting rid of all DMSO remnants. Once more, the cell pellet was resuspended in 10 ml of fresh warm growth medium and transferred to a 10 cm ∅ petri dish.

3.2.2.3. Cell Seeding for Experiments

One day prior to the beginning of the experiment, different cell numbers were seeded, into different multiple well-plates. For details of seeding numbers per experiment and cell line, refer to Table 3-22. Cells were detached by use of PBS-wash and trypsinization and counted in a Neubauer Counting Chamber. The desired amount of cells was resuspended in the respective growth medium and transferred to the experiment-suited dish.

Table 3-22: Cells numbers seeded for different experiments and cell lines

Culture format	*96-well*	*24-well*	*12-well*				*6-well*		*10 cm ∅*
*Experiment**	ELISA	LRA	CF	CV	IF, PLA	CM	WB transfection /induction	qRT-PCR transfection /induction	Lentivirus, co-IP
NOZ	5,000	50,000	125	10,000	50,000	120,000	150,000	100,000	-
G-415	8,000	50,000	500	10,000	70,000	150,000	200,000	150,000	-
GB-d1	8,000	-	-	-	-	-	-	-	-
SNU308	-	-	-	-	-	-	200,000	150,000	-
HEK293T	-	-	-	-	-	-	-	-	$1.2x10^6$ $2x10^6$

* LRA, Luciferase reporter assay; CF, colony formation; CV, cell viability; IF, immunofluorescence; PLA, proximity ligation assay; CM, cell migration; WB, Western Blot; qRT-PCR, quantitative real-time PCR; Co-IP, co-immunoprecipitation

3.2.2.4. Transient Transfection of Micro-RNA Mimics

Transient overexpression of mature miRNAs was accomplished by specific micro-RNA mimics (mimic-145 and mimic-4502) or miRNA-4502 inhibitor with a final concentration of 12,5 pM. AllStars nonsense RNA served as negative control. According to the manufacturer's protocol, separate dilutions of the mimic in Opti-MEM (Mix A) and Lipofectamine RNAiMAX in Opti-MEM (Mix B) were initially prepared (see Table 3-23). After an incubation period of 5 min at room temperate (RT), both dilutions were combined and

further 5 min incubated at RT. Before addition of the transfection mix, the cells' medium was replaced with Opti-MEM serum reduced medium, followed by drop-wise administration of the transfection mix. After 4-6 hours incubation time at 37°C, the Opti-MEM/transfection mix was aspirated and replaced by an equal volume of fresh medium. After 48 hours, the cells were harvested and subjected to further analysis or experiments.

Table 3-23: Reaction mixtures for RNA-mimic transfection

	Culture format	*6-well plate*
	*Experiment**	**qRT-PCR, WB**
Mix A	*mimic-RNA [20µM]*	0,625 µl = 12,5 pmol
	Opti-MEM	ad 150 µl
MIX B	*Lipofectamine RNAiMAX*	9 µl
	Opti-MEM	Ad 150 µl
	Opti-MEM for cell coverage	2 ml

* WB, Western Blot; qRT-PCR, quantitative real-time PCR

3.2.2.5. Transient Transfection of Plasmids

To achieve transient overexpression of one or more specific target genes, plasmids containing the respective target cDNA were transfected via various transfection reagents. Due to high cell toxicity of Lipofectamine™, all cells were transfected with polyethylenimine (PEI [1 mg/ml]) at a cell confluence of 50-70%. The ratio of transfected DNA to PEI was 3:1 and for specific amounts, see Table 3-24. The transfection mixtures were prepared in the following order: 1. DNA was added; 2. Opti-MEM and 3. addition of PEI, followed by an incubation period of 15 min at room temperature. Meanwhile the medium of the cells, which were to transfected, was exchanged to fresh cell growth medium. Afterwards, the transfection mix with the DNA-polymer-complexes was added dropwise to the cells. The cells were harvested 48 post-transfection and subjected to further analysis or experiments. The empty vector backbone (pDEST-ctrl) without the ccdB-cassette was used as negative control.

Table 3-24: Amount and volume of DNA and PEI used for plasmid transfection

Culture format	*6-well*	*10 cm ∅*
*Experiment**	**WB, qRT-PCR**	**Co-IP**
Plasmid	2 µg	15 µg

PEI	6 µl	45 µl
Opti-MEM	150 µl	1000 µl

* qRT-PCR, quantitative real-time PCR; WB, Western blot; Co-IP, Co-immunoprecipitation

3.2.2.6. Lentiviral Transduction of Cells

3.2.2.6.1. Virus Production and Harvest

For the induction of stable gene overexpression, lentivirus-mediated integration of target genes was used. This was achieved by transfection of lentiviral plasmids of the second generation into HEK cells, which then produced virus particles efficiently. To start the experiment, $1.2x10^6$ HEK cells were plated in 10 cm ∅ cell culture dishes, which have previously been coated with PLL solution for 30 min at 37°C. The next day, cells were transfected with PEI, similarly to the details in Table 3-24, with the exception that more total DNA and hence a higher volume of PEI was used. The transfection mix consisted of 10 µg pTRIPZ-GW vector (carrying the target gene), 8 µg of psPAX2 (packaging plasmid for virus particles) and 2.5 µg of pMDG2.G (envelope plasmid), diluted in 1 ml of Opti-MEM, followed by 60 µl of PEI. Further the transfection was carried out as previously described (3.2.2.5). After 24 h at 37°C the cultivation medium was replaced by fresh medium and the cells started to produce viral particles. The virus-containing supernatants were collected at 48 h and 72 h post-transfection. The supernatants were filtered by a 0.45 µM Millex-HA filters and the virus suspensions were either stored for short-term at 4°C or long-term at -20°C.

3.2.2.6.2. Viral Infection of Cells

To integrate the target gene and achieve inducible stable overexpression in the cancer cell lines, NOZ, G-415 and SNU308 were infected with the lentiviral particles in the supernatant. The cells were seeded in 10 cm ∅ petri dishes and infected at 50-80% confluence. Efficient transfection was performed by incubating the cells with 5 ml of their respective cultivation medium, together with 5 ml of the virus containing medium (DMEM) and 8 µg/ml of polybrene. After 24 h, the virus-containing medium was aspirated, the cells were washed twice with PBS and the regular cultivation medium was administrated. After further 24 h (48 h post-transfection), the cells were selected for stable plasmid integration by addition of 1 µg/ml of puromycin, which was from now on added to the cultivation medium at every cell passage.

3.2.2.6.3. Gene Induction by Doxycycline

To induce the overexpression of the target genes FHL1, N1ICD or N3ICD, doxycycline was given to the cells. The doxycycline was previously dissolved in ultra-pure sterile water and a stock solution of 2 mg/ml was prepared. The stock solution of 2 mg/ml was used without dilution to achieve gene induction without intrinsic toxicity by doxycycline for most of the induction experiments, except for the colony formation

experiments. Here, only 1 mg/ml was used to induce gene expression. As negative controls, either cells without the addition of DOX were used or cells with inducible expression of ALB (serum albumin).

3.2.3. Methods of Molecular Biology

3.2.3.1. Micro-RNA Experiments

3.2.3.1.1. Micro-RNA Isolation by TRIzol

Fresh cells from 6-well plates were washed twice with PBS and then resuspended in 1 ml TRIzol in 6-well plate and then transferred to 1.5 ml Eppendorf reaction tube, inverted and vortexed. Frozen cells (from -80°C or N_2(l) were directly resuspended in 1ml TRIzol. For cell lysis, the tubes were incubated 5 min at room temperature (RT). Then, 200 µl of chloroform isoamyl alcohol was added, the tubes were inverted and vortexed. After further 2 min incubation at RT, the tubes were centrifuged at 12,000 g for 15 min at 4°C to separate the RNA and DNA + proteins phases from each other. The total RNA is in the topmost phase and approx. 80% of this phase was carefully transferred by pipetting to a new Eppendorf reaction tube. Then, 500 µl of 100% isopropanol was added to precipitate the RNA. Hence, tubes were mixed and vortexed thoroughly. After 10 min of incubation at RT, the tubes were centrifuged at 12,000 g at 4°C for 15 min. Afterwards the RNA pellet was visible at the bottom of the tubes, the supernatant was discarded carefully and the pellet was washed with 1 ml of 75% EtOH, followed by centrifugation at 7,500 g and at 4°C for 5 min. the supernatant was then carefully removed by decanting and pipetting. The pellet was dried for 15 min under the fume hood and if the pellet was not yet see-through after this time, another few minutes at 37°C was added to dry the RNA pellet completely. Once dry, the pellet was resuspended thoroughly in 30-50 µl of nuclease free water, followed by 10 min incubation at 60°C under shaking, to reassure complete dissolvement of RNA pellet. Finally, the concentration was quantified at 260 nm using the Nanodrop ND-1000 spectrophotometer.

3.2.3.1.2. Micro-RNA cDNA Synthesis

To assess endogenous miRNA-levels and for the control of efficient mimic-RNA transfection the miRNA has to be reverse-transcribed into cDNA. This was achieved by use of the miScript II RT Kit by Qiagen with a total RNA amount of 250 ng. The RNA was mixed with 2 µl of miScript HiSpec Buffer, 1 µl miScript Nucleis Mix and 1 µl of miScript Reverse Transcriptase. Two negative controls were used, one sample with H_2O instead of RNA and one sample with H_2O instead of reverse transcriptase. Amplification was carried out at 37°C for 1 h, followed by 5 min at 95°C for final denaturation.

3.2.3.1.3. MICRO-RNA QUANTITATIVE REAL-TIME PCR (QRT-PCR)

For qRT-PCR of microRNA species, the QuantiTect® SYBR® Green PCR Kit by Qiagen was used together with the miScript primer assays from Qiagen for specific miRNAs. The cDNA produced in the previous step (3.2.3.1.2) served as template for the qRT-PCR after a 1:100 dilution. As internal reference, the ubiquitous RNA from a small nucleolar RNA (SNORD48) was used. The pipetting scheme in Table 3-25 lead to master mixtures for triplicates of each sample. The cycling conditions are shown in Table 3-26 and the PCR was performed on a StepOnePlus real-time PCR device. The relative miRNA expression was calculated using the comparative ΔΔCt method [98].

Table 3-25: qRT-PCR mix for miR-level

Reagents	*Volume*
2 x QuantiTect SYBR Green Mix	25 µl
10 x Universal primer	5 µl
10 x Primer Assay	5 µl
Nuclease-free water	12 µl
cDNA (1:100)	3 µl
Total mix (3x)	50 µl
Final volume per well	13 µl

Table 3-26: Cycling conditions for qRT-PCR of miR-level and melt curve

	PCR phase	*Temperature*	*Time*	*Cycle number*
Polymerase chain reaction	Initial denaturation	95°C	15 min	1
	Denaturation	94°C	15 s	40
	Annealing	55°C	30 s	
	Extension	70°C	30 s	
Melting curve	Denaturation	95°C	15 s	1
	Annealing	60°C	60 s	1
	Dissociation	60-95°C	0.15°C/s	1
	Final denaturation	95°C	15 s	1

3.2.3.2. RNA EXPERIMENTS

3.2.3.2.1. RNA ISOLATION AND CDNA SYNTHESIS

Total RNA either from frozen cell pellets or cultured cells was extracted by using the NucleoSpin® RNA II Kit according to the manufacturer's instructions and the concentration was confirmed using the Nanodrop ND-1000 spectrophotometer.

For cDNA synthesis of mRNA, 0.5-1 µg total RNA was mixed with 1 µl of 1:2 diluted random hexamer primer (50µM, final concentration 5 µM) and nuclease-free water up to a total volume of 6.25 µl. The initial denaturation and primer annealing step was carried for 5 min at 65°C. Subsequently the reaction mixture for the reverse transcription was added. It consisted of 2 µl 5x RT reaction buffer, 1 µl of dNTPs (10 mM each, final concentration 1 mM), 0.25 µl RiboLock (RNAse inhibitor, 20 U/µl) and 0.5 µl of RevertAid H Minus Reverse Transcriptase (200 U/µl). Subsequently, the reaction took place at initial 10 min at 25°C, followed by 2 h at 42°C and terminated by heat-inactivation at 70°C for further 10 min. The original RNA samples were kept at -80°C, whereas the completed cDNA was diluted 1:50 for further analysis, or stored at -20°C.

3.2.3.2.2. QUANTITATIVE REAL-TIME PCR (QRT-PCR)

Gene expression levels of specific genes were analyzed by qRT-PCR with use of the PrimaQUANT qPCR-CYBR-Green-MasterMix-high-ROX, either on a StepOnePlus real-time PCR device or a QuantStudio™ Real-Time PCR. The cycling conditions and the reaction mixtures were identical for both devices. Details for sample preparation and thermocycling are listed in Table 3-27 and Table 3-28. Every sample was measured in duplicates. The gene specific primers can be found in Table 3-14. The internal reference gene for relative quantification was serine/arginine-rich splicing factor 4 (SRSF4). In analogy to the quantification method for miRNA level, relative mRNA expression level were calculated using the ΔΔCt method [98].

Table 3-27: qRT-PCR sample preparations

Reagents	*Volume*
2x qPCR-CYBR-Green-MasterMix-high-ROX	5 µl
Forward primer (1 µM)	0.8 µl
Reverse primer (1 µM)	0.8 µl
Nuclease-free water	1.4 µl
cDNA (1:50)	2 µl

Table 3-28: Cycling conditions of gene expression analyses and melt curve

	PCR phase	*Temperature*	*Time*	*Cycle number*
Polymerase chain reaction	Initial denaturation	95°C	10 min	1
	Denaturation	95°C	15 s	40
	Annealing/ Elongation	60°C	60 s	
Melting curve	Denaturation	95°C	15 s	1
	Annealing	60°C	60 s	1
	Dissociation	60-95°C	0.15°C/s	1
	Final denaturation	95°C	15 s	1

3.2.3.3. Gene Expression Microarray

Another prerequisite study to the experiments of the present dissertation, consisted in a gene expression microarray. Here, the two eCCA cancer cell lines TFK-1 and EGI-1 have been transiently transfected with the mimic-145 or AllStars control (see 3.2.2.4) with subsequent isolation of their RNA in three independent experiments. Quadruplicates of the RNA samples have then been subjected to Human Gene 2.0 ST Arrays from Affymetrix (High Wycombe, UK) in cooperation with the Medical Research Center of the Medical Faculty Mannheim. The analysis has been performed by Prof. Bermejo of the Medical Biometry Facility at the University of Heidelberg.

3.2.3.4. Gateway Cloning

In order to generate plasmids that can be used in virus production for stable gene integration, the Gateway cloning system was used. To succeed at gene transfer, the gene of interests must be contained in a pDONR vector (e.g. pDONR201-FHL1, see Table 3-10). To transfer the gene of interest into the final destination vector (pDEST26, pDEST26-C-FLAG or pTRIPZ-GW) the LR reaction was carried out. To achieve this, 75 ng of the pDONR-gene-of-interest-construct and 75 ng of pDEST26(-C-FLAG)/pTRIPZ-GW were incubated with 1 µl of the LR clonase II enzyme mix and TE buffer up to a final volume of 5 µl. The LR reaction was performed at 25°C overnight. To stop the reaction, 0.5 µl of proteinase K solution was added to the reaction mixture, vortexed and incubated at 37°C for 10 min.

3.2.3.5. Bacterial Transformation and Plasmid Purification

The bacteria transformation was carried out by use of a heat shock mechanism. Therefore, chemically competent Phage-Resistant One Shot™ Mach1™ *E.coli* were mixed with the entire LR clonase reaction mixture (see 3.2.3.4) and incubated on ice for 30 min. This was followed by a 45-60 second heat shock at 42°C and further 2 min incubation on ice. In case of Ampicillin resistance, the bacteria were plated on LB-Agar-Amp (50 µg/µl) afterwards. In case of Kanamycin resistance, 150 µl of SOC Outgrowth Medium was added after the heat shock, followed by incubation at 37°C and shaking for 1 hour. Only after this, the bacteria were plated on LB-Agar plates with Kanamycin (50 µg/µl). All plates were incubated at 37°C overnight to allow growth of bacterial colonies. The next day, single colonies were picked and grown in 3-5 ml of LB medium + antibiotic for a DNA-miniprep or in 150 ml for a DNA-midiprep at 30°C with shaking overnight. Glycerol stocks have been taken from every liquid bacterial culture for long-term storage. Therefore, 500 µl of bacterial culture have been mixed with 500 µl of 70% glycerol and kept at -80°C.

For extraction of plasmid DNA the NucleoSpin® Plasmid kit has been used for miniprep (for plasmid verification of subcloning) and the PureYield™ Plasmid Midiprep System kit has been used for midiprep to obtain DNA for cell transfections. The DNA isolations have been carried out according to the respective manufacturer's instructions.

3.2.3.6. Verification of Gene Sequences

To ensure correct cloning of the plasmids, two different methods of verification were performed. Initially, bacterial clones were digested with the restriction enzyme Bsp1407I. This cleaves the DNA at the att-recombination sites. For the restriction digest, 500 ng of plasmid DNA, 0.5 µl enzyme and 1 µl of 10x enzyme buffer (Tango buffer) were mixed and brought to a final volume of 10 µl with nuclease water. The mixture was incubated at the enzyme-specific duration and temperature (15 min at 37°C). The resulting DNA fragments consisting of the vector backbone and the gene of interest were separated by gel electrophoresis. This was performed as following: an appropriate amount of 6x gel loading dye (blue) was added to the restriction digested samples and separated in a 1-2 % agarose gel (1-2 grams of agarose dissolved in 100 ml of 1x TAE buffer), with GelRed™ nucleic acid stain. A 1 kb DNA ladder was used as reference. The DNA fragments were separated by applying a voltage of 120-150 V for 30-60 min. The DNA was visualized by UV light exposure using the AlphaImager™ gel documentation system. The plasmid with the correct expected band sizes were maintained and subjected to gene sequencing.

To have a final sequence determination, Sanger sequencing of the respective plasmids was performed using the suited sequencing primers (Table 3-13). The sequencing reactions were commercially carried out by Microsynth Seqlab (Göttingen, Germany). The results were analyzed using SnapGene Viewer and ApE (a plasmid editor).

3.2.4. Protein Biochemical Methods

3.2.4.1. Protein Isolation and Quantification

To extract the total protein from cell pellets, either fresh cells or cells frozen in N_2(l) have been used. The cells were resuspended in 30-200 µl of 1x Cell Lysis Buffer (10x Cell Lysis Buffer, 10x PhosStop and 100x Protease Inhibitor Mix G) and sonicated in an ultrasound water bath twice for 30 sec with cooling on ice for 60 sec in between. The cell debris was pelleted at 14,000 g for 15 min at 4°C and the supernatant cell protein lysate was transferred to a new reaction tube. The protein concentration was determined using Bradford's assay according to the manufacturer's instructions. The absorbance was measured at 595 nm using the Omega FLUOStar microplate reader. As reference for the protein concentration a bovine serum albumin (BSA) standard curve was used (0.1 mg/ml, 0.25 mg/ml, 0.5 mg/ml, 1 mg/ml, 1.2 mg/ml and 1.5 mg/ml). The samples were prepared by adjusting the protein lysates with 4x loading buffer and nuclease-free water to solutions with a final concentration of 1 µg/µl and denatured at 95°C for 8 min, before storage at -20°C.

3.2.4.2. Protein Separation and Western Immunoblotting

For further analysis, the proteins were separated according to their molecular weight by sodium dodecyl sulfate polyacrylamide gel electrophoresis (SDS-PAGE). To perform this, 25-50 µl of previously produced cell protein samples (3.2.4.1) and 5 µl of Fisher's EZ-Run™ pre-stained *Rec* protein ladder as reference were loaded onto a 8-12% Bis/Tris polyacrylamide gel. Electrophoresis was carried out at 80 V for 30 min and then at 150 V for 1.5 hours in denaturing electrophoresis buffer. Afterwards the proteins were transferred onto a nitrocellulose membrane by wet blotting for 2.5 hours at 90 V. Blocking was performed by incubating the NC membranes for 1h with 5% milk or 5% BSA in TBST at room temperature. Subsequently, the membranes were incubated with the different primary antibodies (details see Table 3-15) overnight, at 4°C, in a 50 ml falcon tube on a roll shaker. The next day, the NC membranes were washed 3x with TBST and then incubated with the IRDye secondary antibodies (Table 3-16) in blocking solution for 1 h at room temperature. Fluorescence-coupled secondary antibodies were visualized using an Odyssey Sa Infrared imaging system. Protein abundance levels were calculated using the Image Studio Software by normalizing to the internal reference protein (GAPDH or β-actin).

3.2.4.3. Co-Immunoprecipitations

For identification of protein-protein interactions, Co-immunoprecipitation (CoIP) was performed. Depending on the investigated interaction, either Dynabeads® Protein G Magnetic Beads (I) or Anti-FLAG® M2 Magnetic Beads (II) with their corresponding cell lysis buffers (Table 3-6) were used. Firstly, two 10 cm ∅ cell culture plates of HEK293T, which have been previously coated with PLL, were seeded and PEI-

transfected with HA-STAT1 and PTPRF (I) or C-terminally FLAG-tagged N1ICD, FHL1 or RBPJ and controls (II). The IPs were performed 48 hours post-transfection.

(I) CoIP with Dynabeads® Protein G Magnetic Beads: For each IP 50 µl of beads were transferred to a 2 ml reaction tube. The supernatant of the storage solution was discarded by placing the tubes in a 12-Tube magnetic rack. This led to the separation of beads and liquids. The beads were then activated with 50 µl of 50 mM glycine solution (pH 2.8) for 5 min at room temperature, followed by removal of liquids and resuspension in 200 µl of PBST with 2 µg of primary antibody against the protein, which is directly to be pulled down. The negative control was 0.5 µl of mouse or rabbit IgG1 for the bead suspension (depending on the primary antibody host species). The antibody binding to beads took place for 4 h, at 4°C while being rotated, followed by 3x washes with PBST. Cell lysates were prepared by use of the CoIP lysis buffer suitable for the Dynabeads. The cell debris was then agitated by rotating for 15 min at 4°C and centrifuged at 14,000 for 15 min at 4°C. After sufficient time of antibody-binding to beads, 1-2 mg of total protein lysate was added to IP samples/negative ctrl equalized to 1 ml total volume and the pulldown was performed at 4°C for at least 2 h while rotating. Afterwards, the beads were washed 4x with approx. 400 µl PBS. For the final elution of immunoprecipitated proteins, 20 µl of 1x protein sample buffer (dilution of the standardly used 4x protein sample buffer) was added to the beads. They were incubated for 20 min at room temperature while rotating at 500 rpm, followed by boiling at 95°C for 8 min. With the use of the magnetic rack, the protein containing supernatants were removed for further analysis by Western immunoblotting.

(II) For immunoprecipitations of protein interactions including FHL1, Anti-FLAG® M2 Magnetic Beads were used. Furthermore, for the identification of unknown protein interactions partner by subsequent mass spectrometry the IPs were also carried out with the Anti-FLAG beads. Here, 20 µl of bead suspension was used per IP and washed twice with 400 µl of TBS prior to use. Cell lysis was performed in the FLAG-CoIP lysis buffer supplemented with PhosStop and protease inhibitor mix. The cell lysates were rotated for 15 min at 4°C, sonicated twice for 30 sec in an ultrasound water bath und centrifuged at 14,000 g for 15 in at 4°C. The negative control was either no cell lysate at all or non-transfected HEK lysate. The IP took place for 1.5 hours at 4°C while rotating. Afterwards, the beads were washed 3 x with 200 µl TBST. The immunoprecipitated proteins were eluted with 2x non-denaturing sample buffer by boiling the samples for 3 min at 95°C and the protein-containing supernatant were transferred to new reaction tubes by use of the magnetic rack. If mass-spectrometry was applied, the final samples were split equally, one half was analyzed by Western immunoblotting and the other half was used for mass spectrometry.

3.2.4.4. Immunofluorescence (IF)

For visualization of protein abundance and cellular localization *in situ,* immunofluorescence staining of FHL1 was performed. In the beginning of the experiment, glass cover slips were placed in 12-well plates and were coated with PLL for 30 min, at 37°C. After washing 2x with PBS, cells were seeded on the coverslips according to Table 3-22. After 48 hours post-transfection, the cells were washed 2x with PBS and fixed with approx. 500 µl 4%PFA/PBS for 15 min, followed by 2x washing steps with PBS. Cell membranes were then permeabilized by 0.2% Triton X-100/PBS for 7 min. After further PBS-washes, blocking by 0.5% BSA/PBST

for 30 min at room temperature was performed. Subsequently, primary incubation against FHL1 for 1.5 hours in a wet chamber at room temperature was performed as follows: a drop of antibody/blocking solution of approx. 35 µl was placed onto a strip of parafilm. The slides were placed on top with the cells facing the liquid. After this, the slides were washed with PBS 3x for 10 min, followed by Cy3-coupled anti-rabbit secondary antibody incubation (see Table 3-15 and Table 3-16) for 1 h, at room temperature in a wet chamber in the same manner as before and again washed 3x with PBS. Afterwards, cytoskeletal F-actin was stained with 35 µl CytoPainter Phalloidin-iFluor 488 Reagent (1:1000) for 30 min at room temperature After final 3x PBS-washes for 10 min each, the cells were dehydrated in 100% EtOH, air-dried and then mounted on coverslips with DAPI Fluoromount-G.

Images were taken with a Nikon C2+ confocal laser microscope at the Nikon Imaging Center, Heidelberg and subsequent picture analysis was done with Fiji software.

3.2.4.5. Proximity Ligation Assay (PLA)

In addition, proximity ligation assay which is also referred to as '*in cell* Co-IP' was performed. Briefly, the method works as following: Antibody incubation against the two potential interaction partners is carried out with antibodies that work in IF, ideally from two different species. Then, the secondary antibodies from the Duolink® PLA Kit are referred to as MINUS and PLUS probes and each one must target one primary antibody. In case of actual protein-protein interaction, the PLUS and MINUS probes are spatially close to each other, so the incubation with the connector oligos (provided in the Duolink® PLA Kit) results in formation of a complete circular oligonucleotide. This is then amplified in the 'rolling circle incubation' (subsequent Duolink® PLA) step. The now highly abundant oligonucleotides are then hybridized with the detection probes, which are coupled to red fluorophores. Finally, every red spot signal of immunofluorescence pictures is proving the protein-protein interaction.

In the special case of the present experiments, both primary antibodies FHL1 and RBPJ were raised in rabbit, so the available PLUS and MINUS probes were not suitable. This was able to be overcome, by preproducing a MINUS probe, where the antibody can be coupled irrespective of the species it originated in. Thus, a RBPJ-MINUS probe was produced. This was done with the Duolink® In Situ Probemaker MINUS one day prior to use. For this, 20 µl of conjugation buffer was mixed with 20 µl of RBPJ antibody and then added to the lyophilized MINUS probe. After mixing by pipetting, incubation took place overnight at room temperature. The next day, 2 µl of Stop Reagent was added and after 30 min at room temperature the MINUS-probe was ready to be used. The RBPJ-MINUS probe was handled in the experiment and afterwards combined with 24 µl of Storage Solution and stored at 4°C until further use.

The initial steps of the PLA experiments were similar to IF. Cells were seeded, fixed and permeabilized as before. The PLA was performed using the Duolink® In Situ assay according to the manufacturer's protocol. After cell permeabilization, the cells were blocked for 30 min with the provided blocking solution. Primary antibody incubation against FHL1 (1:100 in antibody diluent) was done simultaneously to incubation with the RBPJ-MINUS antibody-probe (1:50 in antibody diluent). The incubation was carried out for 1.5 h at room

temperature in a wet chamber similar to the mechanism described for IF. After washing steps according to the manufacturer's protocol, the coverslips were incubated with the Duolink® In Situ PLA® probe anti-rabbit PLUS (1:5 in PLA probe diluent) for 1 h a 37°C, followed by further washing steps. To detect interactions, the Duolink® In Situ Detection Kit Orange was used subsequently according to the provided instructions. After air-drying of the coverslips, they were mounted onto glass slides using the Duolink® In Situ Mounting Medium with DAPI. Immunofluorescence pictures were taken with the Nikon C2+ microscope and analyzed by using Fiji.

3.2.5. FUNCTIONAL ASSAYS

3.2.5.1. CELL VIABILITY ASSAY

To investigate the effect of FHL1 overexpression on cell viability, 10,000 cells of G-415 and NOZ with inducible expression of FHL1 or ALB have been seeded in triplicates into 12-well plates and induced with 2 µg/ml DOX on day 1 (the measurement on day 0 indicated the cell viability prior to DOX treatment). The cell viability was measured every 24 h (day 0 – day 3), 4 measurements in total. For the measurement, 500 µl of growth medium containing 10% Resazurin was added to the cells and incubated for 1 h at 37°C. Afterwards, 200 µl of every well was transferred to a 96-well plate and fluorescence was measured (λ_{ex} = 560 nm and λ_{em} = 590 nm) with the Omega FLUOstar Microplate Reader. The excess Resazurin-containing medium was aspirated, the cells were washed with PBS and normal growth medium was added until the next time point. Normalization was done with uninduced corresponding cells. As negative control, ALB-inducible cells were used.

3.2.5.2. COLONY FORMATION ASSAY

In order to investigate the clonogenic growth capacity of FHL1 or ALB-overexpression cells, triplicates of 125 NOZ cells and 500 G-415 were seeded into 6-well plates. One day post-seeding, the cells were incubated with 1 µg/ml DOX and colonies were allowed to grow for 8-10 days. Once formed, the cells were washed with PBS and stained with 0.5% crystal violet in 25% MeOH for 45 min at room temperature. Subsequently, the crystal violet staining solution was removed and the 6-well plates were thoroughly washed with ddH_2O until the staining solution was completely removed. Pictures of the plates were taken with the FluorChem M system and the area covered by colonies was counted by use of Adobe Photoshop.

3.2.5.3. Cell Migration Assay

To examine the ability of lateral cell migration after FHL1 or ALB overexpression, the wound healing assay has been performed. 120,000 NOZ and 150,000 G-415 cells were seeded in 12-well plates. As soon as the cell layer was completely confluent, cell proliferation was inhibited by treatment of the cells with 0.1 mg/ml mitomycin C for 3 h. Then, the cells were induced with 2 µg/ml of DOX for 24 h. The following day, a cell gap was created by scratching crosswise from top to bottom and right to left in the single wells using a sterile 10 µl pipette tip. The cells were washed twice with PBS and normal growth medium with/without DOX was re-added to the cells. The gap closure by directional cell migration was documented in a time-resolved manner at 4 different positions using an inverse microscope (Olympus CKX41) with a connected camera at indicated time points after scratching. The cell free area was quantified using the software Fiji.

3.2.5.4. Cell Proliferation Assays

Two different assays have been performed to measure cell proliferation. Firstly, NOZ and G-415 have been immunofluorescently stained for the proliferation marker Ki67 after FHL1-overexpression. For this, cells were grown on coverslips in 12-well plates (see 3.2.4.4 for details) and stained against Ki67. Images were taken with a Nikon C2+ confocal laser microscope at the Nikon Imaging Center, Heidelberg. Five pictures of different areas of each coverslips were taken. Evaluation was performed manually by calculating the ratio of Ki67-positive nuclei and total nuclei.

The second assay to measure proliferation in cells overexpressing FHL1, a bromo-deoxyuridine-incorporation ELISA has been performed. Here, an additional GBC cell line with stable FHL1 expression has been generated. The experiment has been performed according to manufacturer's instructions: Between 5,000 and 8,000 cells have been seeded in sextuplicates into a 96-well plate and stimulated the following day with 2 µg/ml DOX. After 48 h, the medium was aspirated and replaced by growth medium containing 1:10 BrdU (100 µl/well). After incubation for 1-2 h at 37°C, the medium was discarded and fixative solution was added for 30 at room temperature. Afterwards, blocking solution was diluted 1:10 with antibody dilution solution and replaced the fixative for 30 min at room temperature. Then, BrdU-antibody was diluted 1:250 and 50 µl per well were added for 60 min at room temperature. Finally, three washing steps were performed and 50 µl TMB substrate were given to the cells for 30 min at room temperature. To visualize the formed dye, 12.5 µl of 1M H_2SO_4 were added per well and the plate was measured in the Omega FLUOstar Microplate Reader at 450 nm. As negative control, cells have been given 0.1 mg/ml of mitomycin C to inhibit proliferation at the time of DOX stimulation.

3.2.5.5. Dual Luciferase Reporter Assay

Two different kinds of luciferase reporter assay have been performed in NOZ and G-415. (I) The first one was to prove the direct binding of microRNA-4502 to the 3'-UTR of the FHL1-mRNA. This has been done in collaboration with the University of Erlangen. Briefly, the mechanism behind the method: decreased luciferase activity was measured, when microRNA-4502 was overexpressed. Therefore, plasmids containing

the FHL1-3'-UTR coupled to luciferase expression were co-transfected with the mimic-4502 and relevant controls and only after direct binding of the mimic-4502 to the 3'-UTR, the luciferase activity was decreased.

(II) The second dual-luciferase reporter assay was performed to analyze the influence of FHL1 on endogenous N1ICD-driven transcription. The way this was measured was through the RBPJ-mediated N1ICD transcription, since NOTCH1 is not directly binding to the DNA. The DNA sequence where RBPJ binds are 'CSL-sequences'. Therefore, either pDEST-ctrl or pDEST-FHL1 have been transfected, together with Firefly Luciferase reporter vector pGL2-4xCSL-luciferase (expression of Luciferase when RBPJ-N1ICD bind to CSL) and pRL-TK (Renilla Luciferase control reporter vector). Luciferase activity was analyzed by the Dual-Luciferase Reporter Assay System according to the manufacturer's instructions. Measurements were performed using an Omega FLUOstar Microplate Reader. Renilla luciferase was used as internal transfection control and for normalization.

3.2.6. Quantitative Mass-spectrometric Analysis and multiplexing

Quantitative mass-spectrometric analyses were performed with an Orbitrap Fusion™ Lumos™ mass spectrometer. This is the state-of-the-art ion trap mass analyzer for simultaneous analysis of different samples, which are multiplexed with isobaric mass-tags. The general principle of an Orbitrap consists of injection, trapping and excitation and detection. The trapping takes place around the inner electrode where ions cycle around the electrode in elliptical trajectories. This motion is only dependent from the unique mass-to-charge rations m/z. The injected ionized peptides move with the same axial frequency but different rotational frequency around the inner electrode, so every ion creates its own specific oscillation. This oscillation creates a unique current, which can be detected by an outer electrode. Similar to Fourier-transformation-ion-cyclotron-resonance-mass-spectrometry, the m/z ratios can be calculated and hence the ions can be identified as peptides [99].

To further enhance the resolving power, as well as to realize the simultaneous measurement of different samples in shotgun proteomics, isobaric mass labeling is used. Commercially available Tandem Mass Tag Systems are often used, where you can now analyze 16 samples in parallel. In the present study a TMT-10plex™ experiment was carried out. The isobaric tags have an identical structure but contain different numbers and combinations of 13C and 15 N isotopes in the reporter. They contain amine-reactive N-hydroxysuccinimide groups and form a covalent ester bond with the free amino primary amino groups of the digested peptides.

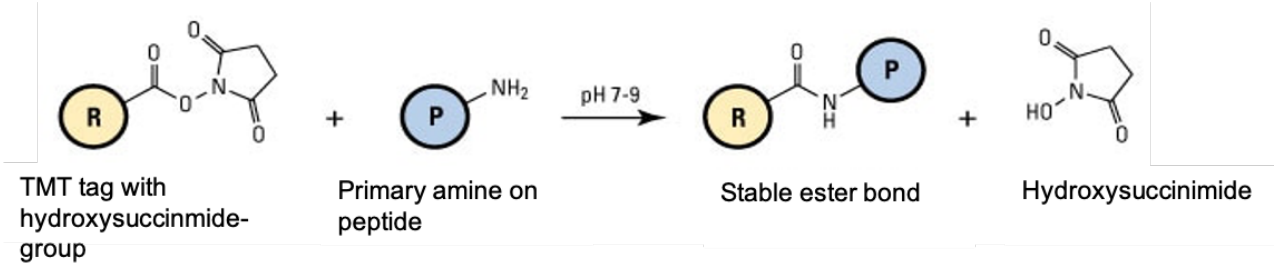

Figure 3-1: Coupling of TMT tags to peptides via formation of N-hydroxysuccinimide esters. Picture taken and modified[2].

This means, each sample was incubated with only one specific tag and afterwards the samples were combined. Since the mass of the tags is known, later on, the peptides were able to be identified and their abundance in every sample too, so this is ultimately how the quantification was performed [100].

3.2.6.1. Sample Preparation from FFPE Blocks

In collaboration with Dr. Alessandro Ori, a successful protocol was established to isolate sufficient proteins from FFPE tissue in order to have a high proteomic resolution after mass spectrometry. In principle the extraction was performed in four steps. 1) protein extraction, 2) protein precipitation, 3) protein digestion and 4) peptide clean-up.

All tumor samples have been micro-dissected before protein extraction and only small areas of tissue (approx. 0.5 mm^3) with a very high tumor cell density have been selected from two different FFPE tissue slides (the same area from two slides) of the same patient. For healthy tissue samples, only the epithelial layer was selected. For protein extraction, the slides were deparaffinized and the area of interest was scraped and transferred to a PCR tube in protein extraction lysis buffer (Table 3-18). Very thorough cell lysis was carried out by sonicating protein lysates in a Bioruptor for 15 cycler (1 min on, 30 sec off) at room temperature followed by 1 h incubation at 99°C. This was repeated and after second heat incubation, the Bioruptor procedure was repeated for 5 cycles, if the lysate was still cloudy. Afterwards, incubation with 200 mM iodoacetamide was carried out to alkylate free cysteine residues. This was afterwards quenched by 200 mM DTT. To precipitate proteins, a 4x volume of ice-cold acetone was added and the samples were frozen at -20°C overnight.

The next day, the protein was pelleted by centrifugation at 14,000 rpm and 4°C for 30 min (further centrifugation steps were performed equally), the acetone was removed and the protein pellet was subsequently washed twice with 500 µl with ice cold acetone and centrifuged. Afterwards the reaction tube was left open, so that the excess acetone could evaporate and the protein pellet dry completely.

For protein digestion, the pellet was resuspended in 13 µl of 3 M urea (in 200 mM HEPES buffer). Then, 1 µl lysozyme C was added (stock: 0.5 µg/µl in HPLC water) and incubated for 4 h at 37°C with shaking of 1000 rpm. This was followed by addition of 13 µl milliQ H_2O. The second protein digestion step was performed

[2] https://www.thermofisher.com/de/de/home/life-science/protein-biology/protein-biology-learning-center/protein-biology-resource-library/pierce-protein-methods/amine-reactive-crosslinker-chemistry.html

by adding 1 µl of trypsin (stock 1 µg/µl in trypsin buffer) and incubation at 37°C for 16 h. Before the peptide clean up, the samples were acidified with approx. 2.5 µl of 10% TFA. The pH should be around 3, which was confirmed by the use of pH test trips.

Finally, to have the pure peptides left in the samples, a peptide clean-up with the Oasis Solid Phase Extraction Technology was performed, according to the manufacturer's instructions (Kit: ProteinWorks™ µElution SPE Clean-up). The eluted peptide samples were dried in a vacuum centrifuge at 45°C for 30-45 min) and reconstituted in reconstitution buffer. The labelling with the isobaric mass tags, also referred to as TMT-10plexing, was performed as described previously [101].

The TMT-labelled samples were subjected to high pH liquid chromatography for fractionation and were injected afterwards into the mass spectrometer.

3.2.6.2. High pH peptide Fractionation for TMT-10plex™-labelled Samples

Offline high pH reverse phase fractionation was performed using an Agilent 1260 Infinity HPLC System equipped with a binary pump, degasser, variable wavelength UV detector (set to 220 and 254 nm), peltier-cooled autosampler (set at 10 °C) and a fraction collector. The column was a Waters XBridge C18 column (3.5 µm, 100 x 1.0 mm) with a Gemini C18, 4 x 2.0 mm SecurityGuard cartridge as a guard column. The solvent system consisted of 20 mM ammonium formate (pH 10.0) as mobile phase (A) and 100% acetonitrile as mobile phase (B). The separation was accomplished at a mobile phase flow rate of 0.1 mL/min using a non-linear gradient from 95% A to 40% B in 100 min. Forty-eight fractions were collected into a microplate along with the LC separation that were subsequently pooled into 16 fractions. Pooled fractions were dried in a speed vacuum centrifuge and then stored at -80°C until LC-MS/MS analysis.

3.2.6.3. Data Acquisition and Processing for TMT-10plex™-labelled Samples

For TMT experiments, fractions were resuspended in 20 µl reconstitution buffer (ca. 2 µg/µl) and 1 µg in 2.5 µl were injected for measurement. Peptides were separated using the nanoAcquity UPLC system fitted with a trapping (nanoAcquity Symmetry C18, 5 µm, 180 µm x 20 mm) and an analytical column (nanoAcquity BEH C18, 2.5 µm, 75 µm x 250 mm). The outlet of the analytical column was coupled directly to an Orbitrap™ Fusion™ Lumos™ using the Proxeon nanospray source. The samples were loaded with a constant flow of solvent A at 5 µl/min, onto the trapping column. Trapping time was 6 min. Peptides were eluted via the analytical column at a constant flow of 0.3 µl/min, at 40 °C. During the elution step, the percentage of solvent B increased in a linear fashion from 5% to 7% in 10 min, then from 7% solvent B to 30% solvent B in a further 105 min and to 45% solvent B by 130 min. The peptides were introduced into the mass spectrometer via a Pico-Tip Emitter 360 µm OD x 20 µm ID; 10 µm tip. A spray voltage of 2.2 kV was applied. The capillary temperature was set at 300 °C. Full scan MS spectra with mass range 375-1500 m/z were acquired in profile mode in the Orbitrap™ with resolution of 60000 FWMH using the quad isolation. The RF

on the ion funnel was set to 40%. The filling time was set at maximum of 100 ms with an AGC target of 4x 10^5 ions and 1 microscan. The peptide monoisotopic precursor selection was enabled along with relaxed restrictions if too few precursors were found. The most intense ions (instrument operated for a 3 second cycle time) from the full scan MS were selected for MS2, using quadrupole isolation and a window of 1 Da. HCD was performed with collision energy of 35%. A maximum fill time of 50 ms for each precursor ion was set. MS2 data were acquired with fixed first mass of 120 m/z. The dynamic exclusion list was with a maximum retention period of 60 seconds and relative mass window of 10 ppm. The instrument was not set to inject ions for all available parallelizable time. For the MS3, the precursor selection window was set to the range 400-2000 m/z, with an exclude width of 18 m/z (high) and 5 m/z (low). The most intense fragments from the MS2 experiment were co-isolated (using Synchronus Precursor Selection = 8) and fragmented using HCD (65%). MS3 spectra were acquired in the Orbitrap™ over the mass range 100-1000 m/z and resolution set to 30000 FWHM. The maximum injection time was set to 105 ms and the instrument was set not to inject ions for all available parallelizable time. For data acquisition and processing of raw data Xcalibur v4.0 and Tune v2.1 were used.

TMT-10plex™ data were processed using Proteome Discoverer v2.0 (Thermo Fisher). Data were searched against the relevant species-specific fasta database (Uniprot database, Swissprot entry only for *homo sapiens*) using Mascot v2.5.1 with the following settings: Enzyme was set to trypsin, with up to 1 missed cleavage. MS1 mass tolerance was set to 10 ppm and MS2 to 0.5 Da. Carbamidomethyl cysteine was set as a fixed modification and oxidation of methionine as a variable. Other modifications included the TMT-10plex™ modification from the used quantification method. The quantification method was set for reporter ions quantification with HCD and MS3 (mass tolerance, 20 ppm). The false discovery rate for peptide-spectrum matches (PSMs) was set to 0.01, using Percolator [102].

Reporter ion intensity values for the peptide-spectrum matches (PSMs) were exported and processed, with procedures written in R (version 3.4.1), as described in [103]. Briefly, PSMs mapping to reverse or contaminant hits, or having a Mascot score below 15, or having reporter ion intensities below 1 x 10^3 in all the relevant TMT channels were discarded. TMT channels intensities from the retained PSMs were then $\log_2$ transformed, normalized and summarized into protein group quantities by taking the median value. At least, two unique peptides per protein were required for the identification and only those peptides with one missing value across all 10 channels were considered for quantification. Protein differential expression was evaluated using the limma package [97]. Differences in protein abundances were statistically determined using the Student's t test moderated by the empirical Bayes method. P-values were adjusted for multiple testing, using the Benjamini-Hochberg method (FDR, denoted as "adj p") [104].

3.2.7. STATISTICAL ANALYSES

Data are presented as mean + standard deviation. Statistical analyses were performed using GraphPad Prism8 or Microsoft Excel. Comparisons of statistical difference between two groups relied on the Student's t-test or the non-parametric two-tailed Mann-Whitney U test. For statistical analysis of correlations, the Spearman's rank correlation coefficient (r_S) was calculated. Overall survival was assessed by Kaplan-Mayer curves and statistically compared using the Log-Rank test. The Fisher's exact test or chi^2-test was applied to assess the significance level of contingency analyses. Significance levels with p-values <0.05 were considered as significant with the following gradation: * $p<0.05$; ** $p<0.01$ and *** $p<0.001$.

4. Results

4.1. MiR-145 and Molecular Consequences

4.1.1. MiRNA Expression Profiling in Gallbladder Cancer

In a previous study, performed by Goeppert *et al.* [72], miRNA profiling of 40 gallbladder cancer and 8 non-neoplastic gallbladder samples has been performed. There, the median survival of the respective patients was 17.2 months and the cutoff point was set to divide the patients in two groups: short- and long-surviving patients. All of the clinicopathological parameters were not correlated with patient survival. The global miRNA-profiling revealed that 608 out of 2006 miRNAs were significantly (FDR <0.001) dysregulated in gallbladder cancer compared to healthy gallbladder tissue. In order to analyze the miRNAs, which were survival-associated, only these miRNAs were selected that were significantly different between healthy and gallbladder cancer and also between short- and long-surviving patients. This led to the identification of 24 differentially expressed miRNAs, 8 downregulated miRNAs and 16 upregulated ones.

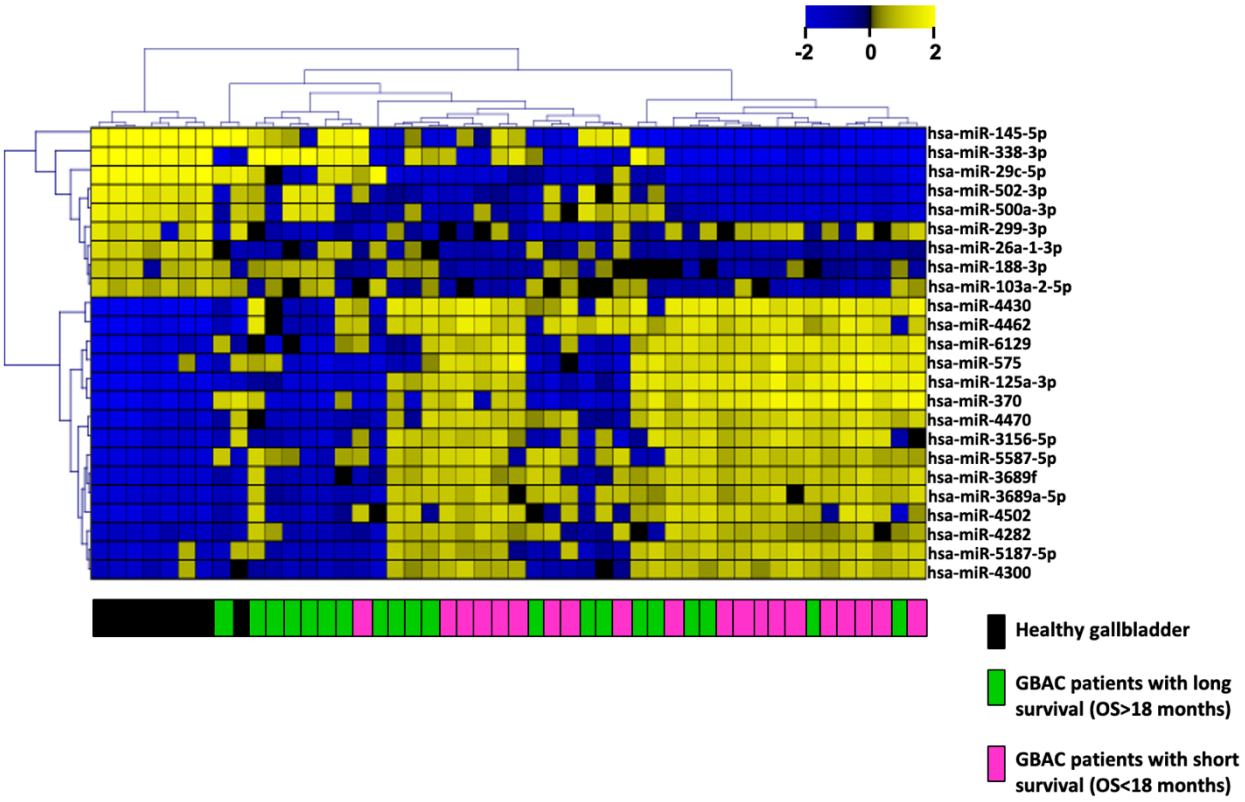

Figure 4-1: MiRNA profiling of normal and gallbladder tissues. Hierarchical clustering of 40 GBC and 8 non-neoplastic gallbladder tissues. Relative expression (log2) values are color coded between -2 and +2 in blue to yellow. Identification of healthy tissues or tissues from short or long surviving patients are shown below the heatmap.

As displayed in Figure 4-1, hierarchical clustering of the 24 miRNAs showed that healthy gallbladder tissues cluster together and GBC cases with short overall survival tend to cluster together separately from long survival patients. This suggests two molecularly distinct subgroups of gallbladder cancer patients.

Table 4-1: MiRNA microarray data. Upregulated miRNAs with positive Log2-fold change and downregulated miRNAs with negative Log2-fold change.

Probes	*Short vs. Long*	*Long vs. Normal*	*Short vs. Normal*	*Ave Expr*	*F*	*P.Value*	*adj.P.Val*
hsa-miR-575	0.573	0.841	1.415	11.069	18.141	1.51E-06	9.70E-06
hsa-miR-370	0.488	1.122	1.611	8.294	13.96	1.79E-05	8.72E-05
hsa-miR-125a-3p	0.43	1.322	1.752	10.135	24.456	5.57E-08	5.25E-07
hsa-miR-6129	0.403	0.95	1.352	7.382	24.99	4.30E-08	4.15E-07
hsa-miR-4430	0.393	2.79	3.183	11.577	103.92	7.18E-18	3.60E-15
hsa-miR-4462	0.295	1.884	2.179	9.343	98.874	1.84E-17	6.40E-15
hsa-miR-4470	0.218	0.719	0.938	7.349	28.457	8.57E-09	1.06E-07
hsa-miR-3156-5p	0.215	0.569	0.784	8.828	15.799	5.84E-06	3.20E-05
hsa-miR-4502	0.202	0.673	0.875	6.153	38.478	1.40E-10	2.78E-09
hsa-miR-299-3p	0.199	-0.541	-0.342	5.837	14.402	1.36E-05	6.81E-05
hsa-miR-3689a-5p	0.161	0.49	0.652	5.432	40.683	6.20E-11	1.34E-09
hsa-miR-5187-5p	0.144	0.29	0.434	5.438	11.374	9.55E-05	0.000391
hsa-miR-5587-5p	0.139	0.698	0.837	5.905	44.857	1.43E-11	3.58E-10
hsa-miR-4300	0.139	0.176	0.315	5.097	13.208	2.88E-05	0.000133
hsa-miR-3689f	0.104	0.623	0.727	5.767	59.311	1.63E-13	7.21E-12
hsa-miR-4282	0.101	0.279	0.38	5.268	21.721	2.19E-07	1.77E-06
hsa-miR-188-3p	-0.068	-0.099	-0.167	4.618	13.64	2.19E-05	0.000104
hsa-miR-26a-1-3p	-0.082	-0.287	-0.368	4.913	25.46	3.43E-08	3.44E-07
hsa-miR-103a-2-5p	-0.09	-0.129	-0.219	4.809	12.144	5.73E-05	0.00025
hsa-miR-500a-3p	-0.224	-0.638	-0.862	5.795	19.726	6.30E-07	4.43E-06
hsa-miR-502-3p	-0.256	-0.845	-1.101	5.661	22.394	1.55E-07	1.32E-06
hsa-miR-29c-5p	-0.405	-2.011	-2.415	6.365	53.015	1.03E-12	3.63E-11
hsa-miR-145-5p	-0.914	-4.032	-4.946	10.787	40.157	7.51E-11	1.59E-09

hsa-miR-338-3p	-1.131	-1.641	-2.772	6.684	14.058	1.68E-05	8.24E-05

Table 4-1 shows the detailed fold-changes of the individual 24 miRNAs that were significantly dysregulated in the study by Goeppert *et al*. Above the double line are the upregulated miRNAs and below are the downregulated ones. Further investigated were miR-575 and miR-370 as potentially oncogenic miRNAs, as well as miR-145-5p and miR-338-3p as potential tumor suppressors by the authors Goeppert *et al.* [72] with the outcome that miR-145-5p showed consistent and significant tumor suppressive effects in cell culture experiments, whereas miR-575 showed oncogenic effects. The other highlighted and potentially oncogenic miR-4502 was further studied later on (see chapter 4.2.2). Taken together, the miRNA profiling of 40 GBC and 8 healthy gallbladder samples revealed 24 significantly different miRNAs, which were associated with a long- and a short-surviving group of patients, thereby suggesting the identified miRNAs to be potentially of tumor suppressive or of oncogenic nature.

4.1.2. MiR-145-5p Expression leads to STAT1 Signaling

Furthermore in previous work by Goeppert *et al* [72], the effect of miR-145-5p overexpression on gene expression was investigated. Therefore, the eCCA cell line TFK-1 was transfected with AllStars negative control or miR-145-5p mimic, followed by whole genome gene expression profiling. Fifty-eight genes were identified as upregulated (adjusted p-value $p<0.05$) and 31 were found downregulated after relaxing the cut-off to an adjusted p-value of $p< 0.1$. Pathway analysis revealed that the miR-145-5p gene signature was mainly regulated by the immune modulatory transcription factor STAT1.

Table 4-2: Abbreviated list of genes upregulated, following miR-145-5p overexpression in eCCA cells.

Gene Name	***MAP***	***fold diff***	***Adj. p value***	***STAT1 target***
IFI44L	1p31.1	7.185	0.0002	
OAS2	12q24.2	6.078	0.0207	
IFITM1	11p15.5	5.776	0.0059	
MX1	21q22.3	4.363	0.0037	Yes
MT2A	16q13	3.495	0.0136	
IFI6	1p35	2.789	0.0024	
ISG15	1p36.33	2.637	0.0248	

STAT1	2q32.2	2.561	0.0071	Yes
IFITM2	11p15.5	2.498	0.0049	
IFITM4P	6p22.1	2.362	0.0024	
IFI27	14q32	2.361	0.0342	Yes
IFI44	1p31.1	2.36	0.0012	
IFI35	17q21	2.341	0.0188	Yes
PNPT1	2p15	2.25	0.0028	
LY6E	8q24.3	2.245	0.0246	
DTX3L	3q21.1	2.128	0.0116	Yes
UBE2L6	11q12	1.987	0.0312	Yes
PLSCR1	3q23	1.973	0.0101	Yes
SAMHD1	20pter-q12	1.829	0.0162	
PARP9	3q21	1.782	0.0018	Yes
USP18	22q11.21	1.71	0.023	
LAP3	4p15.32	1.703	0.0032	Yes
IFI16	1q22	1.547	0.0023	Yes
SPATS2L	2q33.1	1.54	0.0162	
IRF9	14q11.2	1.539	0.0192	Yes
HLA-E	6p21.3	1.517	0.0382	Yes

Table 4-2 shows an abbreviated list of 58 upregulated genes after miR-145-5p overexpression, of which 16 genes are direct STAT1 targets. Here, STAT1 targets are only indicated to be direct, if they have been identified by ChIP sequencing in the cervical adenocarcinoma cell line HeLa [105].

Table 4-3: Abbreviated list of genes downregulated following miR-145-5p overexpression in eCCA cells.

Gene Name	***MAP***	***fold diff***	***Adj. p value***	***Remark***
CRIP1	14q32.33	0.621	0.022	
DANCR	4q12	0.688	0.026	
TSPAN1	1p34.1	0.699	0.069	
PTPRS	19p13.3	0.708	0.034	
MUC5B	11p15.5	0.71	0.083	
ALOX5	10q11.2	0.713	0.06	

PTPRF	1p34	0.731	0.054	
ERBB3	12q13	0.737	0.061	direct miR-145-5p target
MVP	16p11.2	0.747	0.087	
SULT2B1	19q13.3	0.758	0.021	
AHNAK2	14q32.33	0.758	0.019	
CMTM4	16q21-q22.1	0.763	0.002	
ANXA4	2p13	0.769	0.058	
AHNAK	11q12.2	0.778	0.054	

Table 4-3 shows an abbreviated list of 31 genes, which are downregulated after miR-145-5p overexpression. Marked in red are two interesting candidate genes. For instance, ERBB3 has been shown to be a direct target of miR-145-5p [106]. PTPRF and PTPRS are encoding protein phosphatases, being relevant proteins for signal transduction and could be implicated in the detected dysregulated STAT1 signaling. For the comprehensive list, see supplemental material of Goeppert *et al.* [72]. Parts of the above described work was performed within the scope of a Bachelor's thesis in the group of AG Rössler. The experiments following up on the project from this, were carried out as part of the here presented doctoral studies. To sum up, the overexpression of miR-145-5p in the eCCA cell line TFK-1 led to differential expression of a multitude of genes. Many of the upregulated genes belong to the STAT1 signaling pathway and among the downregulated genes are phosphatases or previously confirmed direct miR-145-5p targets.

4.1.2.1. Upregulation of STAT1 and STAT1 Target Genes after miR-145-5p Overexpression

Below described are the first experiments, which were performed in the present study. It began with the validation of the induced STAT1 gene and protein expression. Analyzed were two eCCA (TFK-1 and EGI-1), one hepatoblastoma (HuH1) and one HCC cell line (Hep3B) and STAT1 expression was investigated after overexpression of miR-145-5p. Beforehand, qRT-PCR for the successful overexpression was performed.

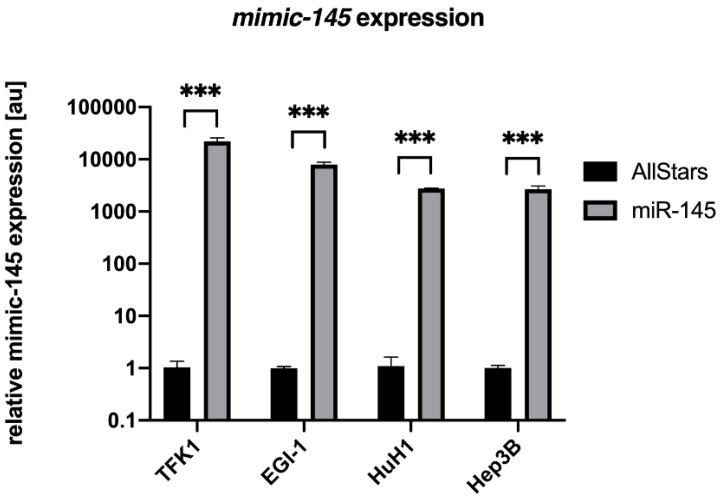

Figure 4-2: Relative miR-145-5p levels after ectopic miR-145-5p overexpression. The eCCA cell lines TFK-1 and EGI-1, as well as the hepatoblastoma and HCC cell lines HuH1 and Hep3B, were transiently transfected with a miR-145-5p mimic and mature miRNA-145-5p level were evaluated. Technical Triplicates are shown. Data was normalized to corresponding AllStars control and is presented as mean ± SD, *p<0.05, **p<0.01, ***p<0.001.

Displayed in Figure 4-2, is an exemplary analysis of mature miR-145-5p level after mimic-145-5p overexpression. The mimic-145-5p is successfully overexpressed in all cell lines to a more than 1,000-fold extent, albeit the overexpression in hepatoblastoma and HCC cell lines is a little bit reduced compared to eCCA cell lines. The overexpression of the mimic-145-5p corresponds to mature miR-145-5p levels, since the qRT-PCR is designed to target mature miRNA level. The overexpression control was routinely performed. Subsequently, the mRNA levels of *STAT1* and STAT1 target genes were investigated.

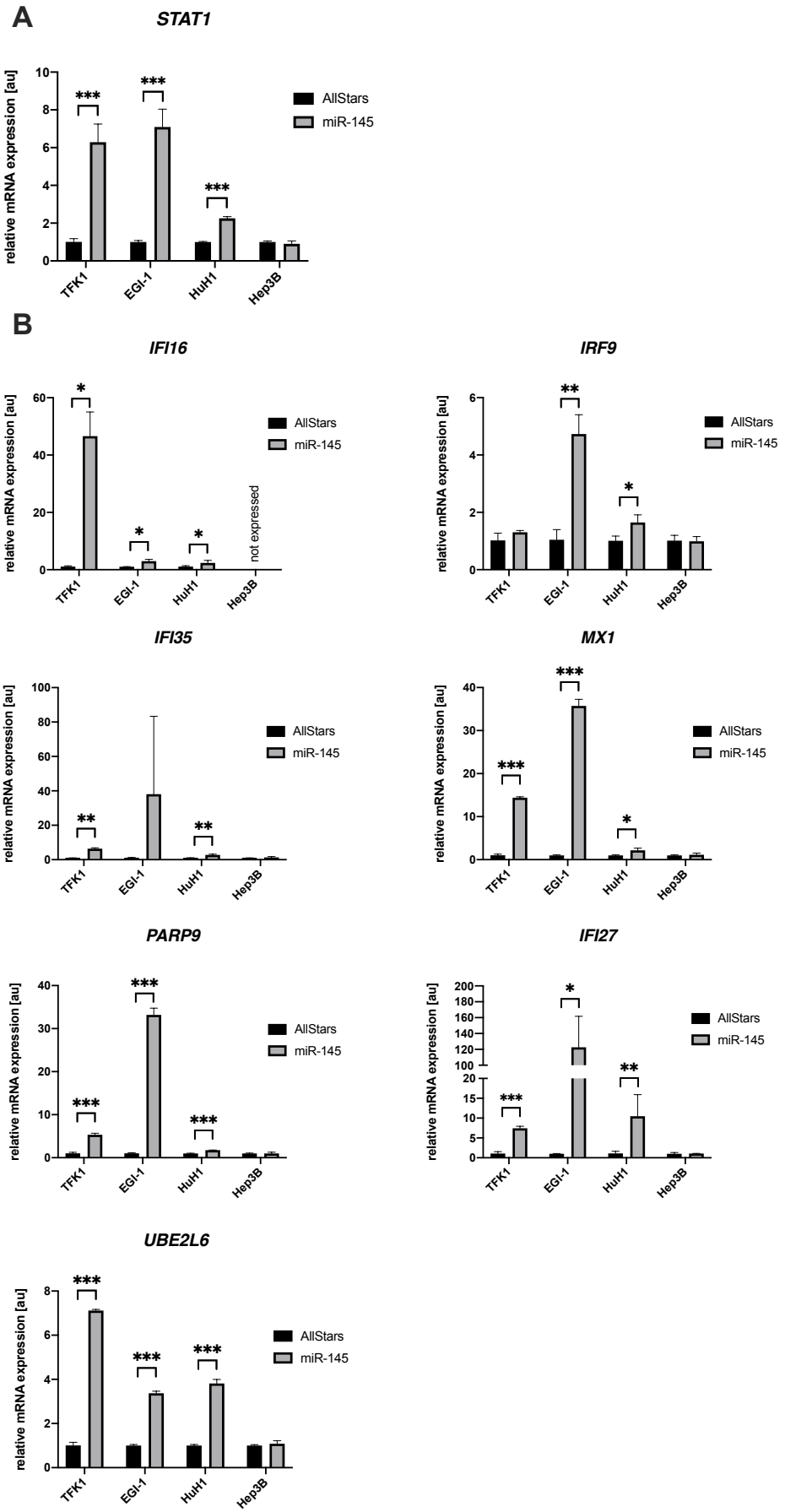
A
STAT1
relative mRNA expression [au]
AllStars
miR-145
TFK1
EGI-1
HuH1
Hep3B
B
IFI16
not expressed
IRF9
IFI35
MX1
PARP9
IFI27
UBE2L6

Figure 4-3: Gene expression analysis of eCCA and HCC cell lines after overexpression of miR-145-5p mimic. (A) *STAT1* gene expression levels are increased in eCCA and one hepatoblastoma cell line, albeit to a lesser extent. (B) Analysis of various STAT1 target genes in the same samples. STAT1 target genes were also upregulated upon miR-145-5p expression. Technical triplicates are shown. Data was normalized to corresponding AllStars control and is presented as mean ± SD, *p<0.05, **p<0.01, ***p<0.001.

As shown in Figure 4-3, overexpression of miR-145-5p leads to an increase in *STAT1* gene expression in TFK-1, EGI-1 and HuH1, albeit to a lesser extent in the hepatoblastoma cell line. No induction is observed in HCC cell line Hep3B. In addition, the expression of multiple STAT1 target genes after miR-145-5p overexpression was observed. Concomitantly with increased *STAT1* mRNA levels, STAT1 induced the expression of target genes. *IFI16* and *UBE2L6* are induced in TFK-1 more strongly than in EGI-1, but in all eCCA cells and in HuH1. *IRF9, IFI35, IFI27, MX1* and *PARP9* are also induced in all eCCA cells, however, in EGI-1 more strongly than in TFK-1, and the genes are also induced in HuH1. Generally, in the hepatoblastoma cells HuH1, the target genes were also induced but less intensely than in the eCCA cell lines. The investigated target genes are all part of the target gene list shown in Table 4-2. No biological triplicates have been performed, as there was no doubt about STAT1 activation after the following Western Blot analyses:

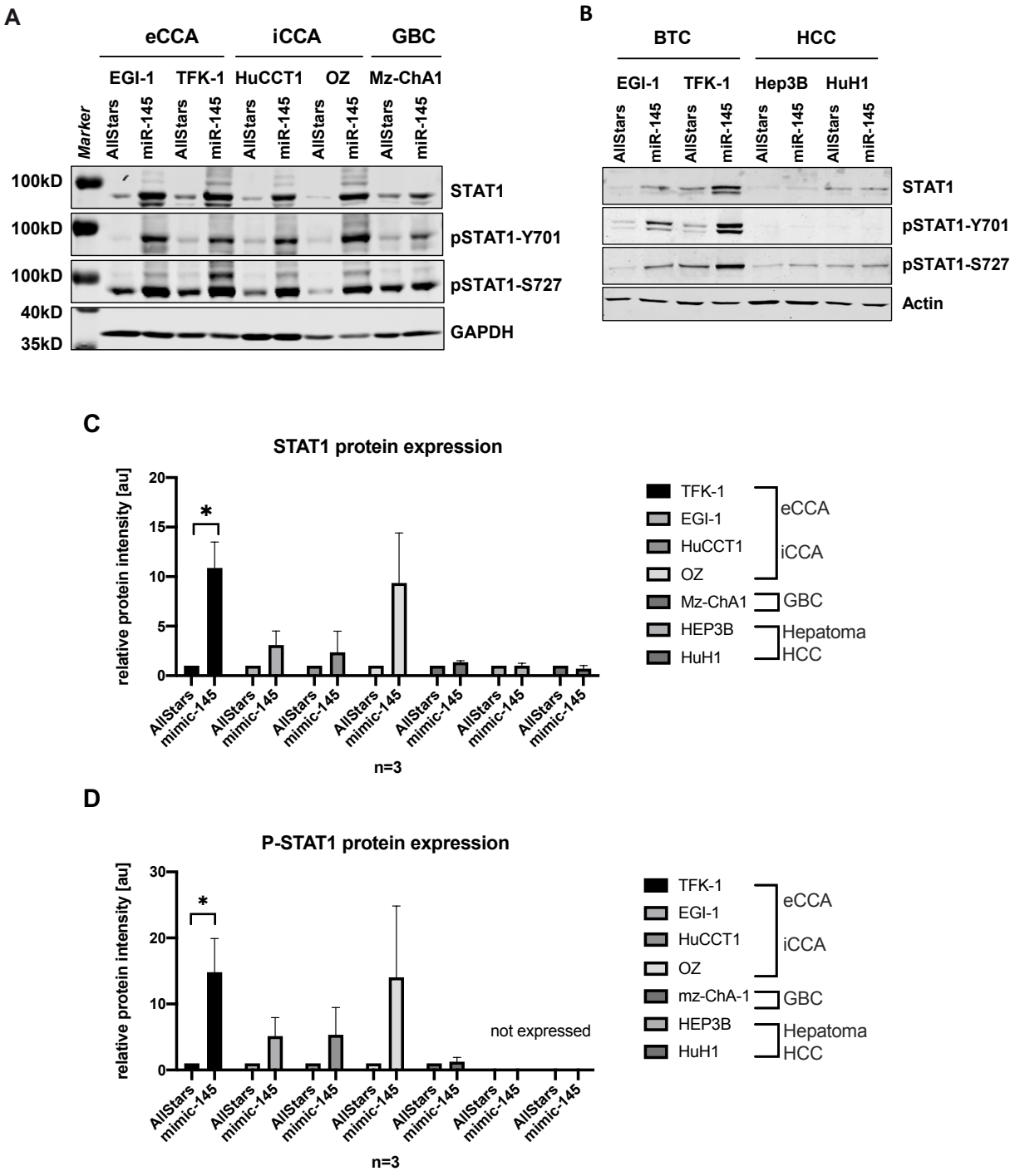

Figure 4-4: Western Blot analyses of STAT1 and P-STAT1 expression. (A) STAT1, P-STAT1 (Y701), P-STAT1 (S727) and GAPDH expression in BTC (eCCA, iCCA and GBC) cell lines. GAPDH was used as internal reference. STAT1 is upregulated and activated after miR-145-5p overexpression. (B) In contrast to CCA cell lines, STAT1 is not upregulated in hepatoma and HCC cell lines, nor activated by miR-145-5p. (C) Protein quantification of three independent experiments of STAT1 in BTC, HCC and hepatoma cell lines after miR-145-5p overexpression. There is significant upregulation of STAT1 in TFK-1 and trend of upregulation in all CCA cell lines, however, not in the GBC or HCC/hepatoma cell lines. GAPDH served as internal reference. (D) In analogy to total

STAT1 protein levels, protein levels of three independent experiments of Y701-phosphorylated STAT1 were assessed. P-STAT1(Y701) was also elevated after miR-145-5p overexpression with significant increase in TFK-1 and trend of upregulation in the other CCA cell lines. Slight activation in the GBC cell line and no expression in HCC/hepatoma cell lines. Biological triplicates are shown. Data was normalized to GAPDH protein levels and is presented as mean ± SD, *p<0.05, **p<0.01, ***p<0.001.

For investigation of STAT1 protein levels, additional cell lines have been investigated. HuCCT1 and OZ are iCCA cell lines and Mz-ChA1 is a GBC cell line. Displayed in Figure 4-4 are the protein levels of STAT1, of STAT1-tyrosine-701-phosphorylated [P-STAT1(Y701)] and of STAT1-serine-727-phosphorylated [P-STAT1(S727)], as well as GAPDH as internal reference in TFK-1 and EGI-1 (eCCA), in HuCCT1 and OZ (iCCA), Mz-ChA1 (GBC), Hep3B and HuH1 (HCC/hepatoma) cell lines. In Figure 4-4 (A) and (B) it is obvious that STAT1 protein expression was upregulated upon overexpression of miR-145-5p. The upregulation of STAT1 was most dominant in eCCA and iCCA cell lines and not so strong in BTC, whereas it was absent in hepatoma and HCC cell lines. Concomitant with the upregulation of STAT1, the activation of STAT1 was also observed, as indicated by the elevated levels of P-STAT1(Y701). Thus, miR-145-5p led to upregulation and activation of STAT1 in CCA, but not in GBC and not in HCC/hepatoma. The upregulation was not caused by different transfection efficiency of miR-145-5p, as the transfection was usually comparable and very strong (see Figure 4-2). In Figure 4-4 (C) and (D), protein levels of STAT1 and P-STAT1(Y701) of three independent experiments were quantified which confirmed the dependency of miR-145-5p overexpression (=mimic-145 in the diagram) and STAT1 induction and activation. The results were significant for TFK-1 and showed the same trend for the other CCA cell lines, but not for the GBC cell line and no P-STAT1(Y701) was at all detected in HCC/hepatoma cell lines. With the above described experiments, it could be confirmed that overexpression of miR-145-5p leads to the overexpression of STAT1 and STAT1 target genes, as well as to sustained STAT1 phosphorylation, predominantly in CCA and not in HCC. This suggests a mechanism of miR-145-5p induced signaling specific for CCA.

4.1.2.2. Downregulation of Genes after miR-145-5p Overexpression

The gene expression array described in chapter 4.1.2, led to the identification of downregulated genes after miR-145-5p overexpression, which are listed in Table 4-3. The expression of a few of these genes was investigated by qRT-PCR in CCA and GBC cell lines, as the study continued to investigate STAT1 signaling and its consequences in BTC.

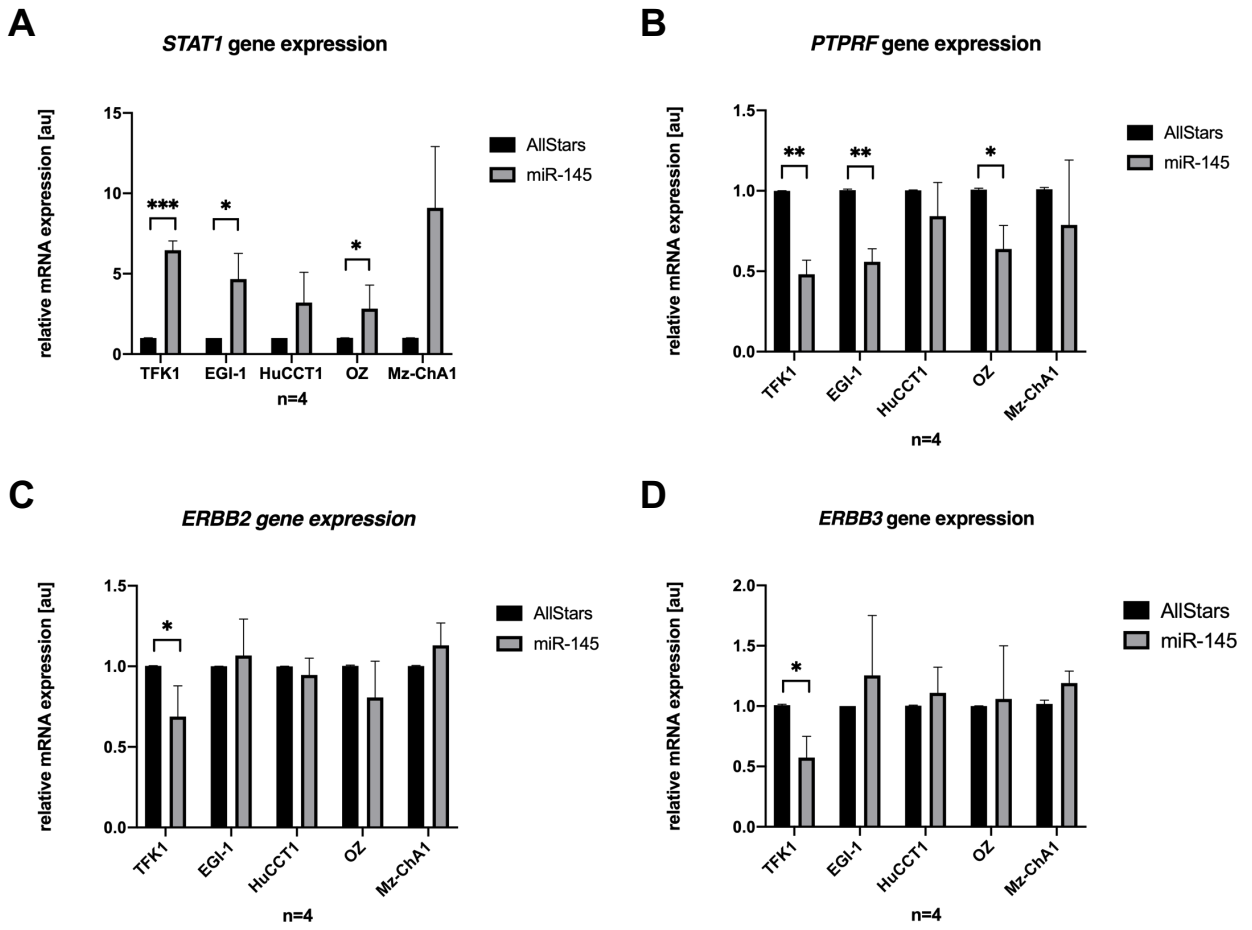

Figure 4-5: Expression of STAT1 and other genes that were downregulated in the gene expression microarray. (A) *STAT1* gene expression is significantly upregulated in TFK-1, EGI-1 and OZ cells after miR-145-5p overexpression in 4 independent biological replicates. HuCCT1 and Mz-ChA1 show the same trend. (B) *PTPRF* gene expression is significantly downregulated in TFK-1, EGI-1 and OZ in 4 independent biological replicates. HuCCT1 and Mz-ChA1 show the same trend. (C) and (D) *ERBB2* and *ERBB3* are significantly downregulated in TFK-1 in 4 independent experiments. Data was normalized to AllStars control and is presented as mean ± SD, *p<0.05, **p<0.01, ***p<0.001.

The analyses of the downregulated genes are displayed in Figure 4-5. First of all, to confirm the observations made during protein level investigation in Figure 4-4, *STAT1* mRNA levels were assessed in 4 independent biological replicates, which were significantly increased in the eCCA cell lines TFK-1 and EGI-1 and in the iCCA cell line OZ, after miR-145-5p overexpression (shown in Figure 4-5). *STAT1* mRNA level were also increased in HuCCT1 and Mz-ChA1, albeit not significantly. Interestingly, the increase in Mz-ChA1 was strong on mRNA level, but not on protein level (see Figure 4-4). The mRNA level for the protein phosphatase *PTPRF* were also significantly downregulated in the aforementioned three cell lines and show a trend of decrease among the other two, however, the standard deviation is high, so there has to be quite strong natural oscillation of PTPRF expression (B). Recent publications have shown that *ERBB3* is a direct target of miR-145-5p in a tumor suppressive context [106]. Hence, there was the expectation of seeing a clear

downregulation of mRNA levels of *ERBB3* after miR-145-5p overexpression. This was not the case [Figure 4-5 (D)], the downregulation of *ERBB3* is only significant in TFK-1, which is also the case for *ERBB2* [Figure 4-5 (C)].

Next, the protein levels for PTPRF, ERBB2 and ERBB3 were assessed. However, the protein expression of ERBB2 and ERBB3 was very low in BTC cell lines and did not give sufficient signal in Western Blot analyses, so the experiment focused on PTPRF:

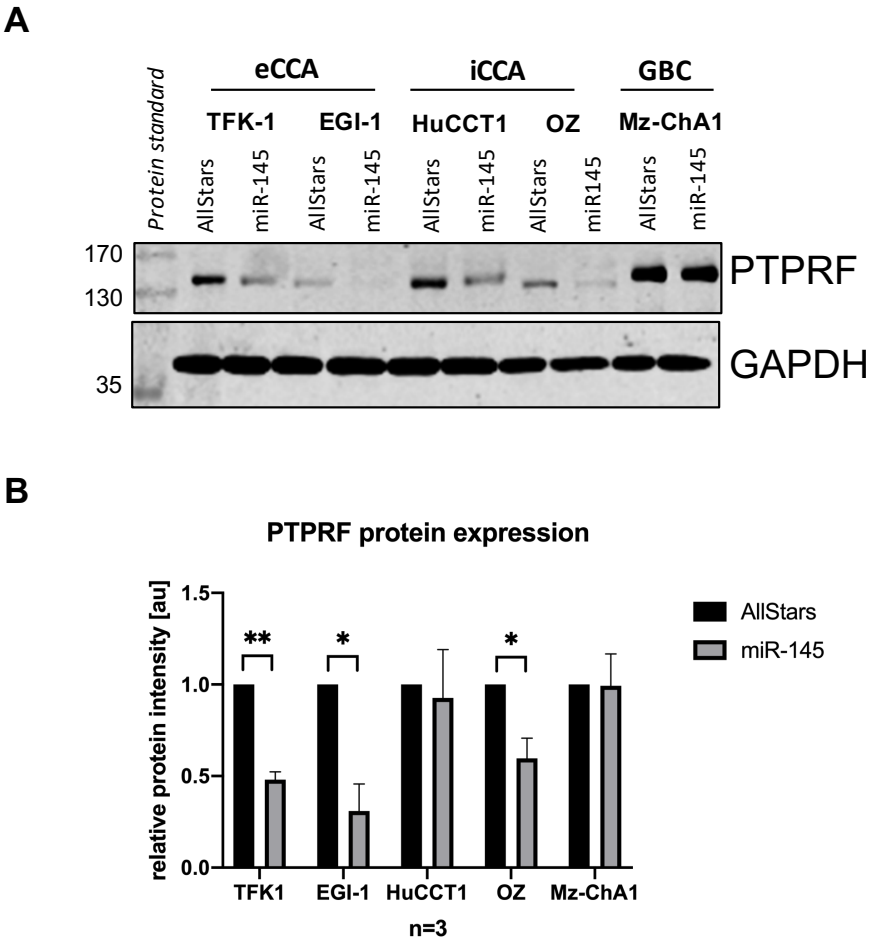

Figure 4-6: Western Blot analysis of PTPRF expression. (A) Exemplary Western Blot of PTPRF expression after miR-145-5p overexpression in BTC cell lines. GAPDH was used as internal reference. (B) Quantification of PTPRF protein level of three independent miR-145-5p overexpression experiments. Data was normalized to GAPDH protein levels and is presented as mean ± SD, *p<0.05, **p<0.01, ***p<0.001.

Figure 4-6 (A) shows an exemplary Western Blot of PTPRF expression upon miR-145-5p overexpression with GAPDH as reference. It is obvious that the protein band for PTPRF was much weaker in TFK-1, EGI-1, HuCCT1 and OZ after miR-145-5p overexpression. This was confirmed through quantification of PTPRF levels of three independent biological experiments displayed in (B), where the protein downregulation of PTPRF was significant in TFK-1, EGI-1 and OZ. The levels of PTPRF in HuCCT1 varied strongly. As shown in the exemplary Western Blot, PTPRF expression was clearly reduced after miR-145-5p overexpression, but no significant

change was observed in combined independent experiments for HuCCT1, as shown in (B). It was interesting to see that the protein level of PTPRF on Mz-ChA1 were consistent and not affected by miR-145-5p, with Mz-ChA1 being the only GBC cell line in contrast to the CCA cell lines. Accordingly, the protein induction of STAT1 was not very strong in Mz-ChA1 after miR-145-5p overexpression (Figure 4-4), supporting the link between miR-145-5p overexpression and STAT1 induction and lastly its effect on target genes. Concomitantly, it was shown that miR-145-5p overexpression lead to reduced PTPRF expression and, to some extent to reduced ERBB2 and ERBB3 expression. Again, this was predominantly observed in CCA.

4.1.3. Interaction between STAT1 and PTPRF

The interesting nature of PTPRF being a phosphatase and its observed downregulation, while STAT1 and P-STAT1(Y701) are upregulated led to the assumption that PTPRF might be able to dephosphorylate STAT1 and hence deactivate the transcription factor. This is further substantiated by the observation that in Mz-ChA1, PTPRF was not downregulated after miR-145-5p overexpression, but at the same time, this cell line showed no induction of STAT1. To prove this idea, co-immunoprecipitation has been performed after overexpression of STAT1 together with different PTPRF-constructs. Through DNA sequencing it was revealed that the commercially acquired PTPRF cDNA sequence harbored a point mutation. Position 1412 of the amino acid sequence of the commercial PTPRF constructs contained a threonine (T) residue, instead of an isoleucine residue (Figure 4-7). This residue has been re-mutated to isoleucine, which is denoted as pDEST-PTPRF, in contrast to the originally bought version PTPRF(T). In a first experiment, the original commercially bought pCMV-PTPRF(T) was used, together with the subcloned original PTPRF(T) sequence in a different vector backbone (pDEST-PTPRF(T)) and further also with the re-mutated PTPRF in pDEST-PTPRF, as shown in Figure 4-7 (A).Due to the lack of overexpression of miR-145-5p and the hereby induced STAT1 activation, a second Co-IP experiment was performed, after stimulation of the cells with IFNγ to ensure the subsequent phosphorylation of STAT1 on tyrosine-701.

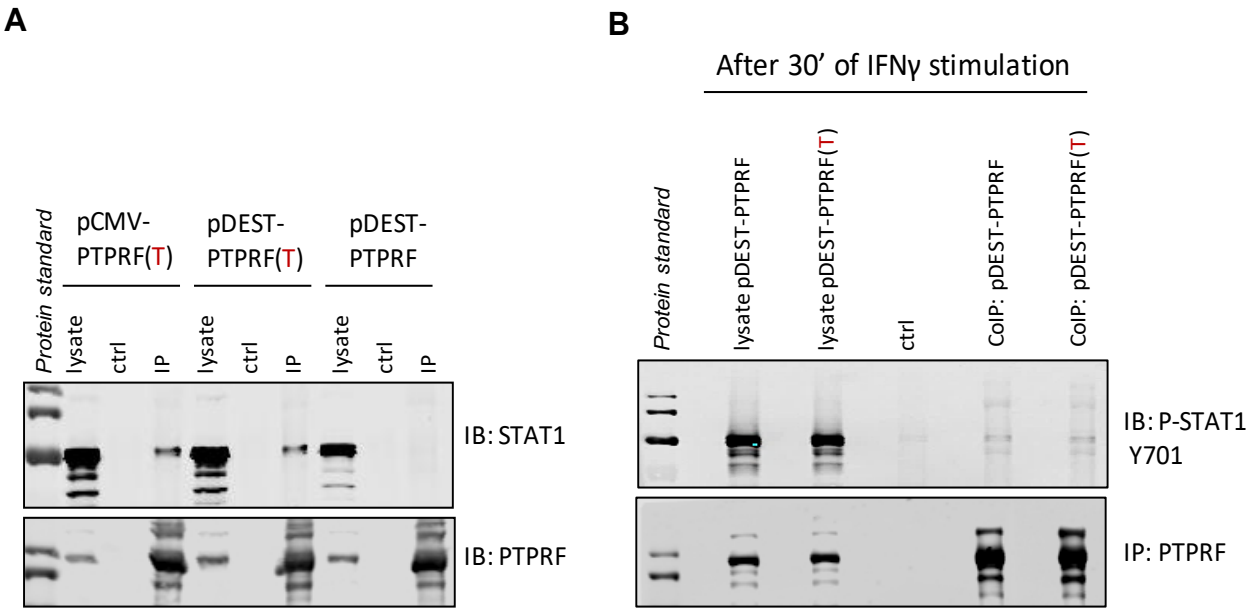

Figure 4-7: Co-Immunoprecipitations between STAT1 and PTPRF with and without stimulation by IFNγ. (A) Western Blot analyses of STAT1 (top) and PTPRF (bottom) in total lysate and after CoIP. STAT1 co-precipitates with PTPRF, containing T at position 1412, instead of the wildtype I at this position. In the right lanes of the CoIP, no STAT1-PTRPF interaction is detected. (B) Western Blot analyses of STAT1 and PTPRF after stimulation of the cells with IFNγ. STAT1 co-precipitates with PTPRF, when STAT1 signaling is activated. This is indicated by detection of P-STAT(Y701) instead of STAT1. IgG in CoIP lysis buffer were used as control samples.

Figure 4-7 shows the immunoblots of STAT1 and PTPRF. The lower blot shows PTPRF, the protein which was directly pulled down and the top blot shows STAT1, the protein potentially associated with PTPRF. In Figure 4-7 (A) the interaction without primary STAT1 induction was tested. Immunoblotted was total protein lysate, next to the IgG control and then the IP samples. In the left and middle panel, it is obvious that STAT1 was detected in the total lysate, as well as in association with PTPRF. This is true only with PTPRF that contained the non-wildtype point mutation PTPRF(T). Wildtype PTPRF did not bind to STAT1, when STAT1 was not previously activated. This may be explained, as PTPRF is a phosphatase and interaction with phosphorylated STAT1 seems to be more likely. Therefore, the association of STAT1 and PTPRF(T) was taking place in unphysiological conditions. Figure 4-7 (B) shows the protein interaction upon STAT1 activation and phosphorylation. It is obvious in the right two lanes that both the mutated PTPRF(T) as well as the wildtype PTPRF were able to bind P-STAT1(Y701). This proved that STAT1 can be bound by PTPRF and hence could likely be a subject to dephosphorylation by PTPRF. This finding concluded the studies on STAT1 pathway implications in BTC.

4.2. Proteomic profiling of Gallbladder Cancer samples

4.2.1. Mass-spectrometric Analysis of Dysregulated Proteins in Gallbladder Cancer

For the quantitative changes in the proteomes between gallbladder cancer samples and healthy gallbladder tissue, the same patient material as previously investigated in the miRNA microarray, was available. This was a very unique opportunity in order to generate in-depth analyses of the molecular changes between healthy and cancerous tissue and then to be able to integrate all of the obtained data. The innovative approach we used was capable of extracting enough protein from FFPE tissues, resulting in a strong resolution of detected proteins. Usually, FFPE tissue does not serve this purpose, but with the administered protocol, the proteomic profiling was feasible. Another advantage was the possibility, to use samples from a large cohort of German GBC samples. Due to the low incidence rates and very different global distribution, this cohort represents a rare collection of local gallbladder cancer samples.

However, due to technical limitations for the chosen proteomics approach, only ten samples were able to be analyzed in a quantitative manner at the same time. This means, 5 samples from healthy tissues, against 5 samples von gallbladder cancer patients.

In total 4,827 proteins were detected, of which 1,766 were significantly dysregulated with the cut-off being: adjusted p-value ≤ 0.05. Of these, 676 proteins were significantly downregulated and 1,090 proteins were significantly upregulated.

The identified proteins per sample led to the following correlation plots: Figure 4-8 (A) shows the similarity of proteins per sample and per group and (B) shows the diversity within the groups of identified proteins. It is not unexpected that the proteins in healthy samples were more homogenous that in the cancer samples and the correlation within this group was stronger, than in the cancer samples. In both groups, there was one exception, namely the samples “Healthy 1” and “Tumor 8”. Healthy 1 was less similar to other healthy gallbladder tissue samples and Tumor 8 was more similar to other healthy samples, mostly Healthy 1. Still, the resolution and the amount of identified proteins was strong enough to serve as basis for further investigation. The shotgun proteomics approach was successful.

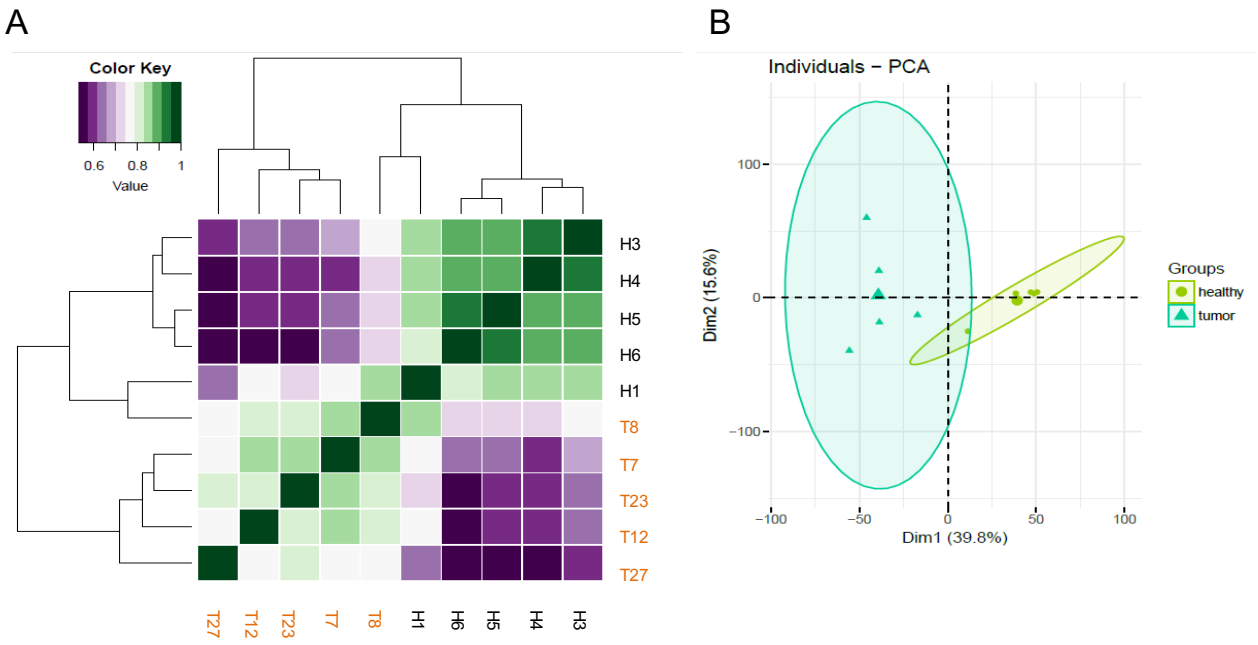

Figure 4-8: (A) and (B) Correlation plots for mass-spectrometric experiment. Healthy gallbladder samples and tumor samples are compared. The Ts stand for tumor and refer to an assigned sample number and the H stands for healthy and refers to an assigned sample number.

Next, pathway analysis for gene enrichment of up- and downregulated genes was performed, by using the web tool 'GOrilla – Gene Ontology enRIchment anaLysis and visuaLizAtion tool '[3]. This tool uses ranked lists of proteins/genes and analyzes enriched pathways represented by these proteins/genes. Further, the GOrilla tool is linked to another online tool: 'REViGO – reduce + visualize gene ontology'[4]. The REViGO tool creates tile plots, representing the dysregulated pathways, with the size of the tiles reflecting the significance of the affected gene ontology terms.

[3] http://cbl-gorilla.cs.technion.ac.il
[4] http://revigo.irb.hr

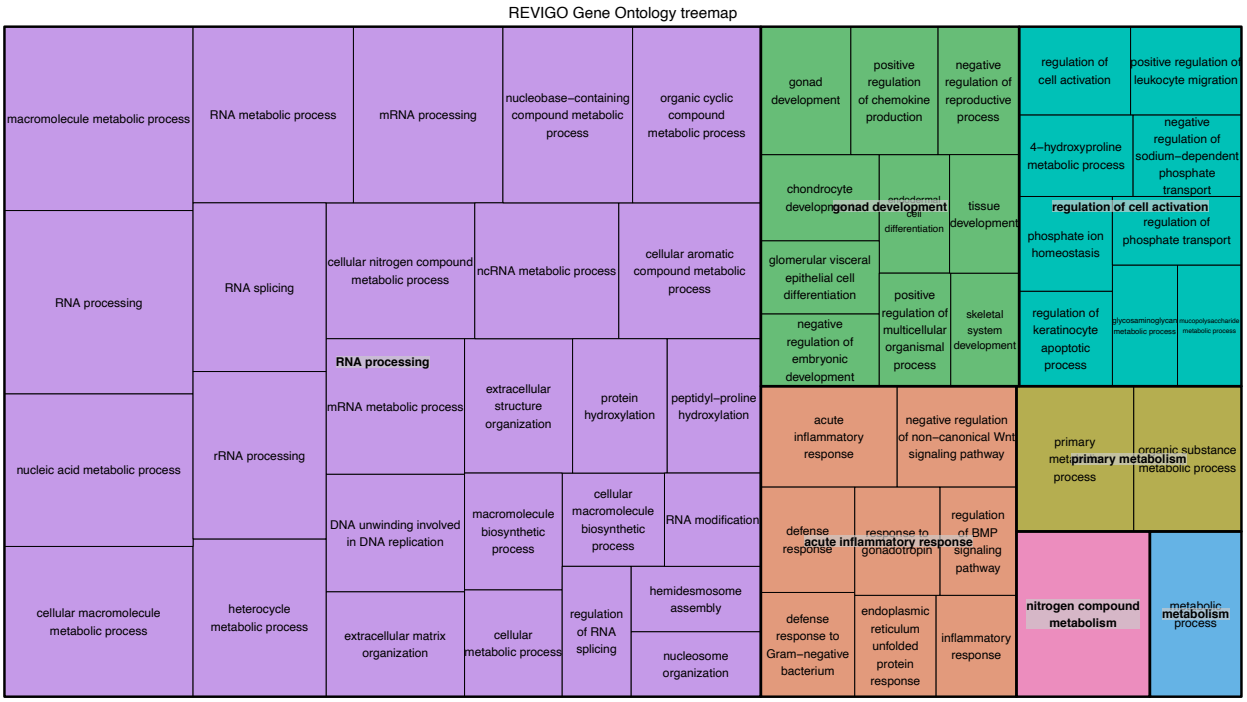

Figure 4-9: Tile plot of gene ontologies upregulated in tumor compared to healthy. The size of the tiles represents the significance.

The biggest generally upregulated GO term was RNA processing, as well as developmental and regulatory genes of cell activation. This is consecutively logical, regarding the general nature of tumor cells. Interesting to see was the upregulation of inflammatory pathways, as it is known that the immune system can either improve or worsen tumor growth, depending on the cell types invading the tissue.

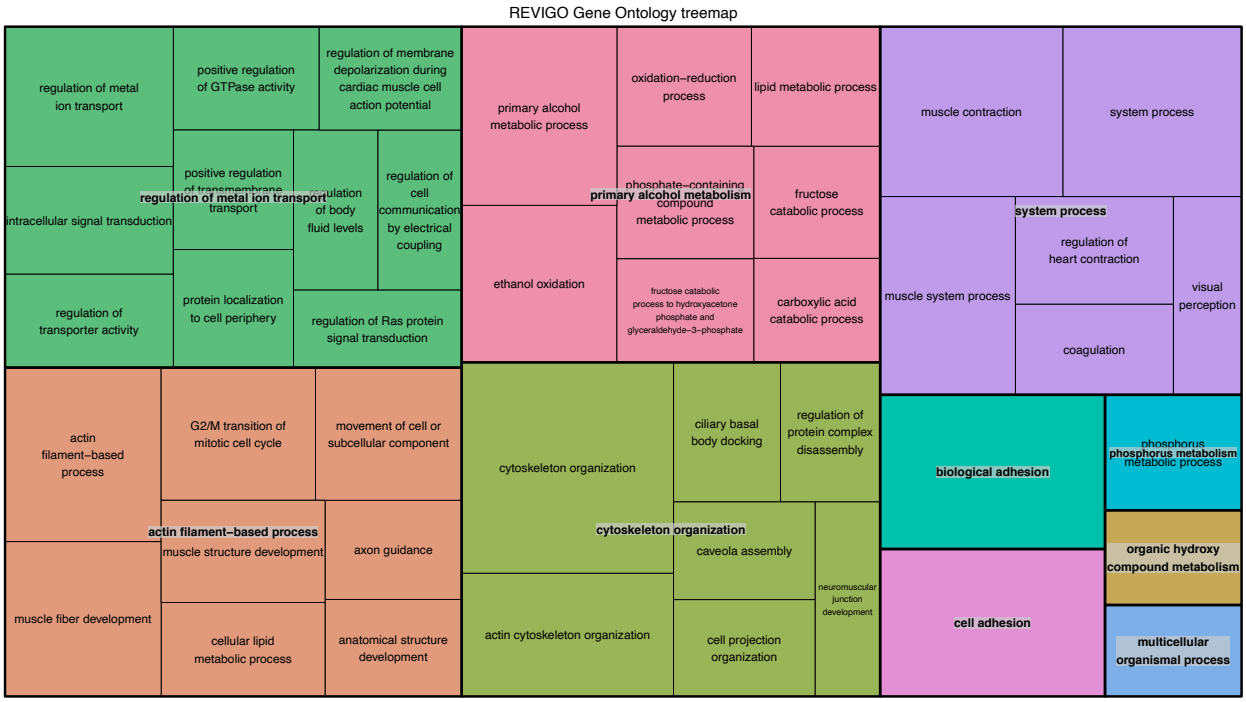

Figure 4-10: Tile plot of gene ontologies downregulated in tumor compared to healthy. The size of the tiles represents the significance.

Figure 4-10 shows the most significantly downregulated GO terms in tumor compared to healthy. The here represented terms are also rational considering what is often downregulated in tumor cells, e.g. the downregulation of controlled cell growth or cell adhesion. Within the scope of this study, we focused on downregulated proteins and hence potential tumor suppressors. In order to do so, the analysis of target proteins continued by firstly: hand-picking of interesting downregulated proteins and secondly, *in silico* determination which of the oncogenic miRs from the above described miRNA microarray (Table 4-1) could target the 'hand-picked' downregulated proteins of the proteomic data. Taken together, quantitative proteomics of 5 healthy gallbladder and 5 GBC samples revealed approximately 5,000 differentially regulated proteins. These were identified in up- and downregulated gene ontology terms, reflecting frequent dysregulated pathways in cancer.

4.2.2. Identification of the Protein FHL1 as a miRNA Target Gene

4.2.2.1. Screening of miRNA Targets that can bind to Target Genes FHL1 and ANK3

In silico analysis of target gene prediction of the individual miRNAs, has been performed by help of the online algorithm MirWalk 2.0 [107]. This analysis also included the comparison between the predictions of other common miRNA target prediction tools, such as miRanda or Targetscan. Only if at least two distinct

algorithms predicted the binding of a miRNA to a certain target gene, was the miRNA included in the study. These computer-aided investigations revealed that the potentially oncogenic miR-4502 is one miRNA with a lot of putative targets within the list of downregulated proteins. Furthermore, it was revealed by using Venn diagrams that a considerable number of predicted miR-4502 targets are downregulated at the protein level. According to MirWalk, miR-4502 has 1,603 potential target genes and as mentioned before, 676 proteins are downregulated in tumor tissue. This led to an overlap of 37 genes, among which are FHL1 and ANK3. This led to the investigation whether miR-4502 could have an influence on FHL1 protein or mRNA levels and if this was a direct effect.

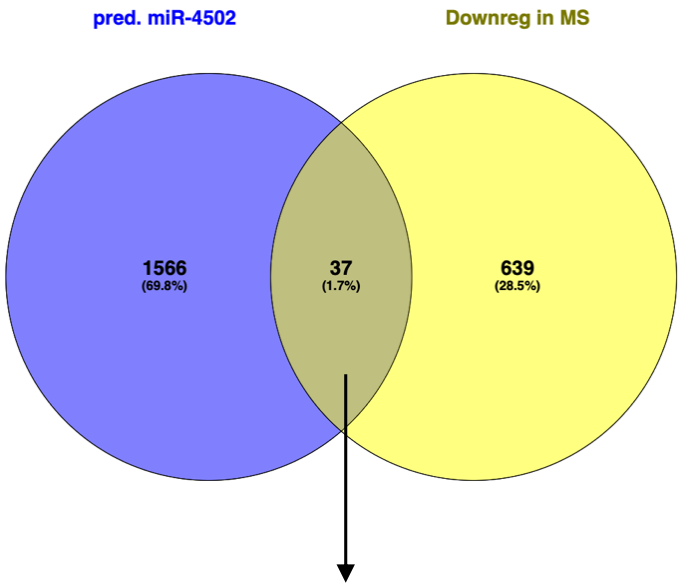

BICD2	TACO1	DDAH1	CD59
TMOD1	DCLK1	JMY	PURA
HSDL2	FARP1	LAMC1	LDB3
LPP	MARC2	RTN1	MYO6
DTNA	EXOC8	NEK9	
MYEF2	NQO1	SYNE1	
TMOD2	PDPR	PALM3	
AOC3	LARP4	SPRY4	
HSPB7	**FHL1**	SGCD	
WNT4	**ANK3**	MRVI1	
SPG21	GIPC2	PARVA	

Figure 4-11: Venn diagram of the overlap of downregulated proteins of the proteomic data and predicted target genes by MirWalk. In total, miR-4502 has 1,603 potential target genes. The proteomic data revealed 676 downregulated target genes. This led to an overlap of 37 genes, which are listed below the Venn diagram. Among them are FHL1 and ANK3.

4.2.2.2. TUMOR SUPPRESSOR FHL1 AS TARGET OF ONCOGENIC MIR-4502

As a first step for the investigation of miR-4502's impact on FHL1, a screening has been performed, where endogenous protein and mRNA levels of FHL1, as well as endogenous miR-4502 levels in various BTC cell lines, have been tested. The results are displayed in Figure 4-12.

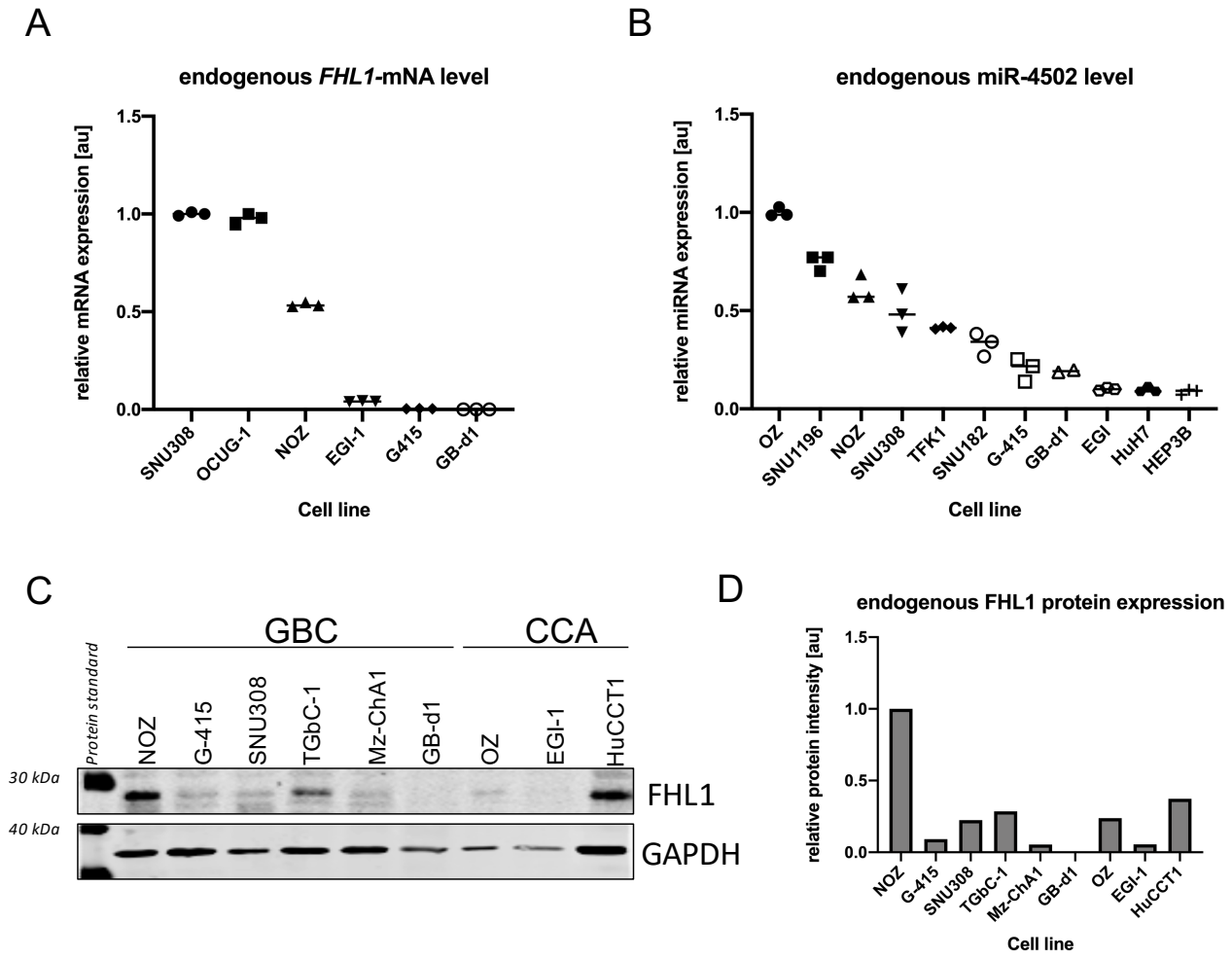

Figure 4-12: Endogenous FHL1 and miR-4502 levels. (A) Endogenous *FHL1* mRNA expression levels in GBC cell lines, relative to the cell line with the highest *FHL1* mRNA expression. (B) Endogenous miR-4502 expression levels in GBC, CCA and HCC cell lines, relative to the cell line with the highest miR-4502 expression. (C) Protein expression levels of FHL1 in GBC and CCA cell lines. (D) Quantification of FHL1 expression levels. GAPDH was used as internal reference. Normalization was performed to the cell line with the highest expression.

In diagram (A) of Figure 4-12, the endogenous *FHL1* mRNA level of GBC and CCA cells were analyzed, relative to the GBC cell line SNU308, which displayed the overall highest expression of *FHL1* mRNA. A few of these cell lines are shown with their respective protein level of FHL1 in Figure 4-12 (C). Here, SNU308 did not show the strongest expression of FHL1, in this cell line the mRNA status was not reflecting the abundance of the protein. As indicated by the mRNA levels, the protein levels of FHL1 were varying along the different cell lines. The same was true for endogenous miR-4502 level, as can be seen in (B). The iCCA cell line OZ showed the highest miR-4502 expression, followed by the HCC cell line SNU1196 and then by GBC cell line NOZ.

Here too, the endogenous expression was different in cell lines and the respective tumor entity they are derived from. For the investigation of the impact of miR-4502 on FHL1 expression, the cell lines NOZ and SNU308 have been chosen, as SNU308 showed a moderate and NOZ showed strong FHL1 expression, while having a comparable miR-4502 expression.

In the following experiments, the effect of overexpression and inhibition of miR-4502 on FHL1 level has been investigated. Also, a luciferase reporter assay was performed with help of the University of Erlangen, to prove the direct binding of miR-4502 to the 3'-UTR of *FHL1* mRNA. (A) and (B) of the following Figure 4-13 show the impact on FHL1 protein level after overexpression of miR-4502. Diagrams (C), (D) and (E) show the effect of miR-4502-inhibitor on FHL1 protein and mRNA level. Diagram (F) shows the results of the luciferase reporter assay.

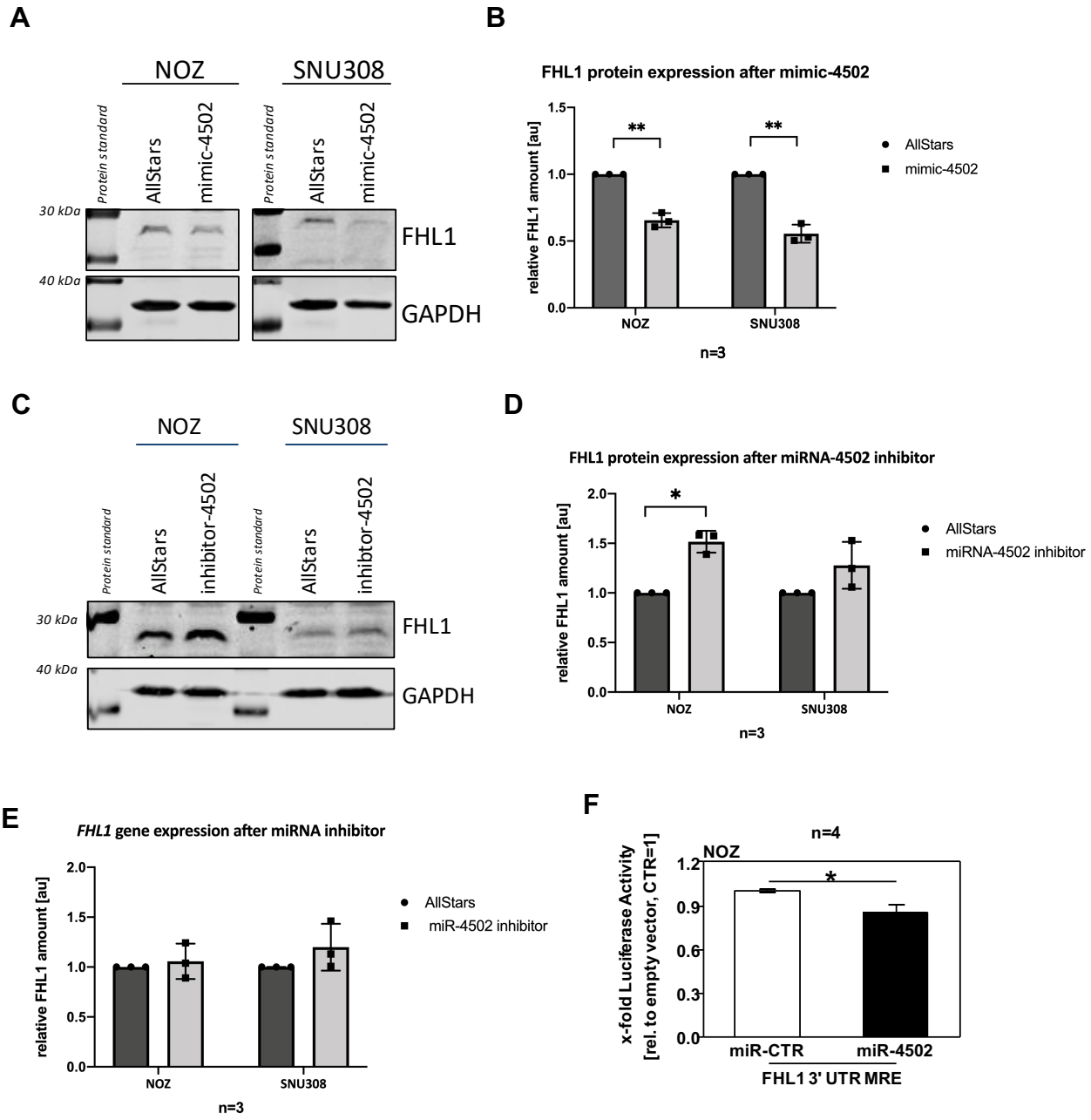

Figure 4-13: The effects of miR-4502 on FHL1 level. (A) Representative Western Blot image of FHL1 protein level after overexpression of mimic-4502 compared to Allstars control. GAPDH was used as internal reference. (B) Quantification of FHL1 protein level, relative to GAPDH after overexpression of mimic-4502 in 3 independent biological experiments. FHL1 is significantly downregulated after mimic-4502 overexpression. (C) Representative Western Blot image of FHL1 protein level after overexpression of miR-4502-inhibitor compared to Allstars control. GAPDH was used as internal reference. (D) Quantification of FHL1 protein level, relative to GAPDH after overexpression of miR-4502-inhibitor in 3 independent biological experiments with significant upregulation of the FHL1 protein level. (E) *FHL1* mRNA level after overexpression of miR-4502-inhibitor in 3 independent biological experiments. (F) Luciferase assay of NOZ overexpressing the 3'-UTR of FHL1 and mimic-4502 or control in 4 independent biological

replicates. Data was normalized to AllStars control and is presented as mean ± SD, *p<0.05, **p<0.01, ***p<0.001.

In Figure 4-13 (A) it is clearly visible that FHL1 protein levels were reduced in both the cell lines NOZ and SNU308 after overexpression of mimic-4502, compared to AllStars control. This observation is reflected in (B), where the FHL1 protein level of three independent biological experiments have been quantified and the downregulation of FHL1 was strongly significant for both cell lines. Next, the FHL1 protein levels are shown after overexpression of a miR-4502-inhibitor and the increase in FHL1 protein level is weak, but was observable, see Figure 4-13 (C). Therefore, the upregulation of FHL1 was only significant in NOZ, as shown in (D), but showed a trend for SNU308 as well. However, the diagram in (D) displays that there was no significant impact on *FHL1* mRNA levels after overexpression of the miR-4502-inhibitor, yet a trend is observable. Finally, the results of the luciferase reporter assay in (E) proved the direct binding of miR-4502 to the 3'-UTR of *FHL1* mRNA in the following manner: Cells have been co-transfected with the mimic-4502 and either an empty construct harboring the luciferase gene or with the 3'-UTR of *FHL1*, followed by the luciferase gene. The experiments showed a significant decrease in luciferase activity in 4 independent biological replicates, thereby proving the downregulation of *FHL1* gene expression after miR-4502 binding to the 3'-UTR in NOZ cells. Thus, this was the first report to show that FHL1 is a direct target of miR-4502.

4.2.3. Identification of Novel Tumor Suppressor FHL1 in Gallbladder Cancer

4.2.2.3. Screening of Downregulated Proteins

Among the most significant and strongest downregulated proteins were FHL1 and ANK3. These were particularly interesting, because they also play roles in the main downregulated GO terms. Overall and individual expression data of the proteomic analysis is displayed in the following figure:

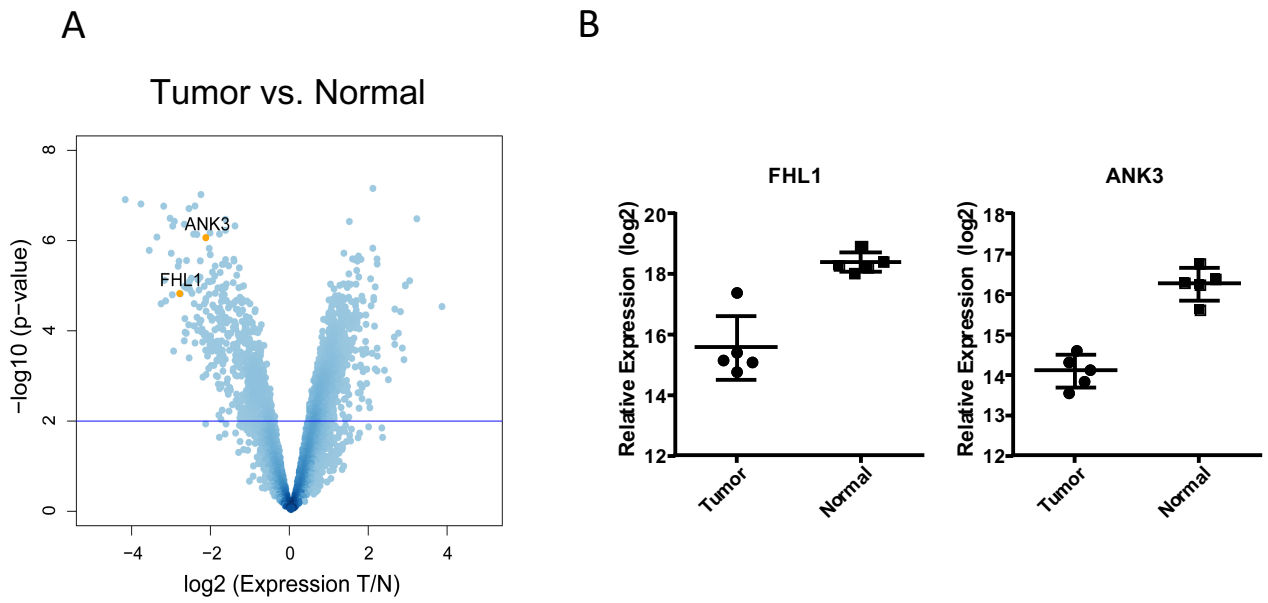

Figure 4-14: Volcano plot of differentially regulated proteins in healthy gallbladder tissue compared to gallbladder cancer and dot plots for the individual downregulation of FHL1 and ANK3. (A) Expression for all detected proteins with special attention drawn to FHL1 and ANK3. (B) Individual expression levels of FHL1 and ANK3 in each sample. After statistical analysis with the limma package in R, for FHL1 the fold difference is 8.6, p-value <0.001 and the FDR is 0.008. For ANK3 the fold difference is 4.5, p-value is <0.001 and the FDR is 0.0002.

The left side of 0 on the x-axis of the volcano plot Figure 4-14 (left), shows proteins that were downregulated in tumor tissues, whereas the right part of the diagram represents proteins, which were expressed to a higher amount in tumor tissue. All proteins above 2 on the y-axis in (A) represent significantly altered proteins. The dot plots on the right side show the individual relative expression values for the proteins FHL1 and ANK3 in the single samples between tumor tissues and normal healthy tissue. For FHL1, the fold-difference was 8.6, the p-value is <0.001 and the FDR is 0.008. For ANK3 the fold-difference was 4.5, the p-value is <0.001 and the FDR is 0.0002. This study then focused on the investigation if FHL1, since it is a smaller protein and according to the human protein atlas, it is expressed in all cellular components, which was in contrast to ANK3. The latter is localized in the plasma membrane [Figure 4-15, (A)]. In addition, ANK3 is a large transmembrane protein with multiple isoforms and no specific antibody could be obtained.

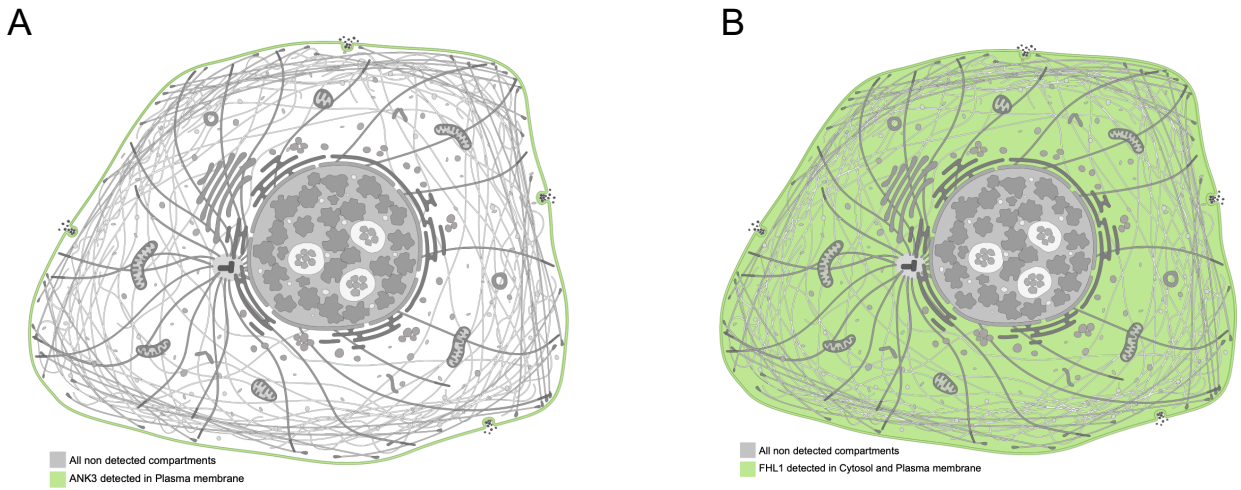

Figure 4-15: Target protein expression in the cell. (A) ANK3 expression, as assessed by the human protein atlas. ANK3 seems to be a membrane protein. **(B)** Expression of FHL1, as assessed by the human protein atlas. FHL1 seems to be a cytosolic and membrane-localized protein. Obtained and modified from the Human Protein Atlas[5].

FHL1 has been described as both a tumor suppressor and oncogene. It is downregulated in a number of different tumors, for example in lung cancer [108] and gastric cancer [109]. There is a tumor suppressive role described in HCC through signaling in a TGFβ-like manner, but independent of the cytokine. In T-cell acute lymphatic leukemia, FHL1 induces apoptosis [110] and in squamous cell carcinoma, FHL1 can induce a cell cycle arrest [111]. However, it has also been described that FHL1 can mediate chemotherapy resistance through caspase 3-regulated mechanisms in HCC [112]. Another interesting study found that FHL1 can be phosphorylated by Src and, depending on the different amino acid residues that are phosphorylated, can act as either a tumor suppressor or as an oncogene [113]. So far, this demonstrates that the clear mechanism of action by FHL1 is still not elucidated and in the context of gallbladder cancer, there is nothing known about FHL1's implications. Furthermore, analyzing Kaplan-Meier survival curves from TCGA data, the context of FHL1 in different cancer entities is controversial, as displayed in Figure 4-16 [114]. Taken together, the information about FHL1 is not unambiguous and therefore, it was decided to study this protein in the present dissertation further and to investigate its role in gallbladder cancer.

[5] https://www.proteinatlas.org

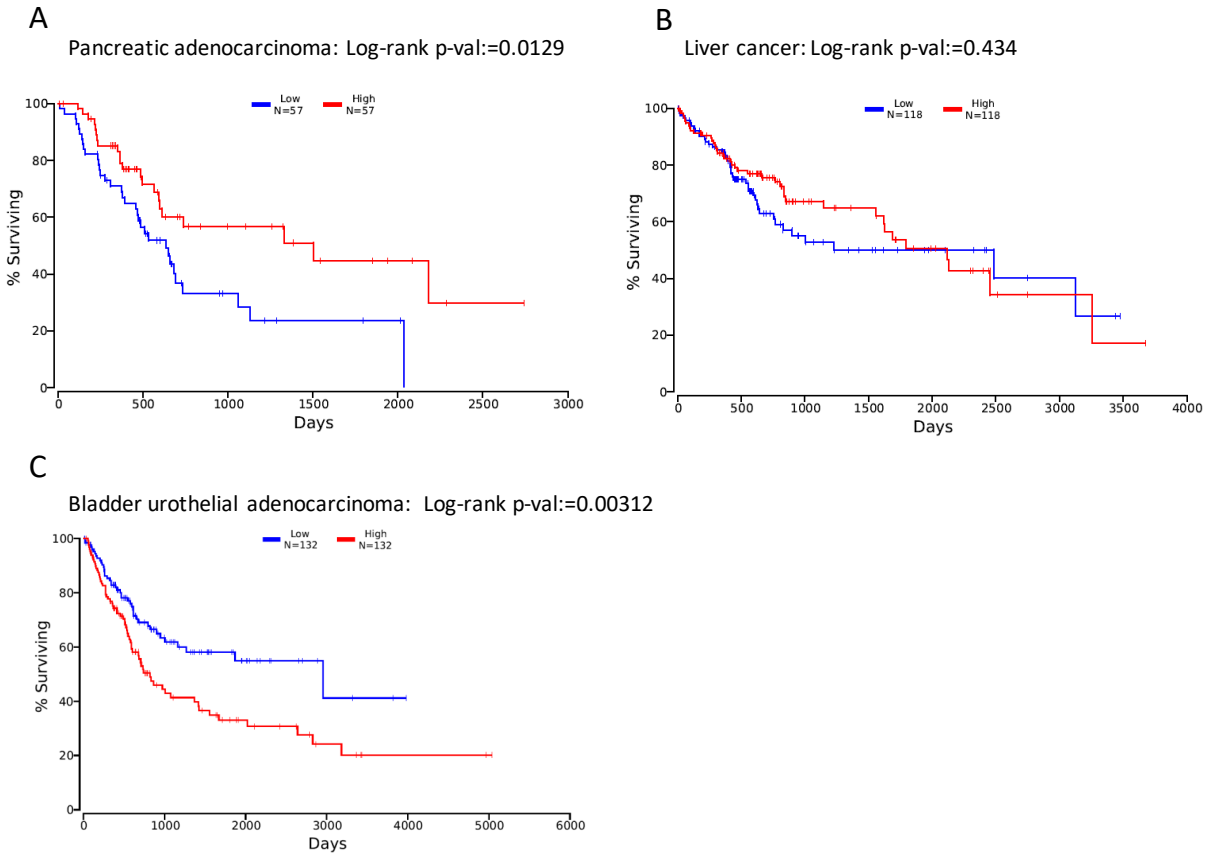

Figure 4-16: Kaplan-Meier survival curves of FHL1 expression in different cancer entities. (A) FHL1 expression in pancreatic adenocarcinoma. High FHL1 expression is favorable for overall survival. (B) FHL1 expression in liver cancer. There is no significant difference in overall survival upon FHL1 expression. (C) FHL1 in bladder urothelial adenocarcinoma, where its expression is unfavorable for overall survival. Source: RNA TCGA Data, analyzed with the help of OncoLnc[6]

4.2.2.4. FHL1 IN GALLBLADDER CANCER TISSUE MICROARRAY

Next, the expression of FHL1 protein in a GBC and healthy gallbladder tissue microarray (TMA) was investigated. After staining, the expression of FHL1 in every tissue punch was investigated by eye and assigned a score. The scores were '0=no expression', '1=weak to moderate expression' and '2-3=intermediate to strong expression'. For exemplary score distribution see Figure 4-17.

[6] http://www.oncolnc.org

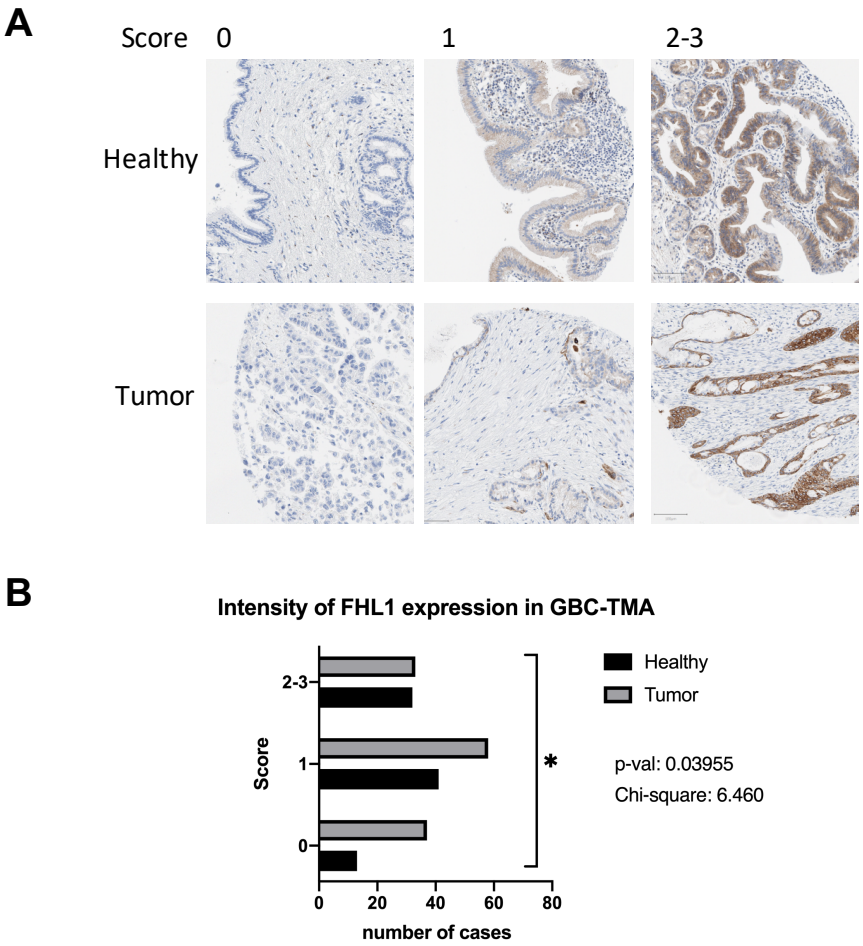

Figure 4-17: TMA of FHL1 protein expression in GBC and healthy gallbladder. (A) Exemplary expression of FHL1 matching the scores for 0 to 3 in healthy and tumor tissue. (B) Evaluation of FHL1 staining of the TMA by the chi^2-test. There was a significant difference in the expression of FHL1 in Healthy and Tumor, with a p-value of 0.03.

Figure 4-17 (A) shows how scores were rated in the tumor or healthy samples of the TMA. As FHL1 is a very abundant protein in muscle cells and therefore smooth muscle cells of blood vessels were usually stained positively, only staining in epithelial cells has been evaluated. After analyzing the score distribution in all samples by the chi^2-test, a significant difference with a p-value of 0.0395 was found between FHL1 expression in healthy and tumor tissue. Thus, FHL1 expression was more abundant in healthy tissue, which also reflects the results from the proteomics data, demonstrating that FHL1 is downregulated in tumor compared to healthy gallbladder.

4.2.3. FHL1 IN CELL SIGNALING PATHWAYS

In order to study the effects of FHL1 expression in GBC cells in different cell signaling pathways, stable inducible FHL1 expression was applied. For this purpose, the cell lines NOZ and G-415 have been selected to integrate the FHL1 gene under the control of a doxycycline (DOX) responsive promotor. The rationale to pick these two cell lines was that NOZ display high endogenous FHL1 protein expression and G-415 very low levels (see Figure 4-12). As control, either uninduced cells or cells with integrated ALB have been used.

To verify the successful induction of FHL1, Western Blot and immunofluorescence staining have been used.

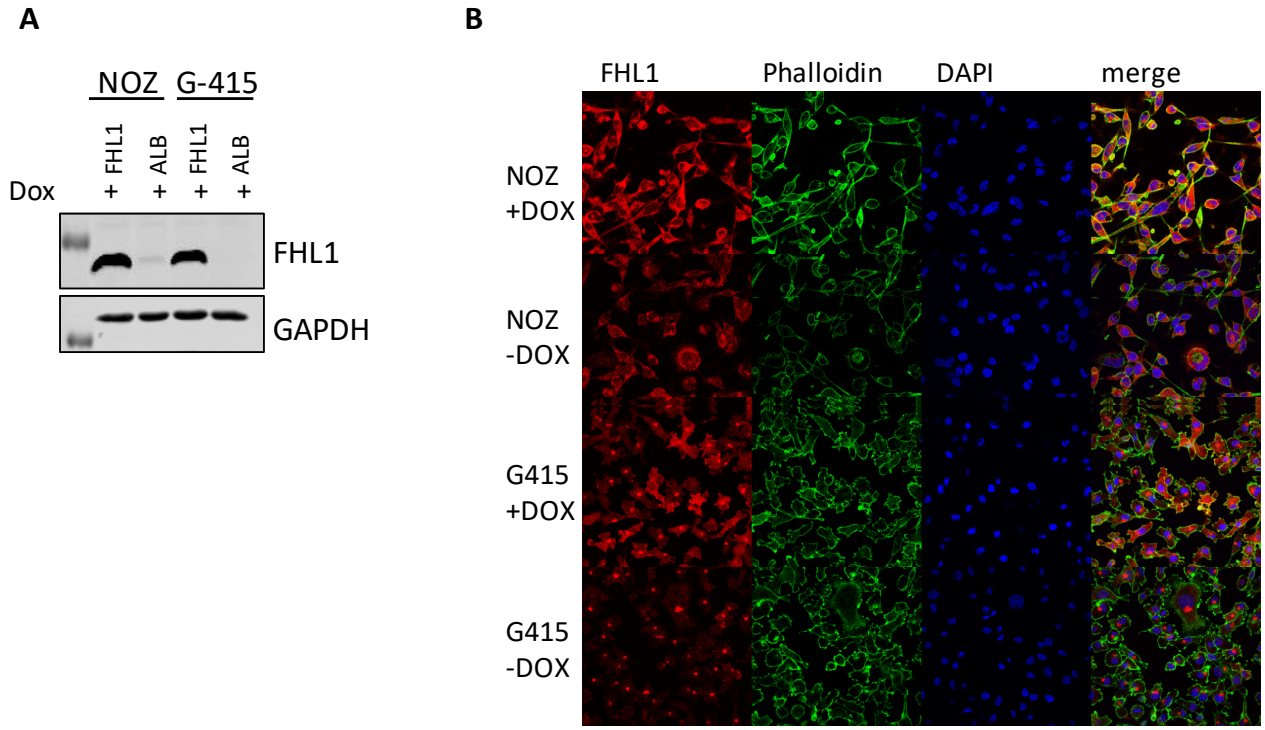

Figure 4-18: Induction of FHL1 expression by doxycycline in NOZ and G-415.(A) Western Blot analysis of FHL1 after DOX addition in NOZ and G-415, with stable integration of either FHL1 or ALB. GAPDH used as internal Reference **(B)** Confocal immunofluorescence microscope pictures of FHL1 expression with and without DOX addition in G-415 and NOZ cells. Phalloidin was used as an actin skeleton marker.

Figure 4-18 (A) shows the successful induction of FHL1 in contrast to ALB after administration of DOX to NOZ and G-415. The earlier observed different basal expression level of FHL1 are also reflected here, with NOZ having a higher FHL1 expression in the ALB+ cells, than G-415. GAPHD served as equal protein amounts loading control. In (B), FHL1 expression with or without DOX and its cellular location was analyzed by immunofluorescence staining. Here too, NOZ showed a higher general FHL1 expression than G-415. Interestingly, G-415 displayed a perinuclear localization of FHL1, especially without forced overexpression,

whereas it was broadly distributed in NOZ cells, including nuclear localization. After the overexpression of FHL1 by DOX induction was confirmed, functional experiments were conducted.

4.2.3.1. FHL1 IN EPITHELIAL-MESENCHYMAL TRANSITION

The literature reported that FHL1 is involved in EMT in a breast cancer adenocarcinoma cell line [115]. Therefore, it was of interest to see, if FHL1 showed an impact on EMT genes and proteins in GBC cells, which could also have been reflected in the downregulated GO terms “actin skeleton organization” and “cell adhesion” (refer to Figure 4-10).

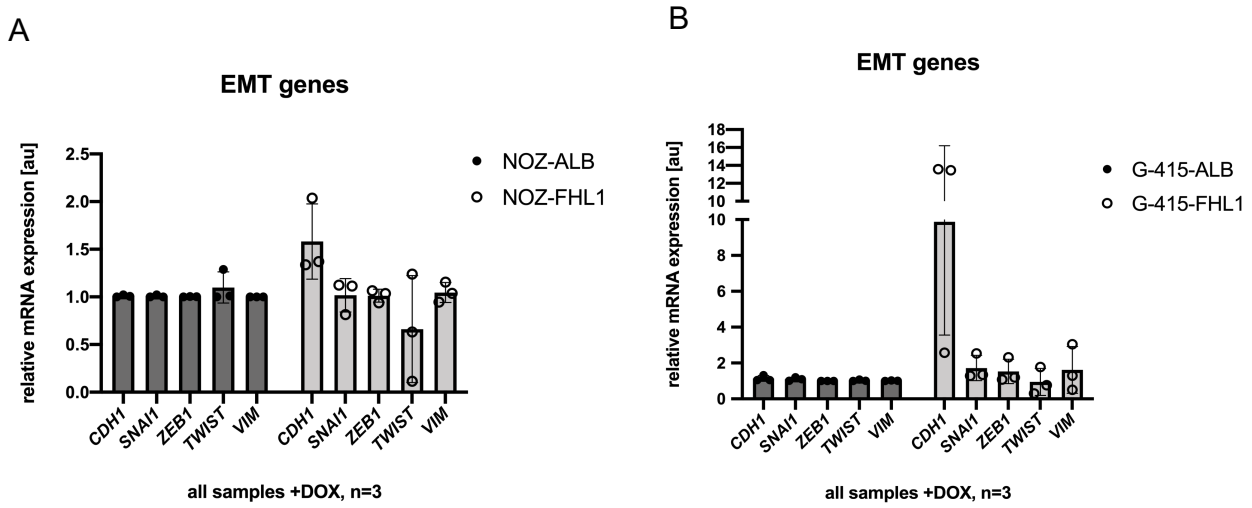

Figure 4-19: EMT gene expression analysis of NOZ and G-415 overexpressing FHL1. (A) NOZ-FHL1 and NOZ-ALB were induced with DOX and 3 independent biological experiments were performed. No significant changes in EMT genes were observed. (B) G-415-FHL1 and G-415-ALB were induced with DOX and 3 independent biological experiments were performed. No significant changes in EMT genes were observed, although a strong trend was observable towards upregulation of E-cadherin.

Figure 4-19 shows the analysis of EMT gene expression in NOZ and G-415 expressing ALB or FHL1, under the control of DOX administration of three independent biological experiments. No significant changes in any gene were observed with broad distributions of single values. However, E-cadherin/CDH1 in G-415-FHL1 cells seemed to be elevated, albeit not significantly and it was also showing a trend of upregulation in NOZ. Concomitantly to CDH1 upregulation, TWIST1 displayed a trend of downregulation. Protein analysis of potential EMT proteins is shown in the representative Western Blot, below in Figure 4-20.

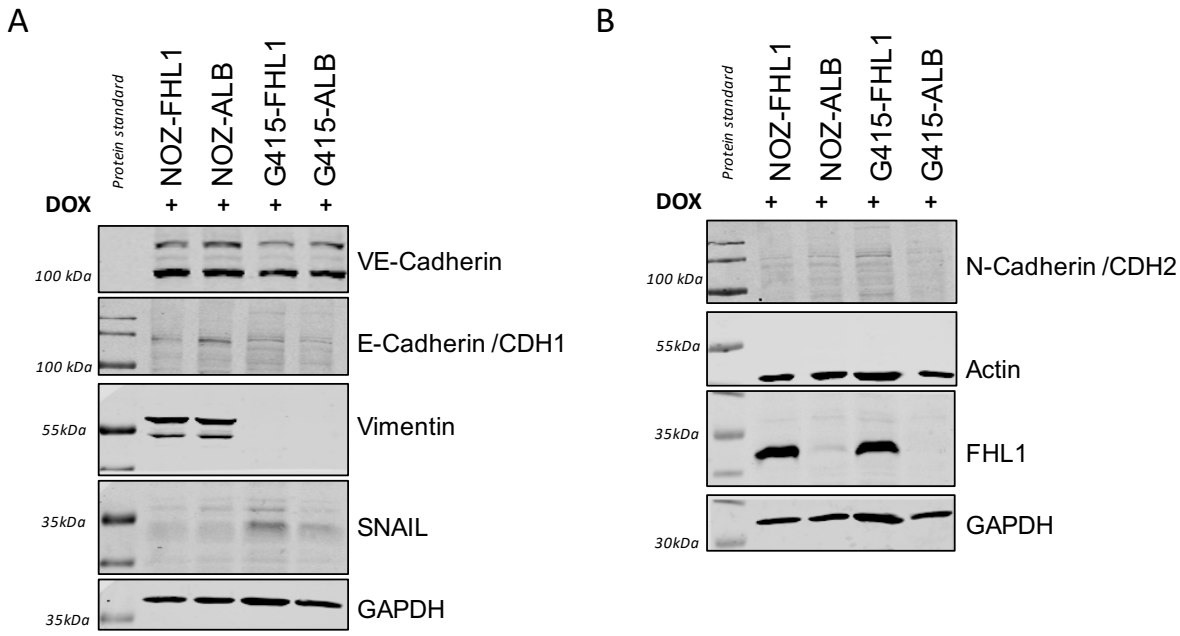

Figure 4-20: Western Blot analysis of EMT proteins in G-415 and NOZ overexpressing ALB or FHL1. (A) Expression of VE-cadherin, E-cadherin, Vimentin, SNAIL in NOZ or G-415 cells, overexpressing FHL1 or ALB after DOX addition. GAPDH was used as internal reference. (B) Expression of N-cadherin, Actin and FHL1 in NOZ or G-415 cells, overexpressing FHL1 or ALB by DOX addition. GAPDH used as internal reference.

Similar to the EMT gene expression analysis, there were no obvious differences in EMT proteins upon overexpression of FHL1 and ALB in NOZ and G415. The marginal differences in protein levels (e.g. actin or SNAIL) seemed to be due to different total protein amounts used for SDS-PAGE, as assessed by GAPDH as internal reference. Taken together, most of the EMT-relevant proteins and genes investigated in FHL1 overexpressing GBC cells were unaffected. For CDH1, there might be an increase in G415 cells, however, no statistical significance was reached.

4.2.3.2. FHL1 IN BILE ACID METABOLISM

Next, investigation of relevant bile acid metabolism genes was performed, as metabolism-related GOs were up- and downregulated in the proteomics data set (see section 4.2.1). According to the Gene Set Enrichment Analysis online database, there are 112 relevant genes for bile acid metabolism[7]. Overlap analysis with all dysregulated proteins of the proteomics data (with an FDR p-value of 0.1 and smaller) found a total of 6 genes. All of these 6 genes were downregulated in the proteomics data and investigated in NOZ and G-415 (Table 4-4 and Figure 4-21).

[7] https://www.gsea-msigdb.org/gsea/msigdb/cards/HALLMARK_BILE_ACID_METABOLISM)

Table 4-4: Proteins of bile acid metabolism that are both significantly dysregulated in GBC cancer samples and downregulated in MS-based proteomics.

Gene	*log2-FC in MS data*	*FDR p-value in MS data*	*Description*
ABCA8	-2.45518828	0.011205718	*ATP-binding cassette sub-family A member 8*
ABCD3	-1.050955392	0.033001639	*ATP-binding cassette sub-family D member 3*
AMACR	-2.241202472	0.035606175	*Alpha-methylacyl-CoA racemase*
LONP2	-0.773345297	0.071742331	*Lon protease homolog 2, peroxisomal*
PECR	-1.359725029	0.06208565	*Peroxisomal trans-2-enoyl-CoA reductase*
PXMP2	-1.235470264	0.077602335	*Peroxisomal membrane protein 2*

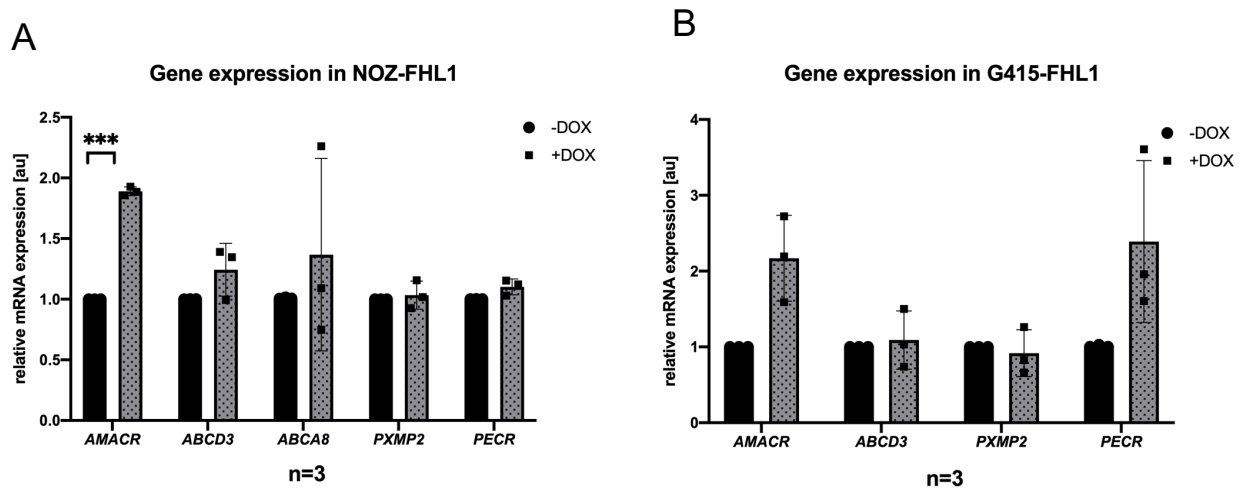

Figure 4-21: Expression analysis of hallmark genes of bile acid metabolism in NOZ and G-415 overexpressing FHL1 in three independent biological experiments. (A) Expression in NOZ-FHL1+/- DOX. The expression of AMACR is significantly increased. (B) Expression in G-415-FHL1+/-DOX cells, which do not exhibit ABCA8 expression in contrast to NOZ cells. No significant changes in gene expression were observed.

To further analyze the expression of these genes after FHL1 overexpression, qRT-PCR was performed. As obvious in Figure 4-21 (B), *AMACR* and *PECR* mRNAs showed a trend of being upregulated in G-415 after FHL1 induction, albeit not significantly. In NOZ-FHL1, *AMACR* was significantly upregulated (A). However, most of the genes varied greatly in their gene expression levels after FHL1 induction compared to no induction. Thus, *AMACR* was induced in GBC cell lines upon FHL1 expression, but the additional bile acid metabolism genes did not change consistently.

4.2.3.3. FHL1 IN SMAD SIGNALING

It has been previously shown that FHL1 expression, together with CK1∂, is capable of phosphorylating SMAD2 and SMAD3 in hepatoma cell lines [116]. For the investigation of SMAD2/3 and their phosphorylated forms after FHL1 overexpression, the presence of CK1∂ was assumed as given, since it is strongly expressed in gallbladder according to the Human Protein Atlas[8].

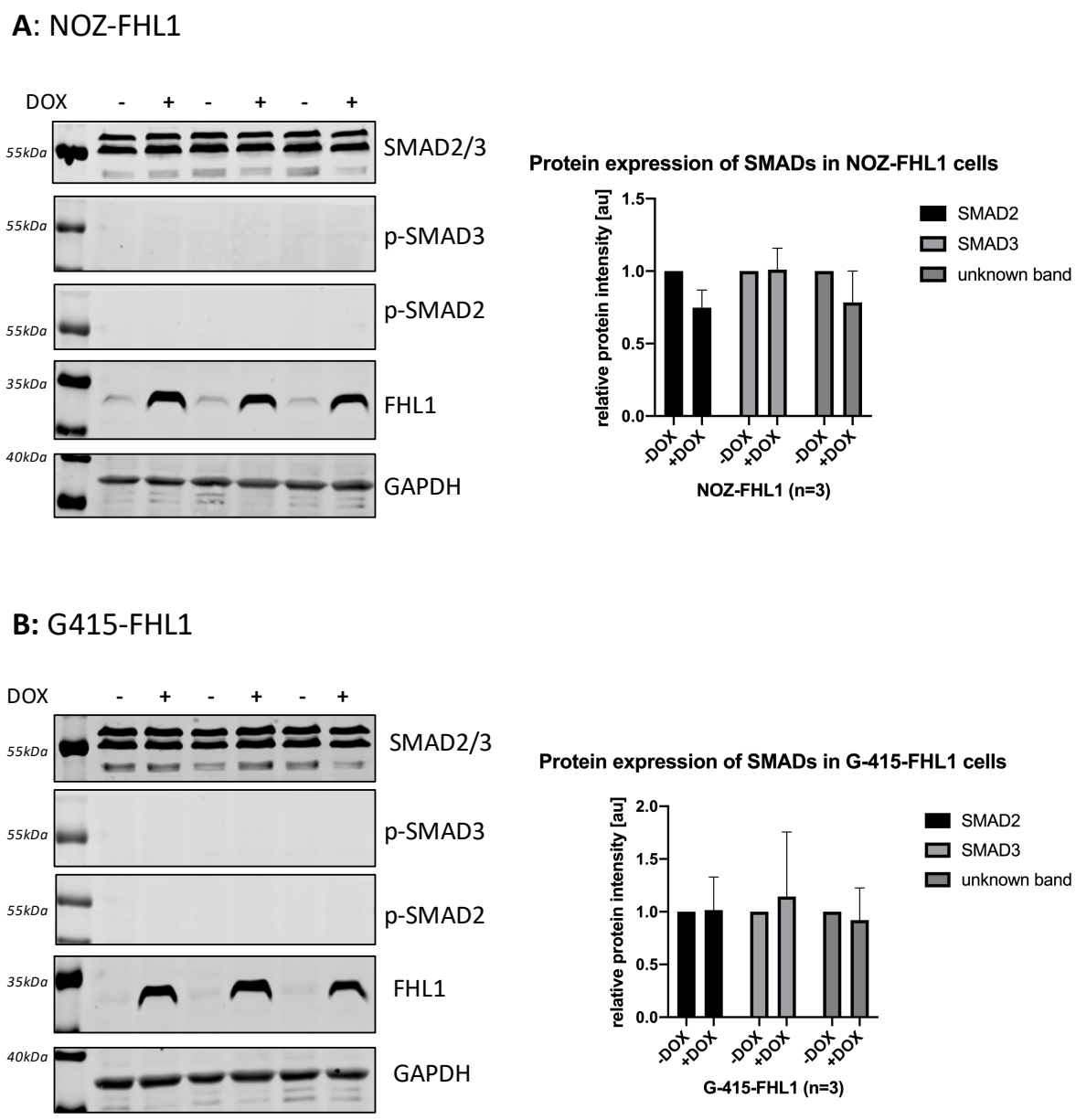

Figure 4-22: SMAD protein status in NOZ and G-415 after overexpression of FHL1. Shown are three independent biological replicates of NOZ/G-415-FHL1 +/-DOX directly next to each other. **(A)** Left: SMAD2/3, P-SMAD2, P-SMAD3 and FHL1 status in NOZ after overexpression of FHL1 +/- DOX. GAPDH was used as internal reference. Right: Quantification of SMAD2, SMAD3 and an unidentified band below SMAD2/3. **(B)** Left: SMAD2/3, P-SMAD2, P-SMAD3 and FHL1 status in

[8] https://www.proteinatlas.org/ENSG00000141551-CSNK1D/tissue

G-415 after overexpression of FHL1 +/- DOX. GAPDH was used as internal reference. Right: quantification of SMAD2, SMAD3 and an unidentified band below SMAD2/3.

The first important observation in Figure 4-22 (A) and (B) in the Western Blot pictures of the left side is that there was no phosphorylation of SMAD2 or SMAD3 induced by the presence of FHL1 in neither NOZ, nor G-415 cells. This is in contrast to findings of the previously published paper [116]. Another interesting observation was the unknown band below SMAD2 and 3 in the topmost WB picture. This band is not to be observed according to the manufacturer of the SMAD2/3 antibody, nor has it been shown in WB pictures of other published research using the same antibody. Plus, this band seemed to vary according to the expression of FHL1. After Quantification of SMAD2/3 and the unknown band in the three different single experiments shown here, there was no clear up- nor downregulation visible, which seemed to depend on FHL1 overexpression. Thus the previously published results of FHL1 action on SMAD activation could not be confirmed.

4.2.3.4. FHL1 IS LINKED TO STAT AND NOTCH SIGNALING

To investigate further in which cell signaling pathways FHL1 is in involved, online research using the STRING database has been performed, to determine protein interaction networks. This has revealed the following for FHL1:

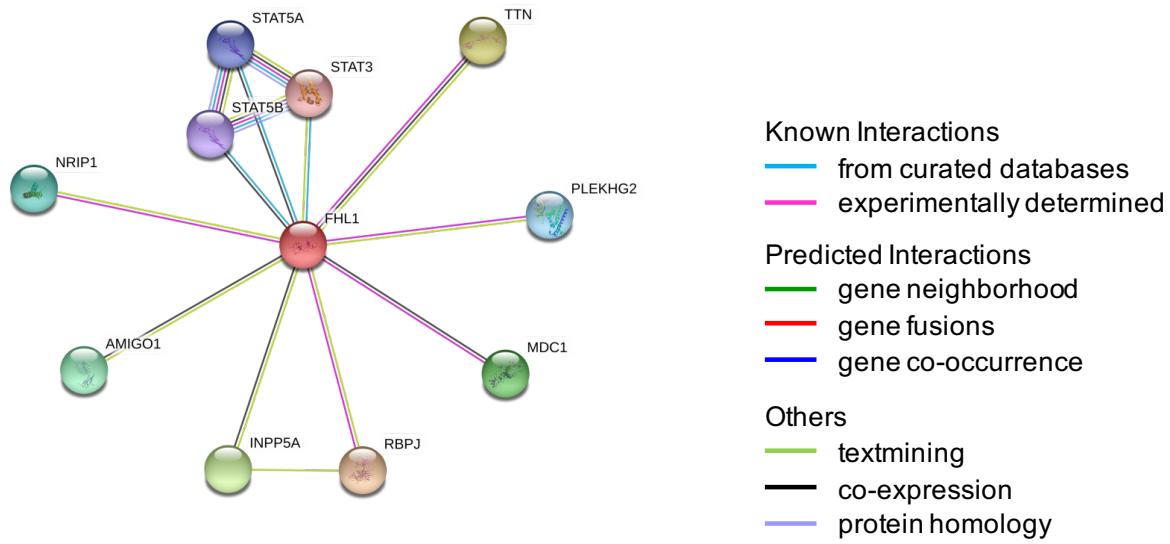

Figure 4-23: Protein interaction network of FHL1 showing the first shell of interactors.

The protein-protein interaction between FHL1 and RBPJ has already been experimentally determined [110]. The interaction with STAT proteins has been identified by analysis of curated databases. To verify these links, a screening of FHL1 expression after IFNγ stimulation or ectopic N1ICD-overexpression was performed in different GBC cell lines:

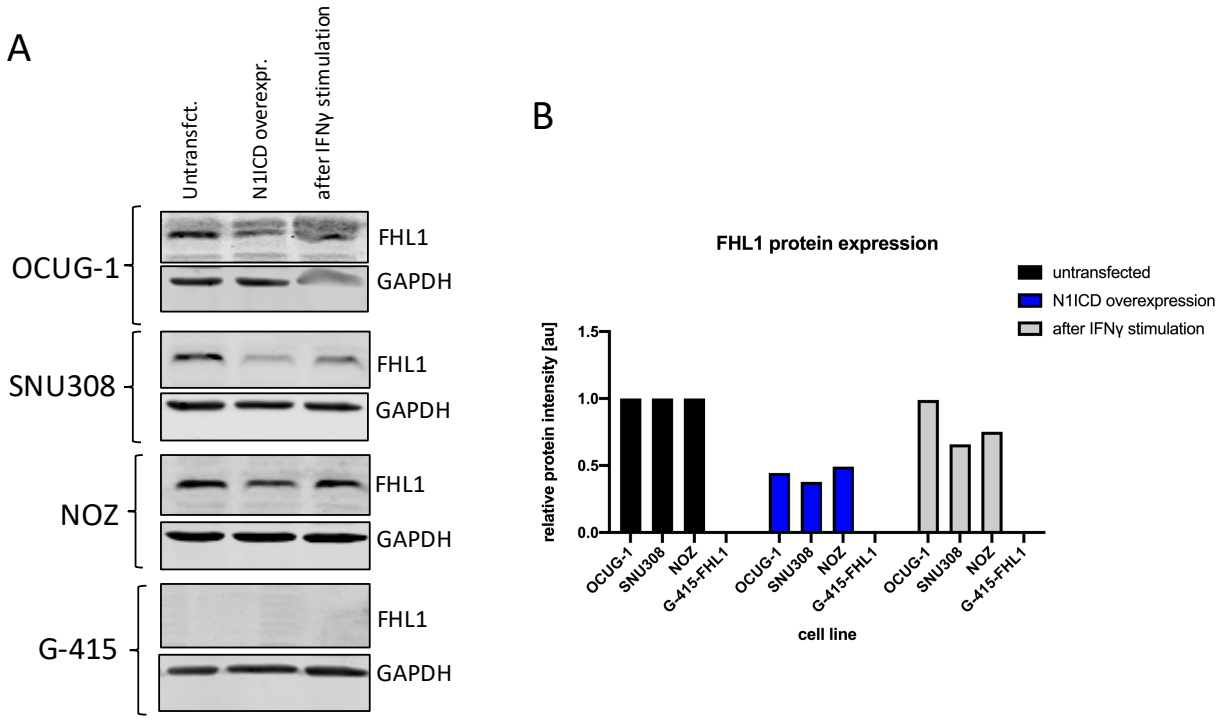

Figure 4-24: FHL1 status in GBC cell lines under different conditions. (A) Western Blot analysis of FHL1 levels in different GBC cell lines under different conditions: Untransfected, after ectopic N1ICD overexpression and after stimulation with IFNγ. (B) Quantification of FHL1 levels under different conditions. GAPDH was used as internal reference.

The three cell lines OCUG-1, SNU308 and NOZ showed endogenous FHL1 expression, whereas G-415 did not, as can be seen in Figure 4-24. This is in line with the previous observations. Interestingly, FHL1 expression was decreased in the top three cell lines after overexpression of N1ICD. The N1ICD was previously proven to be transcriptionally active by members of the research group. The downregulation of FHL1 expression was quite profound, as FHL1 was being reduced to around 50%. The activation of STAT signaling by IFNγ stimulation seemed to have an effect on FHL1 protein level too, more strongly in SNU308 and NOZ, than in OCUG-1. These results supported the suggested links between FHL1 and the interacting proteins of the STRING network and were convincing enough to continue the investigation about FHL1's involvement in NOTCH signaling.

4.2.3.4.1. FHL1 Feedback Inhibition by NOTCH1 and 3

To investigate the mechanism of FHL1 protein regulation by NOTCH1/3 and to verify this on transcriptional level as well, the cell lines SNU308 and NOZ were used to generate stable inducible NOTCH1 and NOTCH3 overexpression systems with their transcriptionally active intracellular domains. The levels of FHL1 protein and mRNA levels have been assessed after successful induction of NOTCH1/NOTCH3 in three independent biological experiments:

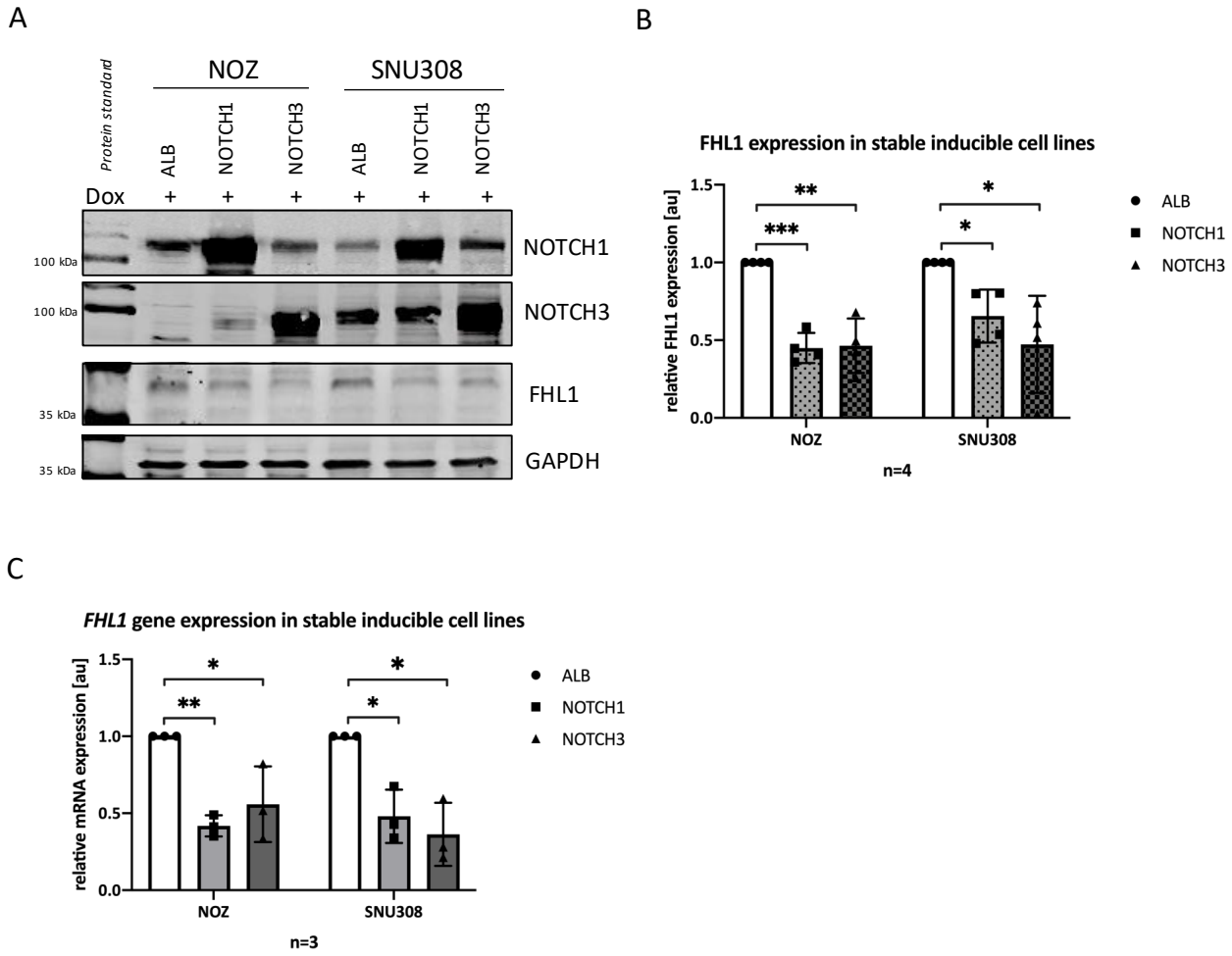

Figure 4-25: Negative regulation of FHL1 gene and protein expression by NOTCH1 and NOTCH3. (A) Representative Western Blot of NOTCH1 and NOTCH3 induction after DOX administration, as well as FHL1 expression in NOZ and SNU308 cells after DOX induction. GAPDH was used as an internal reference. (B) Quantification of FHL1 level of 4 independent experiments after overexpression of NOTCH1/3. The downregulation of FHL1 is significant in both cell lines after overexpression of NOTCH1 and NOTCH3. (C) *FHL1* mRNA expression level after overexpression of NOTCH1/3 in three independent experiments in NOZ and SNU308. The downregulation of FHL1 is significant in both cell lines after overexpression of NOTCH1 and NOTCH3. Data was normalized to ALB +DOX control and is presented as mean ± SD, *p<0.05, **p<0.01, ***p<0.001.

Figure 4-25 (A) shows the successful induction of NOTCH1 or NOTCH3 after administration of DOX, as indicated by the respective +DOX samples. It also shows the different basal levels of active NOTCH1 and NOTCH3 in NOZ and SNU308 in can be seen in the control samples ALB+DOX. NOZ showed more endogenous active NOTCH1 (further called N1ICD) than SNU308, as observable in the first lane of the Western Blot. SNU308 had more NOTCH3 (N3ICD) than NOZ (see second lane). The FHL1 levels are displayed in the third lane. It can be observed that the protein levels decreased upon the overexpression of N1ICD and N3ICD. This is confirmed by the quantification of FHL1 protein levels in four independent experiments, shown in (B). The protein level of FHL1 were highly significantly decreased in NOZ and significantly in SNU308, albeit not as strongly as in NOZ. Diagram (C) proved that the downregulation of FHL1 by N1ICD and

N3ICD takes place on the transcriptional level, as the mRNA for FHL1 is significantly reduced in both cell lines in three independent biological experiments. These results showed that NOTCH1 and NOTCH3 are able to downregulate FHL1. The succeeding question was, if FHL1 would be able to regulate NOTCH signaling as well.

4.2.3.4.2. FHL1 INHIBITS NOTCH1-TARGET GENE TRANSCRIPTION

To investigate the impact of FHL1 on NOTCH1 signaling, the above described experiments has not merely been performed vice versa, but the transcriptional activity of NOTCH1 was monitored after overexpression of a control vector or FHL1. Prerequisite for this was the confirmation that N1ICD was basally expressed in the cell lines used. Therefore, a protein and mRNA screening for N1ICD in cell lines has been performed. This led to the selection of NOZ and G-415, with which the experiments were performed, since NOZ showed quite strong endogenous levels of N1ICD and according to the mRNA levels, G-415 contained even more, in contrast to SNU308, which had weak endogenous N1ICD (see diagram A of the following figure).

A

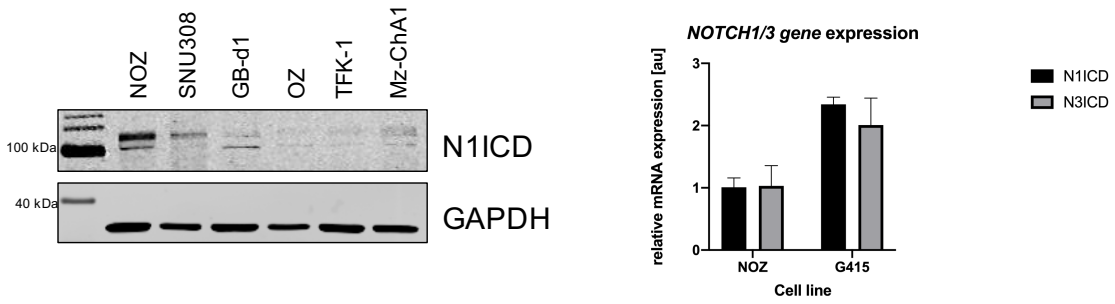

B

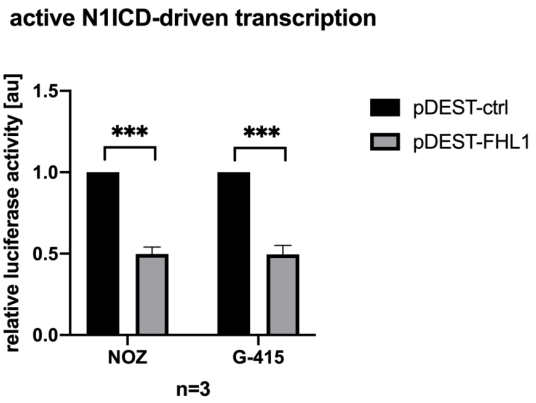

C

		Av Luc act.	SD
G415	pDESTctrl	1	0.207460622
	pDEST-N1ICD	0.54765079	0.00484492
NOZ	pDESTctrl	1	0.058573524
	pDEST-N1ICD	0.55605205	0.038885317

Figure 4-26: Endogenous N1ICD expression in GBC cell lines and reduced N1ICD-mediated transcription upon FHL1 overexpression. (A) Left: Western Blot of endogenous N1ICD in BTC cell lines. Right: *N1ICD* and *N3ICD* mRNA levels in NOZ and G-415. (B) Left: Luciferase assay for the N1ICD-mediated transcription with expression of a control vector or overexpression of FHL1 for 3 independent experiments. The N1ICD-driven transcription is very significantly reduced in NOZ and G-415 upon the overexpression of FHL1. Data was normalized to the luciferase activity in pDEST-

ctrl and is presented as mean ± SD, *p<0.05, **p<0.01, ***p<0.001. (C) Table for average luciferase activities of the three experiments for both cell lines individually.

The diagram and table in (B) of Figure 4-26 show the reduction of N1ICD-mediated transcription after the overexpression of FHL1. The N1ICD-mediated transcription is depending on the N1ICD cofactor RBPJ and the luciferase activity is a reflection of RBPJ-mediated binding to its CSL-binding motif on the DNA. However, RBPJ is also able to bind to FHL1. Here, it can be concluded that overexpression of FHL1 significantly reduced the endogenous N1ICD-driven transcription, as measured by luciferase activity. This gave rise to the question, whether typical N1ICD target genes could also be affected, if FHL1 was overexpressed. Hence, qRT-PCR for some N1ICD target genes was performed. The direct target genes *HES1* and *HEY1, c-MYC* and *HSPB6* [117] were analyzed.

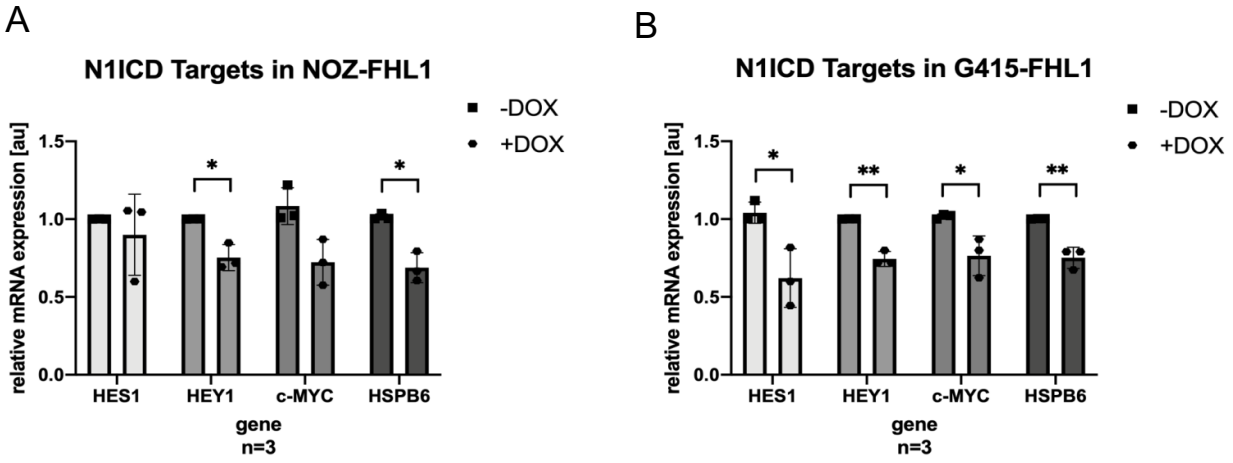

Figure 4-27: Gene expression analysis of N1ICD target genes in NOZ and G-415 after overexpression of FHL1. (A) N1ICD target gene expression analysis of 3 independent biological experiments in NOZ-FHL1 cells. *HEY1* and *HSPB6* are significantly downregulated. *HES1* and *c-MYC* show a trend of downregulation. (B) N1ICD target gene expression analysis of 3 independent biological experiments in G-415-FHL1 cells. All investigated genes are significantly downregulated. Data was normalized to -DOX control and is presented as mean ± SD, *p<0.05, **p<0.01, ***p<0.001.

Figure 4-27 (A) and (B) show the downregulation of the investigated N1ICD target genes in NOZ and G-415 after overexpression of FHL1 in three independent experiments. In G-415, all of the investigated genes were significantly reduced and in NOZ, *HEY1* and *HSPB6* were significantly downregulated, whereby *HES1* and *c-MYC* showed a trend of downregulation. Taken together, with the luciferase assay, this proved that FHL1 decreased the transcriptional activity of N1ICD, resulting in reduced expression of N1ICD target genes in GBC cell lines that have endogenous tumorigenic N1ICD activity.

4.2.3.4.3. FHL1 Binds to RBPJ and Replaces N1ICD in N1ICD-RBPJ Complex.

Since it was previously known that RBPJ can bind to FHL1 and with the above observed downregulation of N1ICD-mediated transcription by FHL1, a closer investigation of the RBPJ protein complexes was performed. Firstly, the interaction between RBPJ and FHL1 was confirmed *in vitro* and *in vivo* by CoIP and PLA. This was followed by the investigation between the protein-protein interactions between N1ICD and RBPJ and a possible interaction between N1ICD and FHL1 by CoIP.

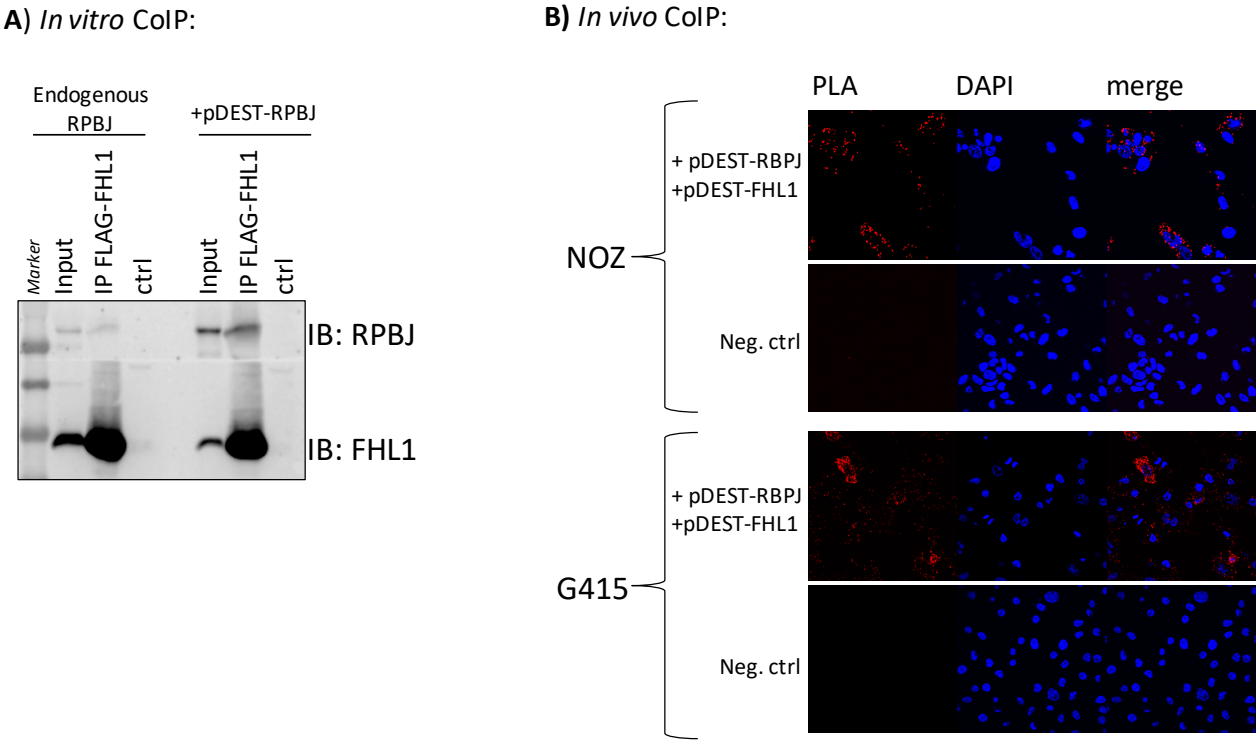

Figure 4-28: *In-vitro* and *in-vivo* CoIP between FHL1 and RBPJ. (A) FLAG-immunoprecipitation of FLAG-tagged FHL1 and the associated RBPJ in HEK cells with endogenous and overexpressed RBPJ. In both experiments, RBPJ is co-immunoprecipitated with FHL1, as proven by immunoblotting. **(B)** *In-vivo* proximity ligation assays in NOZ and G-415 cells after co-overexpression of RBPJ and FHL1 or negative control. Red dots indicate direct binding protein-protein interaction between RBPJ and FHL1. Negative controls were performed with the same protocol, but in the absence of primary antibody incubation.

The previously described interaction between FHL1 and RBPJ was confirmed *in vitro* and *in vivo*. In Figure 4-28 (A) FLAG-tagged FHL1 was immunoprecipitated via its peptide tag in HEK cells. RBPJ was co-immunoprecipitated, as confirmed by Western Blot. The presence of FHL1 and RBPJ in the total protein lysates prior to the immunoprecipitation ('input' lane) was also detected, as well as in the immunoprecipitated samples. The IP to the left of (A) showed the pulldown of FHL1 and endogenous RBPJ and on the right side, after additional RBPJ overexpression. Hence, the band of RBPJ of the left IP sample is stronger. There were no precipitated proteins in the negative control visible. Thus, FHL1 directly bound RBPJ *in vitro*.

The interaction between FHL1 and RBPJ was further confirmed in NOZ and G-415 cell lines by the proximity ligation assay displayed in (B), also known as in-cell co-immunoprecipitation. Red dots in the immunofluorescent microscope pictures indicate the interaction between the proteins. The interaction was detected when RBPJ and FHL1 were expressed together in both cell lines. The interaction is not detected in the negative controls, which were performed in equally treated samples, but in the absence of primary antibody incubation. This ruled out unspecific amplification of the signal, which is responsible for the formation of red fluorescence dots. Taken together, these results confirmed the binding of RBPJ and FHL1 *in vivo.*

Subsequently, extensive studies were performed to investigate the different bi-directional pulldowns between N1ICD/FHL1 and RBPJ and to find out, whether N1ICD and FHL1 could also bind each other, thus giving rise to a potential trimeric complex between the three proteins.

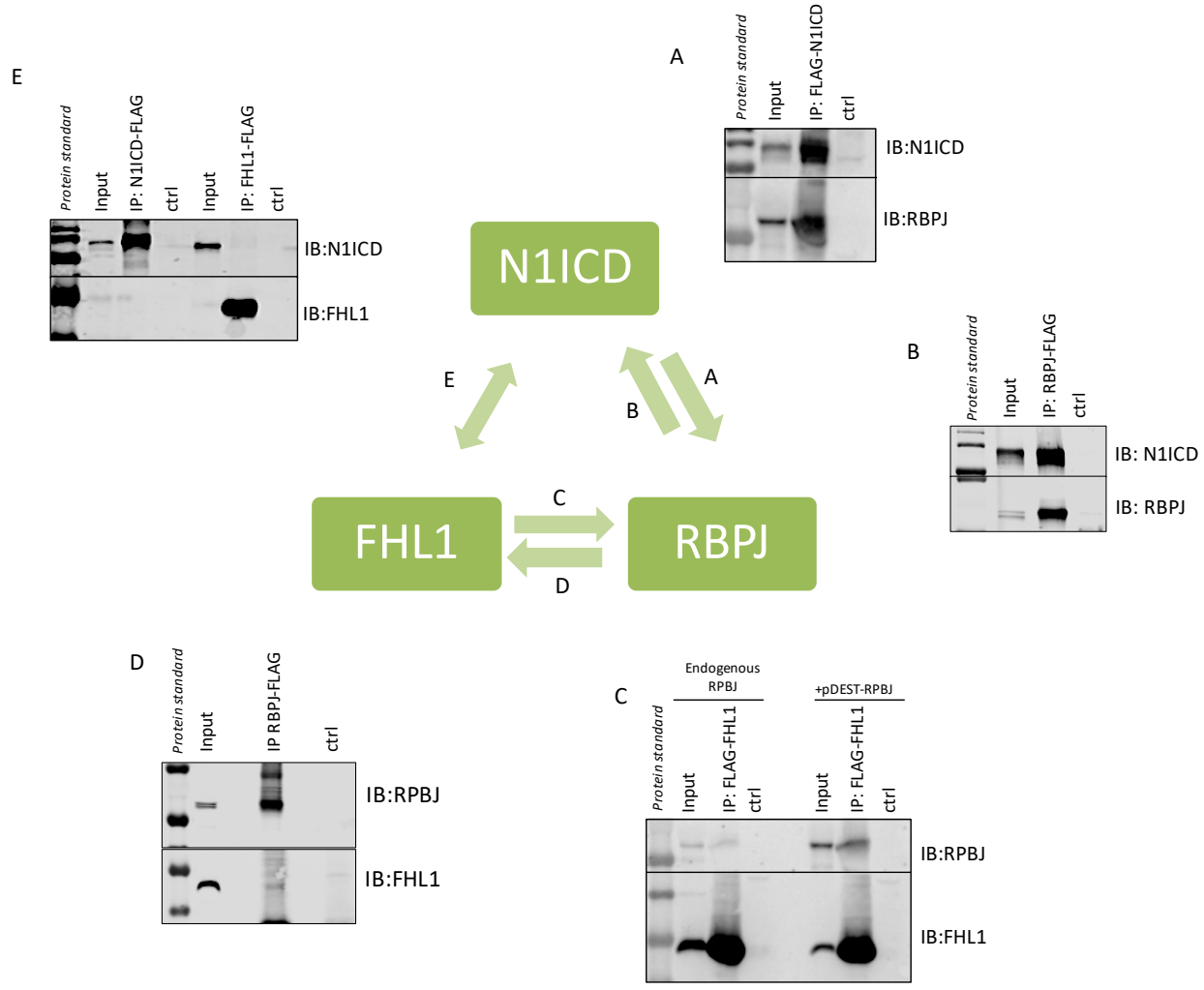

Figure 4-29: Protein interactions between FHL1, RBPJ and N1ICD. (A) N1ICD-pulldown with RBPJ bound. **(B)** RBPJ-pulldown with N1ICD bound. **(C)** FHL1-pulldown with RBPJ bound. **(D)** RBPJ-pulldown with FHL1 bound. **(E)** N1ICD-pulldown does not co-precipitate FHL1 and FHL1-pulldown does not co-precipitate N1ICD.

Figure 4-29 shows the summary of all investigated interactions. Arrow ‘A’ and Western Blot (A) shows the interaction between FLAG-tagged N1ICD and RBPJ after FLAG pulldown. The CoIP was successful, as indicated by the presence of RBPJ and N1ICD bands. The same is true for (B). Here, FLAG-tagged RBPJ was pulled down and N1ICD was co-precipitated. In (C), it was investigated whether FLAG-tagged RBPJ can pulldown RBPJ. This has already been described in Figure 4-28 (A) and it also worked vice versa, as indicated by arrow ‘D’ and Western Blot (D). Here FLAG-tagged RBPJ was precipitated and FHL1 was also pulled down. Lastly, arrow ‘E’ and Western Blot (E) revealed that FLAG-tagged N1ICD pulldown did not co-precipitate FHL1 (left side of the immunoblot) and FHL1 pulldown did not co-precipitate N1ICD (right side of the immunoblot).

These findings suggest that FHL1 and N1ICD are both able to bind RBPJ but failed to bind to each other. This suggested a mutually exclusive manner of binding to RBPJ, creating differences in gene expression regulation.

4.2.4. The Relevance of FHL1 Function *In Vivo*

4.2.4.1. FHL1 does not Influence Migration

Elevated migratory capacity of cells with inhibited proliferation is showing oncogenic properties. Therefore, a wound healing assay has been performed in NOZ and G-415 after overexpression of FHL1 with simultaneous proliferation inhibition by mitomycin C. Due to their inherent different behavior, NOZ were migrating faster than G-415, so the timepoints for the observation of migration was adjusted accordingly.

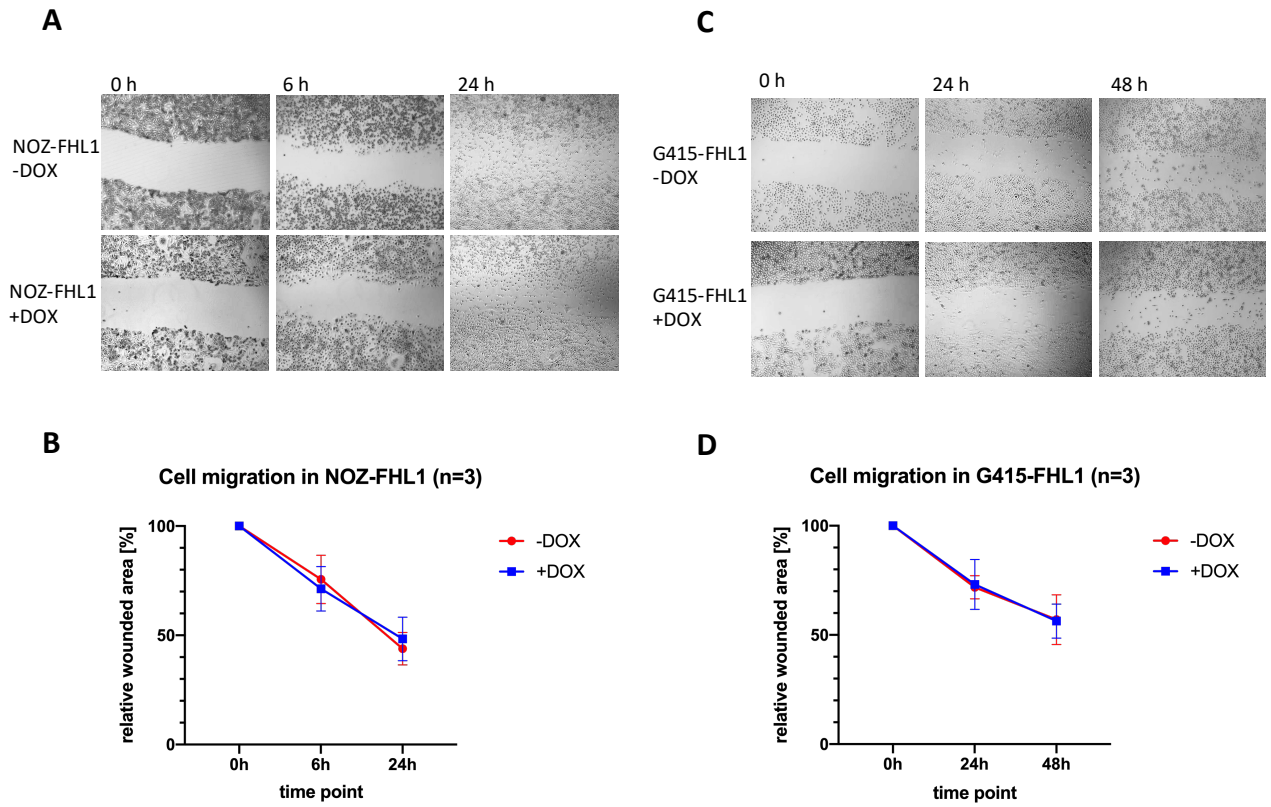

Figure 4-30: Wound healing assay in NOZ and G-415 after overexpression of FHL1. (A) Exemplary microscope pictures of the gap area of NOZ +/- DOX at 0, 6 and 24 h post-wounding. There is no observable qualitative difference in the relative wound area. (B) Quantification of 3 independent biological experiments of the relative wounded area in NOZ +/- DOX at given timepoints. There is no difference in velocity of cell migration. (C) Microscope pictures of the gap area of G-415 +/- DOX at 0h, 24h and 48h post-wounding. There is no observable qualitative difference in the relative wound area. (D) Quantification of 3 independent biological experiments of the relative wounded area in G-415 +/- DOX at given timepoints. There is also no difference in velocity of cell migration.

Figure 4-30 shows that there was no difference in the ability to migrate in both cell lines after the overexpression of FHL1. (A) and (C) show exemplary microscope pictures from the same region of the wounded area. There was no obvious difference in wound closure observable. Further, after calculating the relative wound area and combining three independent experiments, there was no difference found, as shown in (B) and (D). FHL1 overexpression did not affect the migratory capability of the GBC cell lines NOZ and G-415.

4.2.4.2. FHL1 Reduces Cell Viability

Another common functional assay to measure tumorigenic or tumor suppressive potential is the cell viability assay, which was performed next. To rule out an effect of doxycycline on cell viability, the assay has also been performed on NOZ and G-415 overexpressing ALB after DOX addition as control. DOX has only been added after the initial cell viability measurement on day 0.

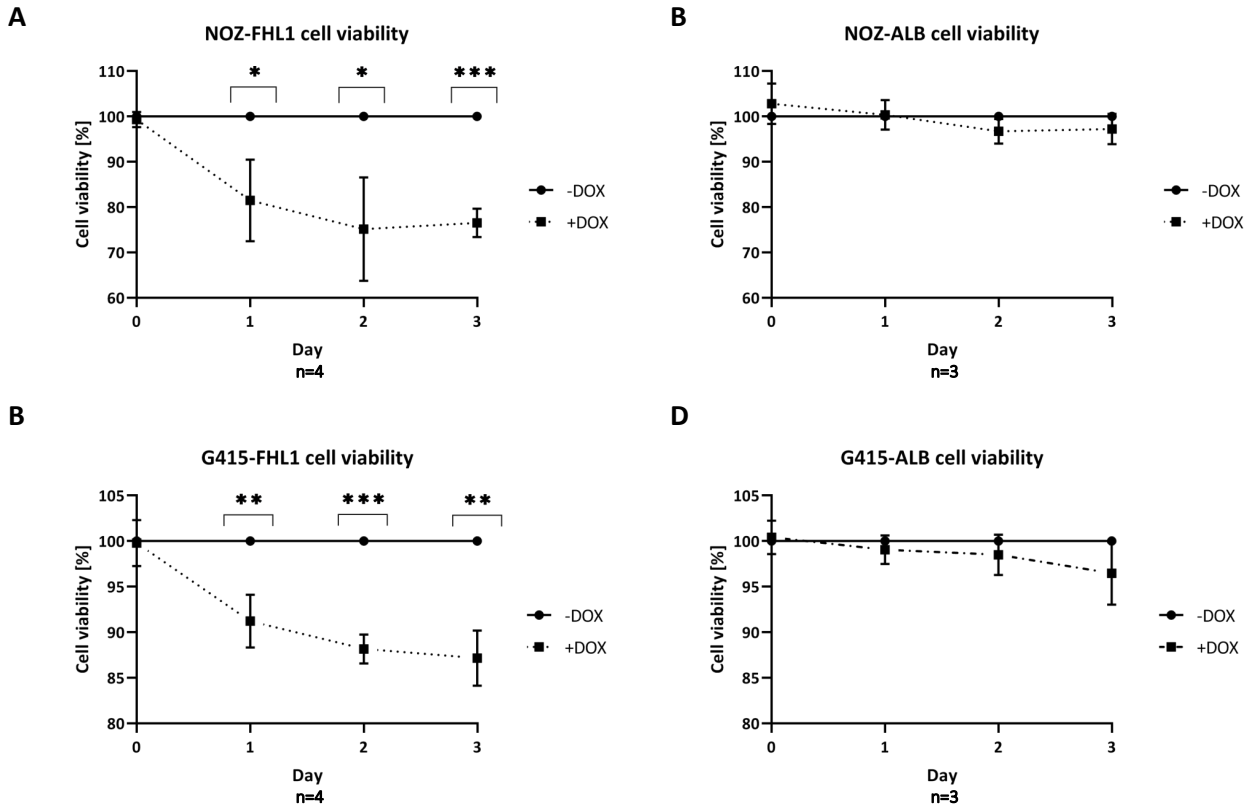

Figure 4-31: Cell viability assay in NOZ and G-415 after overexpression of FHL1 or ALB in three to four independent experiments. (A) The cell viability of NOZ after FHL1 overexpression is significantly decreased. (B) ALB overexpression in NOZ influences cell viability only marginally and without statistical significance. (C) In FHL1 overexpressing G-415 cells, cell viability is slightly but very significantly reduced. (D) After overexpression of ALB in G-415 there is no significant difference. Data was normalized to the respective -DOX control and is presented as mean ± SD, *p<0.05, **p<0.01, ***p<0.001.

The results of the cell viability assay are displayed in Figure 4-31. Diagram (A) shows the significantly reduced cell viability in NOZ after overexpression of FHL1 over a period of 4 days. The effect in G-415 (B) was smaller, yet also highly significant. In NOZ, the effect of DOX on general cell viability was practically non-existent as can be seen in diagram (C): NOZ overexpressing ALB by DOX administration showed almost no decrease in cell viability after 4 days. G-415 cells were a little more sensitive to DOX or strong ALB secretion, because the cell viability was slightly but not significantly reduced on day 4 (D). For the FHL1 overexpression experiment, four independent biological experiments have been combined and for the ALB overexpression,

three experiments were performed. Taken together, FHL1 expression significantly reduced cell viability of GBC cell lines.

4.2.4.3. FHL1 Inhibits Cell Colony Growth

To assess the clonogenic capacity of NOZ and G-415, colony formation assays with both cell lines have been performed under different conditions. In general, the influence of FHL1 induction was investigated, together with AllStars, mimic-4502 or miR-4502-inhibitor overexpression and as control, ALB overexpression was induced. Here, the experiments with mimic-4502 and the miR-4502-inhibitor have been included to investigate synergistic effects with FHL1 overexpression and at the same time, to compare the effects of mimic-4502 and the miR-inhibitor without FHL1 induction. Therefore, all samples have been normalized to the AllStars -DOX condition, which reflects the unaltered cell behavior best.

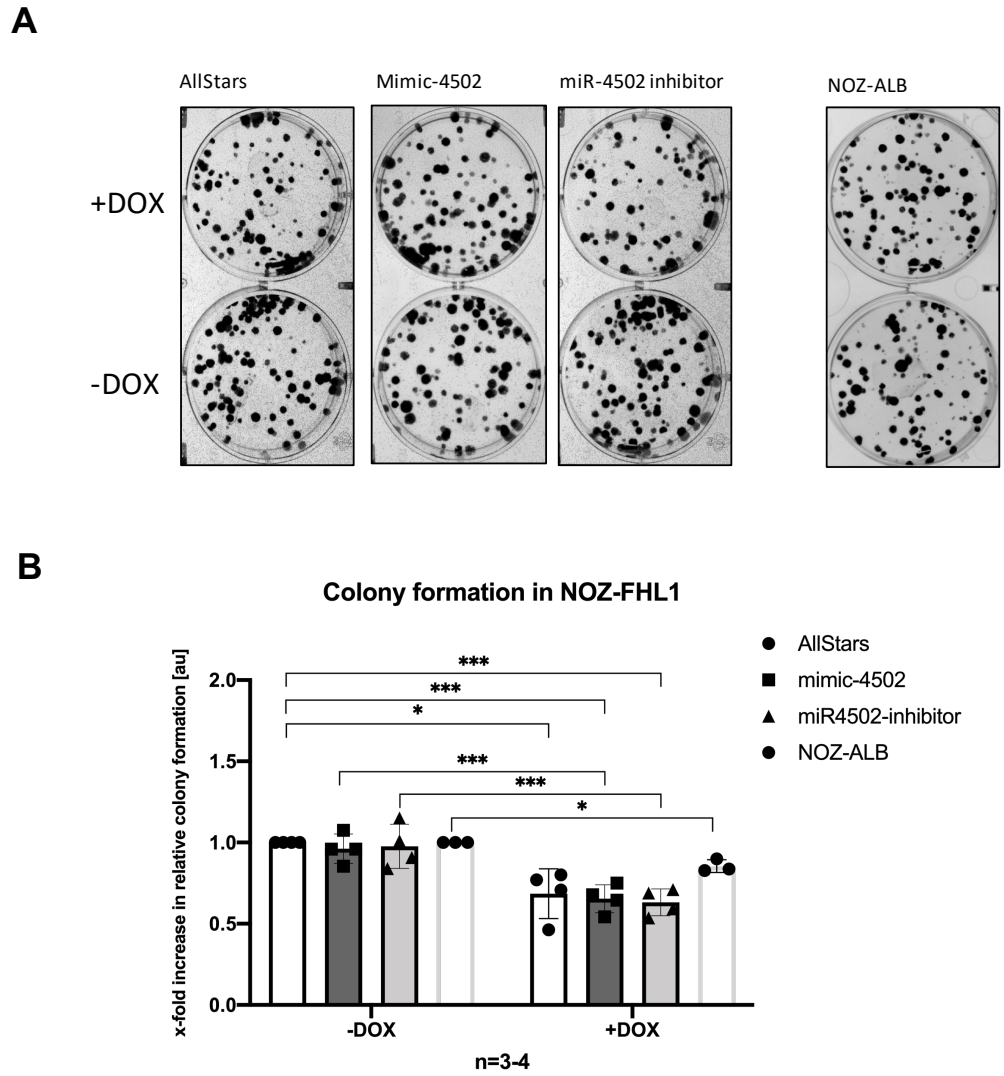

Figure 4-32: Colony formation assay for clonogenic capacity in NOZ cells. (A) Colony formation in NOZ +/- DOX for FHL1 or ALB induction and with overexpression of mimic-4502, miR-4502-inhibitor or AllStars control. For FHL1+/- and +AllStars/mimic-4502/miR-4502-inhibitor, 4 independent biological experiments have been performed. For ALB induction, 3 experiments were combined. (B) Overexpression of FHL1 leads to significant reduction in colony formation ability of NOZ cells, as well as ALB overexpression, albeit to a lesser extent. Data was normalized to the respective -DOX control and is presented as mean ± SD, *p<0.05, **p<0.01, ***p<0.001.

NOZ cells overexpressing FHL1 showed reduced colony formation, the same is true after the induction of ALB, however, the decrease after FHL1 induction was stronger. The comparison of mimic-4502 and miR-inhibitor irrespectively of FHL1, did not show any significant changes. The details are displayed in Figure 4-32 (B). There was a strongly significant decrease in colony formation between NOZ AllStars +DOX and -DOX, as well as to mimic-4502 +DOX and miR-4502-inhibitor +DOX. Further, NOZ mimic-4502 +DOX to -DOX showed highly significantly decreased colony formation. The same is true for NOZ miR-4502-inhibitor +DOX to -DOX. There was also a significant decrease between NOZ-ALB +DOX and -DOX, but the +DOX effect did not reduce the relative colony formation as strongly as FHL1 overexpression did.

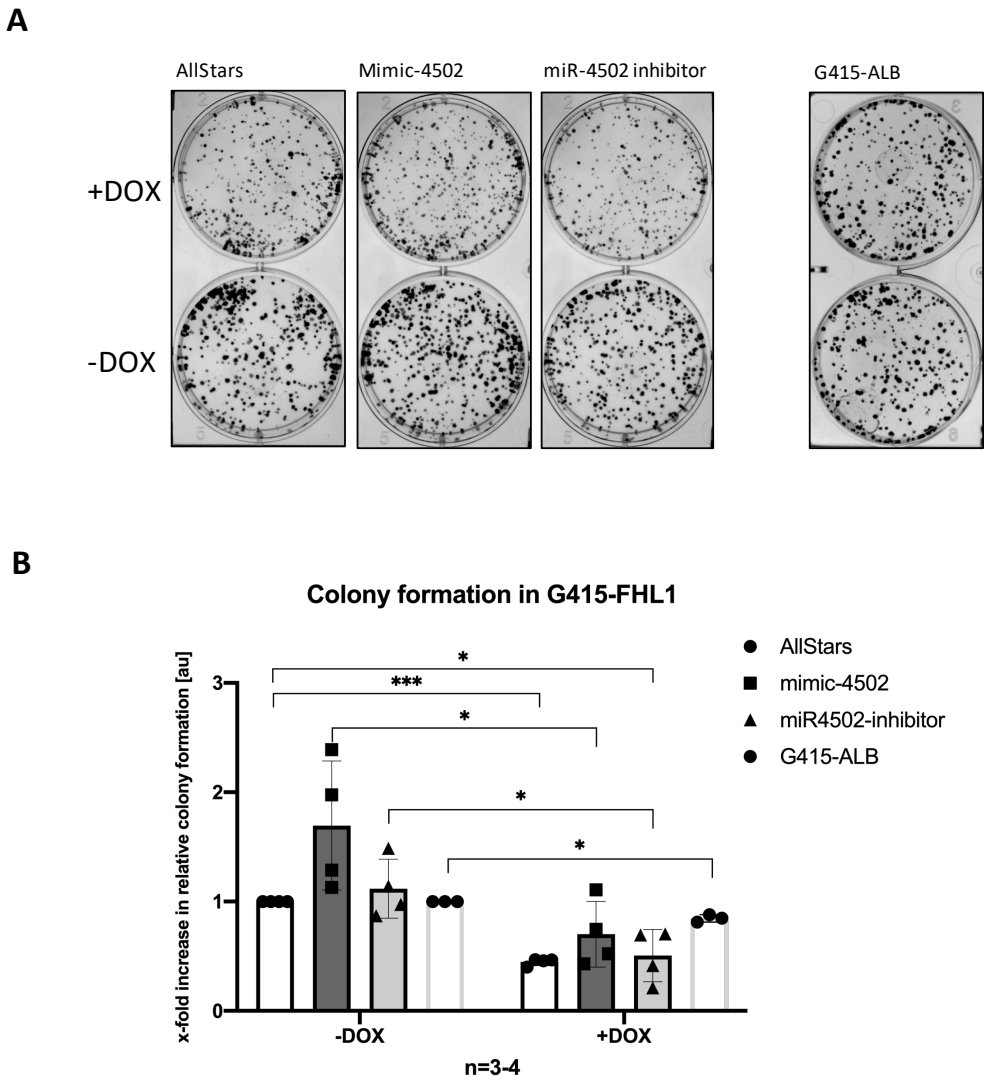

Figure 4-33: Colony formation assay for clonogenic capacity in G-415 cells. (A) Colony formation in G-415 +/- DOX for FHL1 or ALB induction and with overexpression of mimic-4502, miR-4502-inhibitor or AllStars control. for FHL1+/- and +AllStars/mimic-4502/miR-4502-inhibitor, 4 independent biological experiments have been performed. For ALB induction, 3 experiments were combined. (B) Overexpression of FHL1 leads to significant reduction in colony formation ability of G-415 cells, as well as ALB overexpression, albeit to a lesser extent. Data was normalized to the respective -DOX control and is presented as mean ± SD, *p<0.05, **p<0.01, ***p<0.001.

Also, in G-415 cells overexpressing FHL1, the colony formation was significantly reduced. And similarly to NOZ, the induction of ALB led to reduced colony formation, but again not as strong as after FHL1 induction. Between G-415 AllStars and mimic-4502 there was a trend of increased colony formation, in line with the potential oncogenic nature of the miRNA, however, the increase was not significant. The miR-4502-inhibitor did not show an effect compared to AllStars. For the following details see Figure 4-33 (B). There was a strongly significant decrease in colony formation between G-415 AllStars +DOX and -DOX and the decrease was also significant to miR-4502 inhibitor +DOX. G-415 with mimic-4502 +DOX and -DOX also showed significantly decreased colony formation, just as G-415 miR-4502-inhibitor +DOX and -DOX. The decrease in

colony formation between G-415 ALB +DOX and -DOX was also significant, but it did not reduce the relative colony formation to the same extent as FHL1 overexpression did. In summary, expression of FHL1 by DOX significantly reduced the clonogenic capacity of NOZ and G-415 cells.

4.2.4.4. FHL1 Reduces Cell Proliferation

To measure the impact of FHL1 overexpression on cell proliferation, two different experiments have been performed. Firstly, the proliferation was investigated by quantification of Ki67-positive cell nuclei in respect to the total nuclei and the second experiment consisted of a BrdU-ELISA, which reflects the incorporation of nucleotides into new DNA, thereby indicating proliferating cells.

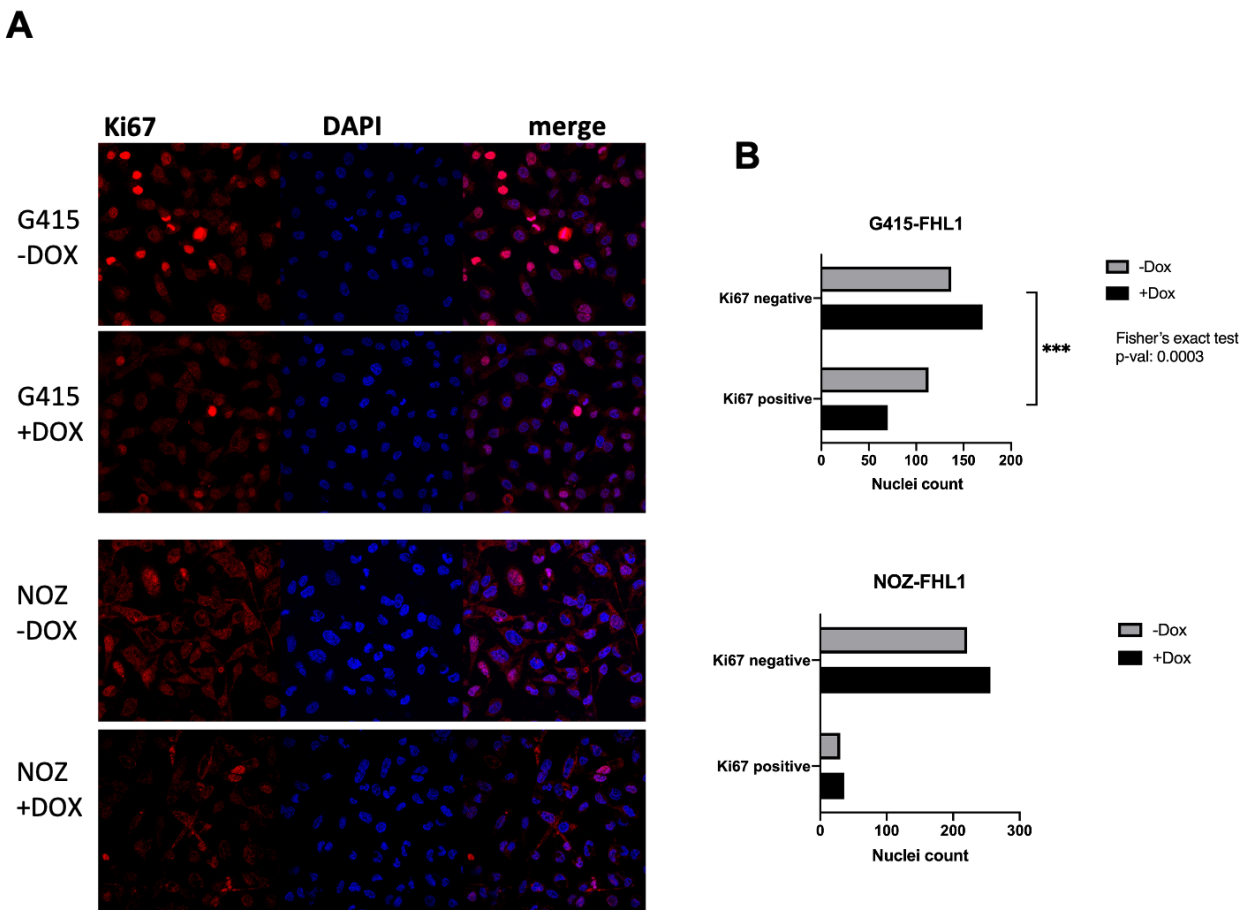

Figure 4-34: Ki67-staining in NOZ and G-415 after overexpression of FHL1. (A) Confocal fluorescence microscopy of G-415 and NOZ cells +/-DOX. The successful overexpression of FHL1 was performed in parallel experiments. Red fluorescence indicates Ki67 staining and blue shows cell nuclei, stained with DAPI. **(B)** Evaluation of total Ki67-positive and negative nuclei in respect to total nuclei by Fisher's exact test. In G-415 overexpressing FHL1 cells, the total number of Ki-67 positive cells is highly significantly decreased, whereas there is no significant change in NOZ cells.

Shown in Figure 4-34 (A) are some exemplary pictures of the Ki67 staining in NOZ and G-415 +/-FHL1 overexpression. In G-415 cells overexpressing FHL1, there was less Ki67 positive staining. In NOZ cells, a slight trend towards less positive cells after FHL1 overexpression was observed. After counting the nuclei and evaluating the numbers of Ki67-positively and negatively stained nuclei, Fisher's exact test revealed that the amount of Ki-67 positive cells was significantly higher in G-415 without FHL1 overexpression, thereby suggesting that FHL1 overexpression lead to decreased cell proliferation. However, there was no such effect observed in NOZ cells.

To complement these observations and also in order to investigate the possibility, if FHL1 overexpression in NOZ cells still has an effect proliferation, the BrdU proliferation assay was performed. To substantiate the findings that FHL1 decreases cell proliferation, additional GBC cell lines were used with assistance of Raisatun Sugyianto. The cell lines GB-d1 and SNU308 contained low levels of endogenous FHL1, whereas TGbC-1 has moderate levels of FHL1 (as shown in Figure 4-12). The overexpression of FHL1 in the additional cell lines has been secured, analogously to the Western Blot analyses shown in Figure 4-18. As control, the inhibition of proliferation was achieved by addition of mitomycin C.

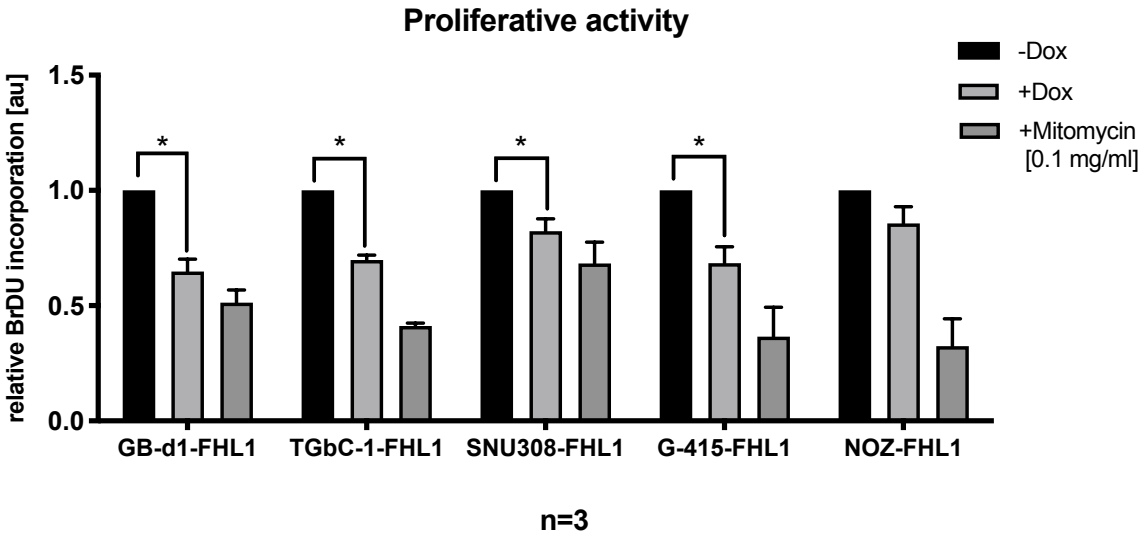

Figure 4-35: BrdU incorporation after FHL1 overexpression in GBC cell lines. The cell proliferation rates after FHL1 overexpression are significantly reduced in Gb-d1, TBbC-1, SNU308 and G-415, thereby indicating downregulation of proliferation. NOZ proliferation rates are marginally reduced after FHL1 overexpression without statistical significance.

Here, in Figure 4-35, the reduction in proliferation in G-415 is reflecting the outcome of the Ki67 staining experiment. This proved that the proliferation rates are decreased in this cell line upon FHL1 induction. GB-d1, SNU308 and TGbC-1 also showed a significant decrease of about 40% in the proliferation rates, whereas NOZ barely showed an effect with a negligible amount of variation. Taken together, these results confirmed that FHL1 overexpression is leading to reduced proliferative activity in GBC cells.

4.2.5. GFT2I is Another Co-precipitated Protein of FHL1 Identified by Mass-spectrometric Analysis.

In order to elucidate the full picture of transcriptional regulation aided by FHL1 –as FHL1 is not binding to DNA by itself– mass-spectrometric analysis of all proteins co-precipitated with FHL1 has been performed. The subsequent table shows an excerpt of all identified proteins, filtered for significance and signal intensity. Besides, only transcription factors were considered and are reflected in Table 4-5.

Table 4-5: Abbreviated list of proteins identified by mass-spectrometry after FHL1 co-immunoprecipitation.

Majority protein IDs	*Gene names*	*Protein names*	*LFQ intensity Sample04*
P78347-2;P78347-4;P78347-3;P78347	**GTF2I**	**General transcription factor II-I**	**1124400000**
Q13263;Q13263-2	TRIM28	Transcription intermediary factor 1-beta	1064900000
P25490;O15391;H0YJV7	YY1;YY2	Transcriptional repressor protein YY1;Transcription factor YY2	163930000
P20290-2;P20290	BTF3	Transcription factor BTF3	94989000
P42224;J3KPM9;P42224-2	STAT1	Signal transducer and activator of transcription 1-alpha/beta; Signal transducer and activator of transcription	30681000
O14776-2;O14776;G3V220	TCERG1	Transcription elongation regulator 1	29852000
O00267-2;O00267	SUPT5H	Transcription elongation factor SPT5	18291000
Q12800-2;Q12800-3;Q12800-4;Q12800;F8VX55;F8VWL0	TFCP2	Alpha-globin transcription factor CP2	18110000
Q6P1K8;Q13888;D6RAW1;D6RIT7;D6RGC9;R4GMS9;D6RJD3;D6RID8	GTF2H2C;GTF2H2	General transcription factor IIH subunit 2-like protein; General transcription factor IIH subunit 2	11285000

K7EN05;K7EPC8;A0A024R7E8;K7EQ44;K7EMV4;P60002	ELOF1	Transcription elongation factor 1 homolog	0
A0A024RAC6;Q14241	TCEB3	Transcription elongation factor B polypeptide 3	0
Q2TAM5;E9PKH5;A0A087X0W8;Q04206-2;Q04206-3;Q04206;Q04206-4;E9PI38;E9PQS6;E9PKV4;A0A087WVP0	RELA	Transcription factor p65	0

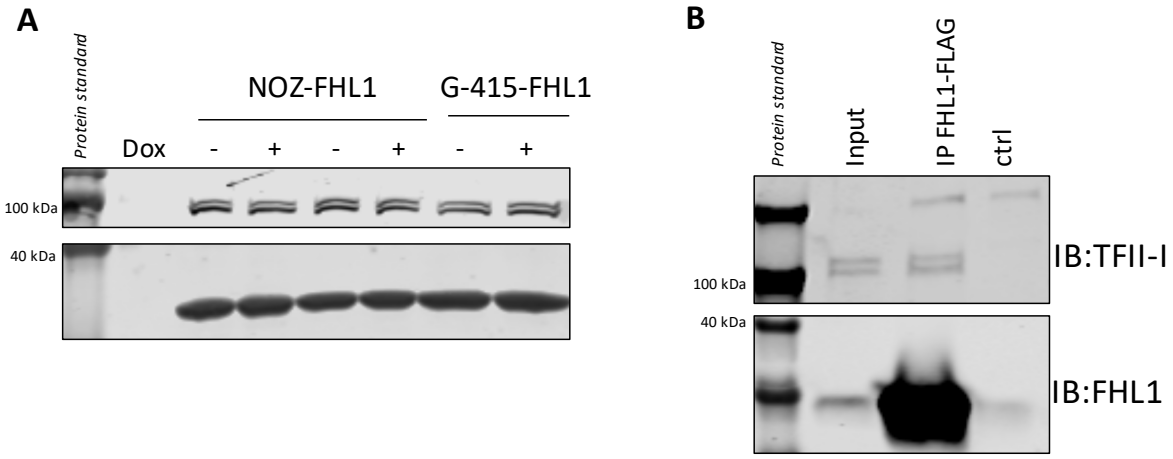

Figure 4-36: Western Blot analyses of protein TFII-I. (A) Endogenous levels of TFII-I in NOZ and G-415 after induction of FHL1 overexpression. (B) TFII-I after FHL1-CoIP. The protein is detected in the input total lysate, as well as co-precipitated with FHL1.

Due to the final phase of the study, preliminary experiments have been performed to prove the binding between FHL1 and the top of the list protein GTF2I alias TFII-I.

The Western Blot image in Figure 4-36 (A) shows the expression of TFII-I in NOZ and G-415 with and without FHL1 overexpression. The protein was endogenously expressed to similar extents in both GBC cell lines, and expression levels did not change upon FHL1 overexpression. After co-immunoprecipitation of FLAG-tagged FHL1, TFII-I was detectable in the positive control of total lysate input and co-precipitated with FHL1. This proved that FHL1 and TFII-I are interacting and could potentially regulate the transcription of target genes.

5. Discussion

5.1. MicroRNA-145-5p and PTPRF

5.1.1. MicroRNA-145-5p induces STAT1 expression and activation

In order to understand the molecular deviations taking place in the formation of cholangiocarcinoma or gallbladder carcinoma more profoundly, it is of great importance to perform genome-wide experiments to identify potential axes of dysregulation. So far, little is known about the pathological mechanisms of CCA and GBC, but due to the fact that these cancer entities usually have a fatal prognosis, it is of great interest to improve patient outcome. This will only be possible with the development of targeted therapies, making use of distinctive molecular mechanism of the disease. To approach this, the previously described microRNA microarray in gallbladder cancer specimens has been performed, revealing potentially oncogenic and tumor suppressive microRNAs.

Up to date, it has not yet been described that the tumor suppressive miR-145-5p can activate STAT1 induction apart from our studies, where miR-145-5p not only leads to STAT1 upregulation, but also to concomitant upregulation of STAT1 target genes in a mRNA microarray in the cholangiocarcinoma cell line TFK-1 [72]. To validate this, miR-145-5p was successfully overexpressed in two CCA and two HCC cell lines with comparably strong overexpression levels. Subsequent analysis of a number of target genes, derived from the microarray, showed that overexpression of miR-145-5p upregulated *STAT1* gene expression, as well as expression of the targets *IFI16, IRF9, IFI27, IFI35, MX1, UBE2L6* and *PARP9* (refer to Figure 4-3). This was predominantly the case in CCA cells. The HCC/hepatoma cells reacted less pronounced (in case of HuH1) or not at all (Hep3B). Nevertheless, given the fact that sustained inflammation also plays a part in hepatocarcinogenesis, this seems unexpected [118]. Another study found dichotomal functions for STAT1 in HCC. They investigated STAT1 in several HCC cell lines, different from the ones used in this study, so it is impossible to reproduce or negate the STAT1 protein status. However, they found that STAT1 protein expression is associated with sustained HCC cell growth, whereas phosphorylated STAT1 inhibits cell growth [119]. The latter finding is in accordance with the tumor suppressive function of STAT1, which has been previously described [64] [67] [68]. In the aforementioned study by Ma *et al.* [119], the signaling is thought to be mediated by IFNα-dependent STAT1 activation, reflecting a type I interferon reaction. This type I reaction of JAK-STAT signaling is leading to formation of activated STAT1/STAT2 heterodimers and together with IRF9, this leads to transcription of genes after binding to the ISRE (interferon-stimulated response element) on the DNA [119]. In contrast to IFNα-dependent STAT1/STAT2 activation, binding of IFNγ leads to formation of phosphorylated STAT1 homodimers and binding to GAS (gamma-activated sequence) response elements. Frequently, ISRE and GAS elements occur in the promotors for the same genes, but it has also been shown that some of these elements are occurring only exclusively, so it is likely that very specific genes can be activated by either STAT1 homodimers or STAT1/2 heterodimers. Hence, the full picture about which genes are activated in which stimulation setting is still not clear [120]. For the study of STAT1 in HCC - as the influence of IFNα-mediated STAT1 induction is leading only to marginal reduction in

cell viability or colony formation in HCC cells [119] - this could mean that the outcome might be different if a type II interferon response would be present.

The fact that STAT1 expression and induction are different in CCA compared to HCC in our own studies suggests that molecular disorders in HCC are distinct from biliary tract cancers and have to be investigated separately (Figure 4-4). Nevertheless, this could be favorable for the development of targeted therapies specific for cholangio- or gallbladder carcinoma, given the limited treatment opportunities up to date. But the questions remain, how the exact mechanism of STAT1 induction works, and how the miR-145-5p does interfere.

A possible explanation to these questions could be via the activation of an immune response. CD4+ T cells are a subset of T-helper cells, who play a major role in mediating the immune response by secretion of cytokines. CD8+ positive T cells are also known as cytotoxic T cells and are recruited to the tumor environment, where their original purpose is the elimination of tumor cells. However, they often get exhausted and dysfunctional due to tumor immune evasion after a short period of time [121]. These two groups of T cells are responsible for IFNγ secretion in the tumor environment and could lead to STAT1 activation to induce tumor suppressive signaling [122]. However, our studies revealed unaltered JAK, TYK, PIAS and SOCS proteins, thereby suggesting that STAT1 activation mediated by miR-145-5p [72] is achieved through a non-canonical mode of action.

Extensive research has been performed to elucidate the mechanism by which miRNAs downregulate proteins at the post-transcriptional level. Nevertheless, this does not seem to be their only mechanism, as studies investigated, how miRNA regulation can also upregulate transcription of a specific target mRNA. One study reports that AGO2, which still has a miRNA bound, associates with another protein, called FX1 (fragile mental X retardation) upon serum starvation (marking a stimulus for the cell, which requires a change in the metabolism) resulting in translation activation [123]. The authors conclude that AGO2 must be a subject to modification and different protein-interactions with AGO2 can lead to the switch from translational repression to induction, without the very detailed understanding of how this is functioning. Further, it has been observed that synthetic dsRNAs can upregulate gene expression through induction of transcription by binding to the promoter regions of the target genes. Since AGO2 is needed for this, the authors hypothesize that the mechanism is mediated by miRNAs or miRNA-like molecules. Because other synthetic dsRNAs fail to induce gene transcription, nor is it working in every cell line equally, this mechanism seems to be highly specific for individual cells [124]. Once more regarding the nature of the JAK-STAT signaling pathway, as being activated as a response to external stimuli, it is interesting to see that miRNAs can be bound by extracellular receptors, such as NRP1. NRP1 can take up miRNAs alone or bound to AGO2 or complexed in beads. The miRNA hereby remains functional in the cell, in which it has been internalized [125]. These observations made it intriguing, to think that miR-145-5p could function as an external stimulus for JAK-STAT signaling, but as mentioned before, no downstream signaling including the canonical proteins of the pathway, was observed in our study. However, it should be taken into account that also no positive controls were included monitoring downstream signaling after IFNγ stimulation, to prove that the pathway is not defective in the cell lines used in the study [72] (see supplemental material).

Therefore, this could be reconsidered, to strictly rule out external stimulation and to pursue the hypothesis of transcriptional activation of STAT1 through a miR-145-5p/AGO2/‘Unknown protein’-complex like in the

above described study. Another study found that STAT1 phosphorylation can be induced by dsRNA independently of INFγ. Here, the underlying mechanism – which resembles the mechanism observed in the study with synthetic dsRNAs – is originally an immune-evasion mechanism of viruses, where the virus RNA is not triggering immune response through IFNγ signaling, but via intracellular proteins that recognize RNAs and can bind them. The authors suggest, STAT1 phosphorylation can be mediated by a yet unknown factor next to the viral RNA recognition protein. The analogy to the previously described mechanism is extended towards the possibility that the unknown factor can also directly be responsible for STAT1 phosphorylation [126]. The authors also mention that STAT1 activation could be achieved by auto-phosphorylation, because it has been reported previously by Tang *et al.* that overexpression of STAT1 can already lead to activation by phosphorylation [127].

What is also interesting, independently from the mechanism of how STAT1 is activated in CCA, is to take a closer look at the downregulated target genes after miR-145-5p overexpression, as revealed by the mRNA microarray in TFK-1. There, the downregulation of the protein phosphatase PTPRF is found. Thus, concerning the regulation of sustained STAT1 activation, the role of PTPRF will be discussed below.

Taken together, STAT1 activation is achieved by a yet unknown mechanism. It is conceivable that miR-145-5p directly interacts with proteins to induce transcription/translation of *STAT1* and also inducing its phosphorylation, or another mechanism of non-canonical miRNA function, such as the stabilization of STAT1 mRNA is carried out by miR-145-5p. Subsequently, elevated levels of STAT1 could lead to STAT1 autophosphorylation, while it still cannot be ruled out that external stimuli are responsible for the initial phosphorylation of STAT1. However, the regulation of STAT1 by miR-145-5p and possibly also by PTPRF and further the regulation of PTPRF itself in dependence of miR-145-5p is very likely to play an important role in the persistence of STAT1 signaling, which could lead to tumor suppression.

5.1.2. PTPRF is Downregulated After miR-145-5p Expression and can Dephosphorylate STAT1

PTPRF is a receptor-type protein tyrosine phosphatase, therefore its classical role is the dampening of signal transduction by removing phosphate residues from proteins. However, protein phosphatases are not merely induced as a consequence of activated kinases, they can activate themselves or be activated by binding of extracellular ligands, just like receptor protein kinases, as the primary signaling event [128]. Therefore, in analogy to kinases, dysregulation of these enzymes can lead to disease. PTPRF localizes in focal adhesions (FA) and at adherens junctions (AJ) [129]. FAs and AJs are undoubtedly important for the integrity of cells in tissues and need to be tightly regulated, therefore, PTPRF could be an important regulator of cell-cell adhesions and cell-ECM interactions during processes like EMT.

Up to date, little is known about the functional implications of PTPRF in pathogenesis. It has been shown that PTPRF (also known as LAR) can target β-catenin and dephosphorylate it, thereby targeting the Wnt signaling pathway in which β-catenin exerts a signaling molecule function, leading to reduced cell migration and inhibition of a rat bladder tumor in a mouse xenograft model [59]. Another study found that PTPRF is remarkedly downregulated in gastric carcinoma and can negatively regulate ERK1/2 signaling in this tumor entity [130]. However, in prostate cancer the extracellular domain of PTPRF is strongly upregulated and was even suggested to serve as a novel plasma biomarker [131]. From a functional point of view, it has been shown that PTPRF can target death associated protein kinase (DAPK), which is presumably involved in colon cancer progression [132]. The picture of PTPRF can even be more complicated within the same tumor entity. For instance, in breast cancer, there is a study showing that PTPRF is associated with breast cancer metastasis, presenting itself as an oncogene [133], whereas another study showed a tumor suppressive effect of PTPRF in breast cancer by attenuating growth factor signaling [134]. In HCC, PTPRF is downregulated in a subset of patients and is thought to play a tumor suppressive role [61]. However, the miR-145-5p/STAT1/PTPRF axis might not be relevant for HCC, but rather for CCA (further discussed below), as there is no STAT1 induction following miR-145-5p overexpression in HCC and further no concomitant downregulation of PTPRF. Apparently, this phosphatase seems to play complicated roles in different cancer types and needs to be carefully looked at, depending on the tumor entity and the respective cellular molecular background.

Our studies showed that PTPRF protein expression was decreased after the overexpression of the tumor suppressive miR-145-5p (Figure 4-6). This observation suggested the assumption that PTPRF mRNA contains a miR-145-5p binding site and is downregulated by the action of the miRNA. The *In silico* miRNA-gene target prediction tool miRWalk2.0[9], when used for 'Putative target genes predicted by chosen algorithms within mRNA selected regions' of miR-145-5p revealed two algorithms (miRWalk and RNA22) predicting the binding of miR-145-5p to the 3'-UTR of PTPRF. However, direct binding could not be observed in this study. This could be due to the experimental setting, or it means that miR-145-5p is not directly interacting with PTPRF mRNA and exerts its regulatory function via intermediate factors or at the protein level.

It is interesting to see that PTPRF reduction is correlating with the STAT1 activation mediated by miR-145-5p. Further, the miR-145-5p mediated STAT1 induction seems to be more relevant in CCA, than in GBC, since in the only GBC cell line Mz-ChA1, miR-145-5p overexpression is neither leading to STAT1 increase nor to activation of STAT1 on protein level and at the same time, also no PTPRF reduction was observed. This suggests a different relevance of the miR-145-5p/STAT1/PTPRF axis in CCA compared to GBC. This hypothesis needs to be validated in further GBC cell lines. Apart from that, the reduction of PTPRF hints towards a negative mechanism of PTPRF expression when STAT1-mediated transcription is active. Since it is very likely for STAT1 to be a direct subject to dephosphorylation by PTPRF, as shown by the co-immunoprecipitation results, PTPRF may attenuate STAT1 signaling, however, it is downregulated after sustained STAT1 signaling. It has not been shown to be a direct STAT1 target so far though. Furthermore, this is the first time describing STAT1 to be a likely candidate of dephosphorylation by PTPRF (Figure 4-7). The reason for successful co-immunoprecipitation between the commercially bought mutated form of PTPRF and STAT1 in an unstimulated manner is presumably attributed to the chemical nature of the amino

[9] http://zmf.umm.uni-heidelberg.de/apps/zmf/mirwalk2/index.html

acid threonine instead of isoleucine. After re-mutation of threonine to isoleucine, interaction between P-STAT1 (Y701) and PTPRF was detectable only after IFNγ stimulation, which proves *in vitro* binding of PTPRF to activated STAT1. An explanation for the co-precipitation of mutated PTPRF and STAT1 could be that threonine contains a polar hydroxyl-group in the side chain, whereas isoleucine carries an aliphatic side chain, hence, it is a non-polar amino acid. The polar hydroxyl group raises the probability for more intermolecular interactions, especially for the formation of hydrogen bonds, whereas the non-polar side chains of isoleucine is restricted to van-der-Waals electrostatic interactions, which are much weaker [135]. Therefore, it could be possible that unphysiological interactions were occurring between mutant PTPRF with the polar side chain and STAT1.

5.1.3. SUMMARY PART I

In summary, PTPRF is reduced by miR-145-5p. Whether this happens in a direct or indirect mechanism remains unresolved. By reducing the expression of PTPRF, the attenuating effect of PTPRF on STAT1 signaling is reduced and the phosphorylated state of STAT1 is sustained with subsequent transcription of tumor suppressive genes. The role for PTPRF in CCA would hence be of oncogenic nature, which would describe a novel role for PTPRF in CCA contrasting its mode of action in HCC.

The activating Y701-phoshorylation of STAT1 is induced after overexpression of miR-145-5p. This might be initially mediated to some extent by a cytokine or growth factor and subsequent intracellular signaling which could lead to substantiation of STAT1 activation. Here, miR-145-5p could act directly or indirectly as an activator of STAT1 signaling. This could create a positive feedback loop where STAT1 will increase its own transcription and because of the high expression levels, auto-phosphorylation could occur. Ultimately this may lead to sustained STAT1-mediated transcription of tumor suppressive genes.

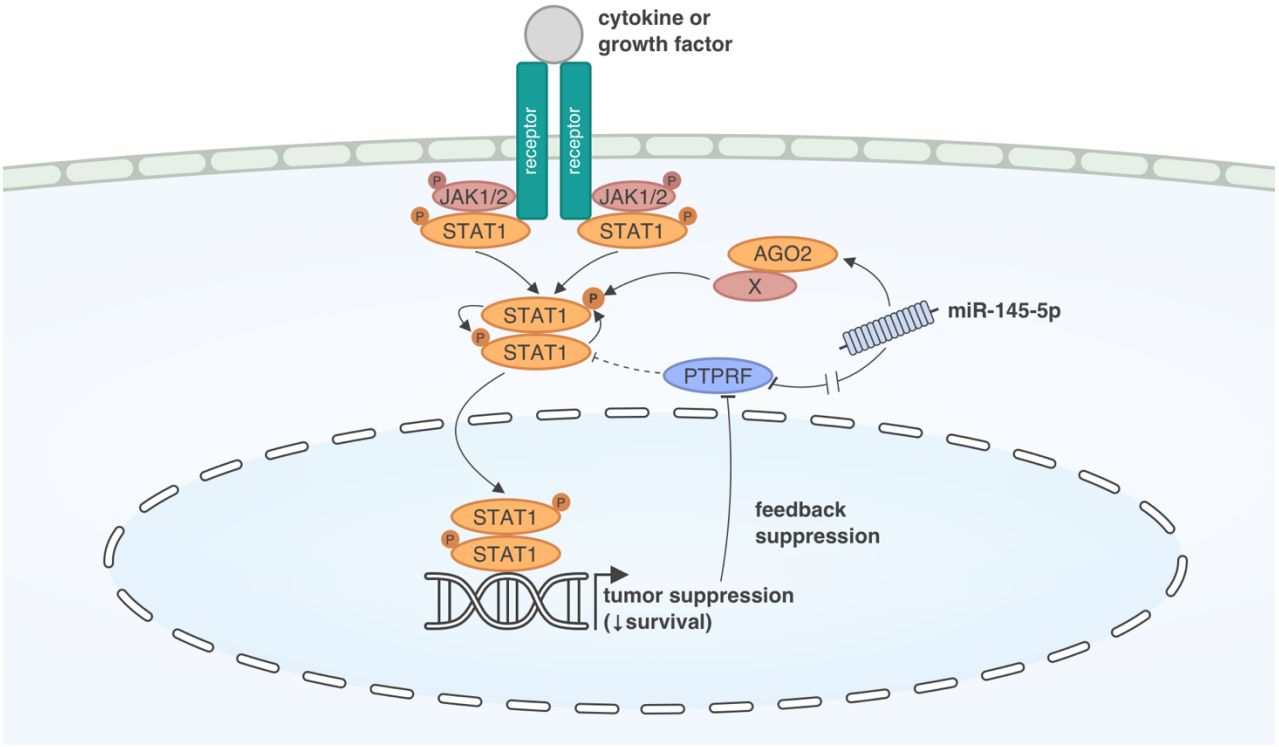

Figure 5-1: Schematic model of miR-145-5p-mediated activation of STAT1 signaling: In CCA tumor cells miR-145-5p expression leads to repression of the phosphatase PTPRF, which reduces the attenuating effect of PTPRF on STAT1 signaling. Ultimately, STAT1 phosphorylation and therefore, STAT1 transcriptional activity is sustained.

5.1.4. Outlook Part I

With our studies, we were able to show that the abundance of the tumor suppressive miR-145-5p is correlating with increased STAT1 expression and also with STAT1 activation, as well as decreased PTPRF expression, leading to tumor suppression in CCA cell lines. This effect seems to be specific for CCA and not occurring in HCC. PTPRF expression is likely to be able to attenuate tumor suppressive signaling by dephosphorylation of STAT1, redirecting STAT1 towards proteasomal degradation. Therefore, it could be a useful therapeutic approach to develop a small molecule inhibitor for PTPRF and investigate its effect on CCA. This could give rise to a targeted therapy for CCA, which is of great interest, due to the lack of specific or effective therapies for unresectable CCA.

From a mechanistic point of view, it would be interesting to deduce the exact mechanism between miR-145-5p and STAT1 induction. This could possibly be achieved by the use of STAT1-mutants which cannot

be phosphorylated anymore and investigate STAT1 status and cellular behavior upon miR-145-5p expression. Another interesting experiment would be to perform AGO-CoIP followed by mass-spectrometric analysis of associated proteins, to identify possible interactors with STAT1 and/or miR-145-5p. This is likely to be challenging basic research in miRNA functions.

5.2. Proteomics Revealed FHL1 as Novel Tumor Suppressor

5.2.1. FHL1 is Downregulated in Gallbladder Cancer

Performing proteomics from FFPE tissues is very challenging, as it is difficult to retrieve proteins from these archived samples with varying conditions, and then still obtain successful proteolytic cleavage to produce peptides small enough for mass-spectrometry. However, our collaborators have previously established a successful protocol to do so, achieving a good resolution of the resulting proteomes providing enough information for deep analysis [101]. Consequently, we were able to apply this technique to identify the proteomes from gallbladder cancer and healthy gallbladder samples using a shotgun approach (Figure 4-8). The discovered proteins were quantified by use of isobaric mass-labeling and allowed for quantitative measurements. On the path to discover new tumor suppressive proteins, which can be put in anti-correlation to the oncogenic microRNAs (primarily to miR-4502) detected in the miRNA profiling of the previous study, we focused on the downregulated proteins.

Analysis of the enriched pathways among the downregulated proteins led to the first general ideas of molecular dysregulation in GBC (see Figure 4-9 and Figure 4-10). It was interesting to see that many proteins involved in cytoskeleton organization and adhesion were downregulated. This is mirroring the nature of GBC, as it is usually not a big growing tumor, but readily metastasizing [136]. Further, the gene ontologies (GOs) identified, provided clues about the nature of relevant candidates. This is how FHL1 was deduced, as it is a very significantly and highly downregulated protein. FHL1 is a zinc-binding protein with multiple protein-protein interaction sites and according to information provided by the UniProtKB database, it is annotated in GOs of biological processes such as cell differentiation and negative regulation of cell-cycle/cell growth. Further, it is known to be distributed all over the cell, including cytosol, nucleus, plasma membrane and in focal adhesions, as can be seen in the UniProtKB entry of FHL1[10]. The protein is very abundant in muscle cells, albeit not exclusively, and mutations in FHL1 can lead to muscular degenerative diseases. However, there is accumulating evidence that dysregulation, but not mutation, of FHL1 is implicated in many cancer types. So far, FHL1 has largely been described as tumor suppressor. For instance, in lung cancer

[10] https://www.uniprot.org/uniprot/Q13642

and tongue squamous adenocarcinoma cells, overexpression of FHL1 exerts growth inhibitory functions by arresting the cell cycle [108] [111]. Further, FHL1 can act on transcriptional regulation. One study found that FHL1 overexpression in estrogen-responsive breast cancer cells downregulates ER-mediated transcription through physically interacting with the ER, resulting in inhibited breast cancer cell growth [137]. Further, apoptosis induction in T cell acute lymphatic leukemia was achieved by overexpression of FHL1. In the respective study, FHL1 was shown to bind the co-activator RBPJ, which is required for NOTCH1 signaling. This results in decreased NOTCH1 target gene expression and subsequent apoptosis induction but this study did not elucidate the exact mechanism of apoptosis induction [110]. Another study suggested tumor cell growth inhibition through FHL1, by mediating TFG-β like-signaling. The authors proposed that FHL1 activates SMAD transcription factors through Casein kinase 1δ and the subsequent expression of tumor suppressive genes, lacking the external stimulation by TFG-β [116]. However, there are also studies describing FHL1 as oncogene. One profound study elucidates that FHL1 is switched from tumor suppressor to oncogene through phosphorylation mediated by Src. This phosphorylation leads to interaction with nuclear BCLAF1, which has already previously been shown to induce colon cancer cell growth. The authors conclusion is that BCLAF1 together with phospho-FHL1 is leading to tumor growth promotion [113]. Another unfavorable scenario mediated by FHL1 is the promotion of chemoresistance in HCC cells through caspase 3 activation, however, no mechanistic explanation was provided [138]. Transcription of FHL1 itself is downregulated by Cas, which is activated by Src, and the downregulation of FHL1 is leading to non-anchored cell growth and migration of tumor cells [139]. This may support the tumor suppressive role of FHL1 by the protein itself.

The epigenetic regulation of FHL1 also seems to play an important role in some malignancies. It has been reported that FHL1 is epigenetically silenced in HCC [140], as well as in head and neck squamous cell carcinoma [141]. It has also been reported that miR-410 can downregulate FHL1 via a direct or indirect mechanism, leading to enhanced tumor cell growth. This shows that FHL1 can also be a subject of regulation by miRNAs [142].

Many of these studies are quite recent, which reflects the huge impact of FHL1 dysregulation, yet without understanding in detail, how FHL1 is regulating cell homeostasis and carcinogenesis in varying cell types. It addition, FHL1 plays conflicting roles in different studies. Combined with the strong and very significant dysregulation we found by mass-spectrometry, this protein constituted a highly interesting candidate as potential tumor suppressor for GBC.

Up to date, no immunohistochemical analysis of FHL1 in GBC has been performed apart from our studies, but concomitant with the observations that FHL1 is frequently downregulated in different tumor entities (such as lung, prostate, breast, ovarian, colon, thyroid, brain, renal, liver, gastric and melanomas [143]), we showed that FHL1 is significantly downregulated in gallbladder cancer samples (see Figure 4-17). Additionally, this observation is confirming the mass spectrometric analysis, where FHL1 was found to be downregulated.

5.2.2. FHL1 IS A DIRECT TARGET OF ONCOGENIC MIR-4502

The miRNA miR-4502 was identified in the aforementioned miRNA profiling as an oncogenic miRNA, which is upregulated in gallbladder cancer samples compared to healthy gallbladder. So far, no targets for miR-4502 have been experimentally established. Using the online mirWalk 2.0 miRNA prediction algorithms, two out of four algorithms (miRanda and TargetScan) predicted *FHL1* mRNA to be a target of miR-4502. This would further substantiate the assumed tumor suppressive role of FHL1. Overexpression of miR-4502 markedly decreased the abundance of FHL1 protein and vice versa, the inhibition of miR-4502 led to an increase of FHL1 in a gallbladder cancer cell line. Subsequently, by using a luciferase assay to investigate binding of miR-4502 to the *FHL1* mRNA, we were able to show that FHL1 is a direct target of miR-4502 in gallbladder cancer in this study. MiR-4502 is targeting the 3'-UTR of *FHL1* mRNA, ultimately leading to decreased protein levels of FHL1 (see Figure 4-13).

5.2.3. FHL1 EXHIBITS TUMOR SUPPRESSIVE EFFECT IN CELL CULTURE FUNCTIONAL ASSAYS

Our studies continued to investigate the tumor suppressive effect of FHL1 in cell culture based functional assays. For this purpose, we used the stable integration of the FHL1 gene in GBC cell lines, with the conditional expression of FHL1 under the control of a doxycyclin-sensitive promoter. Hence, expression of FHL1 is controlled and induced at definite time points. However, it has to be mentioned that FHL1 is already endogenously expressed in NOZ, albeit much less compared to after induction. Interestingly, one study on tongue squamous cell carcinoma (TSCC) found results in logical conjunction to what we found. They detected inhibition of anchorage-dependent growth by silencing FHL1 in a soft agar assay and a subsequently increased number of cell colonies in the assay. This is mirroring our observation with reduced colony formation in GBC cell lines after overexpression of FHL1, being the counterpart of the experiment (Figure 4-32 and Figure 4-33). Our findings could be further substantiated by repetition of the assay with silenced FHL1. The authors of the aforementioned study furthermore found no impact on cell migration or invasion after FHL1 silencing [111]. We did not perform experiments for cell invasion, as there were initially no results for migration (see Figure 4-30). FHL1 overexpression did not alter the velocity of wound closure in our experiments. This is in contrast to other studies showing that FHL1 is implicated in cell-cell contact. Another study by Zhi *et al.* performed in HEK embryonic kidney cells and a neuronal cell line, found an increase of cell migration after FHL1 silencing. The effects they observed are marginal but significant. However, they performed a different assay to measure migration. They used a transwell assay, instead of a wound healing assay which might be a reason for the discrepancy. The increase in proliferation the authors Zhi *et al.* found after FHL1 silencing is also quite small [144]. They state that they performed an assay, which is measuring cell proliferation, but it is based on the sample principle as the cell viability assay in the here

presented studies. To be precise: they were using a CCK8 assay. This chemistry behind this assay consists of a water-soluble tetrazolium salt, which is turned into an orange formazan dye upon a biological reduction reaction. The intensity of the orange staining is allowing the quantification of living cells. Our assay is similar, we used Resazurin, which is a phenoxazine turning from blue to pink when reduced by metabolically active cells. It is believed that these kinds of assay might reflect cell proliferation, but matter-of-factly they are showing cell viability. Nevertheless, this is still a useful assay in order to investigate tumorigenic potential of proteins. The observed effects of the study are in line with our studies, after overexpression of FHL1, the cell viability was reduced in GBC cells (Figure 4-31). In NOZ cells more drastically than in G-415, but still significantly in both cell lines. This decrease is not mediated by the impact of doxycycline on the cells, since the control cells with ALB induction did not show the same effect. Another published study investigating breast cancer cells, shows similar results. There, the authors observed reduced cell viability after FHL1 overexpression and an increase after FHL1 silencing. Further, they found an increase in colony formation after FHL1 silencing [137]. A study on head and neck squamous cell carcinoma (HNSCC) cells also found similar tumor suppressive effects of FHL1 on cell viability and colony formation [141]. Taken together, our experiments on colony formation and cell viability are in accordance with a tumor suppressive phenotype of FHL1 overexpression.

To study further how FHL1 is impacting cellular behavior and if it is targeting cell proliferation, additional assays to measure proliferation have been carried out (Figure 4-34 and Figure 4-35). For instance, the protein status of nuclear Ki67 shows, whether a cell is preparing for division and therefore, the fraction of dividing cells can be measured by calculating Ki67-positive nuclei over total nuclei (excluding cells already in mitosis). Our studies showed that cell proliferation was significantly decreased inG-415 cells after FHL1 overexpression, however, this was not observable in NOZ. This could be partially explained by the stronger endogenous expression of FHL1 in NOZ, meaning that additional FHL1 induction is not having a strong enough impact to alter the cellular homeostasis. However, they do show a trend towards decreased proliferation. To enhance the insight into the proliferation activities, a BrdU-ELISA assay has been performed, to measure cell proliferation of FHL1 overexpressing cells by a different method. Here, additional GBC cell lines were used with the help of Raisatun Sugiyanto. The additionally introduced GBC cell lines were GB-d1, SNU308 and TGbC-1. GB-d1 have very little endogenous FHL1 mRNA expression, SNU308 also shows low levels of FHL1 expression, whereas TGbC-1 has more, but not as much endogenous FHL1 expression as NOZ cells. Apart from the NOZ cell line, all other GBC cell lines displayed a significant decrease in cell proliferation upon FHL1 overexpression. These findings confirmed the Ki67 staining results, in which NOZ cells did not show an effect, but G-415 showed a significant decrease in proliferation. These results led to the conclusion that FHL1 overexpression is inhibiting cell proliferation. This conclusion could further be substantiated by performing cell cycle analysis by FACS or evaluating the status of cell cycle-relevant proteins to show that the cell cycle is arrested by FHL1 overexpression. Previously published literature has shown that FHL1 overexpression is leading to a cell cycle arrest in the G1 phase in squamous cell carcinoma of the tongue (TSCC) [111] and head and neck squamous cell carcinoma (HNSCC) [141].

The role of FHL1 on colony formation has extensively been addressed in our studies (see Figure 4-32 and Figure 4-33). Not only the effect of FHL1 overexpression alone, also if it is concomitantly overexpressed with

the oncogenic miR-4502 or the miR-4502-inhibitor. This also revealed the possibility to compare the off-DOX states (when there is only natural endogenous FHL1 expression), showing the different effects of the AllStars control, the miR-4502 overexpression or the inhibitor. It was expected that overexpressing miR-4502 would increase the colony formation without DOX and be reduced again, when FHL1 is overexpressed after DOX-induction. However, we only saw a partial rescue. In G-415 cells colony formation was increased after miR4502, but due to pronounced variability, no significance was reached between the off-DOX states. In NOZ cells, this trend was not observable, but this could be explained analogously to before with the fact that NOZ cells are endogenously expressing more miR-4502 than G-415, and they might not be impacted by the overexpression (see Figure 4-12). For both cell lines however, when FHL1 was overexpressed, the colony formation was significantly reduced. Another approach was to use miR-4502- inhibitor but it did not lead to a reduction in colony formation. However, we could demonstrate that overexpression of miR-4502-inhibitor is leading to an increase of endogenous FHL1 expression (see Figure 4-13). The strongest factor impacting the capability of forming colonies ,was the stable overexpression of FHL1 alone, which led to a significant decrease of colony formation in both cell lines in the direct comparison of the off/on-DOX states. Taken together, the biological experiments proved that FHL1 is able to decrease cell proliferation and anchorage-dependent cell growth and thus, FHL1 is acting as a tumor suppressor.

5.2.4. FHL1 DOES NOT INFLUENCE EMT, METABOLISM OR PROMOTE SMAD SIGNALING

The investigation of EMT genes was performed, to see if dysregulation of these genes represents the downregulation of the GOs for biological and cell adhesion. Even though FHL1 has been described as tumor suppressor, hardly any studies exist about its implication on EMT of cancer cells. Although this seems to be a relevant idea, given the fact that it is localized in FAs and the plasma membrane. One study describes that FHL1 is interacting with the ZO-1 protein of tight junctions and together, they might mediate the EMT of breast adenocarcinoma cells [145], which would suggest a tumorigenic role of FHL1. However, they were not able to elucidate the exact mechanism. In another study, FHL1 was detected in mesenchymal cells and not in epithelial cells, but due to the complex nature of FHL1 the authors summarized that the function of this protein remains unknown [146]. For this study, we were investigating a few EMT genes relevant for HCC, to find out if FHL1 overexpression would interfere with EMT gene expression [147]. However, no significant changes in the EMT genes *CDH1* (coding for E-cadherin), *SNA1, ZEB, TWIST* or *VIM* were found (refer to Figure 4-19). The only finding, which is potentially supporting a dampening effect of FHL1 on EMT, is the trend of increase in *CDH1* expression in gallbladder cancer cells. This could be further investigated in additional cell lines to evaluate, whether FHL1 could have an impact on EMT.

Another question we asked was, whether FHL1 can impact cell metabolism, as we identified multiple proteins downregulated in the mass-spec data that are implied in bile acid metabolism. The only gene regulated by FHL1 overexpression we could confirm was *AMACR,* which was upregulated. The encoded enzyme interconverts pristanoyl-CoA and C27-bile acyl-CoAs between their (R)- and (S)-stereoisomers, which is necessary for subsequent beta oxidation. So far, it has been investigated for the use as prognostic marker in GBC and was found upregulated and associated with advanced primary tumor status [148]. This is in contrast to what we found, because in our data, AMACR was significantly downregulated (refer to Table 4-4). Further, being upregulated in cancer and being associated with poorer survival, it is likely not to exert tumor suppressive functions.

An interesting finding of our studies was the failure to reproduce SMAD activation by FHL1 (Figure 4-22). There is a single study suggesting that FHL1 was interacting with CK1δ, which in turn would phosphorylate SMAD2 and SMAD3 in HCC cells. SMAD4 was also necessary to finally lead to the transcription of tumor suppressor p21 [116]. To the present knowledge, this is the only study reporting that SMAD is activated through FHL1. We were not able to detect any phosphorylation of SMAD2/3 upon the overexpression of FHL1. However, SMAD4 and CK1δ expression was not investigated separately in these samples, so it is not to be entirely ruled out that these proteins might not be expressed, and therefore no activation of SMAD2/3 is achieved. But according to the human protein atlas, CK1δ is ubiquitously highly expressed and SMAD4 also exhibits medium to strong expression in gallbladder, therefore it is unlikely that these proteins are not expressed, and we simply were not able to show the same effect of FHL1. Another possible explanation could be – as repeatedly pointed out before – that the situation in hepatocellular carcinoma might be differing from the mechanism in gallbladder cancer and this pathway might not be implicated in the latter.

5.2.5. FHL1 IS COMPETING WITH NOTCH1 AND CAN DOWNREGULATE NOTCH1 TARGET GENES

Our initial approach to investigate the possible regulators of FHL1 led us to the idea that FHL1 and NOTCH signaling interact. This was further substantiated by the analysis of FHL1 and its interactors, curated by the STRING database for protein-protein interactions. There, it was found that FHL1 is binding to RBPJ, which is the main mediator for NOTCH-dependent transcriptional activity [80].

It has been previously shown that FHL1 is able to inhibit NOTCH-mediated transcription in the mammalian cell line COS-7[149]. This cell line is derived from the African green monkey, so it was not proven that FHL1 could also downregulate NOTCH-mediated transcription in human cells. However, in our studies, we were able to confirm the FHL1-dependent decrease of: firstly NOTCH1-mediated transcriptional in activity human cancer cells (Figure 4-26) and secondly that this reduced NOTCH1 activation is also leading to downregulated oncogenic NOTCH1 target genes (Figure 4-27). Therefore, this would explain at least partially how FHL1 can act as tumor suppressor, namely by the downregulation of oncogenic NOTCH1 signaling. Also, FHL1 is

downregulated by NOTCH signaling, most likely in a negative feedback mechanism. We then tried to elucidate, whether FHL1 can bind the RBPJ-NOTCH1 complex at the same time to affect NOTCH1 target gene transcription, or if FHL1 and NOTCH1 are excluding each other. Up to date, this has not been investigated. We found that FHL1 and RBPJ co-precipitate, as well as RBPJ and NOTCH1, but FHL1 and NOTCH1 are not binding to each other, which suggested that FHL1 and NOTCH1 are excluding each other in a protein complex.

It has been shown that FHL1 (formerly known as KyoT protein) is able to bind to RBPJ, resulting in the downregulation of NOTCH1 and EBNA2-mediated transcription in mouse [149]. Our studies confirm the direct decrease of NOTCH1-mediated transcriptional activity of about 50% in gallbladder cancer cell lines with intrinsic N1ICD expression by luciferase reporter assays. Subsequently, this resulted in the downregulation of the investigated NOTCH1 target genes *HES1, HEY1, C-MYC* and *HSPB6* [150]. The NOTCH1 pathway is relevant for gallbladder cancer formation, as it has been reported that upregulation of NOTCH1 signaling by mutated Kras is leading to early stages of gallbladder carcinoma in a mouse model. Concomitantly with our studies, upregulation of *Hes1* and *Hey1* have been detected in a study by Xu *et al.* [151]. However, there are some issues that have to be mentioned. First of all, using an animal model to study gallbladder cancer is very rare, as there is no knockout/knockdown mouse model specific for GBC available. Further, they a used mouse model that makes use of mutated Kras, which is a mutation found mainly in GBCs that arise from abnormal pancreatobiliary junctions (APBJ) and are found only in late stages in GBCs arising from cholelithiasis. So, there might be the possibility that only a subset of GBCs is represented in the study, which might be slightly different in the genetic background. Furthermore, the developing cancers reflect early onset adenomas and low-grade adenocarcinoma and do not progress into invasive carcinomas. This suggests that additional molecular changes are required. Nevertheless, this study proved that upregulated NOTCH1 signaling with the target genes *Hes1* and *Hey1* has a tumor-promoting effect in GBC.

C-MYC is a well-known proto-oncogene and is upregulated in gallbladder cancer, however, not to a very strong extent. In a study of 126 gallbladder cancer samples, c-MYC was only upregulated in about 9% of primary GBCs and 26% in metastases, but with 23 as the total sample size of metastatic lesions, the upregulation of c-MYC was rather low. Taken together, c-MYC expression has been detected in about 10% of cases and is significantly higher expressed in metastases than primary GBCs [152]. From a functional point of view, it has been found that c-MYC upregulates miR-19a, which leads to GBC cell migration and invasion [153]. For HSPB6, there are no studies about its implication in gallbladder cancer. In HCC, it has been shown that phosphorylated HSPB6 inhibits cell migration and invasion, therefore displaying tumor suppressive functions [154]. In GBC the function remains unclear. Thus, the majority of the investigated genes, which were affected by FHL1-mediated NOTCH1 inhibition, exhibits potential tumorigenic effects in GBC and FHL1 may exert its tumor suppressive function at least partially through attenuation of NOTCH1-mediated oncogenic signaling.

In addition, our findings showed that FHL1 and N1ICD most likely bind mutually exclusively to RBPJ, as there is no co-immunoprecipitation between FHL1 and N1ICD possible. However, it is still not be ruled out that both proteins bind to RBPJ without physical interaction between themselves. Nevertheless, FHL1 is dampening the transcriptional activity of N1ICD, which supports the tumor suppressive role of FHL1 in a

context of N1ICD tumorigenic activity. Furthermore, as FHL1 has also been shown to co-precipitate with the transcription factor TFII-I (Figure 4-36) in our studies, modulation of RBPJ activity is likely not to be the only way of how FHL1 could interfere with transcriptional regulation.

Interestingly, FHL1 seems to be regulated by NOTCH1 and NOTCH3 both on protein, as well as on transcriptional level. It has not been investigated so far, how FHL1 can be controlled, so our studies provide the first hint that FHL1 is downregulated after NOTCH signaling. This could mean that the FHL1-mediated functions for the cell are in contrast to the NOTCH-mediated ones. More precisely, this suggests that FHL1 is actively repressed by the cells when they are in need of developmental or proliferative programs. This would support an indispensable role for FHL1 in cell homeostasis, rather than for FHL1 being relevant for dynamic changes in the cellular behavior. Furthermore, this notion would support the experimental outcomes in the previous section (chapter 5.2.3), meaning that in cell culture assays for functional characterization, FHL1 overexpression is leading to rather mild tumor suppressive effects. This could be explained, with FHL1 showing indeed tumor suppressive characteristics, but probably being more important for the steady state of cells.

5.2.6. Summary Part II

The mass-spectrometric analyses of gallbladder cancer specimens and healthy gallbladder tissues revealed that FHL1 is one of the most strongly and significantly downregulated proteins in GBC compared to healthy. Thus, taken together with FHL1 belonging to downregulated gene ontology terms in GBC, the protein constituted a promising target to be investigated further in terms of potential tumor suppression. Pro- and anti-tumorigenic functions of FHL1 have previously been reported in different tumor entities, however its role in gallbladder cancer has never been addressed. We showed that FHL1 is a direct target of the previously identified oncogenic miR-4502, resulting in downregulation of FHL1. Further, FHL1 is binding to RBPJ, which is the main mediator of NOTCH1-induced signaling. Either, only FHL1 or N1ICD seems to be able to bind to RBPJ at the same time, suggesting that N1ICD and FHL1 are competitors. NOTCH1 signaling is also leading to the transcriptional and translational repression of FHL1. If FHL1 is overexpressed, NOTCH1 target genes are reduced, suggesting a 'balance mechanism' between the complexes FHL1-RBPJ and NOTCH1-RBPJ, with FHL1-RBPJ shifting the equilibrium to its side, resulting in reduced NOTCH-mediated transcriptional activation. This is the first time observing this balance mechanism with FHL1 as a direct competitor of NOTCH in binding to RBPJ in GBC. Whether FHL1, together with additional cofactors, could lead to a transcriptionally active complex, which actually induces the expression of other tumor suppressive target genes remains to be resolved.

In the oncogenic environment in GBC cell lines, NOTCH signaling is overactive and miR-4502 is downregulating FHL1, hence the decreased levels of FHL1 are incapable of counter-balancing the oncogenic signaling through NOTCH1. By restoring or inducing FHL1, there is competition between FHL1 and N1ICD in

favor of binding to RBPJ, which leads to a reduction in NOTCH1-mediated transcription and leading from an oncogenic to more tumor suppressive phenotype.

Another aspect of FHL1-mediated tumor suppression is the ability to decrease cancer cell proliferation and anchorage dependent cell growth, however, the exact mechanisms behind this remain to be resolved. Given the implication of FHL1 in plasma membrane structures, such as FAK and junctions, it is perceivable that the investigated functions of FHL1 in transcriptional regulation might not be the only relevant functions FHL1 could have. Here, additional studies have to be addressed.

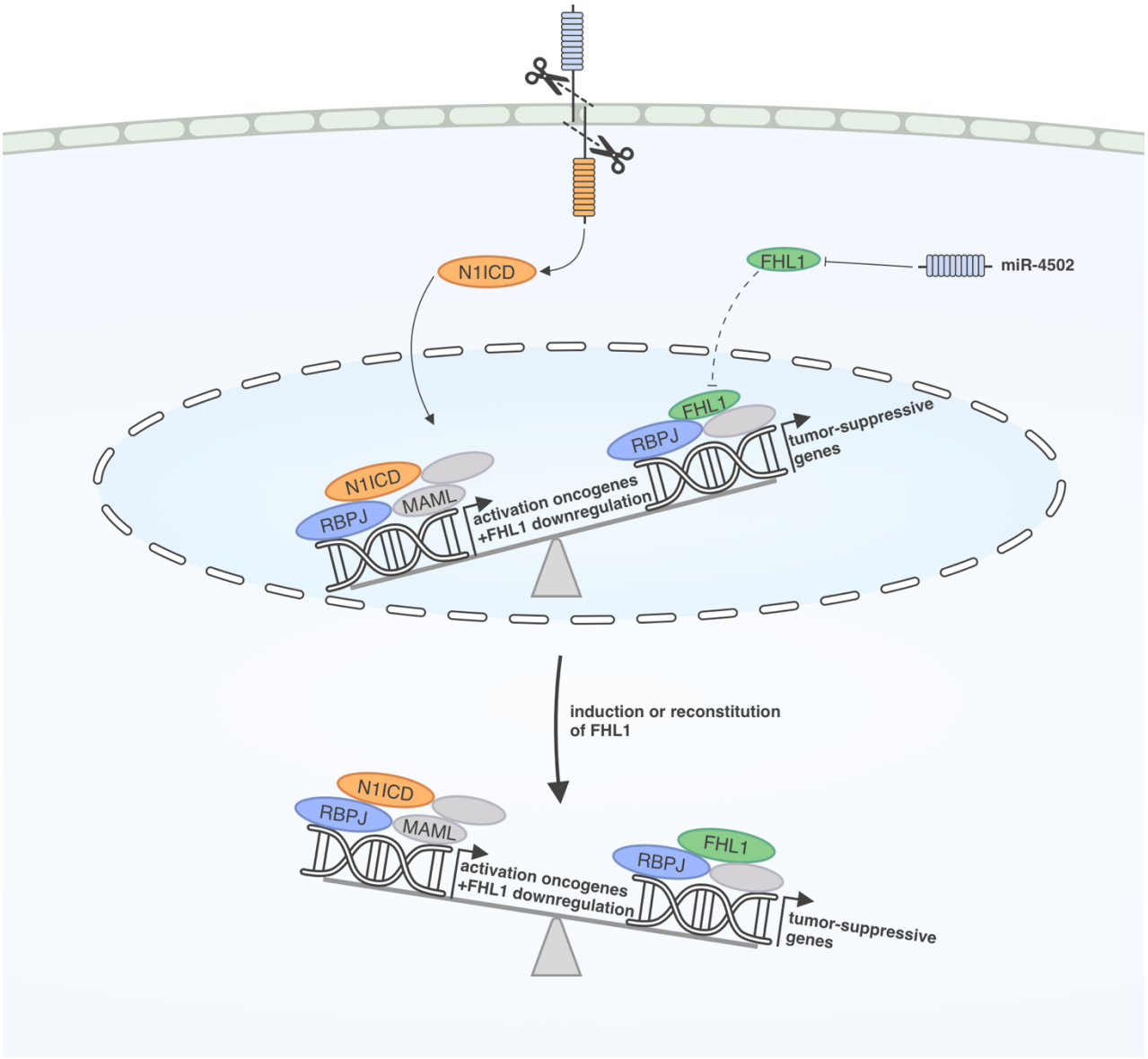

Figure 5-2: Schematic model for the role of FHL1 in GBC in respect to NOTCH1 signaling. Overactive NOTCH1 signaling and the presence of miR-4502 creates an oncogenic environment in GBC, with subsequent downregulation of FHL1. Hence, FHL1 cannot exert its dampening effect on oncogenic NOTCH1-mediated transcription. When FHL1 is reconstituted in GBC, the balance

between NOTCH1-medited oncogenic signaling is shifted towards repressed NOTCH1 transcription, leading to a more tumor suppressive environment for the cells.

5.2.7. OUTLOOK PART II

In this study, FHL1 was identified as potential tumor suppressor in GBC. It is likely to regulate transcriptional activity, however, FHL1 target genes are unknown so far. In order to elucidate the impact on gene expression mediated by FHL1, it needs to be deduced if there are genes directly regulated by FHL1. In initial experiments, we performed a mRNA microarray in the absence and presence of FHL1 overexpression but due to technical issues, no statistically significant results could be obtained. However, another way of addressing transcriptional regulation by FHL1, would be to perform FHL1 ChIP-Seq analyses to reveal important genes regulated by FHL1.

Additionally, the role of FHL1 as tumor suppressor needs to be confirmed by *in vivo* experiments. To date, only few mouse models for gallbladder cancer exist. These include models using ErbB2 overexpression in the biliary epithelium, but these animals also develop skin tumors and only about 50% of mice develop GBC. Another possibility to study GBC in mice is by xenograft mouse models of cancer cells in immune-deficient mice.

The evidence for FHL1 to be a tumor suppressor in GBC is solid, however, most likely it is not an 'all-or-nothing' mechanism. FHL1 alone is not completely repressing tumor cell growth and survival, but it should be taken in account that modulating FHL1 together with other tumor suppressors or oncogenic proteins could result in a synergistic effect, mediating strong tumor suppression. One of these additional factors might be NOTCH signaling. Therefore, this study provides the foundation to develop targeted therapies by addressing FHL1 in combination therapies. It has not been shown that FHL1 is a direct target of the oncogenic miR4502 before, so targeting this axis could result in sufficient tumor suppression. FHL1 could – apart from inducing the protein on transcriptional level – potentially be activated by blocking miR-4502, resulting in stronger induction of FHL1. However, more functional studies on miR-4502 need to provide better insight in its molecular function, apart from targeting FHL1, to see if this could serve as an additional cornerstone in developing a targeted therapy for GBC.

Furthermore, the datasets generated in this study by mass-spectrometric analysis resulted in the identification of a large number of dysregulated proteins in GBC. Thus, there is still a plethora of information about potential tumor suppressors and oncogenes in GBC available, which will be followed up in future studies.

REFERENCES

1. Tariq NU, McNamara MG, Valle JW. Biliary tract cancers: current knowledge, clinical candidates and future challenges. Cancer Manag Res 2019;**11**:2623-42 doi: 10.2147/cmar.S157092
2. Netter FH. *Atlas der Anatomie des Menschen*: Novartis, 2000.
3. Lüllmann-Rauch R. *Histologie*: Thieme, 2009.
4. Heinrich S, Birth M, König S, Markus PM. Anatomie und Physiologie. Hepatobiliäre und Pankreastumoren. Berlin, Heidelberg: Springer Berlin Heidelberg, 2010:2-13.
5. Manohar R, Li Y, Fohrer H, et al. Identification of a candidate stem cell in human gallbladder. Stem Cell Res 2015;**14**(3):258-69 doi: 10.1016/j.scr.2014.12.003
6. Schott E, Bergk A, Büchsel R, et al. Epidemiologie, Ätiologie und Pathogenese. Hepatobiliäre und Pankreastumoren. Berlin, Heidelberg: Springer Berlin Heidelberg, 2010:14-37.
7. Bridgewater JA, Goodman KA, Kalyan A, Mulcahy MF. Biliary Tract Cancer: Epidemiology, Radiotherapy, and Molecular Profiling. American Society of Clinical Oncology Educational Book 2016(36):e194-e203 doi: 10.1200/edbk_160831
8. Mondaca S, Nervi B, Pinto M, Abou-Alfa GK. Biliary tract cancer prognostic and predictive genomics. Chinese Clinical Oncology 2019;**8**(4):13
9. https://www.cancer.net/cancer-types/bile-duct-cancer-cholangiocarcinoma/statistics. Cholangiocarcinoma: Statistics
10. https://www.cancer.net/cancer-types/gallbladder-cancer/statistics. Gallbladder Cancer: Statistics
11. Zhu AX, Hong TS, Hezel AF, Kooby DA. Current management of gallbladder carcinoma. Oncologist 2010;**15**(2):168-81 doi: 10.1634/theoncologist.2009-0302
12. Sharma A, Dwary AD, Mohanti BK, et al. Best supportive care compared with chemotherapy for unresectable gall bladder cancer: a randomized controlled study. J Clin Oncol 2010;**28**(30):4581-6 doi: 10.1200/jco.2010.29.3605
13. Marcano-Bonilla L, Mohamed EA, Mounajjed T, Roberts LR. Biliary tract cancers: epidemiology, molecular pathogenesis and genetic risk associations. Chinese Clinical Oncology 2016;**5**(5):4
14. Wistuba II, Gazdar AF. Gallbladder cancer: lessons from a rare tumour. Nature Reviews Cancer 2004;**4**(9):695-706 doi: 10.1038/nrc1429
15. Sasaki M, Yamaguchi J, Itatsu K, Ikeda H, Nakanuma Y. Over-expression of polycomb group protein EZH2 relates to decreased expression of p16INK4a in cholangiocarcinogenesis in hepatolithiasis. The Journal of Pathology 2008;**215**(2):175-83 doi: 10.1002/path.2345
16. House MG, Wistuba, II, Argani P, et al. Progression of gene hypermethylation in gallstone disease leading to gallbladder cancer. Ann Surg Oncol 2003;**10**(8):882-9 doi: 10.1245/aso.2003.02.014
17. Bickenbach K, Galka E, Roggin KK. Molecular mechanisms of cholangiocarcinogenesis: are biliary intraepithelial neoplasia and intraductal papillary neoplasms of the bile duct precursors to cholangiocarcinoma? Surg Oncol Clin N Am 2009;**18**(2):215-24, vii doi: 10.1016/j.soc.2008.12.001
18. Chakravarty D, Gao J, Phillips SM, et al. OncoKB: A Precision Oncology Knowledge Base. JCO Precis Oncol 2017;**2017** doi: 10.1200/po.17.00011
19. Ross JS, Wang K, Javle MM, et al. Comprehensive genomic profiling of biliary tract cancers to reveal tumor-specific differences and frequency of clinically relevant genomic alterations. Journal of Clinical Oncology 2015;**33**(15_suppl):4009-09 doi: 10.1200/jco.2015.33.15_suppl.4009
20. Hanada K, Tsuchida A, Iwao T, et al. Gene mutations of K-ras in gallbladder mucosae and gallbladder carcinoma with an anomalous junction of the pancreaticobiliary duct. Am J Gastroenterol 1999;**94**(6):1638-42 doi: 10.1111/j.1572-0241.1999.01155.x
21. Roa JC, Anabalón L, Tapia O, Melo A, de Aretxabala X, Roa I. [Frequency of K-ras mutation in biliary and pancreatic tumors]. Rev Med Chil 2005;**133**(12):1434-40

22. Li M, Zhang Z, Li X, et al. Whole-exome and targeted gene sequencing of gallbladder carcinoma identifies recurrent mutations in the ErbB pathway. Nature Genetics 2014;**46**(8):872-76 doi: 10.1038/ng.3030
23. Valle JW, Lamarca A, Goyal L, Barriuso J, Zhu AX. New Horizons for Precision Medicine in Biliary Tract Cancers. Cancer Discovery 2017;**7**(9):943 doi: 10.1158/2159-8290.CD-17-0245
24. Lamarca A, Barriuso J, McNamara MG, Valle JW. Molecular targeted therapies: ready for „prime time" in biliary tract cancer. Journal of Hepatology doi: 10.1016/j.jhep.2020.03.007
25. Li M, Liu F, Zhang F, et al. Genomic ERBB2/ERBB3 mutations promote PD-L1-mediated immune escape in gallbladder cancer: a whole-exome sequencing analysis. Gut 2019;**68**(6):1024 doi: 10.1136/gutjnl-2018-316039
26. Ambros V. The functions of animal microRNAs. Nature 2004;**431**(7006):350-55 doi: 10.1038/nature02871
27. van Rooij E, Kauppinen S. Development of microRNA therapeutics is coming of age. EMBO Mol Med 2014;**6**(7):851-64 doi: 10.15252/emmm.201100899
28. Lee Y, Kim M, Han J, et al. MicroRNA genes are transcribed by RNA polymerase II. Embo j 2004;**23**(20):4051-60 doi: 10.1038/sj.emboj.7600385
29. Gregory RI, Chendrimada TP, Shiekhattar R. MicroRNA Biogenesis: Isolation and Characterization of the Microprocessor Complex. In: Ying S-Y, ed. MicroRNA Protocols. Totowa, NJ: Humana Press, 2006:33-47.
30. Öhman M. A-to-I editing challenger or ally to the microRNA process. Biochimie 2007;**89**(10):1171-76 doi: https://doi.org/10.1016/j.biochi.2007.06.002
31. Huntzinger E, Izaurralde E. Gene silencing by microRNAs: contributions of translational repression and mRNA decay. Nat Rev Genet 2011;**12**(2):99-110 doi: 10.1038/nrg2936
32. Bartel DP. MicroRNAs: target recognition and regulatory functions. Cell 2009;**136**(2):215-33 doi: 10.1016/j.cell.2009.01.002
33. Cipolla GA. A non-canonical landscape of the microRNA system. Frontiers in Genetics 2014;**5**(337) doi: 10.3389/fgene.2014.00337
34. Kloosterman WP, Plasterk RHA. The Diverse Functions of MicroRNAs in Animal Development and Disease. Developmental Cell 2006;**11**(4):441-50 doi: https://doi.org/10.1016/j.devcel.2006.09.009
35. Friedman RC, Farh KK, Burge CB, Bartel DP. Most mammalian mRNAs are conserved targets of microRNAs. Genome Res 2009;**19**(1):92-105 doi: 10.1101/gr.082701.108
36. Thorsen SB, Obad S, Jensen NF, Stenvang J, Kauppinen S. The therapeutic potential of microRNAs in cancer. Cancer J 2012;**18**(3):275-84 doi: 10.1097/PPO.0b013e318258b5d6
37. Sarver AE, Li L, Kartha RV, Subramanian S. microRNAs in the Malignant Transformation Process. In: Santulli G, ed. microRNA: Cancer: From Molecular Biology to Clinical Practice. Cham: Springer International Publishing, 2015:1-21.
38. Peng Y, Croce CM. The role of MicroRNAs in human cancer. Signal Transduction and Targeted Therapy 2016;**1**(1):15004 doi: 10.1038/sigtrans.2015.4
39. Calin GA, Dumitru CD, Shimizu M, et al. Frequent deletions and down-regulation of micro- RNA genes miR15 and miR16 at 13q14 in chronic lymphocytic leukemia. Proceedings of the National Academy of Sciences 2002;**99**(24):15524 doi: 10.1073/pnas.242606799
40. Akcakaya P, Ekelund S, Kolosenko I, et al. miR-185 and miR-133b deregulation is associated with overall survival and metastasis in colorectal cancer. Int J Oncol 2011;**39**(2):311-8 doi: 10.3892/ijo.2011.1043
41. Li X, Zhang Y, Zhang Y, Ding J, Wu K, Fan D. Survival prediction of gastric cancer by a seven-microRNA signature. Gut 2010;**59**(5):579 doi: 10.1136/gut.2008.175497
42. Kojima M, Sudo H, Kawauchi J, et al. MicroRNA markers for the diagnosis of pancreatic and biliary-tract cancers. PloS one 2015;**10**(2):e0118220-e20 doi: 10.1371/journal.pone.0118220
43. Kishimoto T, Eguchi H, Nagano H, et al. Plasma miR-21 is a novel diagnostic biomarker for biliary tract cancer. Cancer Science 2013;**104**(12):1626-31 doi: 10.1111/cas.12300

44. Shigehara K, Yokomuro S, Ishibashi O, et al. Real-Time PCR-Based Analysis of the Human Bile MicroRNAome Identifies miR-9 as a Potential Diagnostic Biomarker for Biliary Tract Cancer. PLOS ONE 2011;**6**(8):e23584 doi: 10.1371/journal.pone.0023584
45. Tryndyak VP, Ross SA, Beland FA, Pogribny IP. Down-regulation of the microRNAs miR-34a, miR-127, and miR-200b in rat liver during hepatocarcinogenesis induced by a methyl-deficient diet. Molecular Carcinogenesis 2009;**48**(6):479-87 doi: 10.1002/mc.20484
46. Wang R, Wang ZX, Yang JS, Pan X, De W, Chen LB. MicroRNA-451 functions as a tumor suppressor in human non-small cell lung cancer by targeting ras-related protein 14 (RAB14). Oncogene 2011;**30**(23):2644-58 doi: 10.1038/onc.2010.642
47. Liu T, Tang H, Lang Y, Liu M, Li X. MicroRNA-27a functions as an oncogene in gastric adenocarcinoma by targeting prohibitin. Cancer Letters 2009;**273**(2):233-42 doi: https://doi.org/10.1016/j.canlet.2008.08.003
48. Lehmann U, Hasemeier B, Christgen M, et al. Epigenetic inactivation of microRNA gene hsa-mir-9-1 in human breast cancer. The Journal of Pathology 2008;**214**(1):17-24 doi: 10.1002/path.2251
49. Janssen HL, Reesink HW, Lawitz EJ, et al. Treatment of HCV infection by targeting microRNA. N Engl J Med 2013;**368**(18):1685-94 doi: 10.1056/NEJMoa1209026
50. van Zandwijk N, Pavlakis N, Kao SC, et al. Safety and activity of microRNA-loaded minicells in patients with recurrent malignant pleural mesothelioma: a first-in-man, phase 1, open-label, dose-escalation study. Lancet Oncol 2017;**18**(10):1386-96 doi: 10.1016/s1470-2045(17)30621-6
51. Aaronson DS, Horvath CM. A Road Map for Those Who Don't Know JAK-STAT. Science 2002;**296**(5573):1653 doi: 10.1126/science.1071545
52. Sekimoto T, Imamoto N, Nakajima K, Hirano T, Yoneda Y. Extracellular signal-dependent nuclear import of Stat1 is mediated by nuclear pore-targeting complex formation with NPI-1, but not Rch1. The EMBO Journal 1997;**16**(23):7067-77 doi: 10.1093/emboj/16.23.7067
53. Igaz P, Tóth S, Falus A. Biological and clinical significance of the JAK-STAT pathway; lessons from knockout mice. Inflammation Research 2001;**50**(9):435-41 doi: 10.1007/PL00000267
54. Darnell JE, Jr., Kerr IM, Stark GR. Jak-STAT pathways and transcriptional activation in response to IFNs and other extracellular signaling proteins. Science 1994;**264**(5164):1415-21 doi: 10.1126/science.8197455
55. Tamiya T, Kashiwagi I, Takahashi R, Yasukawa H, Yoshimura A. Suppressors of Cytokine Signaling (SOCS) Proteins and JAK/STAT Pathways. Arteriosclerosis, Thrombosis, and Vascular Biology 2011;**31**(5):980-85 doi: 10.1161/ATVBAHA.110.207464
56. Kershaw Nadia J, Murphy James M, Lucet Isabelle S, Nicola Nicos A, Babon Jeffrey J. Regulation of Janus kinases by SOCS proteins. Biochemical Society Transactions 2013;**41**(4):1042-47 doi: 10.1042/BST20130077
57. Xu D, Qu CK. Protein tyrosine phosphatases in the JAK/STAT pathway. Front Biosci 2008;**13**:4925-32 doi: 10.2741/3051[published Online First: Epub Date]|.
58. Mander A, Hodgkinson CP, Sale GJ. Knock-down of LAR protein tyrosine phosphatase induces insulin resistance. FEBS Lett 2005;**579**(14):3024-8 doi: 10.1016/j.febslet.2005.04.057
59. Muller T, Choidas A, Reichmann E, Ullrich A. Phosphorylation and free pool of beta-catenin are regulated by tyrosine kinases and tyrosine phosphatases during epithelial cell migration. J Biol Chem 1999;**274**(15):10173-83 doi: 10.1074/jbc.274.15.10173
60. Xu YY, Liu H, Su L, et al. PPARgamma inhibits breast cancer progression by upregulating PTPRF expression. Eur Rev Med Pharmacol Sci 2019;**23**(22):9965-77 doi: 10.26355/eurrev_201911_19563
61. Bera R, Chiou CY, Yu MC, et al. Functional genomics identified a novel protein tyrosine phosphatase receptor type F-mediated growth inhibition in hepatocarcinogenesis. Hepatology 2014;**59**(6):2238-50 doi: 10.1002/hep.27030
62. Sarhan AR, Patel TR, Cowell AR, et al. LAR protein tyrosine phosphatase regulates focal adhesions through CDK1. J Cell Sci 2016;**129**(15):2962-71 doi: 10.1242/jcs.191379

63. Shuai K, Liu B. Regulation of gene-activation pathways by PIAS proteins in the immune system. Nature Reviews Immunology 2005;**5**(8):593-605 doi: 10.1038/nri1667
64. Avalle L, Pensa S, Regis G, Novelli F, Poli V. STAT1 and STAT3 in tumorigenesis: A matter of balance. JAKSTAT 2012;**1**(2):65-72 doi: 10.4161/jkst.20045
65. Yu H, Pardoll D, Jove R. STATs in cancer inflammation and immunity: a leading role for STAT3. Nature Reviews Cancer 2009;**9**(11):798-809 doi: 10.1038/nrc2734
66. Rani A, Murphy JJ. STAT5 in Cancer and Immunity. J Interferon Cytokine Res 2016;**36**(4):226-37 doi: 10.1089/jir.2015.0054
67. Stephanou A, Latchman DS. STAT-1: a novel regulator of apoptosis. Int J Exp Pathol 2003;**84**(6):239-44 doi: 10.1111/j.0959-9673.2003.00363.x
68. Chin YE, Kitagawa M, Kuida K, Flavell RA, Fu XY. Activation of the STAT signaling pathway can cause expression of caspase 1 and apoptosis. Mol Cell Biol 1997;**17**(9):5328-37 doi: 10.1128/mcb.17.9.5328
69. Battle TE, Lynch RA, Frank DA. Signal transducer and activator of transcription 1 activation in endothelial cells is a negative regulator of angiogenesis. Cancer Res 2006;**66**(7):3649-57 doi: 10.1158/0008-5472.Can-05-3612
70. Critchley-Thorne RJ, Yan N, Nacu S, Weber J, Holmes SP, Lee PP. Down-regulation of the interferon signaling pathway in T lymphocytes from patients with metastatic melanoma. PLoS Med 2007;**4**(5):e176 doi: 10.1371/journal.pmed.0040176
71. Dokduang H, Techasen A, Namwat N, et al. STATs profiling reveals predominantly-activated STAT3 in cholangiocarcinoma genesis and progression. Journal of Hepato-Biliary-Pancreatic Sciences 2014;**21** doi: 10.1002/jhbp.131
72. Goeppert B, Truckenmueller F, Ori A, et al. Profiling of gallbladder carcinoma reveals distinct miRNA profiles and activation of STAT1 by the tumor suppressive miRNA-145-5p. Scientific Reports 2019;**9**(1):4796 doi: 10.1038/s41598-019-40857-3
73. Dexter JS. The Analysis of a Case of Continuous Variation in Drosophila by a Study of Its Linkage Relations. The American Naturalist 1914;**48**(576):712-58 doi: 10.1086/279446
74. Wilson A, Radtke F. Multiple functions of Notch signaling in self-renewing organs and cancer. FEBS Lett 2006;**580**(12):2860-8 doi: 10.1016/j.febslet.2006.03.024
75. Brzozowa-Zasada M, Piecuch A, Dittfeld A, et al. Notch signalling pathway as an oncogenic factor involved in cancer development. Contemp Oncol (Pozn) 2016;**20**(4):267-72 doi: 10.5114/wo.2016.61845
76. Louvi A, Artavanis-Tsakonas S. Notch and disease: A growing field. Seminars in Cell & Developmental Biology 2012;**23**(4):473-80 doi: https://doi.org/10.1016/j.semcdb.2012.02.005
77. Bray SJ. Notch signalling in context. Nature Reviews Molecular Cell Biology 2016;**17**(11):722-35 doi: 10.1038/nrm.2016.94
78. Aster JC, Pear WS, Blacklow SC. The Varied Roles of Notch in Cancer. Annu Rev Pathol 2017;**12**:245-75 doi: 10.1146/annurev-pathol-052016-100127
79. Munro S, Freeman M. The Notch signalling regulator Fringe acts in the Golgi apparatus and requires the glycosyltransferase signature motif DxD. Current Biology 2000;**10**(14):813-20 doi: https://doi.org/10.1016/S0960-9822(00)00578-9
80. Kopan R, Ilagan MXG. The Canonical Notch Signaling Pathway: Unfolding the Activation Mechanism. Cell 2009;**137**(2):216-33 doi: https://doi.org/10.1016/j.cell.2009.03.045
81. Schweisguth F. Regulation of Notch Signaling Activity. Current Biology 2004;**14**(3):R129-R38 doi: https://doi.org/10.1016/j.cub.2004.01.023
82. Andersson ER, Sandberg R, Lendahl U. Notch signaling: simplicity in design, versatility in function. Development 2011;**138**(17):3593 doi: 10.1242/dev.063610
83. Petrovic J, Formosa-Jordan P, Luna-Escalante JC, et al. Ligand-dependent Notch signaling strength orchestrates lateral induction and lateral inhibition in the developing inner ear. Development 2014;**141**(11):2313 doi: 10.1242/dev.108100

84. van Tetering G, Vooijs M. Proteolytic cleavage of Notch: "HIT and RUN". Curr Mol Med 2011;**11**(4):255-69 doi: 10.2174/156652411795677972
85. Steinbuck MP, Winandy S. A Review of Notch Processing With New Insights Into Ligand-Independent Notch Signaling in T-Cells. Frontiers in Immunology 2018;**9**(1230) doi: 10.3389/fimmu.2018.01230
86. Yeh C-H, Bellon M, Nicot C. FBXW7: a critical tumor suppressor of human cancers. Mol Cancer 2018;**17**(1):115 doi: 10.1186/s12943-018-0857-2
87. Bruckner K, Perez L, Clausen H, Cohen S. Glycosyltransferase activity of Fringe modulates Notch-Delta interactions. Nature 2000;**406**(6794):411-5 doi: 10.1038/35019075
88. Lee TV, Sethi MK, Leonardi J, et al. Negative regulation of notch signaling by xylose. PLoS Genet 2013;**9**(6):e1003547 doi: 10.1371/journal.pgen.1003547
89. VanHook AM. Dishevelled Mediates Wnt-Notch Crosstalk. Science Signaling 2012;**5**(251):ec298 doi: 10.1126/scisignal.2003786
90. Weng AP, Ferrando AA, Lee W, et al. Activating mutations of NOTCH1 in human T cell acute lymphoblastic leukemia. Science 2004;**306**(5694):269-71 doi: 10.1126/science.1102160
91. Wang NJ, Sanborn Z, Arnett KL, et al. Loss-of-function mutations in Notch receptors in cutaneous and lung squamous cell carcinoma. Proc Natl Acad Sci U S A 2011;**108**(43):17761-6 doi: 10.1073/pnas.1114669108
92. Ntziachristos P, Lim Jing S, Sage J, Aifantis I. From Fly Wings to Targeted Cancer Therapies: A Centennial for Notch Signaling. Cancer Cell 2014;**25**(3):318-34 doi: https://doi.org/10.1016/j.ccr.2014.02.018
93. Yoon HA, Noh MH, Kim BG, et al. Clinicopathological significance of altered Notch signaling in extrahepatic cholangiocarcinoma and gallbladder carcinoma. World J Gastroenterol 2011;**17**(35):4023-30 doi: 10.3748/wjg.v17.i35.4023
94. Zender S, Nickeleit I, Wuestefeld T, et al. A Critical Role for Notch Signaling in the Formation of Cholangiocellular Carcinomas. Cancer Cell 2013;**23**(6):784-95 doi: https://doi.org/10.1016/j.ccr.2013.04.019
95. Ishimura N, Bronk SF, Gores GJ. Inducible Nitric Oxide Synthase Up-Regulates Notch-1 in Mouse Cholangiocytes: Implications for Carcinogenesis. Gastroenterology 2005;**128**(5):1354-68 doi: https://doi.org/10.1053/j.gastro.2005.01.055
96. Bizama C, García P, Espinoza JA, et al. Targeting specific molecular pathways holds promise for advanced gallbladder cancer therapy. Cancer Treatment Reviews 2015;**41**(3):222-34 doi: https://doi.org/10.1016/j.ctrv.2015.01.003
97. Ritchie ME, Phipson B, Wu D, et al. limma powers differential expression analyses for RNA-sequencing and microarray studies. Nucleic Acids Research 2015;**43**(7):e47-e47 doi: 10.1093/nar/gkv007
98. Livak KJ, Schmittgen TD. Analysis of relative gene expression data using real-time quantitative PCR and the 2(-Delta Delta C(T)) Method. Methods 2001;**25**(4):402-8 doi: 10.1006/meth.2001.1262
99. Hu Q, Noll RJ, Li H, Makarov A, Hardman M, Graham Cooks R. The Orbitrap: a new mass spectrometer. Journal of Mass Spectrometry 2005;**40**(4):430-43 doi: 10.1002/jms.856
100. Thompson A, Schafer J, Kuhn K, et al. Tandem mass tags: a novel quantification strategy for comparative analysis of complex protein mixtures by MS/MS. Anal Chem 2003;**75**(8):1895-904 doi: 10.1021/ac0262560
101. Buczak K, Ori A, Kirkpatrick JM, et al. Spatial Tissue Proteomics Quantifies Inter- and Intratumor Heterogeneity in Hepatocellular Carcinoma (HCC). Mol Cell Proteomics 2018;**17**(4):810-25 doi: 10.1074/mcp.RA117.000189
102. Brosch M, Yu L, Hubbard T, Choudhary J. Accurate and Sensitive Peptide Identification with Mascot Percolator. Journal of Proteome Research 2009;**8**(6):3176-81 doi: 10.1021/pr800982s
103. Heinze I, Bens M, Calzia E, et al. Species comparison of liver proteomes reveals links to naked mole-rat longevity and human aging. BMC Biology 2018;**16**(1):82 doi: 10.1186/s12915-018-0547-y
104. Benjamini Y, Drai D, Elmer G, Kafkafi N, Golani I. Controlling the false discovery rate in behavior genetics research. Behav Brain Res 2001;**125**(1-2):279-84 doi: 10.1016/s0166-4328(01)00297-2

105. Satoh J-I, Tabunoki H. A Comprehensive Profile of ChIP-Seq-Based STAT1 Target Genes Suggests the Complexity of STAT1-Mediated Gene Regulatory Mechanisms. Gene Regul Syst Bio 2013;**7**:41-56 doi: 10.4137/GRSB.S11433
106. Yan X, Chen X, Liang H, et al. miR-143 and miR-145 synergistically regulate ERBB3 to suppress cell proliferation and invasion in breast cancer. Mol Cancer 2014;**13**:220-20 doi: 10.1186/1476-4598-13-220
107. Sticht C, De La Torre C, Parveen A, Gretz N. miRWalk: An online resource for prediction of microRNA binding sites. PLOS ONE 2018;**13**(10):e0206239 doi: 10.1371/journal.pone.0206239
108. Niu C, Liang C, Guo J, et al. Downregulation and growth inhibitory role of FHL1 in lung cancer. Int J Cancer 2012;**130**(11):2549-56 doi: 10.1002/ijc.26259
109. Xu Y, Liu Z, Guo K. Expression of FHL1 in gastric cancer tissue and its correlation with the invasion and metastasis of gastric cancer. Mol Cell Biochem 2012;**363**(1-2):93-9 doi: 10.1007/s11010-011-1161-2
110. Fu W, Wang K, Zhao JL, et al. FHL1C induces apoptosis in Notch1-dependent T-ALL cells through an interaction with RBP-J. BMC Cancer 2014;**14**:463 doi: 10.1186/1471-2407-14-463
111. Ren W, Lian P, Cheng L, et al. FHL1 inhibits the growth of tongue squamous cell carcinoma cells via G1/S cell cycle arrest. Mol Med Rep 2015;**12**(3):3958-64 doi: 10.3892/mmr.2015.3844
112. Zhou L, Ding L, Liu J, et al. Four-and-a-half LIM protein 1 promotes paclitaxel resistance in hepatic carcinoma cells through the regulation of caspase-3 activation. J Cancer Res Ther 2018;**14**(Supplement):S767-s73 doi: 10.4103/0973-1482.187304
113. Wang X, Wei X, Yuan Y, et al. Src-mediated phosphorylation converts FHL1 from tumor suppressor to tumor promoter. J Cell Biol 2018;**217**(4):1335-51 doi: 10.1083/jcb.201708064
114. Anaya J. OncoLnc: linking TCGA survival data to mRNAs, miRNAs, and lncRNAs. PeerJ Computer Science 2016;**2**:e67 doi: 10.7717/peerj-cs.67
115. Zhao JL, Liang SQ, Fu W, et al. The LIM domain protein FHL1C interacts with tight junction protein ZO-1 contributing to the epithelial-mesenchymal transition (EMT) of a breast adenocarcinoma cell line. Gene 2014;**542**(2):182-9 doi: 10.1016/j.gene.2014.03.036
116. Ding L, Wang Z, Yan J, et al. Human four-and-a-half LIM family members suppress tumor cell growth through a TGF-beta-like signaling pathway. J Clin Invest 2009;**119**(2):349-61 doi: 10.1172/jci35930
117. Li Y, Hibbs MA, Gard AL, Shylo NA, Yun K. Genome-wide analysis of N1ICD/RBPJ targets in vivo reveals direct transcriptional regulation of Wnt, SHH, and hippo pathway effectors by Notch1. Stem Cells 2012;**30**(4):741-52 doi: 10.1002/stem.1030
118. Farazi PA, DePinho RA. Hepatocellular carcinoma pathogenesis: from genes to environment. Nature Reviews Cancer 2006;**6**(9):674-87 doi: 10.1038/nrc1934
119. Ma B, Chen K, Liu P, et al. Dichotomal functions of phosphorylated and unphosphorylated STAT1 in hepatocellular carcinoma. J Mol Med (Berl) 2019;**97**(1):77-88 doi: 10.1007/s00109-018-1717-7
120. Platanias LC. Mechanisms of type-I- and type-II-interferon-mediated signalling. Nature Reviews Immunology 2005;**5**(5):375-86 doi: 10.1038/nri1604[published Online First: Epub Date]|.
121. Farhood B, Najafi M, Mortezaee K. CD8(+) cytotoxic T lymphocytes in cancer immunotherapy: A review. J Cell Physiol 2019;**234**(6):8509-21 doi: 10.1002/jcp.27782
122. Gajewski TF, Schreiber H, Fu Y-X. Innate and adaptive immune cells in the tumor microenvironment. Nature Immunology 2013;**14**(10):1014-22 doi: 10.1038/ni.2703
123. Vasudevan S, Tong Y, Steitz JA. Switching from Repression to Activation: MicroRNAs Can Up-Regulate Translation. Science 2007;**318**(5858):1931 doi: 10.1126/science.1149460
124. Li L-C, Okino ST, Zhao H, et al. Small dsRNAs induce transcriptional activation in human cells. Proceedings of the National Academy of Sciences 2006;**103**(46):17337 doi: 10.1073/pnas.0607015103
125. Prud'homme GJ, Glinka Y, Lichner Z, Yousef GM. Neuropilin-1 is a receptor for extracellular miRNA and AGO2/miRNA complexes and mediates the internalization of miRNAs that modulate cell function. Oncotarget 2016;**7**(42):68057-71 doi: 10.18632/oncotarget.10929

126. Dempoya J, Matsumiya T, Imaizumi T, et al. Double-Stranded RNA Induces Biphasic STAT1 Phosphorylation by both Type I Interferon (IFN)-Dependent and Type I IFN-Independent Pathways. Journal of Virology 2012;**86**(23):12760 doi: 10.1128/JVI.01881-12
127. Tang L, Roberts PC, Kraniak JM, Li Q, Tainsky MA. Stat1 Expression Is Not Sufficient to Regulate the Interferon Signaling Pathway in Cellular Immortalization. Journal of Interferon & Cytokine Research 2006;**26**(1):14-26 doi: 10.1089/jir.2006.26.14
128. Mohebiany AN, Nikolaienko RM, Bouyain S, Harroch S. Receptor-type tyrosine phosphatase ligands: looking for the needle in the haystack. FEBS J 2013;**280**(2):388-400 doi: 10.1111/j.1742-4658.2012.08653.x
129. Serra-Pagès C, Kedersha NL, Fazikas L, Medley Q, Debant A, Streuli M. The LAR transmembrane protein tyrosine phosphatase and a coiled-coil LAR-interacting protein co-localize at focal adhesions. The EMBO Journal 1995;**14**(12):2827-38 doi: 10.1002/j.1460-2075.1995.tb07282.x
130. Tian Xa, Yang C, Yang L, Sun Q, Liu N. PTPRF as a novel tumor suppressor through deactivation of ERK1/2 signaling in gastric adenocarcinoma. Onco Targets Ther 2018;**11**:7795-803 doi: 10.2147/OTT.S178152
131. Whitmore TE, Peterson A, Holzman T, et al. Integrative Analysis of N-Linked Human Glycoproteomic Data Sets Reveals PTPRF Ectodomain as a Novel Plasma Biomarker Candidate for Prostate Cancer. Journal of Proteome Research 2012;**11**(5):2653-65 doi: 10.1021/pr201200n
132. Wang W-J, Kuo J-C, Ku W, et al. The Tumor Suppressor DAPK Is Reciprocally Regulated by Tyrosine Kinase Src and Phosphatase LAR. Molecular Cell 2007;**27**(5):701-16 doi: https://doi.org/10.1016/j.molcel.2007.06.037
133. Levea CM, McGary CT, Symons JR, Mooney RA. PTP LAR expression compared to prognostic indices in metastatic and non-metastatic breast cancer. Breast Cancer Res Treat 2000;**64**(2):221-8 doi: 10.1023/a:1006410509740
134. Du WW, Fang L, Li M, et al. MicroRNA miR-24 enhances tumor invasion and metastasis by targeting PTPN9 and PTPRF to promote EGF signaling. J Cell Sci 2013;**126**(Pt 6):1440-53 doi: 10.1242/jcs.118299
135. Zeegers-Huyskens T, Huyskens P. Intermolecular Forces. In: Huyskens PL, Luck WAP, Zeegers-Huyskens T, eds. Intermolecular Forces: An Introduction to Modern Methods and Results. Berlin, Heidelberg: Springer Berlin Heidelberg, 1991:1-30.
136. Fahim RB, Mc DJ, Richards JC, Ferris DO. Carcinoma of the gallbladder: a study of its modes of spread. Ann Surg 1962;**156**:114-24 doi: 10.1097/00000658-196207000-00021
137. Ding L, Niu C, Zheng Y, et al. FHL1 interacts with oestrogen receptors and regulates breast cancer cell growth. Journal of Cellular and Molecular Medicine 2011;**15**(1):72-85 doi: 10.1111/j.1582-4934.2009.00938.x
138. Zhou L, Ding L, Liu J, et al. Four-and-a-half LIM protein 1 promotes paclitaxel resistance in hepatic carcinoma cells through the regulation of caspase-3 activation. Journal of Cancer Research and Therapeutics 2018;**14**(10):767-73 doi: 10.4103/0973-1482.187304
139. Shen Y, Jia Z, Nagele RG, Ichikawa H, Goldberg GS. Src Uses Cas to Suppress Fhl1 in Order to Promote Nonanchored Growth and Migration of Tumor Cells. Cancer Research 2006;**66**(3):1543 doi: 10.1158/0008-5472.CAN-05-3152
140. Wang J, Huang F, Huang J, Kong J, Liu S, Jin J. Epigenetic analysis of FHL1 tumor suppressor gene in human liver cancer. Oncol Lett 2017;**14**(5):6109-16 doi: 10.3892/ol.2017.6950
141. Cao W, Liu J, Xia R, et al. X-linked FHL1 as a novel therapeutic target for head and neck squamous cell carcinoma. Oncotarget 2016;**7**(12):14537-50 doi: 10.18632/oncotarget.7478
142. Wang Y, Fu J, Jiang M, et al. MiR-410 is overexpressed in liver and colorectal tumors and enhances tumor cell growth by silencing FHL1 via a direct/indirect mechanism. PLoS One 2014;**9**(10):e108708 doi: 10.1371/journal.pone.0108708

143. Shathasivam T, Kislinger T, Gramolini AO. Genes, proteins and complexes: the multifaceted nature of FHL family proteins in diverse tissues. Journal of cellular and molecular medicine 2010;**14**(12):2702-20 doi: 10.1111/j.1582-4934.2010.01176.x
144. Zhi Z, Zhu H, Lv X, et al. IGF2-derived miR-483-3p associated with Hirschsprung's disease by targeting FHL1. Journal of cellular and molecular medicine 2018;**22**(10):4913-21 doi: 10.1111/jcmm.13756
145. Zhao J-L, Liang S-Q, Fu W, et al. The LIM domain protein FHL1C interacts with tight junction protein ZO-1 contributing to the epithelial–mesenchymal transition (EMT) of a breast adenocarcinoma cell line. Gene 2014;**542**(2):182-89 doi: https://doi.org/10.1016/j.gene.2014.03.036
146. Kiemer AK, Takeuchi K, Quinlan MP. Identification of genes involved in epithelial-mesenchymal transition and tumor progression. Oncogene 2001;**20**(46):6679-88 doi: 10.1038/sj.onc.1204872
147. Giannelli G, Koudelkova P, Dituri F, Mikulits W. Role of epithelial to mesenchymal transition in hepatocellular carcinoma. J Hepatol 2016;**65**(4):798-808 doi: 10.1016/j.jhep.2016.05.007
148. Wu LC, Chen LT, Tsai YJ, et al. Alpha-methylacyl coenzyme A racemase overexpression in gallbladder carcinoma confers an independent prognostic indicator. J Clin Pathol 2012;**65**(4):309-14 doi: 10.1136/jclinpath-2011-200489
149. Taniguchi Y, Furukawa T, Tun T, Han H, Honjo T. LIM protein KyoT2 negatively regulates transcription by association with the RBP-J DNA-binding protein. Molecular and cellular biology 1998;**18**(1):644-54 doi: 10.1128/mcb.18.1.644
150. Li Y, Hibbs MA, Gard AL, Shylo NA, Yun K. Genome-wide analysis of N1ICD/RBPJ targets in vivo reveals direct transcriptional regulation of Wnt, SHH, and hippo pathway effectors by Notch1. Stem cells (Dayton, Ohio) 2012;**30**(4):741-52 doi: 10.1002/stem.1030
151. Chung WC, Wang J, Zhou Y, Xu K. Kras(G12D) upregulates Notch signaling to induce gallbladder tumorigenesis in mice. Oncoscience 2017;**4**(9-10):131-38 doi: 10.18632/oncoscience.368
152. Roa I, Araya JC, Shiraishi T, et al. [Gallbladder carcinoma: expression of the c-myc and ras-p-21 oncogene products]. Rev Med Chil 1994;**122**(7):754-9
153. Li H, Jin Y, Hu Y, et al. The PLGF/c-MYC/miR-19a axis promotes metastasis and stemness in gallbladder cancer. Cancer science 2018;**109**(5):1532-44 doi: 10.1111/cas.13585
154. Matsushima-Nishiwaki R, Toyoda H, Nagasawa T, et al. Phosphorylated Heat Shock Protein 20 (HSPB6) Regulates Transforming Growth Factor-α-Induced Migration and Invasion of Hepatocellular Carcinoma Cells. PLOS ONE 2016;**11**(4):e0151907 doi: 10.1371/journal.pone.0151907

PUBLICATIONS

Parts of this doctoral thesis have been published in:

Peer-reviewed article

Benjamin Goeppert, Felicia Truckenmueller, Alessandro Ori, Valerie Fritz, Thomas Albrecht, Angelika Fraas, Dominique Scherer, Rosa González Silos, Carsten Sticht, Norbert Gretz, Arianeb Mehrabi, Melanie Bewerunge-Hudler, Stefan Pusch, Justo Lorenzo Bermejo, Peter Dietrich, Peter Schirmacher, Marcus Renner, Stephanie Roessler

Profiling of gallbladder carcinoma reveals distinct miRNA profiles and activation of STAT1 by the tumor suppressive miRNA-145-5p, Scientific Reports. 2019 Mar 18. DOI: 10.1038/s41598-019-40857-3

Katarzyna Buczak, Joanna M. Kirkpatrick, Felicia Truckenmueller, Deolinda Santinha, Lino Ferreira, Stephanie Roessler, Stephan Singer, Martin Beck, Alessandro Ori

Spatially resolved analysis of FFPE tissue proteomes by quantitative mass spectrometry, Springer Nature Experiments. 2020 Sep 09. DOI: 10.1038/s41596-020-0356-y

Conference Posters

Felicia Truckenmueller, Benjamin Goeppert, Stefan Pusch, Ivonne Heinze, Joanna Kirkpatrick, Peter Schirmacher, Alessandro Ori, Stephanie Roessler

Mass-spectrometric analysis of deregulated proteins in gallbladder carcinoma

International Liver Congress (ILC), 2019, Vienna, Austria

FIGURE INDEX

TABLE INDEX

ACKNOWLEDGEMENTS

Mein Dank gilt zuvorderst Prof. Dr. Peter Schirmacher und PD Dr. Stephanie Rössler für die Möglichkeit, meine Doktorarbeit am Pathologischen Institut des Universitätsklinikums Heidelberg durchführen zu können.

Besonderer Dank gilt dabei Dr. Stephanie Rössler für die Überlassung des spannenden Themas und ihrer offenen Tür, die eine umfassende Betreuung und rat- und tatkräftige Unterstützung mit sich brachte. Danke Dir, für das in mich gesetzte Vertrauen und die Unterstützung beim Umsetzen der Projekte, unter anderem der tollen Möglichkeit ein Teil der Experimente in Jena durchführen zu kommen. Danke auch für die vertrauensvolle Arbeitsatmosphäre in deiner Gruppe und die sorgfältige Begutachtung meiner Arbeit. Außerdem danke ich dir für dein Verständnis und deinen Rückhalt während der schweren privaten Zeit für mich.

Des Weiteren danke ich meinem Doktorvater Prof. Dr. Ralf Bartenschlager, für seine Bereitschaft diese Dissertation zu begutachten und vor der Biowissenschaftlichen Fakultät der Universität Heidelberg zu vertreten.

Frau Prof. Ilse Hoffmann und Herrn Prof. Peter Angel danke ich für ihre Bereitschaft, als Prüfer in meiner Disputation zu fungieren.

Zudem möchte ich mich bei allen Kollaborationspartnern bedanken, die einen wesentlichen Beitrag zum Gelingen dieser Arbeit geleistet haben:

- Dr. Alessandro Ori und seiner gesamten Arbeitsgruppe (Joanna, Svenja, Simone und Yvonne) für die großartige Möglichkeit Proteomics Analysen durchführen zu können, sowie auch die Auswertungen zu verstehen. Und natürlich auch danke dafür, dass immer eine Laborgruppen-Aktivität geplant war, als ich zu Besuch war.
- Dr. Stefan Pusch für Bereitstellung der Plasmide.
- Dr. Christian Ackermann und Dr. Ulrike Engel vom Nikon Imaging Center.
- Prof Dr. Peter Friedrich und seiner Gruppe für den Nachweis direkter MicroRNA Bindung.
- Ariani für die tatkräftige Unterstützung im Rahmen ihrer Masterarbeit
- Veronika für die ganzen IHC-Färbungen der TMAs.

Ein ganz besonders großes Dankeschön geht an Geli, Sarah, Caro und Sofia für eure zahlreichen Antworten auf praktische Fragen und Antworten auf theoretische Fragen, mit denen ich mich jederzeit an euch wenden konnte. Außerdem großen Dank an Michaela, ich konnte dich nicht nur immer in Labordingen fragen, sondern habe die letzten Monate neben dir sitzend sehr viel Spaß und sehr gute Gespräche gehabt. Lena, Thorben und Fabi - schade, dass wir nicht länger zusammen gearbeitet haben.

Ein riesengroßes Dankeschön, geht an meine 0711-Gang und die Mädels aus meiner Schulzeit, die immer noch super Freundinnen sind, egal wo wir uns zurzeit befinden. Ihr bildet ein Netz, in das man sich immer reinfallen lassen kann.

Mein größter Dank gilt meiner Mama im Universum, meinen Großeltern und meiner ganzen Familie, Sonia, meinem Bruder und natürlich meinem Partner Leon. Danke für eure Unterstützung, Liebe und dass ihr immer – wirklich immer – meinen Rücken stärkt.

EIDESSTATTLICHE VERSICHERUNG GEMÄß §8 DER PROMOTIONSORDNUNG

Bei der eingereichten Dissertation zu dem Thema “Dysregulated microRNAS in Biliary Tract Cancer and Characterization of the target Tumor Suppressor FHL1” handelt es sich um meine eigenständig erbrachte Leistung. Ich habe nur die angegebenen Quellen und Hilfsmittel benutzt und mich keiner unzulässigen Hilfe Dritter bedient. Insbesondere habe ich wörtlich oder sinngemäß aus anderen Werken übernommene Inhalte als solche kenntlich gemacht. Die Arbeit oder Teile davon habe ich bislang nicht an einer Hochschule des In- oder Auslandes als Bestandteil einer Prüfungs- oder Qualifikationsleistung vorgelegt.

Stuttgart, den Felicia Truckenmüller